Nanocomposites: Incorporation of Cellulose Nanocrystals into Polymers and Addition of Zwitterionic Functionality

Keith Doubrava Hendren

Dissertation submitted to the faculty of the Virginia Polytechnic Institute and State University in partial fulfillment of the requirements for the degree of

Doctor of Philosophy

In

Material Science and Engineering

E. Johan Foster, Chair

Paul A. Deck, Co-Chair

Kevin J. Edgar

Michael J. Bortner

Travis W. Baughman

Michael O. Hunt

3-18-2020

Blacksburg Virginia

Keywords: Composite, Catalyst, Polyethylene, Cellulose Nanocrystal, Norbornene, Surface Modification

Nanocomposites: Incorporation of Cellulose Nanocrystals into Polymers and Addition of Zwitterionic Functionality

Keith Doubrava Hendren

ACADEMIC ABSTRACT

Cellulose nanocrystals (CNCs) are nanomaterials that have shown promise as reinforcement filler materials. Their small size, high modulus, and high aspect ratio makes CNCs good reinforcing materials. CNCs are typically introduced into softer polymer materials, which can have incompatible surface chemistry such as aliphatic chains, leading to aggregation and poor reinforcement of the material. The intrinsic hydrophobicity of the CNC surfaces suggests that dispersal into hydrophobic polymer matrices, which the CNCs could potentially reinforce, represent a significant challenge. Therefore, new non-traditional strategies are needed to introduce CNCs into polymer materials. The hydroxyl groups on the surfaces of CNCs can be functionalized using a variety of chemical techniques to yield materials that can interact better with solvents or polymers. Additionally, surface groups can allow the CNCs to react with environmental stimuli (smart materials).

The primary focus of this work is the incorporation of CNCs in hydrophobic matrices. Herein we introduce a new method of dispersing CNCs in polyethylene (PE), a substance of legendary hydrophobicity that is also the most common synthetic polymer used in consumer packaging. The prospect of increasing the mechanical strength of PE by incorporating CNC materials as fillers may lead to the possibility of using less polymer to obtain the same strength.

This thesis approaches the problem of dispersing CNCs within PE by first functionalizing the CNCs with a catalyst capable of polymerizing ethylene and other α-olefins. The catalyst 1,1'-bis(bromodimethylsilyl)zirconocene dibromide (catalyst **1**) is equipped with anchoring groups that are capable of attachment to the surface hydroxyl groups of CNC particles. After immobilizing catalyst **1** onto various CNC samples, introduction of solvent, organoaluminum cocatalyst, and monomer (ethylene alone or ethylene *plus* 1-hexene) afforded high density polyethylene (HDPE) and linear low-density polyethylene (LLDPE) samples, respectively, containing well-dispersed CNCs as filler materials.

Chapter 2 provided important information on the attachment of catalyst **1** to cellulose nanocrystals and the successful polymerization of ethylene from the cellulose nanocrystals. The resulting composite materials showed a in Young's modulus that was three-fold that of PE samples we tested (1600 ± 100 vs 500 ± 30) and about 10% greater relative to a commercial high modulus PE sample (1450 MPa). The increase in Young's modulus along with the lack of macroscopic aggregates led to the conclusion that we have developed a viable method to disperse CNCs in polyolefin matrices.

Chapter 3 focused on the dispersal of CNCs in a softer, more pliable polyethylene grade known as linear low-density polyethylene (LLDPE). LLDPE incorporates a small fraction of 1-hexene into polyethylene as a randomly inserted comonomer, giving rise to properties suitable for applications in plastic films and bags among other end uses. Catalyst **1** functionalized CNCs were added to a reaction vessel with both ethylene and 1-hexene to afford LLDPE CNC composites. Different loading of catalyst **1** on CNC aerogels afforded the same amount of catalyst in each reaction but allowed for different CNC loadings in

each reaction. The composite materials showed increasing Young's modulus with increasing cellulose nanocrystal content.

Chapter 4 describes how CNCs were functionalized with the intention of filling reverse osmosis membrane materials to have surface chemistry that could be impart antibacterial properties and increase flux. CNCs were functionalized with carboxylic acid by 2,2,6,6-tetramethylpiperidin-1-yl)oxyl (TEMPO)-mediated oxidation, then amine functionalization by carbodiimide coupling chemistry, and finally functionalized with a zwitterionic group by β-propiolactone ring opening. Amine coupling was confirmed with X-ray photoelectron spectroscopic analysis, and a second carboxylic acid peak was confirmed using infrared spectroscopy. These results were further verified with conductometric titration showing that after each respective reaction there were 1060 mmol kg^{-1} of carboxylic acid groups, 520 mmol kg^{-1} of amine groups, and 240 mmol kg^{-1} of zwitterionic groups. This CNC material was left to undergo future testing for desirable membrane properties.

Chapter 5 assesses the possible value in creating a new composite material using a functionalized polynorbornene, poly(5-triethoxysilyl-2-norbornene) (PTESN). The composites were fabricated by using the solvent casting method, dispersing the CNCs in a toluene solution of polymer and drying. The composite materials showed an increase in Young's modulus with increased loading. The 20 wt% CNC in PTESN had a Young's modulus of 970 MPa, a significant increase over the Young's modulus of the polymer lacking the filler (540 MPa).

In summary, this dissertation advances new techniques for the incorporation of CNCs as fillers in polymer-based nanocomposites. We are confident that further refinement and development of our results will find wide-ranging application. s

Nanocomposites: Incorporation of Cellulose Nanocrystals into Polymers and Addition of Zwitterionic Functionality

Keith Doubrava Hendren

GENERAL AUDIENCE ABSTRACT:

Cellulose nanocrystals (CNCs) are materials that can be added to polymers to form composite materials having increased stiffness. CNCs have the primary advantages over other filler materials of providing significant reinforcement without changing the color or increasing the density of the overall composite. CNCs are therefore good for designing polymer composites that need to be lightweight and aesthetically pleasing. Packaging materials (especially plastic bags and plastic films) are dominated by polyolefin materials such as polyethylene, which is already lightweight and colorless. The challenge of mixing polyethylene and CNCs is that their surface chemistry is incompatible, "like oil and water." To overcome the natural tendency for the CNC filler material to separate from the surrounding polyethylene matrix, a catalyst was attached to the surface of the CNCs and polymerization ensued from that catalyst leading to a composite material in which tiny CNC particles were trapped in the matrix Good dispersal of the component substances in the composite and of excellent overall reinforcement were proven by physical analysi

Acknowledgements:

In this endeavor, I had assistance from many people who gave me good advice, worked with me, or helped me with instrumentation. I would first acknowledge the efforts of my dissertation committee, as they have continually reviewed my work, served as resources of information and insight, and challenged me to grow as a scientist. With their help I now have developed a better sense of experimental design, project management, data analysis, critical reading of the literature, and communicating my work to peers and superiors alike. Of course, my committee also helped me tremendously in the preparation of this dissertation, which represents the culmination of several diverse, multidisciplinary efforts.

I would like to acknowledge the contributions of Ethan Smith, Morgan Higgins, Travis Baughman, Paul Deck, Kenneth Knott, Sarita Hough, Stephen Martin, Jacob Haag, and Johan Foster to the research presented herein. Their helped ranged from oversight of the research to substantive intellectual contributions to the many papers that will arise from this work, to key technical contributions such as help with catalyst synthesis, physical testing, etc. Their work in particular rises to the co-authorship level.

I am thankful for the time and expertise of the several individuals who either trained me on equipment or gave me necessary advice on how to proceed with various instruments. Thomas Staley and Carlos Suchicital maintained the material science and engineering laboratories. Priya Venkatramen, Dana Kazarooni, Adwoa Baah-Dwomoh, Raffaella De Vita, and Britannia Vondrasek helped me with tensile data. Charles Carfagna, Mark Cashman, and Cameron Crowell helped me acquire differential scanning calorimetry (DSC) data. I'm thankful for all of the help with advanced with XPS (Feng Xu), TEM

(Chris Winkler), microtome (Ya-Peng Yu), AFM and SEM (Steve McCartney), and Joel Serrano and Eric Gilmer (FTIR). I'm especially grateful to Wei Lu and Ilir Koliqi at TOSOH for their expertise and help with GPC.

This dissertation was completed with much needed support from my parents, siblings, and fiancé Caitlin. I would like to thank my friends at the Virginia Tech Bujinkan Budo Taijutsu club for making my stay at Virginia Tech enjoyable especially Joel Serrano and Brittany Bonnet.

Table of Contents

List of Figures:

List of Schemes:

List of Tables:

Abbreviations and acronyms:

ACNC	tertiary amine functionalized CNC
AFM	atomic force microscopy
catalyst **1**	1,1'-bis(bromodimethylsilyl)zirconocene
CNC	cellulose nanocrystals
CNF	cellulose nanofibril
CNT	carbon nanotube
DMA	dynamic mechanical analysis
DMAP	4-dimethyl amino pyridine
DMF	N,N-dimethylformamide
EDC	1-ethyl-3-(3-dimethylaminopropyl)carbodiimide
EtOAc	Ethyl acetate
FTIR	Fourier transform infrared spectroscopy
GHDPE	high-density polyethylene from Goodfellow
HCl	hydrochloric acid
HDPE	high density polyethylene
LDPE	low density polyethylene
LLDPE	linear low-density polyethylene
MAO	methylalumoxane
MMAO-12	modified methylalumoxane
M_n	number average molecular weight
M_w	weight average molecular weight
NMR	nuclear magnetic resonance spectroscopy
PDI	polydispersity index
PE	Polyethylene
PMC	polymer matrix composite
RO	reverse osmosis
ROMP	ring opening metathesis polymerization
SEM	scanning electron microscopy
TEM	transmission electron microscopy
TEMPO	2,2,6,6-tetramethylpiperidin-1-yl)oxyl
THF	tetrahydrofuran
UHMWPE	ultra-high molecular weight polyethylene
UPy	ureido-4[1H]pyrimidinone
vol%	volume percentage
wt%	weight percentage
XPS	X-ray photoelectron spectroscopy
ZCNC	zwitterion functionalized cellulose nanocrystal
ZCNT	zwitterion functionalized carbon nanotube

Chapter 1: Introduction

The introduction provides information in the form of short overviews about subjects that are covered later chapters of this thesis, to serve as a backdrop to understand the state of current technologies.

1.1 Polymer Nanocomposites and Mechanics:

Polymer nanocomposites are functional unions of polymers and nanoscale filler materials. Polymers are a material class with a very broad range of properties and are produced both in biological and synthetic processes. Nanomaterials are most broadly defined as materials that have at least one dimension less than 100 nm,[1] and they are commonly thought of as the bridge between molecular and macroscopic materials.

Nanofiller materials come in a wide variety of shapes: rods, sheets, plates, and spheres. Inorganic nanofillers include clay, exfoliated silica,[1] and the carbon-based nanoparticles graphene, carbon nanotubes (CNTs), and carbon black. Biologically-based filler particles include cellulose nanofibrils (CNFs), cellulose nanocrystals (CNCs), bacterial cellulose, and chitin nanocrystals.

Polymer nanocomposites comprise a continuous phase of matrix polymer and a nanoparticle filler. The filler material often enhances or adds a property to the continuous matrix polymer. The most common property targeted is reinforcement of the matrix material, which leads to an increase in the stiffness or modulus of the material. Other targeted properties are typically filler-specific. Some examples include silver nanoparticles which may add antibacterial properties, carbon-based filler which may add electrical conductivity, and silica-based clay nanomaterials may improve barrier properties.

The reinforcement of materials by nanofillers has been termed a “nano effect.” Some studies have stated that adding nanofiller materials reinforce beyond what composite theory for macroscopic particles would predict. These claims have been met with resistance, but nanofillers persist as they are able to reinforce in many planes and may

reinforce without having much of an aesthetic downside, such as a minimally affected surface finish.[1]

Examining nanoparticle reinforcement with traditional composite theory, for ideal situations the two components of the composite material act as continuous phases. When both continuous phases undergo the same strain, a larger amount of stress is placed on stiffer material, leading to an ideal reinforcement or the upper bounds of the rule of mixtures. In this case, the modulus of the composite material approaches the sum of the weighted volume fractions of the filler and polymer matrix (**Equation 1**); the Young's modulus is represented by E, volume fraction by φ, and the subscripts denote the composite (C), filler (F), and matrix polymer(M).[2] This is based on Hooke's law, and the situation of maximum reinforcement where the filler material and the matrix material undergo the same strain. This is illustrated in **Figure 1.1**.

$$E_C = \varphi_F E_F + \varphi_M E_M \qquad \text{Upper bounds of mixing rule} \qquad (1)$$

Traditional composite theory also accounts for non-ideal situations, using continuous phases. When each material in a composite instead undergoes the same stress, the softer portions of the material undergo the stress first. This is the lower bound rule of mixtures (**Equation 2**).[3]

$$E_C = \left(\frac{\varphi_F}{E_F} + \frac{\varphi_M}{E_M}\right)^{-1} \qquad \text{Lower bounds of mixing rule} \qquad (2)$$

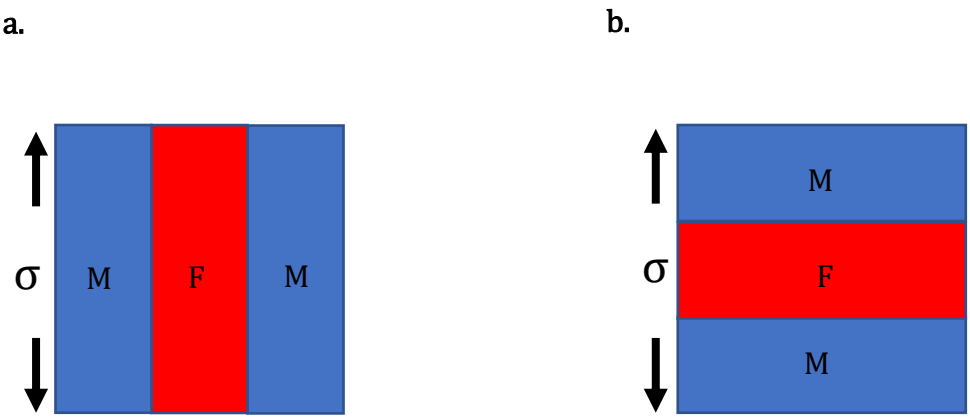

Figure 1.1: Composites above demonstrate upper and lower bounds of the mixing rule. **a:** Composite material components matrix (M) and filler (F) undergo the same strain demonstrating the upper rule of mixtures. **b:** Components (M) and (F) undergo the same stress demonstrating the lower bound rule of mixtures.

The traditional composite models are made for continuous phases of materials. To better predict the mechanical properties of composite systems with non-continuous filler materials, such as short fiber composites and particle composites other models have been created. For particle composites, shape is considered by Halpin-Tsai model, by the shape factor θ in **Equation 3**.[2]

$$E_C = E_M \frac{1+\theta\varphi_F\frac{(\frac{E_F}{E_M}-1)}{(\frac{E_F}{E_M}-\theta)}}{1-\varphi_F\frac{(\frac{E_F}{E_M}-1)}{(\frac{E_F}{E_M}-\theta)}} \qquad \text{Halpin Tsai model} \qquad (3)$$

The lower bound of the Halpin Tsai model where (θ=0) follows the inverse rule of mixtures **Equation 3**, which implies that the filler material undergoes the same stress throughout the composite material. As a consequence, the material follows the transverse loading shown in **Figure 1.1b.** In contrast, for θ=∞ the Halpin-Kardos model follows the upper

bound rule of mixtures, which implies that the filler material is acting as a continuous phase in the direction axial to the stress and undergoing the same strain as the composite.

The Halpin-Tsai model best describes short fiber composites, but other composite models further focus on other filler particle geometries such as disks.[2] However, these models do not exceed the upper bounds to the rule of mixtures. However, in practice the modulus of a composite material can fall below the lower bounds of the rule of mixtures if the materials do not interact well with one another.

Surface area and surface chemistry determine how well filler materials interact with matrix materials. Nanomaterials have a larger surface area per volume than their macroscopic counterparts. This feature allows for increased interaction between the polymer and the filler, and in some cases interaction among the filler particles through networking often referred to as percolation. Macroscopic discontinuous filler particles have low surface areas and are too large to reinforce a material. For the case of rubber, a well-studied material, it is generally accepted that particles larger than 1 μm do not reinforce rubbers well, while nanoscale particles of less than 100 nm in a dimension offer exceptional reinforcement.[4]

Interactions at the nanoscale have been shown to have effects on the composite crystallization and glass transition temperature deemed to be "nano-effects."[1] Interactions between the filler and the polymer are classified as interfacial interactions. Weak interactions of polymer-filler interfaces can result in void spaces within the material, while strong interfacial interactions of soft rubbers and carbon fillers has led to rubbers becoming glassy near nanoparticles.[5] In composite systems that do not allow covalent bonding to filler particles changes in the glass transition temperature (T_g) of typically ≤ 3 °C.[1] Increases

in T_g have been attributed to strong interfacial interactions, while decreases in the T_g have been attributed to weak interfacial interactions.[1] Nanofillers can also affect crystallite size by not affording crystallites the space to grow.[1]

Filler-filler interactions being continuous throughout a composite system are described as percolation effects. Key outcomes of percolation effects include electrical conductivity and reinforcement. For electrically conductive filler materials, such as CNTs, there is a critical volumetric concentration based on their aspect ratio that determines when there is a continuous network. When this threshold is met throughout the matrix, the resulting composite is electrically conductive.[6]

Mechanical percolation stems from the same concept, the observation that for some composites there is more substantial reinforcement above a critical volumetric concentration of filler. Polymers filled with some materials can show that there is little reinforcement with the addition of filler at low volume concentration, but with increased addition of filler particles there is substantial reinforcement. The increase in reinforcement is more substantial for particles that have strong interaction with one-anther such as pi-pi interactions[7] or hydrogen bonding.[8] A relationship used to predict the percolation threshold of thin rod-shaped particles such as CNCs and CNTs is 0.7/A, where (A) is the aspect ratio. This approximation is only technically valid for particles with A>50 and does not account for end-end interaction of rod-shaped particles.

A reinforcement model was created to account for mechanical percolation in composite materials with rod-shaped filler materials such as CNCs and CNTs.[8-9] The mechanical percolation model is represented as a piecewise equation, where below the percolation threshold the lower bound rule of mixing is used, while above the critical

volume concentration (φ_C) **Equation 4** is followed. The percolation threshold can be determined by fitting the data to the model, or it can be found as 0.7/A.

$$E_C = \frac{(1-2(\tau)+(\tau)\varphi_F)+(\varphi_M)\tau E_F^2}{(\varphi_M)E_F+(\varphi_F-\tau)E_F}$$ Young's modulus above percolation threshold (4)

$$\tau = \varphi_F \left(\frac{\varphi_F-\varphi_C}{1-\varphi_C}\right)^b$$ Percolating fraction (5)

The percolating fraction τ is involved in the transfer of the load going from one particle to another and can be calculated from **Equation 5**. The variable φ_C refers to the critical concentration required for percolation and b is the percolation exponent.[8]

The percolation model does not exceed the upper bounds of the rule of mixtures but come close to following it when filler exceeds the critical concentration. For filler materials that are not aligned to the applied stress, the percolation model typically adjusts the Young's modulus of the filler material (E_F) to fit the data set. The percolation model is based on infinite aggregates of filler materials forming, so changing this (E_F) to be closer to a value expected from a film composed only of aggregated filler material rather than a solid film of filler material is reasonable.[8-9] Similarly, the Halpin-Kardos model adjusts the shape parameter θ, which can be adjusted based on experimental observations such as aspect ratio, orientation, and reinforcement to fit the observed changes in stiffness.

1.2 Cellulose Nanocrystals

Cellulose is a major structural component of plants, and it consists of linked 1,4 β D-glucose or repeating "cellobiose" units **Figure 1.2**. Cellulose nanocrystals (CNCs) are natural materials that are isolated from cellulose by removing the non-crystalline regions of the cellulose leaving crystalline units of the cellulose material. After isolating cellulose from other materials, initial treatment with strong acids afforded fast decomposition followed by a second slower rate of decomposition.[10] Isolation of the resulting products

showed that the faster rate was the decomposition of low crystallinity material, and the slower decomposition rate was associated with highly crystalline material.[10]

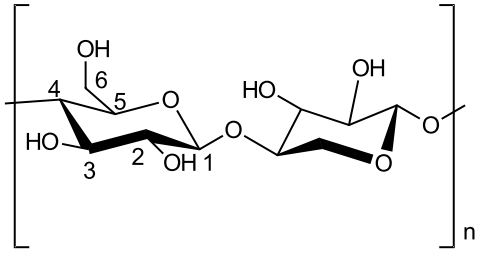

Figure 1.2: The chemical structure of cellulose is shown with the six labeled carbons.

Isolation of CNCs requires a source of cellulose and a technique to remove the amorphous regions of the cellulose. Many sources of cellulose have been used for the isolation of CNCs including ramie fibers,[11-13] kenaf fibers,[14-16] cotton, tunicin,[17] banana pseudostems,[18] pistachio shells,[19] hardwood,[20] softwood,[21] bacteria,[22] and bamboo pulp.[23] CNCs size and aspect ratio is dependent on source and isolation method.[24]

To fabricate CNCs, purified cellulose is often subjected to a strong acid at high concentration for a set time.[19, 21] An increased duration of exposure to strong acid will decrease the size of the resulting CNCs, and a study found that spherical CNCs could be obtained with increased hydrolysis time.[22] Broadly, two kinds of acid can be used to obtain CNCs from cellulose: acids that impart functional groups such as sulfuric acid[21] or phosphoric acid[25] and acids which do not such as hydrochloric acid[26] or hydrobromic acid.[27] Notably the charged groups from sulfuric acid or phosphoric acid help to stabilize the CNCs as they are dispersed in polar liquids. Additionally, researchers have found that the addition of citric acid or formic acid can impart functional groups to the CNCs as they are being hydrolyzed by hydrochloric acid.[28]

Other methods of converting cellulose to more crystalline nanomaterials utilize either a mechanical, biological, or oxidative means of removing the amorphous portion of the cellulose.[24] However, with these methods typically less of the amorphous portion is removed relative to acid hydrolysis leading to a lower crystalline content material such as those in cellulose nanofibrils (CNFs).[24] CNCs have been definitively obtained through a high pressure, high shear homogenization process.[29]

While CNCs are physically more crystalline than the parent cellulose and more crystalline than CNFs from the same source, CNCs are not entirely a crystalline material. For sulfuric acid isolated CNCs the crystalline fractions were found to be 0.72 from bacteria, 0.80 from tunicin, and 0.60 from wood.

CNCs are most often rod-shaped, and typically have diameters of 5-30 nm, well below the threshold of being less than 100 nm in any dimension to qualify as a nanomaterial. Examples sulfuric acid CNCs diameters are bacteria 14.0 ± 7.4 nm, tunicin 9.4 ± 5 nm, and wood 5.9 ± 1.8 nm.[24] The corresponding lengths of CNCs are bacteria 94 ± 79 nm, tunicin 148 ± 147 nm, and wood 23 ± 12 nm.[24] The aspect ratio of CNCs is often greater than 10, and high aspect ratios are advantageous as they allow more pronounced reinforcement at a lower loading for composite materials.

The most common crystalline morphology is cellulose I, commonly referred to as natural cellulose. Other types are cellulose II, III, and IV. Cellulose II can be formed through regenerating cellulose from a soluble cellulose derivative of cellulose (such as cellulose nitrate), or treatment with aqueous sodium hydroxide. Cellulose III can be formed by treating cellulose I or cellulose II with liquid ammonia; subsequent heat treatment of cellulose III can yield cellulose IV. While cellulose II has applications as transparent films

and Rayon, cellulose I has the highest elastic modulus in the axial direction and occurs naturally.[30]

Cellulose I has two polymorphs, Iα and Iβ. They are in naturally occurring cellulose sources and their relative ratio depends on the natural source of cellulose. Cellulose Iα is the major component of algae and bacteria, while cellulose Iβ is more common in tunicin and multicellular plants. These two polymorphs have different crystalline arrangements; Iα is triclinic and Iβ is monoclinic. A notable difference between the polymorphs is the monoclinic crystalline arrangement of cellulose Iβ polymorph, which has stronger hydrogen bonding leading to a higher thermal degradation temperature.[30]

As cellulose is sourced from biological media, the formation of the elementary cellulose crystals varies in terms of chain arrangements for different biological organisms. For wood, the crystalline regions are formed as 36 chains forming a cellulose Iβ elementary crystal structure with a rectangular cross section. Other sources can have different cross sections such as maize cellulose for which a hexagonal cross section has been proposed.[30]

Hydroxyl groups on CNCs are subject to modification through many chemical reactions resulting in robust covalent bonds. CNCs have been successful modified by polymer grafting, click chemistry, esterification, adsorption of surfactants, acetylation, silylation, and acylation.[30] Efforts to functionalize CNCs have been driven by applications including dispersing CNCs in a polymer matrix, making CNCs electrically conductive,[31] increasing the thermal stability of the CNCs,[32] and other functions.

Thermal properties of CNCs are of great concern. The surface chemistry of the CNCs predict how the CNCs will respond to increased temperature. Sulfuric acid CNCs tend to degrade at lower temperatures than neutral CNCs (without acidic groups), which is

attributed to the sulfate ions on the surface of the CNCs. Additionally, any residual acid from the hydrolysis of cellulose will cause early degradation of the CNCs.[10]

CNCs are primarily used as fillers in composites, but CNCs have also been used to alter the rheological properties of some fluids. As filler materials, the effect of CNCs have been investigated on barrier, optical, thermal, and mechanical properties.[10, 30] The barrier property unfunctionalized CNCs contribute to polymer composites is an increase in water permeability. Adding CNCs to a polymer may increase or decrease oxygen permeability, and the result is dependent on the polymer and surface chemistry of the CNCs. CNCs can be incorporated to form translucent films but will scatter some light.[30] Light scattering occurs as nanomaterials that are larger than ten times the wavelength of interest scatter light and this includes CNCs. However, CNCs with a typical 10-nm diameter would not appear as macroscopic particles when well dispersed in a matrix.

CNC composites have been used for the reinforcement of materials due to their high tensile modulus (axial 110-220 GPa, transverse 10-50 GPa), typically high aspect ratio(>10), and low density (1.6 $g \cdot cm^{-3}$).[30] The literature describes CNCs as filler in rubber, poly(vinyl alcohol), epoxies, linear low-density polyethylene, polypropylene, polystyrene, poly(lactic acid), polycarbonate, polyurethanes, and a variety of other polymers.

Appendix A features a list of polymers reinforced by CNCs. This list includes CNC source, refinement method, surface modification, and mechanical data from tensile tests. Tensile tests in Appendix A show a general increase in Young's modulus with increasing volume fraction of CNCs. This Appendix shows processing methodologies and by extension which processing methodologies are most common with a polymer type. For example, polyurethanes are frequently grafted onto functional CNCs, and poly(lactic acids)

are most often mechanically mixed with CNCs in roller blade mixers and twin-screw extruders.

Appendix A is in part meant to be a useful tool in conjunction with other useful reviews by providing relevant results that have previously been published. This database can be used to design materials based on known properties or to extrapolate based on trends to design a material with the needed properties. An example would be the need to have a higher modulus linear low-density polyethylene material (LLDPE) material without decreasing elongation at break. Appendix A presents two processes for creating CNC LLDPE composite materials from Borjesson et al.[32] and from Natterodt et al.[33] In these composites, Borjesson had greater Young's modulus but the elongation at break decreased. The example from Natterodt did not decrease the elongation at break, so that is the better starting point for a material that doesn't decrease elongation at break.

A feature of Appendix A is translating the data from many studies from weight percentage (wt%) to volume percentage (vol%). This allows for the concentration of CNCs to be used directly in models such as the Halpin-Kardos and the percolation model. With this data, future studies can generate materials of the desired modulus by predicting the modulus of a composite material based on the corresponding model chosen.

Appendix A can be used in conjunction with a variety of review papers such as a review of surface chemistry.[34] In this work, many of the possible interactions of CNCs with matrix polymers are detailed, including silane coupling, peptide coupling, silanizing, urethanization, click chemistry, peptide coupling, and surface initiated radical polymerization.[34] Studies can be easily found that had such reactions occurring[35-39] in

Appendix A. From Appendix A, the potential mechanical benefit of performing a reaction can be predicted.

1.3 Polyethylene

Polyethylene was first developed as a material in 1930, by Carl Shipp Marvel at du Pont de Nemours and Company. However, the first commercial production and patent began with low-density polyethylene (LDPE) at Imperial Chemical Industries. Later high-density polyethylene (HDPE) was discovered by Karl Ziegler of the Max Planck Institute for Coal Research. Ziegler and his colleague Erhard Holzkamp used an organometallic catalyst. Later, Giulio Natta improved the process and applied it to the polymerization of propylene, leading to the name Ziegler-Natta catalyst[40] and their joint receipt of the Nobel Prize in Chemistry in 1963. The use of metallocene catalysts was reported soon thereafter by Breslow & Newburg[41] but their work gained little traction until Kaminsky showed that a combination of trimethylaluminum and water (essentially, methylalumoxane) as an activator demonstrated appreciable catalytic activity and novel, desirable product properties.[42]

Variations in polyethylene structure are obtained by changing the concentration of alkene comonomer(if any), the structure of the catalyst, and reaction conditions such as pressure and temperature. Higher pressures usually result in higher molecular weight, while higher temperatures have the opposite effect.[43]

Initiating ethylene polymerization with free radicals leads to the randomly branched polyethylene structures characteristic of LDPE. As free-radicals are not well-behaved chemical species there is backbiting and branching as the polymerization ensues.[44] High-density polyethylene (HDPE) in contrast is formed by coordination polymerization using

a transition metal catalyst. (**Figure 1.3**). Because the reaction is controlled at the catalyst site, there is not a population of unstable intermediates.[45] Differences in molecular weight separate HDPE and ultra-high molecular weight polyethylene (UHMWPE) where the higher molecular weight product UHMWPE begins at molecular weights of three million daltons.[46]

Linear low-density polyethylene (LLDPE) is similar to HDPE in that an addition catalyst is used. However, the addition of a co-monomer introduces short branches from the main backbone. The amount of monomer incorporation depends on the amount of monomer in the feed and the selectivity of the catalyst to incorporate the monomer.

For the polymerizations of HDPE and UHMWPE the Cossee-Arlman mechanism adequately describes the use of a Ziegler-Natta or metallocene catalyst system, as illustrated in **Figure 1.3.** For LLDPE, the mechanism would be the same, except for the addition of linear α-olefins like propene, butene, hexene or octene.

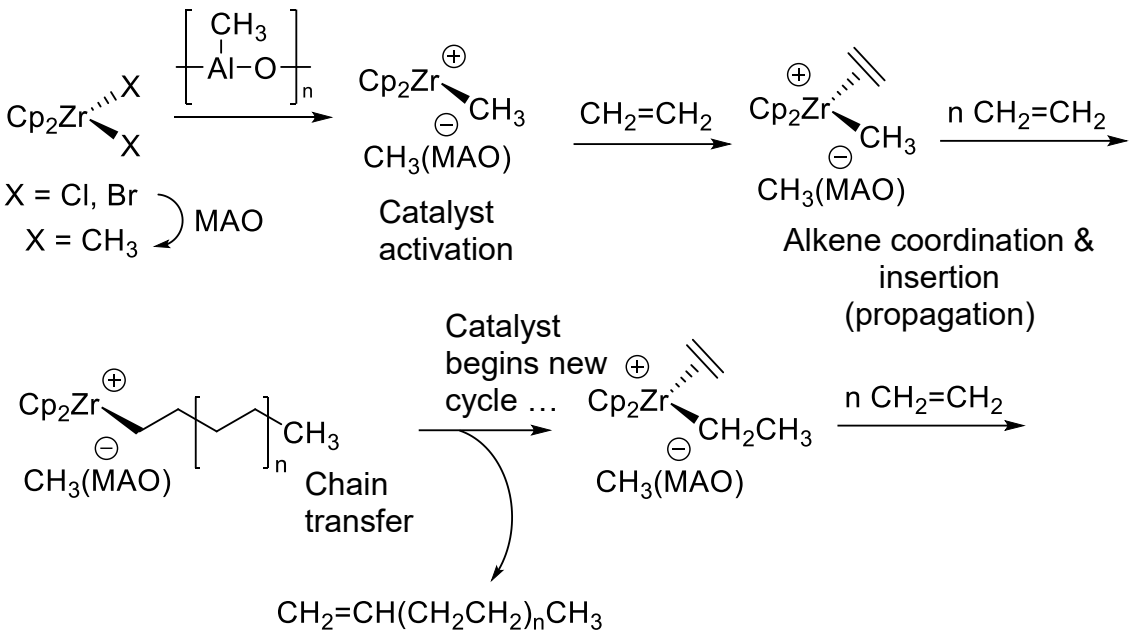

Figure 1.3: The Cossee-Arlman mechanism for ethylene polymerization catalysts such as zirconocene dichloride shows the crucial steps of activation and coordination with a co-catalyst, absorption of an alkene (propagation), followed by the eventual chain termination in which the catalyst can being a new alkyl chain.

The Ziegler-Natta catalyst systems are those that are transition-metal based and activated by an organic aluminum compound. The classic Ziegler-Natta catalyst $TiCl_4$ is activated with triethylaluminum. Most Ziegler-Natta catalysts take the form of tiny solid particles that have active catalytic sites on their surfaces. Polymerization ensues when these particles combine with monomer in the gas phase. A more efficient "second generation" of Ziegler-Natta catalysts followed, in which the more expensive transition metal component was coated onto the surface of an inorganic support such as magnesium chloride, which also contributed better control over the catalyst particle size distribution.

Another type of ethylene polymerization catalyst is the Phillips catalyst, which is a chromium oxide species immobilized on silica gel, generated by infusing silica gel with chromium(III) acetate and subsequent calcination. The Phillips catalyst differs in that no

alkylaluminum activator is required; instead the catalyst activates during an induction period in which the surface oxide species is reduced to a chromium alkyl by the monomer itself. The mechanism of this critical process remains one of the great unsolved mysteries of modern chemistry. This catalyst accounts for a substantial portion of the world's production of HDPE but is not especially versatile and cannot yet be adapted to the formation of either LLDPE or polypropylene.[47]

The Kaminsky Catalyst, as the combination of MAO (formed by partial hydrolysis of trimethylaluminum) and Cp_2ZrCl_2 is now known, showed extremely high activity for ethylene and gave much narrower molecular weight distributions, at or near the ideal value for single-site coordination polymerization (PDI = 2.0).[42] These however, did not have the same ability to anchor as the classic Ziegler Natta catalyst or the Phillips catalyst, so the Kaminsky catalyst and its congeners were confined to polymerizations in solution, so their value was limited to niche markets where special properties of the resin such as precise control of branching and other microstructural features would compensate for the high cost of solvent volatilization and recycling.[48]

In response, efforts were made to find anchoring chemistry, through synthetic elaboration of the metallocene ligand structure. 'Hybrid' catalysts featuring the single-site characteristics of metallocenes and the particle-size control of an inorganic support promised to extend metallocene technology into the gas phase. Complementary approaches, in which the cocatalyst (organoaluminum or organoboron compound) is anchored first to the inorganic support, have been developed more recently and have the advantage that any soluble polymerization catalyst can, in theory, be used, obviating a lot of complex ligand synthesis.[49]

Bulk material properties of polyethylene are dependent on synthesis method and processing method. Microscale structures of polyethylenes such as their crystal morphologies have been extensively studied. Single crystals of polyethylene form as 10-nm thick ribbons and can be pulled from dilute solutions. Other polyethylene crystal structures known as spherulites exist as stacks of crystalline regions with amorphous regions between the stacks.[50] Polyethylene single crystals have high strengths and have moduli from 240-360 GPa in the axial direction.[50] This property explains the high stiffness of >90% crystalline UHMWPE used in high performance applications.

The crystalline content in polyethylene varies, and the addition of branch points to polyethylenes decreases the crystalline content.[51] For LLDPE, addition of α-olefin comonomers decreases the crystallinity of the polyethylene. Except for ethylene propylene copolymers which have only single-carbon branches, crystalline regions are not formed at all when sufficient branch point populations are present, there are decreases in the melting point and crystallinity of polyethylene with the addition of 1-butene, 1-hexene, or 1-octene. The current understanding is that for random distributions of comonomer in polyethylene (excluding propene), the melting point is decreased in proportion to the number of branch points and weakly dependent the specific comonomer. Chain lengths can also have an effect on the physical properties of LLDPE. High molecular weights of LLDPE copolymers with the same comonomer content have lower melting temperatures for the range (3-3,000 kDa).[51] Melting points are reduced as consequence of a reduction in crystallite thickness, due to an increase in entanglements.[51]

HDPE has inherent chemical resistance, as the rare methyl ($-CH_3$) and common methylene ($-CH_2-$) units are very stable. Both HDPE and LLDPE can have terminal alkene

groups that while very uncommon are subject to the effects of aging. . High energy radiation can affect polyethylene species by causing it to crosslink, but stabilizers can mitigate this effect.[46] LLDPE has branch points, tertiary carbons (>CH-), and these carbons are able to form more stable radicals and carbocations, making LLDPE less chemically inert. Notably, sufficient branching enables most LLDPE and LDPE to be solubilized in common solvents such as toluene and xylene. HDPE may be solubilized in xylene or chlorinated benzene derivatives, while UHMWPE is almost exclusively solubilized in 1,2,4-trichlorobenzene.

One of the more notable attributes of polyethylene its low cost of starting material, as ethylene is an inexpensive monomer.[52] Alpha olefins likely add to the cost of LLDPE materials but little comonomer is typically needed.

LDPE can be processed in a variety of ways; some of the most common are extrusion and injection molding. Additionally, there are exotic methods often used to process UHMWPE such as ram extrusion[53] and fiber spinning and drawing.[54] Ram extrusion can lead to increased crystallinity from annealing in UHMWPE and ram extrusion allows for high melt viscosity materials unlike twin screw extrusion.[53] Tape or fiber drawing allows for chain alignment and the development of high crystallinity UHMWPE products.[54] Polyethylene species exhibit strength properties that vary strongly with polyethylene type and crystalline morphology.

Polyethylene composites come in a variety of forms as there are various polyethylene types. The goals for most polyethylene composites include reinforcement, electrical conductivity, and flame retardation. Current technologies focus on the use of

natural fibers, nanocarbon materials, and layered clay-based materials such as montmorillonite.[55]

The carbon-based materials are intrinsically some of the best materials for reinforcement of polyethylene as they are often better distributed throughout the polymer matrix than raw natural fibers or exfoliating clays. Carbon nanotubes have been shown to be an excellent filler material and able to reinforce at low loading but are also among the costliest filler materials.

Clays such as montmorillonite have been shown reinforce polyethylene at low loadings and impart flame retardant properties. However, they afford a rather poor interface with the polyethylene and have trouble dispersing in the polymer matrix. There have been notable efforts with clay materials to add organic functional groups such as fatty acids to the surface or add quaternary ammonium salts to facilitate dispersion.[56]

Natural fibers have a distinct advantage over the clay and carbon-based materials in that they are renewable materials that can be easily acquired. For natural fibers, the source materials with the highest cellulose content as opposed to hemicellulose or lignin tend to be better at providing stiffness to the polyethylene materials.[57] There is however, the limitation that the natural fiber materials to be blended with the polyethylene have hydrophilic characteristics that can lead to poor mixing within the system. To overcome this problem, polyethylene has been grafted with maleic anhydride to improve hydrophilicity. A similar approach can be taken with natural fibers, instead silanizing the hydroxyl groups on the natural fibers which has shown mechanical reinforcements at high filler loadings.[58]

1.4 Desalination Membranes:

Clean fresh water is a critical need for societies to live in healthy conditions as it is used for drinking, hygiene, and agriculture. It is estimated that each person uses 1000 m^3 of freshwater per year.[59] Fresh water demand can exceed availability, and it is estimated that 35% of the world's population suffers from water stress.[60] Instead, some sources of water such as seawater and brackish water are purified to meet the demands of the people.[59] Membranes are materials that allow for selective permeability and are materials that can be possibly improved.

Important membrane separation methods include electrodialysis, membrane distillation,[61] and reverse osmosis. These processes use different driving forces to generate water with reduced concentrations of cations and anions. Electrodialysis uses a potential difference to force salt anions across a membrane, membrane distillation uses thermal energy on one side of the membrane to force vapor across the membrane, and reverse osmosis uses a pressure difference to force salt free water across the membrane. While all these technologies are important, reverse osmosis (RO) is the most widely used. Additionally, RO membranes that have been generated with nanoparticles have had success improving key properties.[62]

The current discussion of RO membranes dates back Gerald Hassler in the 1940s, but earlier records can be found discussing osmosis in the forward direction. His early account hypothesized that evaporation was a necessary step to move water through the membrane. Later, in 1959, C.E. Reid and E.J. Brenton were able to show that cellulose acetate membranes were able to reject 96% of chlorides while allowing for 14 gallons per day with a 3.7 μm thick membrane.[63]

Importantly after this, the first asymmetric membranes for reverse osmosis membranes were developed allowing for much thinner membranes. Cellulose acetate membranes were developed that were able to have a ten-fold increase in flux due to having a thin coherent portion of cellulose acetate of 0.2 μm with a backing of cellulose acetate that allowed the membrane to remain a sturdy material.[63]

Reverse osmosis is used either for the recovery of pure water from a water source with dissolved or suspended solids or the recovery of dissolved or suspended solids by removing water. Applications in which reverse osmosis is used are removal of sodium ions for boilers, ultrapure water for microelectronics, concentrating corn-based sweeteners, concentrating dairy products,[64] purification of waste water, and purification of sea and brackish waters.[63]

Osmosis in the forward direction allows the flow of a liquid through a membrane without allowing the flow of dissolved solids suspended solids. The flow of osmosis in this direction is driven by a difference in solute concentration. The solution with the higher concentration of solutes will incur the flow of water across the membrane until both sides have reached equilibrium.[65]

Reverse osmosis uses an applied pressure on the surface of the membrane forcing pure water through, while the membrane rejects the dissolved solids. The efficiency of the membrane is reflected in terms of both salt rejection and flux or flow through the membrane. It can be understood that from a non-equilibrium state the flux N_m is the difference between the osmotic pressures π and applied pressures P, these pressures are illustrated in **Figure 1.4**. However, as it is membrane dependent the permeability of the membrane P_M and the thickness L_M influence how the amount of water that is passed

through the membrane. Therefore, efforts to make the membranes more efficient would have greater permeability, or mechanically robust membranes to allow for thinner or higher applied pressures.[65] The relationship between flux (N_m), permeability (P_m), osmotic pressure (π), and applied pressure (P) is shown in **Equation 6**.

$$N_m = \frac{P_m}{L_m}(\Delta P - \Delta\pi) \qquad \text{Transport across reverse osmosis membrane} \qquad (6)$$

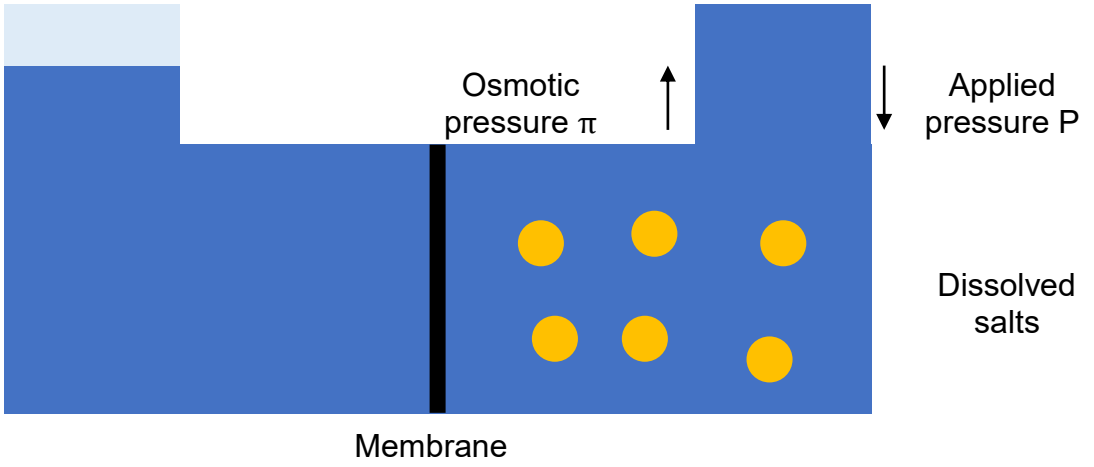

Figure 1.4: For a system separated by a membrane, the region with more dissolved salts will attract more water (osmotic pressure), and to overcome the osmotic pressure an applied pressure is placed on this water to force water through the membrane.

More recent developments in membrane technologies have focused on the addition of nanomaterials to the membranes. Additions to modern aromatic crosslinked polyamide membranes have included carbon nanotubes,[66] silver nanoparticles,[67] metal organic frameworks,[68] and zeolites.[69] The functional portion or "skin" layer of a polyamide membrane is about 200 nm in thickness. Studies have used porous nanoparticles to serve as physical channels for the water to pass through; this effectively provides a shortcut to increase flux by reducing the amount of polyimide that needs to be penetrated by water.

As more nanoparticles are examined, relationships regarding what allows for high flux and good salt rejection though a membrane may become more clear.[62]

1.5 Polynorbornenes:

Norbornenes are bicyclic rings with a π bond and are created by the Diels-Alder reaction of ethylene and cyclopentadiene (**Figure 1.5**). They are produced to the extent that patents for different industrial synthetic processes have been previously filed in 1986[70] and in 2000.[71] Interestingly norbornenes derivatives with side chains and functional groups can be made by starting with a substituted ethylene as shown in **Figure 1.5**.[72] Derivatives are not limited to aliphatic substitutions but can be trimethylsilyl groups and halogens among countless others. The stereochemistry of substitution (exo vs. endo) influences the subsequent reactivity of the double bond in ring-opening metathesis polymerization (ROMP), so chemists have devised ways to control this stereochemistry during the cycloaddition reaction and to separate the isomers when the selectivity problem cannot be entirely overcome. Generally, the *exo* substituted isomer is more reactive than the *endo* isomer towards ROMP.[72]

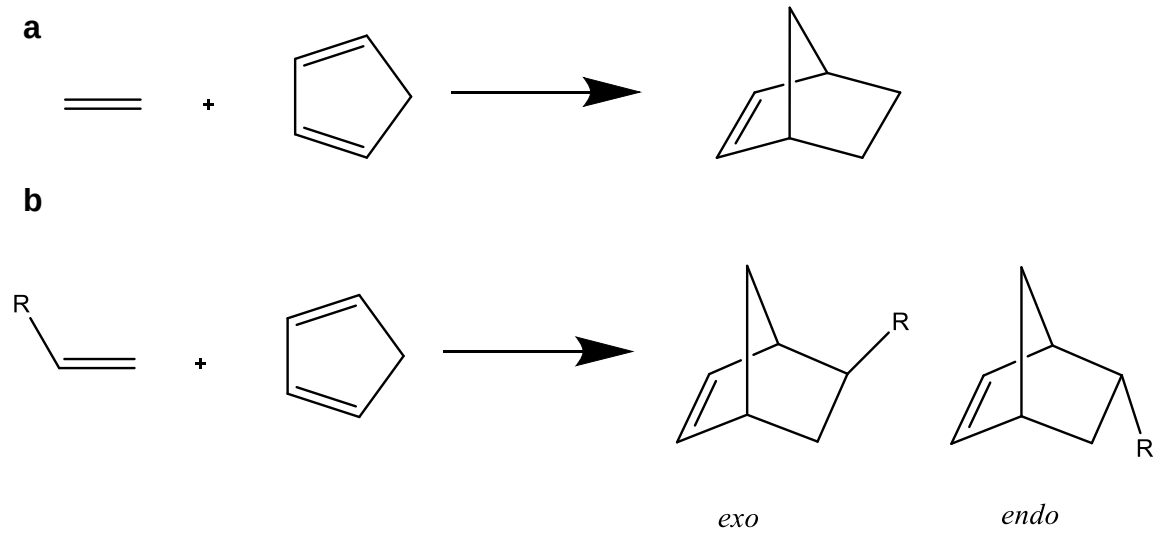

Figure 1.5: Formation of norbornene derivatives is shown **a:** Reaction scheme of cyclopentadiene and ethylene to give norbornene. **b:** Reaction of a substituted ethylene with cyclopentadiene to give a substituted norbornene.

Norbornenes are especially useful unsaturated monomers because the pi-bond is located within a strained ring system. There are two methods for making polynorbornenes, the ring opening metathesis polymerization (ROMP) and addition polymerization. The reaction scheme below shows the reactions of each scheme, **Figures 1.6a** (ring opening) and **1.6b (**addition reaction). The reactions can result in stereospecific products but the most basic reaction scheme is shown.[72]

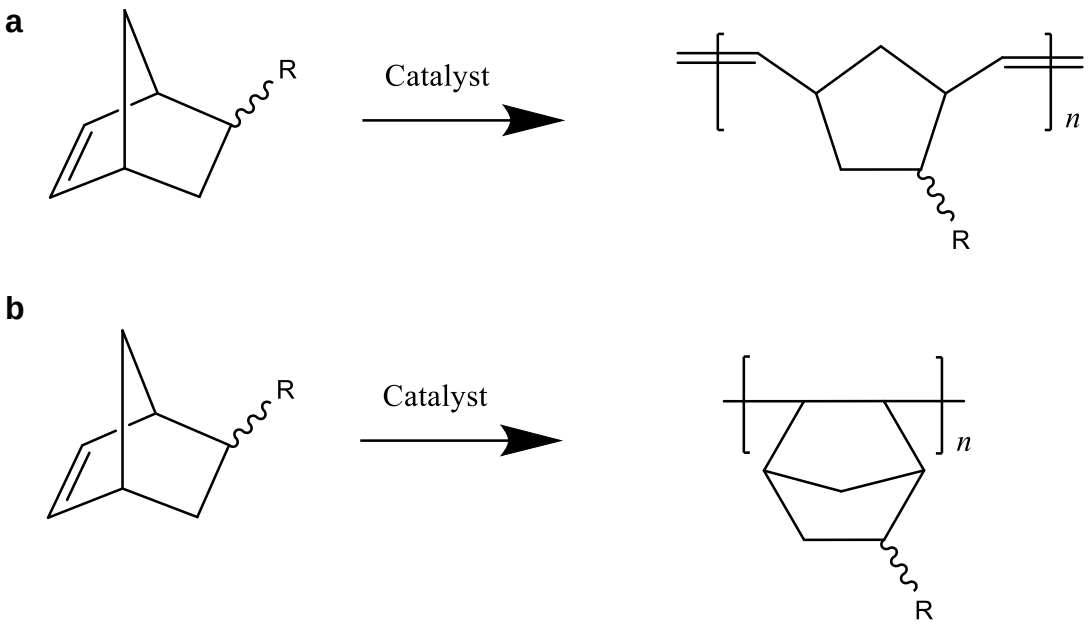

Figure 1.6: Above is **a:** polymerization of norbornene in the presence of a ring opening metathesis catalyst and **b:** polymerization of norbornene in the presence of an addition catalyst.

ROMP of norbornenes has been more successful than addition polymerization and can produce high molecular weight polymers. ROMP is mediated by a metal catalyst containing titanium, ruthenium, molybdenum, or tungsten. ROMP allows for a great degree of control and small polydispersity indexes. These polymerizations can be both continuous (living) and discontinuous (non-living) depending on the catalyst used.[73] Higher molecular weight ROMP products have use in industry as a soft but strong rubber, and these can be used as a low hardness damping compound. Blending ROMP polynorbornenes with polyisoprene leads to materials that can be used to make bellows, roller coverings, and seals.[74] Pure ROMP polynorbornenes are also used for gas separation technologies for selective separation of hydrocarbons.[72]

Products from **Figure 1.5.1b** involve the polymerization of bicyclic rings. At high molecular weights these polymers are glassy materials have been used for gas separation

technologies for gasses such as hydrocarbons, nitrogen, and carbon dioxide.[75] Applications in making the polynorbornene have focused on the change of side groups of the rings with Si-O-Si side groups being especially selective for hydrocarbons.[76]

1.6 Scope and Objectives

It is difficult to disperse cellulose nanocrystals (CNCs) in hydrophobic polymers because CNC particles are hydrophilic and tend to interact strongly with one another. To overcome the different surface chemistries and combine CNCs into a polymer material mixing strategies are employed. The hydroxyl groups on CNCs are responsible for strong interaction with other CNCs through hydrogen bonding, so it is important that the CNCs interact strongly with one another and that is most likely when there is minimal surface functionalization of CNCs.

These studies focus on key points of CNC composite materials introducing new surface functionalities and using CNCs for reinforcing polymers. Chapters 2, 3, and 5 are concerned with the application of incorporating CNCs into polymer systems. Chapter 4 is focused on functionalizing CNCs for an industrial application. The following research objectives are hypothesis and the following chapters are steps towards answering them.

1. The hydrophobic and hydrophilic interactions of polyolefins and CNCs can be overcome by using the growth of polyolefin chains from the surface of the filler material leading to a composite material with well dispersed CNCs.
2. Functionalized CNCs with charged surface groups are capable of strong interactions with the current state of the art polyamide reverse osmosis membranes, allowing for increased flux of water through the membrane material while maintaining high salt rejection.

3. Incorporating CNCs into functionalized vinyl addition polynorbornene materials such as poly(5-triethoxysilyl-2-norbornene) will have improved mechanical properties common of CNC polymer composites and can serve as a platform for creating specialty materials.

References:

1. Paul, D. R.; Robeson, L. M., Polymer nanotechnology: Nanocomposites. *Polymer* **2008,** *49* (15), 3187-3204.
2. Fornes, T. D.; Paul, D. R., Modeling properties of nylon 6/clay nanocomposites using composite theories. *Polymer* **2003,** *44* (17), 4993-5013.
3. Kim, H. S.; Hong, S. I.; Kim, S. J., On the rule of mixtures for predicting the mechanical properties of composites with homogeneously distributed soft and hard particles. *Journal of Materials Processing Technology* **2001,** *112* (1), 109-113.
4. Ma, J.; Zhang, L. Q.; Dai, J., Interface Modification and Characterization. In *Rubber Nanocomposites*, Thomas, S.; Stephen, R., Eds. 2010; pp 87-112.
5. Berriot, J.; Montes, H.; Lequeux, F.; Long, D.; Sotta, P., Evidence for the Shift of the Glass Transition near the Particles in Silica-Filled Elastomers. *Macromolecules* **2002,** *35* (26), 9756-9762.
6. Bauhofer, W.; Kovacs, J. Z., A review and analysis of electrical percolation in carbon nanotube polymer composites. *Composites Science and Technology* **2009,** *69* (10), 1486-1498.
7. Pérez, E. M.; Martín, N., π–π interactions in carbon nanostructures. *Chemical Society Reviews* **2015,** *44* (18), 6425-6433.
8. Favier, V.; Cavaille, J. Y.; Canova, G. R.; Shrivastava, S. C., Mechanical percolation in cellulose whisker nanocomposites. *Polymer Engineering & Science* **1997,** *37* (10), 1732-1739.
9. Sapkota, J.; Shirole, A.; Foster, E. J.; Martinez Garcia, J. C.; Lattuada, M.; Weder, C., Polymer nanocomposites with nanorods having different length distributions. *Polymer* **2017,** *110*, 284-291.
10. Dufresne, A., *Nanocellulose: from nature to high performance tailored materials*. Walter de Gruyter GmbH & Co KG: 2017.
11. Junior de Menezes, A.; Siqueira, G.; Curvelo, A. A. S.; Dufresne, A., Extrusion and characterization of functionalized cellulose whiskers reinforced polyethylene nanocomposites. *Polymer* **2009,** *50* (19), 4552-4563.
12. Furtak-Wrona, K.; Kozik-Ostrowka, P.; Jadwiszczak, K.; Maigret, J. E.; Aguie-Beghin, V.; Coqueret, X., Polyurethane acrylate networks including cellulose nanocrystals: a comparison between UV and EB- curing. *Radiation Physics and Chemistry* **2018,** *142*, 94-99.
13. Yue, L.; Maiorana, A.; Khelifa, F.; Patel, A.; Raquez, J. M.; Bonnaud, L.; Gross, R.; Dubois, P.; Manas-Zloczower, I., Surface-modified cellulose nanocrystals for biobased epoxy nanocomposites. *Polymer* **2018,** *134*, 155-162.
14. Zakuwan, S. Z.; Ahmad, I.; Ramli, N., Preparation of Hybrid Nano Biocomposite kappa-Carrageenan/Cellulose Nanocrystal/Nanoclay. In *2013 Ukm Fst Postgraduate*

Colloquium, Murad, A.; Yen, C. C.; Ismail, E. S.; Maskat, M. Y.; Noorani, M. S. M.; Ibrahim, N.; Karim, N.; Yahya, R.; Khalid, R. M.; Ismail, W. R.; Ling, W. S.; Ibrahim, Z., Eds. Amer Inst Physics: Melville, 2013; Vol. 1571, pp 738-743.
15. Kargarzadeh, H.; Sheltami, R. M.; Ahmad, I.; Abdullah, I.; Dufresne, A., Cellulose nanocrystal reinforced liquid natural rubber toughened unsaturated polyester: Effects of filler content and surface treatment on its morphological, thermal, mechanical, and viscoelastic properties. *Polymer* **2015,** *71*, 51-59.
16. Zarina, S.; Ahmad, I., Biodegradable Composite Films based on kappa-carrageenan Reinforced by Cellulose Nanocrystal from Kenaf Fibers. *Bioresources* **2015,** *10* (1), 256-271.
17. Cao, L. M.; Huang, J. R.; Chen, Y. K., Dual Cross-linked Epoxidized Natural Rubber Reinforced by Tunicate Cellulose Nanocrystals with Improved Strength and Extensibility. *Acs Sustainable Chemistry & Engineering* **2018,** *6* (11), 14802-14811.
18. Pereira, A. L. S.; do Nascimento, D. M.; Souza Filho, M. M.; Morais, J. P. S.; Vasconcelos, N. F.; Feitosa, J. P. A.; Brigida, A. I. S.; Rosa, M. F., Improvement of polyvinyl alcohol properties by adding nanocrystalline cellulose isolated from banana pseudostems. *Carbohydr Polym* **2014,** *112*.
19. Marett, J.; Aning, A.; Foster, E. J., The isolation of cellulose nanocrystals from pistachio shells via acid hydrolysis. *Industrial Crops and Products* **2017,** *109*, 869-874.
20. Long, K. Y.; Cha, R. T.; Zhang, Y. P.; Li, J. J.; Ren, F. P.; Jiang, X. Y., Cellulose nanocrystals as reinforcements for collagen-based casings with low gas transmission. *Cellulose* **2018,** *25* (1), 463-471.
21. Bondeson, D.; Mathew, A.; Oksman, K., Optimization of the isolation of nanocrystals from microcrystalline celluloseby acid hydrolysis. *Cellulose* **2006,** *13* (2), 171.
22. Lam, N. T.; Saewong, W.; Sukyai, P., Effect of varying hydrolysis time on extraction of spherical bacterial cellulose nanocrystals as a reinforcing agent for poly(vinyl alcohol) composites. *Journal of Polymer Research* **2017,** *24* (5).
23. Dhar, P.; Kumar, A.; Katiyar, V., Magnetic Cellulose Nanocrystal Based Anisotropic Polylactic Acid Nanocomposite Films: Influence on Electrical, Magnetic, Thermal, and Mechanical Properties. *Acs Applied Materials & Interfaces* **2016,** *8* (28), 18393-18409.
24. Sacui, I. A.; Nieuwendaal, R. C.; Burnett, D. J.; Stranick, S. J.; Jorfi, M.; Weder, C.; Foster, E. J.; Olsson, R. T.; Gilman, J. W., Comparison of the properties of cellulose nanocrystals and cellulose nanofibrils isolated from bacteria, tunicate, and wood processed using acid, enzymatic, mechanical, and oxidative methods. *ACS Appl Mater Interfaces* **2014,** *6* (9), 6127-38.
25. Nicharat, A.; Shirole, A.; Foster, E. J.; Weder, C., Thermally activated shape memory behavior of melt-mixed polyurethane/cellulose nanocrystal composites. *Journal of Applied Polymer Science* **2017,** *134* (27), 45033.
26. Xie, D. Y.; Qian, D.; Song, F.; Wang, X. L.; Wang, Y. Z., A Fully Biobased Encapsulant Constructed of Soy Protein and Cellulose Nanocrystals for Flexible Electromechanical Sensing. *Acs Sustainable Chemistry & Engineering* **2017,** *5* (8), 7063-7070.

27. Sucaldito, M. R.; Camacho, D. H., Characteristics of unique HBr-hydrolyzed cellulose nanocrystals from freshwater green algae (Cladophora rupestris) and its reinforcement in starch -based film. *Carbohydrate Polymers* **2017,** *169*, 315-323.
28. Yu, H. Y.; Yao, J. M., Reinforcing properties of bacterial polyester with different cellulose nanocrystals via modulating hydrogen bonds. *Composites Science and Technology* **2016,** *136*, 53-60.
29. Jalvo, B.; Mathew, A. P.; Rosal, R., Coaxial poly(lactic acid) electrospun composite membranes incorporating cellulose and chitin nanocrystals. *Journal of Membrane Science* **2017,** *544*, 261-271.
30. Moon, R. J.; Martini, A.; Nairn, J.; Simonsen, J.; Youngblood, J., Cellulose nanomaterials review: structure, properties and nanocomposites. *Chemical Society Reviews* **2011,** *40* (7), 3941-3994.
31. Meulendijks, N.; Burghoorn, M.; van Ee, R.; Mourad, M.; Mann, D.; Keul, H.; Bex, G.; van Veldhoven, E.; Verheijen, M.; Buskens, P., Electrically conductive coatings consisting of Ag-decorated cellulose nanocrystals. *Cellulose* **2017,** *24* (5), 2191-2204.
32. Borjesson, M.; Sahlin, K.; Bernin, D.; Westman, G., Increased thermal stability of nanocellulose composites by functionalization of the sulfate groups on cellulose nanocrystals with azetidinium ions. *Journal of Applied Polymer Science* **2018,** *135* (10), 10.
33. Natterodt, J. C.; Sapkota, J.; Foster, E. J.; Weder, C., Polymer Nanocomposites with Cellulose Nanocrystals Featuring Adaptive Surface Groups. *Biomacromolecules* **2017,** *18* (2), 517-525.
34. Chakrabarty, A.; Teramoto, Y., Recent Advances in Nanocellulose Composites with Polymers: A Guide for Choosing Partners and How to Incorporate Them. *Polymers* **2018,** *10* (5).
35. Wu, G. M.; Liu, D.; Liu, G. F.; Chen, J.; Huo, S. P.; Kong, Z. W., Thermoset nanocomposites from waterborne bio-based epoxy resin and cellulose nanowhiskers. *Carbohydrate Polymers* **2015,** *127*, 229-235.
36. Girouard, N. M.; Xu, S. H.; Schueneman, G. T.; Shofner, M. L.; Meredith, J. C., Site-Selective Modification of Cellulose Nanocrystals with Isophorone Diisocyanate and Formation of Polyurethane-CNC Composites. *Acs Applied Materials & Interfaces* **2016,** *8* (2), 1458-1467.
37. Atifi, S.; Su, S. X.; Hamad, W. Y., Mechanically tunable nanocomposite hydrogels based on functionalized cellulose nanocrystals. *Nord. Pulp Paper Res. J.* **2014,** *29* (1), 95-104.
38. Cao, X. D.; Habibi, Y.; Lucia, L. A., One-pot polymerization, surface grafting, and processing of waterborne polyurethane-cellulose nanocrystal nanocomposites. *Journal of Materials Chemistry* **2009,** *19* (38), 7137-7145.
39. Yang, J.; Han, C. R., Mechanically Viscoelastic Properties of Cellulose Nanocrystals Skeleton Reinforced Hierarchical Composite Hydrogels. *Acs Applied Materials & Interfaces* **2016,** *8* (38), 25621-25630.
40. Kaminsky, W.; Sinn, H., Methylaluminoxane: Key Component for New Polymerization Catalysts. In *Polyolefins: 50 years after Ziegler and Natta II: Polyolefins by Metallocenes and Other Single-Site Catalysts*, Kaminsky, W., Ed. Springer Berlin Heidelberg: Berlin, Heidelberg, 2013; pp 1-28.

41. Breslow, D. S.; Newburg, N. R., Bis-(cyclopentadienyl)-titanium Dichloride-Alkylaluminum Complexes as Soluble Catalysts for the Polymerization of Ethylene. *Journal of the American Chemical Society* **1957,** *79* (18), 5072-5073.
42. Kaminsky, W., Zirconocene catalysts for olefin polymerization. *Catalysis Today* **1994,** *20* (2), 257-271.
43. D'Agnillo, L.; Soares, J. B. P.; Penlidis, A., Effect of operating conditions on the molecular weight distribution of polyethylene synthesized by soluble metallocene/methylaluminoxane catalysts. *Macromolecular Chemistry and Physics* **1998,** *199* (6), 955-962.
44. Wells, G. J.; Ray, W. H., Prediction of Polymer Properties in LDPE Reactors. *Macromolecular Materials and Engineering* **2005,** *290* (4), 319-346.
45. Cossee, P., Ziegler-Natta catalysis I. Mechanism of polymerization of α-olefins with Ziegler-Natta catalysts. *Journal of Catalysis* **1964,** *3* (1), 80-88.
46. Sastri, V. R., 6 - Commodity Thermoplastics: Polyvinyl Chloride, Polyolefins, and Polystyrene. In *Plastics in Medical Devices (Second Edition)*, Sastri, V. R., Ed. William Andrew Publishing: Oxford, 2014; pp 73-120.
47. McDaniel, M. P., Chapter 3 - A Review of the Phillips Supported Chromium Catalyst and Its Commercial Use for Ethylene Polymerization. In *Advances in Catalysis*, Gates, B. C.; Knözinger, H., Eds. Academic Press: 2010; Vol. 53, pp 123-606.
48. Lee, B. Y.; Oh, J. S., Preparation of Anchored Metallocene Complexes on Dehydroxylated Silica and Their Use in the Polymerization of Ethylene. *Macromolecules* **2000,** *33* (9), 3194-3195.
49. Kaminsky, W.; Funck, A.; Klinke, C., In-situ Polymerization of Olefins on Nanoparticles or Fibers by Metallocene Catalysts. *Topics in Catalysis* **2008,** *48* (1), 84.
50. Gedde, U. W.; Mattozzi, A., Polyethylene Morphology. In *Long Term Properties of Polyolefins*, Albertsson, A.-C., Ed. Springer Berlin Heidelberg: Berlin, Heidelberg, 2004; pp 29-74.
51. Alamo, R. G.; Mandelkern, L., The crystallization behavior of random copolymers of ethylene. *Thermochimica Acta* **1994,** *238*, 155-201.
52. Selke, S. E.; Hernandez, R. J., Packaging: Polymers for Containers. In *Encyclopedia of Materials: Science and Technology*, Buschow, K. H. J.; Cahn, R. W.; Flemings, M. C.; Ilschner, B.; Kramer, E. J.; Mahajan, S.; Veyssière, P., Eds. Elsevier: Oxford, 2001; pp 6646-6652.
53. Haichen, Z.; Yong, L., Extrusion Processing of Ultra-High Molecular Weight Polyethylene. In *Extrusion of Metals, Polymers and Food Products*, Qamar, S. Z., Ed. IntechOpen: 2018.
54. An, M.; Xu, H.; Lv, Y.; Tian, F.; Gu, Q.; Wang, Z., The effect of chitin nanocrystal on the structural transition of shish-kebab to fibrillar crystals of ultra-high molecular weight polyethylene/chitin nanocrystal fibers during hot-stretching process. *European Polymer Journal* **2017,** *96*, 463-473.
55. Visakh, P. M.; Morlanes, M. J. M., 1. Introduction - HDPE and UHMWPE. In *Polyethylene-Based Blends, Composites and Nanocomposites*, John Wiley & Sons: 2015.
56. Rives, V.; Labajos, F. M.; Herrero, M., 6. Double layered hydroxides as nanofillers of composites and nanocomposite materials based on polyethylene. In *Polyethylene-Based Blends, Composites and Nanocomposites*, Visakh, P. M.; Morlanes, M. J. M., Eds. John Wiley & Sons: 2015.

57. Fernandes, E. M.; Mano, J. F.; Reis, L. R., 5. Polyethylene Composites with Lignocellulosic Material. In *Polyethylene-Based Blends, Composites and Nanocomposites*, Visakh, P. M.; Morlanes, M. J. M., Eds. John Wiley & Sons: 2015.
58. Raj, R. G.; Kokta, B. V., Linear Low-Density Polyethylene Filled with Silane-Coated Wood Fibers. In *High-Tech Fibrous Materials*, American Chemical Society: 1991; Vol. 457, pp 102-113.
59. Rogers, P., Facing the Freshwater CRISIS. *Scientific American* **2008,** *299* (2), 46-53.
60. Wada, Y.; van Beek, L. P. H.; van Kempen, C. M.; Reckman, J. W. T. M.; Vasak, S.; Bierkens, M. F. P., Global depletion of groundwater resources. *Geophysical Research Letters* **2010,** *37* (20).
61. Galanakis, C. M.; Agrafioti, E., Membrane distillation development. In *Sustainable Water and Wastewater Processing*, Elsevier: 2010.
62. Chan, W.-F.; Chen, H.-y.; Surapathi, A.; Taylor, M. G.; Shao, X.; Marand, E.; Johnson, J. K., Zwitterion Functionalized Carbon Nanotube/Polyamide Nanocomposite Membranes for Water Desalination. *ACS Nano* **2013,** *7* (6), 5308-5319.
63. Kucera, J., Introduction and History of Development. In *Reverse Osmosis*, Kucera, J., Ed. 2010; pp 1-13.
64. Hiddink, J.; de Boer, R.; Nooy, P. F. C., Reverse Osmosis of Dairy Liquids. *Journal of Dairy Science* **1980,** *63* (2), 204-214.
65. Greenlee, L. F.; Lawler, D. F.; Freeman, B. D.; Marrot, B.; Moulin, P., Reverse osmosis desalination: Water sources, technology, and today's challenges. *Water Research* **2009,** *43* (9), 2317-2348.
66. Kim, H. J.; Choi, K.; Baek, Y.; Kim, D.-G.; Shim, J.; Yoon, J.; Lee, J.-C., High-Performance Reverse Osmosis CNT/Polyamide Nanocomposite Membrane by Controlled Interfacial Interactions. *ACS Applied Materials & Interfaces* **2014,** *6* (4), 2819-2829.
67. Ben-Sasson, M.; Lu, X.; Bar-Zeev, E.; Zodrow, K. R.; Nejati, S.; Qi, G.; Giannelis, E. P.; Elimelech, M., In situ formation of silver nanoparticles on thin-film composite reverse osmosis membranes for biofouling mitigation. *Water Research* **2014,** *62*, 260-270.
68. Kadhom, M.; Hu, W.; Deng, B., Thin Film Nanocomposite Membrane Filled with Metal-Organic Frameworks UiO-66 and MIL-125 Nanoparticles for Water Desalination. *Membranes (Basel)* **2017,** *7* (2), 31.
69. Li, L.; Dong, J.; Nenoff, T. M.; Lee, R., Desalination by reverse osmosis using MFI zeolite membranes. *Journal of Membrane Science* **2004,** *243* (1), 401-404.
70. Baumann, W.; Firnow, J.; Gloede, K.; Hertzog, G.; Hessler, M.; Moll, K. K.; Ramhold, K.; Reinecke, U.; Roschka, E.; et, a. Simplified distillative norbornene purification. DD237987A1, August 6, 1986, 1986.
71. Lattner James, R.; Sanchez Leonel, E.; Becker Christopher, L.; Devoy Bruce, C. Production Of Alkenyl Bridged Ring Compounds. US 6093865 A, 1998, 2000.
72. Finkelshtein, E. S.; Bermeshev, M. V.; Gringolts, M. L.; Starannikova, L. E.; Yampolskii, Y. P., Substituted polynorbornenes as promising materials for gas separation membranes. *Russian Chemical Reviews* **2011,** *80* (4), 341-361.
73. Sutthasupa, S.; Shiotsuki, M.; Sanda, F., Recent advances in ring-opening metathesis polymerization, and application to synthesis of functional materials. *Polymer Journal* **2010,** *42* (12), 905-915.

74. Ash, M.; Ash, I., Polynorbornene. In *Handbook of Plastics and Rubber Additives, Volumes 1-2 (2nd Edition)*, Synapse Information Resources, Inc.: 2013.
75. Gmernicki, K. R.; Hong, E.; Maroon, C. R.; Mahurin, S. M.; Sokolov, A. P.; Saito, T.; Long, B. K., Accessing Siloxane Functionalized Polynorbornenes via Vinyl-Addition Polymerization for CO2 Separation Membranes. *ACS Macro Letters* **2016,** *5* (7), 879-883.
76. Bermeshev, M. V.; Syromolotov, A. V.; Starannikova, L. E.; Gringolts, M. L.; Lakhtin, V. G.; Yampolskii, Y. P.; Finkelshtein, E. S., Glassy Polynorbornenes with Si–O–Si Containing Side Groups. Novel Materials for Hydrocarbon Membrane Separation. *Macromolecules* **2013,** *46* (22), 8973-8979.

Chapter 2: *In situ* dispersion and polymerization of polyethylene cellulose nanocrystal-based nanocomposites

This chapter is adapted from the publication: "In situ dispersion and polymerization of polyethylene cellulose nanocrystal-based nanocomposites." In the publication *Journal of Applied Polymer Science*.

I recognize the contributions of the coauthors Travis W. Baughman, Paul A. Deck, and E. Johan Foster. All co-authors contributed ideas, procedures, and significant editing to the document, and Paul A. Deck synthesized the catalyst 1,1'-bis(bromodimethylsilyl)zirconocene dibromide.

In situ dispersion and polymerization of polyethylene cellulose nanocrystal-based nanocomposites

Keith D. Hendren, Travis W. Baughman, Paul A. Deck, and E. Johan Foster

Abstract:

This study describes a novel method of forming a nanocomposite comprising cellulose nanocrystals (CNC)s as the reinforcing filler and a high-density polyethylene matrix. The method involves covalent attachment of a metallocene catalyst, 1,1'-bis(bromodimethylsilyl)zirconocene dibromide **1**, to the hydroxyl-rich surfaces of the CNCs and subsequent slurry polymerization with excess alumoxane (MMAO-12) as the co-catalyst. Polymerization proceeds with activities reaching 500 kg mol^{-1} atm^{-1} h^{-1}, while the CNCs are simultaneously dispersed to afford robust, well-dispersed nanocomposites. Films of these composites (ca. 7 vol% CNC) showed excellent dispersal of the filler (optically translucent; no CNC aggregation observed by AFM). The composites (ca. 7 vol% CNC) also revealed an increase in Young's modulus (10-100%) and comparable yield strength relative to commercially produced polyethylenes (PE). The experimental simplicity of this approach suggests that our method could be scaled beyond the present laboratory scale and extended to reinforce other polyolefin grades.

2.1. Introduction:

Nanomaterials are ideal composite fillers; their high surface area leads to increased interfacial interactions with the matrix material.[1] High-modulus nanoscopic fillers can improve the mechanical properties of a material by increasing the stiffness more than their microscopic counterparts.[1] As a filler material, cellulose nanocrystals (CNCs) have substantial reinforcing potential as they have high aspect ratios and high Young's moduli.[2] In addition, surface hydroxyl groups enable CNCs to associate with one another through hydrogen-bonding, resulting in a percolated network of rod-like filler particles within the matrix at a critical concentration determined by the aspect ratio of the CNCs.[3] CNCs at critical concentrations of typically 6-10 vol% have been shown to dramatically increase the stiffness of soft polymers (> 400%),[4] of low-density polyethylene (LDPE) (> 300%),[5] and of a rigid polypropylene by up to 54%.[6] Production of CNCs is increasing globally, and manufacturers are actively seeking new applications for these bio-based materials.[3] Since polyethylene (PE) is manufactured on an enormous scale, an efficient method of dispersing CNCs into PE would provide a key market for these new nanofillers. Market projections show that demand for nanofilled PE will increase dramatically in coming years.[7]

A previous study using the solvent-exchange method obtained LDPE CNC composites with more than two times the storage modulus and three times the tensile modulus compared to the same polymer lacking a reinforcing filler.[5] However, the solvent exchange method consumes both time and solvent (typically 5-7 days and 4-11 L, respectively) for the incorporation 0.9-3 g of CNCs.[8] Additionally, the solvent-exchange method cannot be readily extended to less soluble polymers such as high-density polyethylene (HDPE). Another approach for CNC LDPE composite fabrication has been

surface modification of the highly polar CNCs with hydrophobic groups to compatibilize them with the aliphatic LDPE chains.[9] Unfortunately, this approach also tends to disrupt hydrogen bonding between CNCs, weakening filler-filler interactions.[10] The efficient incorporation of minimally modified CNCs into hydrophobic matrices therefore remains an important challenge.

In order to achieve high dispersion of filler in a polymer without sacrificing interfacial characteristics, an alternative approach to preparing the composite attaches a polymerization catalyst to the filler; the growing polymer chains originate in close proximity to the filler, ideally dispersing the filler in the matrix. Previous work has mostly focused on the method introduced by Kaminsky of adsorbing a cocatalyst, generally methylalumoxane (MAO), to the filler material, binding a catalyst through cocatalyst-metallocene ionic interactions, and then polymerizing.[11] This polymerization-filling approach has been successful using a variety of metallocene single site systems.[12-24] The bio-derived supports chitin, starch, and cellulose have been previously used with this method.[25] In a particularly compelling and recent report, Mülhaupt et al. supported MAO on nanofibrillar cellulose,[23] adhered an iron catalyst, and polymerized ethylene to obtain mechanically reinforced composite materials. As far as we are aware, this method has not been applied to CNCs as nanofillers for PE.

Herein we report a method to prepare CNC-filled PE nanocomposites that have significantly greater stiffness when compared with conventional HDPEs, in a hitherto unavailable, industrially scalable process. We selected wood-derived CNCs because they have a theoretical modulus in the transverse direction of 18-50 GPa and an aspect ratio of ca. 20.[26] Moreover, this type of CNC is presently in commercial production.[27] Importantly,

our method of supporting the metallocene catalyst represents a significant departure from the methods reported by Kaminsky, Mülhaupt, and others. Whereas their method used a nanofibrillar cellulose-bound alumoxane so that the metallocene would become activated only at the CNC surface, we have chosen a complementary approach using a metallocene that can engage in robust covalent bonding through tethering groups attached to the cyclopentadienyl ligands.[28-29] Mälder adsorbed $TiCl_4$ directly to a cellulose surface and polymerized ethylene therefrom, with the aid of an alumoxane cocatalyst.[30] That result shows that a covalently-bound transition metal catalyst can still polymerize ethylene, but $TiCl_4$-based catalysts typically do not exhibit single-site characteristics such as narrow molecular weight distribution.[30] Moreover, advantages of supporting the catalyst directly onto the CNCs is that the stability of metallocenes relative to supported alumoxanes allows for thorough and convenient washing via centrifuge in air making it an ideal process for nanomaterials that are difficult to filter and wash under inert conditions, such as CNCs. The other advantage is that the polymerization can be conducted as a slurry using an excess of alumoxane in the solvent, which also serves to scavenge adventitious poisons; this eliminates the need for an additional, non-activating scavenger such as triisobutylaluminum. On the other hand, the primary advantage of supporting the alumoxane before supporting the catalyst is that this method is compatible with a variety of metallocene catalysts and allows a wide variety of catalysts to be screened quickly.

We will show that in our preliminary study, we bound metallocene catalyst to CNCs, and we achieved a practical activity for polymerization ca. 500 $kg_{PE}\ mol_{Zr}^{-1}\ h^{-1}$. In tensile testing, the 7 vol% CNC in polyethylene material showed a 10-100% greater Young's modulus relative to commercial HDPE,[31-32] though there is a noticeable decrease

in elongation at break 200-600% vs ca. 4%.[31-32] We also tested a commercial ultra-high molecular weight polyethylene (UHMWPE) sample at a low crystallinity and found that our composite, 7 vol% CNC in PE, had a Young's modulus fivefold greater than the UHMWPE. The resulting films exhibited promising translucency, although characterization of filler dispersion, as will be discussed, proved difficult.

2.2 Results and Discussion:

This article describes first the attachment of functionalized metallocene dibromide catalysts onto the surface of cellulose nanocrystal (CNC) aerogel particles (**Scheme 1**), the polymerization of ethylene from the surfaces of those particles, and the physical characterization of the resulting CNC-PE composite materials.

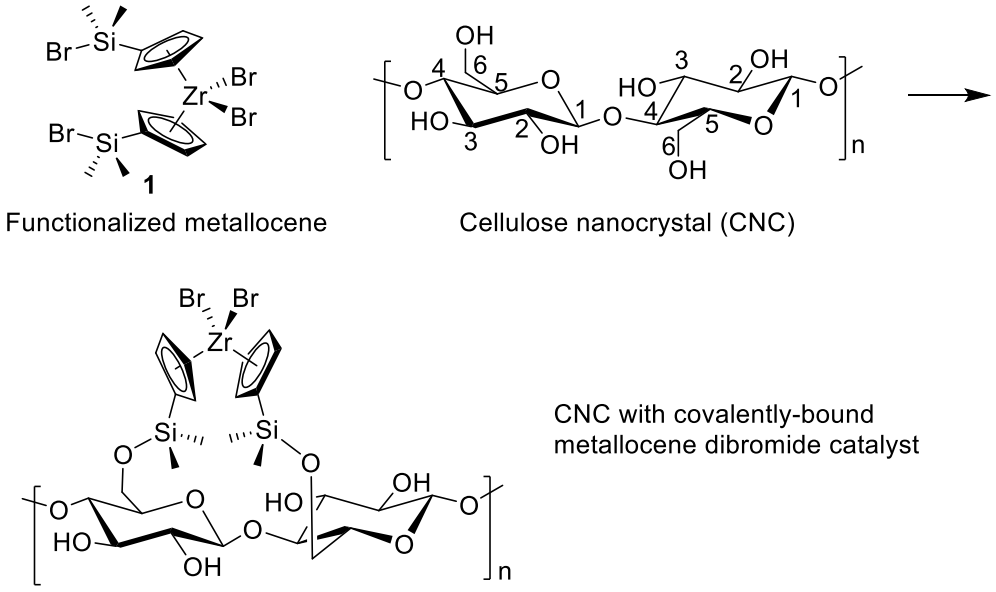

Scheme 2.1: The proposed reaction for bromodimethylsilyl-functionalized zirconocene dibromide catalyst **1** with cellulose nanocrystals (CNC)s is shown. Substitution of the reactive Si-Br bonds results in formation of strong silyloxy linkages to the CNC.

2.2.1 Attachment of catalysts to cellulose nanocrystals (CNC)s:

We chose CNC aerogels to serve as heterogeneous supports for our metallocene ethylene polymerization catalyst, with the idea that the flaky aerogel particles (**Figure 2.1**) would break apart and become well dispersed during polymerization and then serve as a nanofiller for the resulting PE resin. Our strategy for attaching metallocene catalysts to CNCs is based on prior work of Deck and co-workers,[28] who showed that bromodimethylsilyl-functionalized zirconocene dibromides adsorb to hydroxylated surfaces (e.g., silica) by reaction of the surface hydroxyl groups (Si-OH) with the reactive substituent (Br-Si) to form covalent silyloxy linkages (Si-O-Si). Prior methods of silanizing CNCs (solvent exchange methods or amine chemistry) would not be compatible with our functionalized metallocene, which is quite sensitive toward hydrolysis of the Si-Br (and Zr-Br) bonds.[28-29]

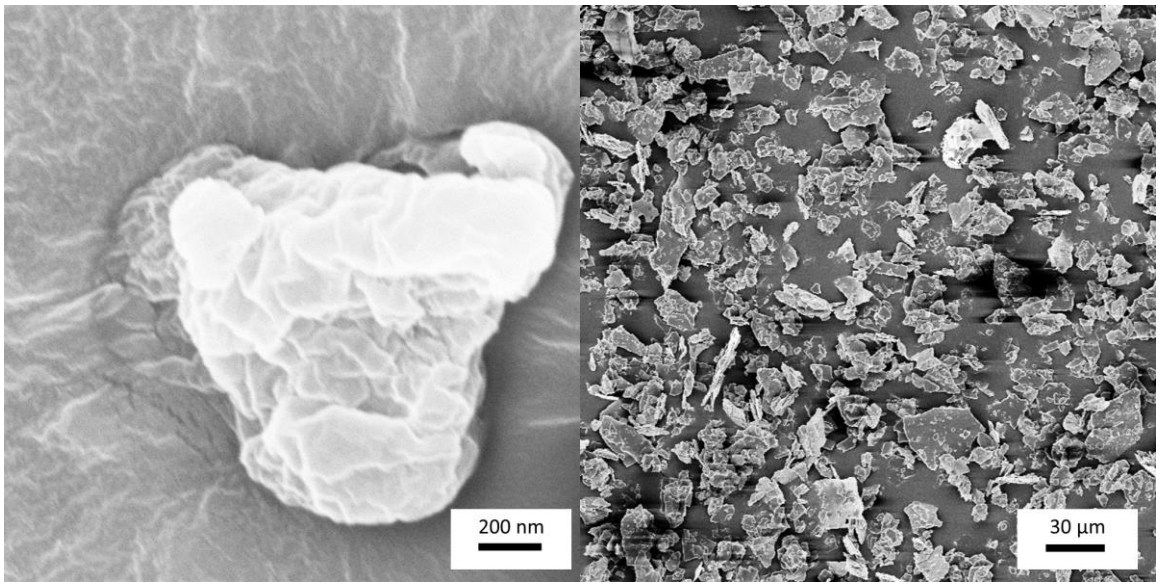

Figure 2.1: Scanning electron microscopy (SEM) images show functionalized CNCs as aerogel powder particles for Entries 2 and 3 (**Table 1**). The images show the flaky texture of the CNC aerogel particles (left), as well as their large size (right).

Aqueous CNC dispersions with concentrations of 60 mg mL^{-1} (in water) were selected to prepare our aerogels. At higher concentrations, gelation (excessive physical crosslinking) can occur, which could decrease the overall surface area upon freeze-drying.[33] At this concentration, freeze-drying resulted in minimal apparent shrinkage, which has been observed when freeze-drying CNCs from more dilute solutions. We also prepared one sample using 2:1 *tert*-butanol:water, which previous studies have shown yields a higher surface area,[34] but discovered (see below) that this approach did not result in a higher activity.

CNCs are constructed of anhydroglucose units having three possible positions for attaching a silyl group the hydroxyl groups at the O-2, O3, and O-6 positions. While have not yet been able to determine the exact mode of binding (to which hydroxyl groups or even to how many) in our materials, we expect the primary hydroxyls at the O-6 position to be the most reactive largely due to steric effects. The O-2 position has been shown to be otherwise equally reactive towards etherification, however the formation of a pentavalent silicon intermediate during silylation might tend to amplify steric effects on relative site reactivities.[35-36] Prior studies have shown that, theoretically, for ideally dispersed CNCs about half of the sites are available for functionalization.[36] However, we only needed to attach our catalyst to a small fraction of these available hydroxyl sites in order to obtain the desired polymerization activity levels. Proposing (a) our supported catalyst would have an activity approximately 1% that of zirconocene dichloride,[28] (b) that we would run our polymerizations for 1 h, and (c) that we wanted to form about 1 g of material having 20-30% of CNC by weight, we estimated that we would need to adsorb about 4 mg (6.1 μmol)

of our catalyst for every 300 mg of CNC support. Each of our CNC samples (300 mg) should contain ca. 0.88 mmol of anhydroglucose units and 0.44 mmol of primary surface hydroxyl groups. At a maximum we could attach 0.22 mmol of our metallocene catalyst assuming that both $BrSiMe_2$ groups react at the surface and that all of the surface hydroxyl groups are engaged. These calculations suggest that we only need to functionalize about 2.8% of the available hydroxyl groups. Additionally, using previous analysis and measurements, the 36 cellulose chain rosette model, the average length of wood CNCs, and nominal length of 5 Å per anhydroglucose unit, we estimate that there are roughly 65 catalyst molecules available per CNC.[2, 37] These calculations show that there are enough catalyst particles per CNC to effect the growth of numerous PE chains from the surface of each individual CNC leading to a proposed separation of CNCs as they are clustered as aerogel sheets. It is imperative for the reader to understand that these calculations are based on a highly idealized model. In reality, the CNCs are significantly aggregated as aerogels, so fewer surface hydroxyl groups are available for catalyst immobilization. In the immobilization procedure, the CNCs are washed to remove any metallocene species that are not covalently bound. Thus, the proportion of immobilized metallocene will certainly be lower than we have projected, and immobilization may not be uniform throughout the CNC material. As a result, productivities reported here represent a lower bound on the true productivities of the competent surface-adsorbed catalytic species.

Accordingly, samples of CNCs (300 mg) were treated with (4 mg, 6.1 μmol) portions of catalyst **1** in toluene, washed with solvent, and vacuum dried. Washing the CNC-supported catalyst required some exploration because the CNC particles are so fine that they flow easily through fine-porosity fritted-glass filters. Rather than search for even

finer-pored filtration apparatus, we found that using a centrifuge was a much more convenient alternative, which we could even carry out under ambient atmosphere without degrading the supported catalyst.[38] This catalyst loading predicts a Zr:C ratio of 0.00055, but X-ray photoelectron spectroscopy (XPS) characterization showed Zr:C ratio range of 0.0005 to 0.002. This suggests an even a higher loading of Zr than was provided in our protocol. This result can be explained as our CNC-supported catalyst samples contain particles in the micron size range in contrast to the penetration depth of XPS is only about 5 nm, and the catalyst molecules will be more concentrated at the surface.

In our XPS measurements we also analyzed the Br:Zr ratio to explore the mode of binding of the catalyst to the CNC surface. Several possibilities are shown in **Scheme 2**. The "ideal" structure (b) should have a Br:Zr ratio of 2:1, however the ratio observed was actually 1:1 or even lower. We surmise that partial hydrolysis of the Zr-Br bonds from adventitious moisture (likely introduced during catalyst washing procedures that included some exposure to air) or "face-down" binding of the metallocene (forming Zr-O linkages at the CNC surface) can account for the observed relative atomic concentrations. However, the catalyst is still found to be active upon treatment with alumoxane cocatalyst (described in a subsequent section), so we propose that if the alternative structures (d), (e), and (f) are formed, they are rectified upon treatment with MMAO-12 to the ideal, active form of the catalyst (c). Importantly, our washing procedures did not disrupt the vital Si-O bonds retaining the metallocene on the CNC surface (see the section on washing studies below). Silyl ethers bound to cellulose have been previously shown to be quite resistant toward hydrolysis.[39] XPS data is available in **Figure S2.1**. It should be noted that XPS is a great technique for detecting small amounts of a chemical and doing so quantitatively. How

accurate XPS at this surface concertation for an uneven surface is not well understood. We hope to support these finding using a chromophore with similar anchoring chemistry under similar conditions, absorbance spectra are also sensitive at low concentrations.

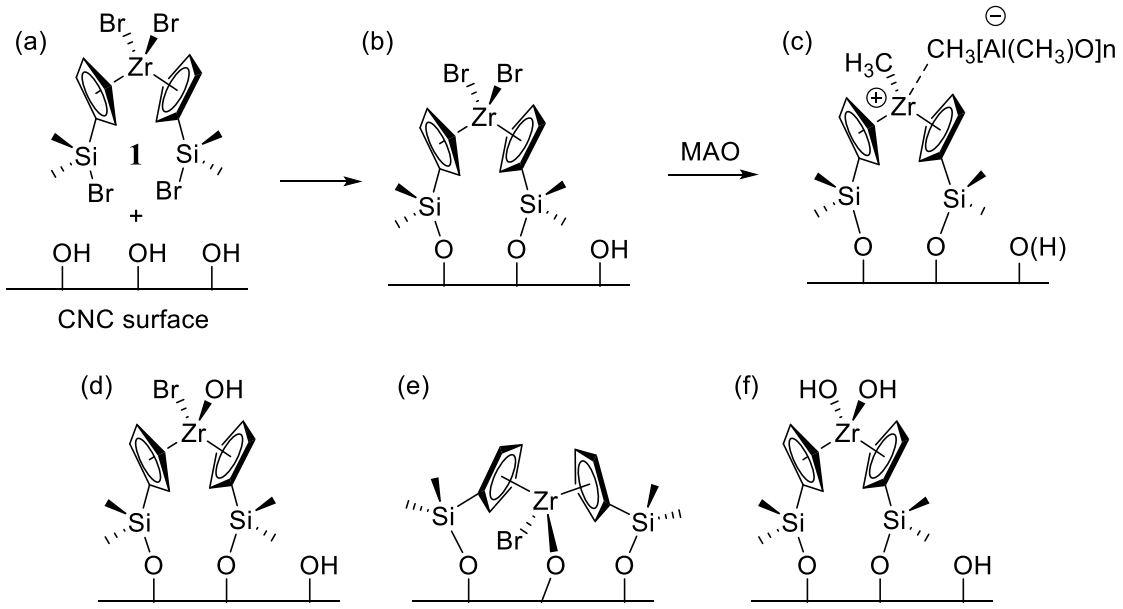

Scheme 2.2: These proposed reactions lead to the robust adsorption of metallocene **1** on CNC surfaces.[28-29] (a) Functionalized metallocene dibromide **1** and the putative, hydroxylated CNC surface; (b) "face-up" metallocene dibromide bound to the CNC surface through two covalent silyloxy linkages; (c) alumoxane-activated, surface-tethered metallocene; (d) and (e) partially hydrolyzed, surface-tethered metallocenes; (f) "face-down" metallocene bound to the CNC surface through two silyloxy linkages and a Zr–O linkage; Structures (d) – (f) are proposed to account for Br:Zr ratios less than 2:1 observed by XPS. We propose that structures such as (d) – (e), if they are formed, are reactivated upon treatment with excess alumoxane to generate the activated structure (c).

2.2.2 Polymerizations of ethylene from CNC supports:

Polymerizations from **Table 1** resulted in similar activities, despite many of them having minor procedural differences. For example, there were similar activities when comparing polymerizations conducted on the higher surface area *tert*-butyl alcohol freeze-dried sample when compared to other entries in the table. Entry 5 had an increase in scale with a comparable activity to other entries. The slightly lower activities of

Entries 7-9 are in part because we assumed, in the calculation, that the CNCs from the initial 300 mg are present and therefore all of the catalyst is still on the CNCs, while, in fact, as much as a third of the CNCs are lost during centrifuge washing.

Table 2.1: Studies of PE polymerizations of catalyst supported on CNCs were activated with a 1100:1 Al:Zr ratio, catalyst loading of 1.3 wt%, washed by centrifuge, and polymerized at 25 °C under 1 atm of ethylene for 0.5 h. The differences in polymerization conditions for each sample are noted below the table as superscripts, and information concerning TGA can be found in the supporting information.

Entry	CNCs dried before slurry polymerization	Washing (# x mL)	Mass of Resin (g)	Mass of CNCs (g)	Activity (kg_{PE} mol_{Zr}^{-1} h^{-1})	vol% CNC (TGA)
1[i]	Yes	3 x 35	0.116	0.020	500	8%
2[ii]	Yes	3 x 35	0.121	0.020	500	7%
3[ii,iv]	Yes	3 x 35	0.187	0.020	400	6%
4	Yes	3 x 35	0.096	0.020	400	10%
5	Yes	3 x 35	0.738	0.094	700	7%
6[iii]	Yes	2 x 35	0.034	0.020	70	17%
7[v]	No	3 x 35	0.824	0.3	200	17%
8[v]	No	2 x 35	0.862	0.3	200	16%
9[v]	No	2 x 35	0.629	0.3	100	23%

[(i)] Light aerogel freeze-dried from 150 mg and *tert*-butyl alcohol water solution; [(ii)] Used the same aerogel; [(iii)] Dried in air; [(iv)] Polymerized for 1 h; [(v)] Estimated values are based on original aerogel mass.

The activities attained from this study (ca. 500 kg_{PE} mol_{Zr}^{-1} h^{-1}) supported on CNCs were comparable to a work from Deck and coworkers (1,300 kg_{PE} mol_{Zr}^{-1} h^{-1}) supported on silica gel. The lower activity in the present study is partly explained by the lower temperature of 25 °C, compared to 50 °C used by Deck and coworkers.[28] This study seems to imply that the two supports effect similar activities, but only a direct comparison under identical reaction conditions could confirm this finding.

2.2.3 Physical Characterization of CNC-PE Composite:

Samples representative of the best process of CNC composite fabrication, Entries 2 and 3 (**Table 2.1**), were analyzed for dispersion as films. The films used were obtained

from the gentlest processing methods possible; these processes are detailed in the experimental section (**2.4.7**). This was done to ensure that possible residual acid did not cause early oxidation the CNCs during processing. Minimal composite processing and melting of the PE crystals was done to avoid a false positive conclusion regarding CNC dispersion, ensuring the CNCs did not disperse because of processing. To find the crystallinity of the composites and control films, the enthalpy of melting was found by linear integration of DSC thermograms using the first heating cycle **Figure S2.3.** The enthalpy of melting was compared with that of 100% crystalline polyethylene at 290 J g^{-1}.[40] The translucency shown in **Figure 2.2** suggests that CNCs are well-dispersed in the PE matrix at ca. 6 vol%. These films were deemed good for mechanical testing, both DMA and DSC, as they were cohesive and uniform.

Characterization of CNC dispersion in PE on a smaller scale done with atomic force microscopy (AFM) to distinguish the stiffer CNCs from the softer PE. AFM images (**Figure 2.3**) imply that aggregate bundles of CNCs are not present as the large aerogel particles shown in **Figure 2.1**. While it is not shown that CNCs are individualized in the polymer matrix, AFM should resolve micron size particles of CNCs.[2] Additionally, we were unable to find evidence of aggregation by SEM as shown in **Figure S2.2**. Unfortunately, PE forms crystals that have comparable and greater dimensions to CNCs;[41] this would complicate further characterization by transmittance measurements as the PE crystals would scatter light. We infer from our results that the CNCs are well dispersed. SEM is the standard technique to see objects on the nanoscale, but there is little contrast between CNCs and PE. We hoped to overcome this lack of contrast with AFM imaging which can see differences in modulus from the phase angle image. However, PE has

crystals that are similar in size, we thus used both tests to conclude there was no aggregation. These results were supported by the DMA and tensile data that show good reinforcement.

6 vol% CNC PE Entry 3	Commercial UHMWPE

Figure 2.2: Optical photographs of a 150-micron melt-pressed film of a 6 vol% CNC PE composite obtained as shown in Entry 3 of **Table 2.1** (**A**) and of a 150-micron melt-pressed film of commercial UHMWPE (**B**).

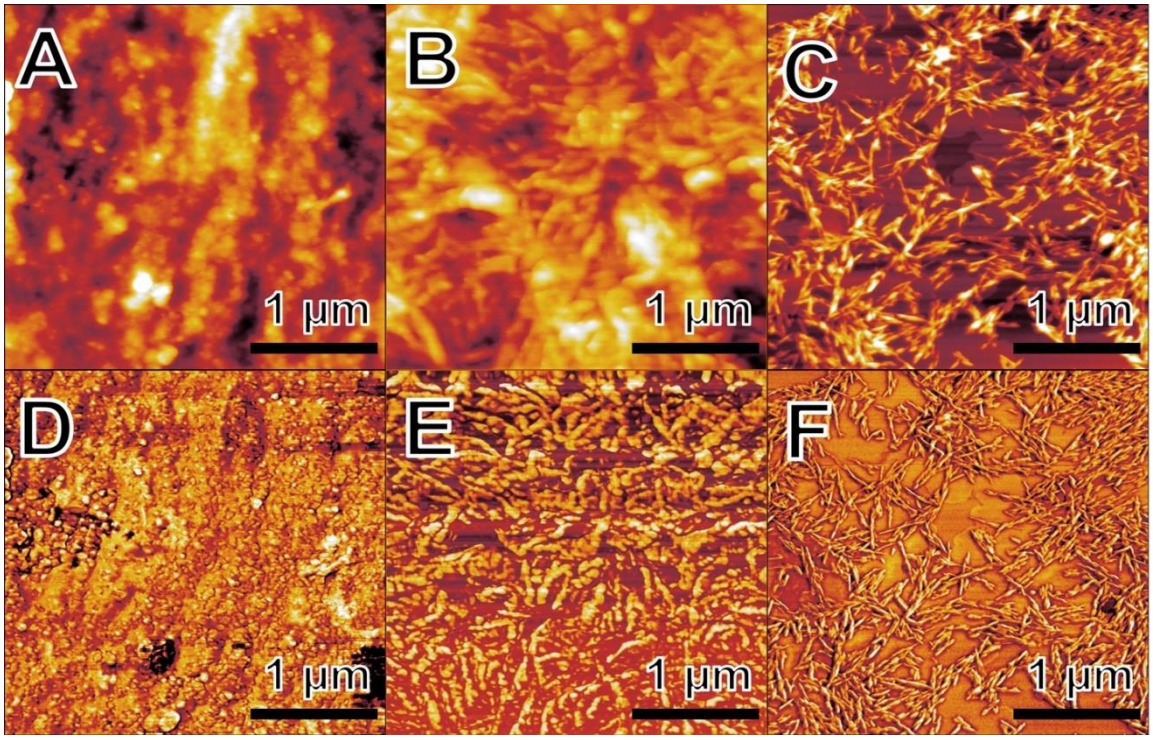

Figure 2.3: Atomic force micrographs (AFM) show polished composite surface, a polished PE surface, and CNCs: **A)** the height image of a 6 vol% CNC PE film (Entry 3, **Table 2.1**), **B)** the height image for commercial UHMWPE, **C)** the height image for CNCs. Images **D**, **E**, and **F** are phase images that correspond to their above height image. Composite phase image **D** does not show signs of aggregation when compared with PE phase image **E** and CNC phase image **F**.

Mechanical data in **Figure 2.4** shows a greater in storage modulus for the ca. 7 vol% CNC PE composites (Entries 2, 3, and 5 **Table 2.1**) ca. 4000 MPa, HDPE controls from Goodfellow (GHDPE)-1 ca. 1800 MPa, a second control from Goodfellow (GHDPE)-2 ca. 2100, UHMWPE ca. 1200 MPa respectively at 20 °C). We acknowledge that the lower crystallinity of the commercial products, analyzed below, contributes to this difference.[5] For comparison, other groups have achieved similar storage moduli at 20 °C in HDPE with higher filler loadings: 20 vol% copper nanoparticles ca. 4100 MPa (neat HDPE ca. 2000 MPa),[42] 20% v/v graphite ca. 4500 MPa (neat HDPE ca. 1800 MPa),[43] and 10 vol% graphite ca. 3100 MPa (neat HDPE 1800 MPa).[43] DMA tensile analysis is difficult to replicate as small deviations in sample prep can cause large scale differences in modulus.

We overcame this by carefully pulling the materials taut and observing both sides of the film to ensure they were both equally taut. We did tensile testing to confirm that the relative differences in storage modulus were similar to the differences in Young's modulus.

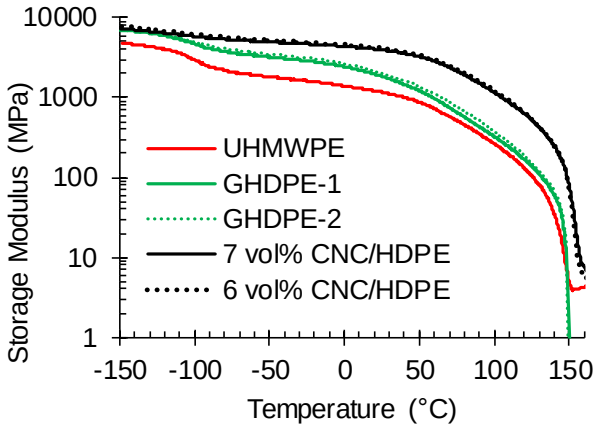

Figure 2.4: The graph shows temperature representative traces of sweeps conducted from -150 °C to 160 °C on rectangular coupons at 1 Hz and an amplitude of 15 µm at 5 °C min^{-1} with the films of PE CNC composite 6 vol% (Entry 3, **Table 2.1**), PE CNC 7 vol% (Entry 2), GHDPE-1, GHDPE-2, UHMWPE, and 7 vol % (Entry 5) were tested by DMA.

Tensile data and crystallinity data comparing UHMWPE, 7 vol% CNC in PE, tested GHDPEs, and commercial HDPE products are summarized in **Table 2.2.** Tensile data comparing 7 vol% CNC (Entry 5 in **Table 2.1**), commercial UHMWPE at a low crystallinity, commercial HDPE, and typical values for HDPE products imply that there is an increased stiffness of the composite. Young's modulus values were 1600 ± 100 MPa 7 vol% CNC composite material, 300 ± 30 MPa for UHMWPE, 500 ± 30 MPa GHDPE-1 and 350 ± 30 MPa GHDPE-2. Yield strength of the 7 vol% CNC composite, 29 ± 6 MPa, greater than the yield strengths of the control samples and comparable to commercial HDPE values 22-32 MPa. [31-32] There was however, a large decrease in elongation at break for the composite material ca. 4%, when compared to controls and commercial products

Table 2.2. The low elongation at break may be attributed to the occasional voids present as is visible in the SEM images **Figure S2.2**.

Tensile testing successfully measured the primary quantities of interest the Young's modulus and yield strength. Notably though the small size of these materials and crosshead speed may have led to premature failure of the GHDPE-1, GHDPE-2, and 7 wt% CNC composite samples. This limitation can be overcome with larger scale production allowing for testing at multiple crosshead speeds and with larger samples.

Table 2.2: Physical property values below for UHMWPE,12 GHDPE-1, GHDPE-2, and 7 vol% CNC in PE were determined experimentally and values for HDPE 1 and HDPE 2 were taken from indicated sources.

Sample	Young's Modulus (MPa)	Elongation at Break (%)	Yield Strength (MPa)	Crystallinity (%) (DSC)
UHMWPE	300 ± 30	500 ± 70	21 ± 1	47
7 vol% CNC in PE	1600 ± 100	4 ± 2	29 ± 6	75
GHDPE-1	500 ± 30	40 ± 20	24 ± 1	61
GHDPE-2	350 ± 30	70 ± 10	20 ± 1	55
HDPE 1[32]	1450	200	32	79
HDPE 2[31]	800	1000	22	64

The first heating from the DSC found that the melting points of our composites (Entries 2 and 3 in **Table 2.1**) were ca. 139 °C, UHMWPE was ca. 132 °C, and GHDPE-1 and GHDPE-2 were ca. 128 °C. Notably the PE of the composites was much more crystalline, ca. 75%, in the processed state and only ca. 40% on the second heating **Figure S2.3**. In contrast the UHMWPE was 47% crystalline on the first heating and 45% crystalline on the second heating. GHDPEs showed a similar trend decreasing GHDPE-1

went from 61% to 55% crystalline, and GHDPE-2 went from 55% to 52% crystalline. The comparatively low crystallinity value for UHMWPE was surprising, and is likely due to the high melt viscosity which may make processing this material into a more crystalline form difficult.[44] Additionally, this may account for the surprisingly low Young's modulus observed for UHMWPE, and unfortunately processing it at a low temperature to maintain its natural crystallinity proved difficult. GHDPE products were tested as additional controls, using both methods of processing, they resulted in fair yield strength but lower than expected elongation at break and Young's moduli. As such, mechanical data for commercial HDPE products (62-79% crystalline) was included for an additional reference.[31-32]

Crystallinity data from DSC is not suitable for composites of unknown filler content. TGA results were used to find the amount of CNCs in each sample and remove the known mass fraction of the CNCs, as they do not have a thermal event **Figure S2.5**. The calculated mass of PE from the composite was then used to calculate the heat of fusion/melting.

The molecular weights of Entries 2, 3, and 7 as analyzed by TOSOH Bioscience LLC, were found to have molecular weights (PDIs) of 1.77 Mg mol-1 (5.2), 1.74 Mg mol-1 (3.4), and 0.726 Mg mol-1 (2.4) respectively. These high molecular weights were unexpected, and they explain why the crystallinity of the second heating was comparable to the commercial UHMWPE. The somewhat high polydispersity indices also suggest that the catalyst may not be a truly single-site species. Interestingly, the ability to process the composite materials below the melting temperature of the PE may be due to a low degree entanglement of the PE chains; in order to form disentangled PE crystals, the catalyst sites

need to be distributed far away from one another and the polymerization must occur below the crystallization temperature.[45] These two conditions may have been met with the polymerization conditions allowing for a lower than expected processing temperature of the composites, and this disentanglement could allow for advanced processing conditions such as oscillation shear injection molding.[46]

In comparing the mechanical properties of the 7 vol% CNC in PE in our work, we chose an UHMWPE that we thought would be a good basis of comparison and added GHDPE-1 and GHDPE-2 as additional controls. However, the low crystallinity lead to much lower than expected values for Young's modulus for all controls involved, as such we chose another polyethylene to add as a comparison "HDPE 1" that likely has a lower molecular weight than our material but a greater crystallinity. We think the properties of the polyethylene we produced lies somewhere between the low crystallinity UHMWPE and the highly crystalline HDPE 1.[32] Therefore, we claim that there is a minimum of 10% increase of Young's modulus, showing reinforcement of the polymer material through the presence of CNCs.

2.3 Conclusions:

We were successfully able to fabricate PE CNC composites in an efficient manner. GPC data indicated, serendipitously, that we were able to make PE CNC composites with MW near UHMWPE, that were implied to be well dispersed. Furthermore, this composite material would be very difficult to synthesize using conventional mixing methods,[47] whereas the method shown here should be scalable, tunable, and act as a platform method for further nanocellulose reinforced polyolefin composites. Mülhaupt and Sapkota produced polyethlene nanocellulose composites with similar Young's moduli (ca. 1600

MPa). Although higher strength and comperable stiffness values are observed by Mülhaupt, we attribute this to polymer and filler alignment during injection molding.[48] Although beyond the scope of this paper, we hope to use conventional processing such as injection molding with the current materials will hopeful yield even stiffer and stronger PE CNC composites, which may then serve well in roles which require stiffness and are subject to minor strains such as a component of sandwich composites for which carbon fiber composites are largely used.[49] The utilitarian value of this work makes it easily substituted into current industrial polymerization processes. As such, further studies will be done analyzing the scaling up this process, optimizing control of this process and creating alternative methods to alter the molecular weights of resulting PE.

2.4 Experimental:

2.4.1 Materials:

ACS grade toluene from Fisher Scientific USA, was further purified by distillation from sodium and benzophenone. All other reagents were used without further purification. Grade 5.0 ethylene gas, 99.999% purity, was obtained from Praxair USA, HPLC grade hexanes were purchased from Fisher Scientific. High density polyethylene (HDPE) MW 0.125 Mg mol^{-1} was purchased from Goodfellow, USA and is noted in the manuscript as GHDPE. Ultra-high molecular weight polyethylene (UHMWPE) MW 3-6 Mg mol^{-1}, MMAO-12 solution (7 wt.% aluminum in toluene ca. 2.3 mmol/mL), *tert*-butyl alcohol, and sodium bicarbonate were purchased from Sigma Aldrich, USA. Methanol, USP grade, was obtained from Pharmco USA, and ACS grade hydrochloric acid was purchased from Spectrum Chemical, USA. Water was purified to resistivity ≥16.7 MΩ using a Sybron Barnstead purification system. Sulfuric acid hydrolyzed CNCs from wood (1.00 wt%

sulfur, ca. 300 mmol kg^{-1})[50] were found to be 90 ± 40 nm length and 7 ± 2 nm height, as shown in **Figure 2.3** and **Figure S2.4**, and were obtained as a 11.8 wt% gel in water from the Forest Products Laboratory, University of Maine USA. The 1,1'-bis(bromodimethylsilyl)zirconocene dibromide catalyst **1** was made using previously described methods.[29]

2.4.2 CNC Aerogel Formation:

CNCs were diluted to 60 mg mL^{-1} with deionized water and dispersed at 90 °C with vigorous stirring followed by sonication in a Branson 2800 Ultrasonic bath. This process was repeated until the CNC dispersion appeared homogeneous when viewed with crossed-polarized films. Aqueous CNC dispersions (5 mL), measured by syringe, were then placed into 50 mL Schlenk flasks. Sealed flasks were frozen in liquid nitrogen and vacuum-freeze-dried while gradually warming over 8 h using a conventional vacuum pump. After the samples had reached a pressure of 30 mTorr or less, they were dried using the same vacuum system for at least 8 h at 80 °C, again a final pressure of 30 mTorr or less was reached.

One sample (Entry 1, **Table 2.1**) was prepared as above, except that *tert*-butanol (45 mL) and (15 mL) of a 10 mg mL^{-1} aqueous dispersion of CNCs (150 mg) were combined, in order to compare our aqueous protocol to a previously published method.[34]

2.4.3 Centrifuge-Washing:

To each aerogel (300 mg CNCs), contained in the same Schlenk flask used for its preparation, anhydrous toluene (20 mL) was added under a nitrogen atmosphere. A stir bar was fitted, and the aerogel was ground into a powder (slurry) by magnetic stirring overnight. The catalyst **1** (4 mg, 6.1 μmol) was then added as a toluene solution, and the mixture was stirred overnight at 30 °C to adsorb the metallocene onto the CNCs. For Entry

1, catalyst **1** (2 mg, 3.1 μmol) was added to keep the ratio of CNCs to catalyst the same. Under air, the slurry was transferred to a 50 mL conical centrifuge tube. Hexanes was added to reach a total volume of 35 mL. The tube was inserted into an Eppendorf 5810 centrifuge fitted with an FA-45-6-30 rotor and spun at 10,000 rpm for 20 min to form a pellet. The supernatant was decanted and discarded. Additional washes with hexane were conducted for each experiment as shown in **Table 2.1**. Each wash included a cycle of vortex mixing, centrifugation, and decantation of the supernatant. CNC aerogels for Entries 1-5 were vacuum dried to remove hexanes and stored in a nitrogen glovebox while, the aerogel for Entry 6 was allowed to dry under air in a centrifuge tube. The sample was not finely divided, so toluene (10 mL) was added, the sample was agitated briefly, and the toluene was removed under vacuum to obtain a dry powder, which was stored in a nitrogen glovebox. For Entries 7-9, samples were left wet with the hexanes that remained after the last decantation, and these were used directly in the ensuing polymerization experiments.

2.4.4 Polymerization of Ethylene:

Entries 7-9 (**Table 2.1**) were conducted using the entire sample of CNCs that remained after solvent washing (see above). To each 50 mL Schlenk flask containing the catalyst-infused CNCs (nominally 300 mg), dry toluene (20 mL), and MMAO-12 solution (3-mL, 6.9 mmol Al) solution was added. A stir bar was fitted, and the flask was equilibrated with a water bath at 25 °C. Ethylene was introduced into the flask using a needle, and polymerization ensued for 0.5 h. Excess pressure was released through a mineral oil bubbler, thereby maintaining the reaction at atmospheric pressure. Reactions were then quenched with acidified methanol (prepared from concentrated aqueous HCl (5

mL) and methanol (45 mL)). The resulting polymer was collected on a medium glass fritted funnel, washed with methanol, and dried under vacuum.

Polymerizations of Entries 2-4 and 6 (**Table 2.1**) were conducted using catalyst bound CNCs (20 mg) weighed into each 50-mL Schlenk flask in a nitrogen glovebox. Then, toluene (20 mL) and MMAO-12 solution (0.2 mL, 0.46 mmol Al) was added to each flask. A stir bar was fitted, and the reaction mixture was stirred and equilibrated with a water bath at 25 °C. Ethylene was introduced into the flask using a needle, and polymerization ensued for 0.5 h, except for polymerization of Entry 3, in which polymerization ensued for 1 h. The reactions were quenched, and the polymer composites collected and washed as above.

Polymerization of Entry 5 was conducted as Entries 2-4 and 6, with the exception of being done in a 100-mL Schlenk flask fitted with a stir bar with catalyst bound CNCs (94 mg), MMAO-12 solution (0.94 mL, 2.26 mmol Al), and toluene (100 mL). To prevent oxidation of the CNCs after the final methanol rinse, the resin was placed in aqueous sodium bicarbonate solution (100 mg dissolved in 100 mL of water).

2.4.5 Scanning Electron Microscopy:

SEM images were obtained to determine the size of the CNC aerogel particles used prior to polymerization. This powder was used for Entries 2 and 3 (**Table 2.1**) and examined using a LEO Zeiss scanning electron microscope (SEM) with an in-lens detector at 3 keV. The sample was spread onto double-stick carbon tape on the SEM mount and then coated with 5 nm of iridium using a Leica sputter-coater. Images show that the CNC particles, prior to polymerization reactions, were nominally 1-20 microns in diameter **Figure 2.1**. Additional images of the cryo-microtomed surface of Entry 5 were prepared

and analyzed in the same manner (**Figure S2.2**). Micrographs revealed occasional voids in the processed films which likely negatively affected the elongation at break and yield strength of the composite materials.

2.4.6 X-ray Photoelectron Spectroscopy:

Dried CNCs from Entries 1-4 and 6 in **Table 2.1** were analyzed using X-ray photoelectron spectroscopy (XPS) on a PHI Versa Probe III. Samples were mounted on adhesive tape and transferred to the ultra-high vacuum chamber anaerobically. Spectra were acquired using a monochromatic Al Kα X-ray source at 100 W over a 1400 x 100 μm area at a 45° takeoff angle. A survey scan (280 eV pass energy) was acquired, followed by element scans (C, O, Br, Si, and Zr) using a 26-eV pass energy. These data were used to estimate elemental composition of the CNCs with adsorbed metallocene catalyst.

2.4.7 Film Processing:

Samples from the best fabrication method, Entries 2, 3, and 5 in **Table 2.1**, were pressed using a Carver press equipped with heating platens with 150 μm shims at 120 °C for 5 min at 1 metric ton and at 7 metric tons for 5 min, then cooled overnight at 7 metric tons (during the cooling period the pressure decreased from 7 to ca. 3 metric tons). The first control GHDPE-1 was processed in the same manner but milled beforehand in a Spex Cryomill for 9 minutes for good particle association. The UHMWPE sample from Sigma Aldrich was treated in the same manner at a higher pressing temperature (180 °C) and the second control GHDPE-2 was processed in this manner.

For the composites materials Entries 2, 3, 5 and GHDPE 1 a low temperature (120 °C) was chosen to obtain films to minimize the possibility of thermal degradation of the CNCs, and this process, heating and holding is important for understanding the thermal

history of these materials. For the UHMWPE, the lowest temperature capable of producing transparent cohesive films was chosen.

2.4.8 Dynamic Mechanical Thermal Analysis:

Three samples each from the polymers prepared in Entries 2, 3, 5, (**Table 2.1**) GHDPE-1, GHDPE-2, and the UHMWPE control sample films were cut into rectangular coupons greater than 10 mm length 3 mm width and 150 μm thickness with a razorblade. Samples were analyzed at 1 Hz frequency with a ca. 5 mm clamp distance with a set amplitude of 15 μm at a rate of 5 °C per minute in the temperature range of −150 °C to 160 °C using a TA Instruments DMA Q800 equipped with a tension clamp. Data for the temperature range −150 °C to 160 °C is shown in **Figure 2.4**. Above 160 °C the sample has melted. Entry 5 is omitted from **Figure 2.4** as it is well represented by Entry 2 at 6 vol% CNC content.

2.4.9 Tensile Testing:

Samples of UHMWPE and CNC PE composite Entry 5 (**Table 2.1**) were cut as dog bones with a 7 mm gauge length, 3 mm width, and measured thickness (ca. 150 μm) using a punch indent and gently tracing with a razorblade to ensure dog bone edges were clean. Samples were firmly clamped on an Instron Electroplus e1000 with a 1 kN load cell and were pulled in tensile mode at a rate of 5 mm/min until broken. The zero-strain point was set at 0.5 N force; Young's moduli were calculated from 0 to 1% strain using linear regression; yield stress was taken as the highest point on CNC/PE, GHDPE-1, and GHDPE-2 curves and as the highest point from 0 to 20% strain for UHMWPE; elongation at break was taken manually. Five samples were run for both commercial UHMWPE and

the CNC PE Composite Entry 5 **Table 2.1**, and representative curves are available in **Figure S2.6**.

2.4.10 Thermogravimetric Analysis (TGA):

Samples from Entries from **Table 2.1**, UHMWPE, and CNCs (ca. 8 mg) were analyzed using a TA Instruments TGAQ50, sweeping from room temperature to 600 °C at 20 °C min^{-1}, under nitrogen atmosphere. The CNC content was approximated using equations in **Figure S2.5** and thermogravimetric data in the Supplemental Information. **Equation S1** in **Figure S2.5** uses the volume fraction and the ratio of densities of PE and CNCs to convert to volume fraction of CNCs in the sample. **Equation S2** uses mass fractions from TGA data to approximate the mass fraction of CNCs.

2.4.11 Gel Permeation Chromatography:

Gel permeation chromatography was performed by TOSOH using an EcoSEC high temperature GPC system equipped with a refractive index detector. Tests were performed at 1.0 mL/min at 1.0-1.5 mg/mL in 1,2,4-trichlorobenzene on Entries 2, 3, and 7 (**Table 2.1**).

2.4.12 Atomic Force Microscopy:

All atomic force microscopy (AFM) images were obtained using a Veeco Multimode scanning probe AFM in dynamic mode. Films from polymerization Entry 3 (**Table 2.1**) were embedded in epoxy and cryo-polished on an RMC cryo-microtome by cutting 250 nm sections of polymer. The commercial UHMWPE sample was polished in the same manner without prior embedding in epoxy. To compare these images to neat CNCs, one drop of an aqueous CNC solution (0.1 mg/mL) was placed onto a silicon wafer

and allowed to dry under air. Each of these samples were used to obtain the micrographs shown in **Figure 2.3**.

2.4.13 Differential Scanning Calorimetry:

Films from Entries 2, 3, GHDPE-1, GHDPE-2 and neat UHMWPE (ca. 5 mg) were analyzed using a TA Instruments DSCQ100, with a heat cool heat cycle at 10 °C/min from room temperature to 160 °C, −150 °C, and then 160 °C. Melting point data was taken using the initial peak melting temperature, and crystallization data was taken integrating the melt using TA Universal Analysis software for integration using 290 J/g as the 100% crystallinity PE basis.[40]

2.4.14 Washing Studies:

In order to ensure that our centrifuge washed polymerization experiments are entirely heterogeneous, CNCs that were treated with metallocene **1** were washed at least twice with hexane to remove any excess metallocene **1**. The supernatant from the second hexane wash from Entries 7-9 (**Table 2.1**) was tested for ethylene polymerization activity (a sensitive test for the presence of a soluble metallocene!) by adding MMAO-12 solution (3 mL, 6.9 mmol Al), bubbling ethylene through the solution for 0.5 h at room temperature, quenching in acidified methanol, collecting any PE product on a filter, and drying under vacuum. For these three experiments, 950 mg, 11 mg, and 68 mg of PE were obtained. In the case of Entry 7, in which 950 mg of PE was produced, a third hexane wash was carried out, which gave a supernatant that was inactive toward ethylene polymerization. We conclude that two washes with hexane is sufficient to ensure that no soluble metallocene remained.

Acknowledgments:

The authors thank Dr. Xu Feng and the Surface Analysis Laboratory at Virginia Tech for the XPS analysis, Steve McCartney for assistance with AFM micrographs, and Adwoa Baah-Dwomoh for assistance with tensile testing. The authors would also like to gratefully thank Ilir Koliqi and Wei Lu from TOSOH Bioscience LLC for the difficult GPC of the PE/CNC system. Work was completed with support from the Institute for Critical and Applied Sciences (ICTAS) Doctoral Scholars Program, the Material Science and Engineering Department and Chemistry Departments at Virginia Tech.

References:

1. Bhattacharya, M., Polymer Nanocomposites—A Comparison between Carbon Nanotubes, Graphene, and Clay as Nanofillers. *Materials* **2016,** *9* (4), 262.
2. Moon, R. J.; Martini, A.; Nairn, J.; Simonsen, J.; Youngblood, J., Cellulose nanomaterials review: structure, properties and nanocomposites. *Chemical Society Reviews* **2011,** *40* (7), 3941-3994.
3. Trache, D.; Hussin, M. H.; Haafiz, M. K. M.; Thakur, V. K., Recent progress in cellulose nanocrystals: sources and production. *Nanoscale* **2017,** *9* (5), 1763-1786.
4. Favier, V.; Cavaille, J. Y.; Canova, G. R.; Shrivastava, S. C., Mechanical percolation in cellulose whisker nanocomposites. *Polymer Engineering & Science* **1997,** *37* (10), 1732-1739.
5. Sapkota, J.; Jorfi, M.; Weder, C.; Foster, E. J., Reinforcing poly (ethylene) with cellulose nanocrystals. *Macromolecular rapid communications* **2014,** *35* (20), 1747-1753.
6. Nagalakshmaiah, M.; El Kissi, N.; Dufresne, A., Ionic Compatibilization of Cellulose Nanocrystals with Quaternary Ammonium Salt and Their Melt Extrusion with Polypropylene. *Acs Applied Materials & Interfaces* **2016,** *8* (13), 8755-8764.
7. Nowlin, T. E., Global Polyethylene Business Overview. In *Business and Technology of the Global Polyethylene Industry*, John Wiley & Sons, Inc.: 2014; pp 1-45.
8. Capadona, J. R.; Van Den Berg, O.; Capadona, L. A.; Schroeter, M.; Rowan, S. J.; Tyler, D. J.; Weder, C., A versatile approach for the processing of polymer nanocomposites with self-assembled nanofibre templates. *Nat Nanotechnol* **2007,** *2* (12), 765-9.
9. Junior de Menezes, A.; Siqueira, G.; Curvelo, A. A. S.; Dufresne, A., Extrusion and characterization of functionalized cellulose whiskers reinforced polyethylene nanocomposites. *Polymer* **2009,** *50* (19), 4552-4563.
10. Dufresne, A., *Nanocellulose: from nature to high performance tailored materials*. Walter de Gruyter GmbH & Co KG: 2017.
11. Kaminsky, W., Metallocene Based Polyolefin Nanocomposites. *Materials* **2014,** *7* (3), 1995-2013.

12. Kaminsky, W., Zirconocene catalysts for olefin polymerization. *Catalysis Today* **1994,** *20* (2), 257-271.
13. Rosehr, A.; Luinstra, G. A., Polypropylene composites with finely dispersed multi-walled carbon nanotubes covered with an aluminum oxide shell. *Polymer* **2017,** *120*, 164-175.
14. Stürzel, M.; Kempe, F.; Thomann, Y.; Mark, S.; Enders, M.; Mülhaupt, R., Novel graphene UHMWPE nanocomposites prepared by polymerization filling using single-site catalysts supported on functionalized graphene nanosheet dispersions. *Macromolecules* **2012,** *45* (17), 6878-6887.
15. Boggioni, L.; Scalcione, G.; Ravasio, A.; Bertini, F.; D'Arrigo, C.; Tritto, I., Ethylene-co-Norbornene Copolymers Grafted Carbon Nanotube Composites by In Situ Polymerization. *Macromolecular chemistry and physics* **2012,** *213* (6), 627-634.
16. Bahuleyan, B. K.; Atieh, M. A.; De, S. K.; Jabarulla Khan, M.; Al-Harthi, M. A., Easy one-pot method to control the morphology of polyethylene/carbon nanotube nanocomposites using metallocene catalysts. *Journal of Polymer Research* **2012,** *19* (2), 9744.
17. Ravasio, A.; Boggioni, L.; Tritto, I.; D'arrigo, C.; Perico, A.; Hitzbleck, J.; Okuda, J., A non-PFT (polymerization filling technique) approach to poly (ethylene-co-norbornene)/MWNTs nanocomposites by in situ copolymerization with scandium half-sandwich catalyst. *Journal of Polymer Science Part A: Polymer Chemistry* **2009,** *47* (21), 5709-5719.
18. Toti, A.; Giambastiani, G.; Bianchini, C.; Meli, A.; Bredeau, S.; Dubois, P.; Bonduel, D.; Claes, M., Tandem Action of Early− Late Transition Metal Catalysts for the Surface Coating of Multiwalled Carbon Nanotubes with Linear Low-Density Polyethylene. *Chemistry of Materials* **2008,** *20* (9), 3092-3098.
19. Kaminsky, W.; Funck, A.; Klinke, C., In-situ Polymerization of Olefins on Nanoparticles or Fibers by Metallocene Catalysts. *Topics in Catalysis* **2008,** *48* (1), 84.
20. Trujillo, M.; Arnal, M.; Müller, A. J.; Bredeau, S.; Bonduel, D.; Dubois, P.; Hamley, I.; Castelletto, V., Thermal fractionation and isothermal crystallization of polyethylene nanocomposites prepared by in situ polymerization. *Macromolecules* **2008,** *41* (6), 2087-2095.
21. Bonduel, D.; Mainil, M.; Alexandre, M.; Monteverde, F.; Dubois, P., Supported coordination polymerization: a unique way to potent polyolefin carbon nanotube nanocomposites. *Chemical Communications* **2005,** (6), 781-783.
22. Funck, A.; Kaminsky, W., Polypropylene carbon nanotube composites by in situ polymerization. *Composites Science and Technology* **2007,** *67* (5), 906-915.
23. Hees, T.; Zhong, F.; Rudolph, T.; Walther, A.; Mülhaupt, R., Nanocellulose Aerogels for Supporting Iron Catalysts and In Situ Formation of Polyethylene Nanocomposites. *Advanced Functional Materials* **2017,** *27* (11), 1605586-n/a.
24. Alexandre, M.; Martin, E.; Dubois, P.; Marti, M. G.; Jérôme, R., Polymerization-Filling Technique: An Efficient Way To Improve the Mechanical Properties of Polyethylene Composites. *Chemistry of Materials* **2001,** *13* (2), 236-237.
25. Eberhardt, A. M.; Ferreira, M. L.; Damiani, D. E., Heterogeneization of polymerization catalysts on natural substances. *Polymer Engineering & Science* **2001,** *41* (6), 946-954.

26. Lahiji, R. R.; Xu, X.; Reifenberger, R.; Raman, A.; Rudie, A.; Moon, R. J., Atomic Force Microscopy Characterization of Cellulose Nanocrystals. *Langmuir* **2010,** *26* (6), 4480-4488.
27. Cowie, J.; BILEK, E.; Wegner, T. H.; Shatkin, J. A., Market projections of cellulose nanomaterial-enabled products. *Tappi Journal* **2014,** *13* (6).
28. Cheng, X.; Lofthus, O. W.; Deck, P. A., Ethylene polymerization using silica-supported zirconocene dibromide/methylalumoxane catalysts. *Journal of Molecular Catalysis A: Chemical* **2004,** *212* (1), 121-126.
29. Deck, P. A.; Fisher, T. S.; Downey, J. S., Boron−Silicon Exchange Reactions of Boron Trihalides with Trimethylsilyl-Substituted Metallocenes. *Organometallics* **1997,** *16* (6), 1193-1196.
30. Mälder. Ziegler-Natta-Polymerisation unter Verwendung von Stärke und Stärkeabbauprodukten. University of Hamburg, 1987.
31. SABIC, SABIC HDPE F4520: High Density Polyethylene. Revision 20190506, 2018.
32. SABIC, SABIC HDPE M864SE: High Density Polyethylene. Revision 20181012, 2018.
33. De France, K. J.; Hoare, T.; Cranston, E. D., Review of Hydrogels and Aerogels Containing Nanocellulose. *Chemistry of Materials* **2017,** *29* (11), 4609-4631.
34. Shamskar, K. R.; Heidari, H.; Rashidi, A., Preparation and evaluation of nanocrystalline cellulose aerogels from raw cotton and cotton stalk. *Industrial Crops and Products* **2016,** *93*, 203-211.
35. Impens, N. R. E. N.; van der Voort, P.; Vansant, E. F., Silylation of micro-, meso- and non-porous oxides: a review. *Microporous and Mesoporous Materials* **1999,** *28* (2), 217-232.
36. Eyley, S.; Thielemans, W., Surface modification of cellulose nanocrystals. *Nanoscale* **2014,** *6* (14), 7764-7779.
37. Sacui, I. A.; Nieuwendaal, R. C.; Burnett, D. J.; Stranick, S. J.; Jorfi, M.; Weder, C.; Foster, E. J.; Olsson, R. T.; Gilman, J. W., Comparison of the properties of cellulose nanocrystals and cellulose nanofibrils isolated from bacteria, tunicate, and wood processed using acid, enzymatic, mechanical, and oxidative methods. *ACS Appl Mater Interfaces* **2014,** *6* (9), 6127-38.
38. Hlatky, G. G.; Upton, D. J., Supported Ionic Metallocene Polymerization Catalysts. *Macromolecules* **1996,** *29* (24), 8019-8020.
39. Klebe, J.; Finkbeiner, H., Silyl celluloses: a new class of soluble cellulose derivatives. *Journal of Polymer Science Part A: Polymer Chemistry* **1969,** *7* (7), 1947-1958.
40. Hatakeyama, T.; Liu, Z., *Handbook of Thermal Analysis*. John Wiley and Sons, Inc: Chichester, 1998.
41. Miao, W.; Zhu, H.; Duan, T.; Chen, H.; Wu, F.; Jiang, L.; Wang, Z., High-density polyethylene crystals with double melting peaks induced by ultra-high-molecular-weight polyethylene fibre. *Royal Society Open Science* **2018,** *5* (7), 180394.
42. Molefi, J. A.; Luyt, A. S.; Krupa, I., Comparison of the influence of copper micro- and nano-particles on the mechanical properties of polyethylene/copper composites. *Journal of Materials Science* **2009,** *45* (1), 82.

43. Tavman, I.; Krupa, I.; Omastova, M.; Sarikanat, M.; Novak, I.; Sever, K.; Ozdemir, I.; Seki, Y.; Podhradska, S.; Moskova, D., Effects of conductive graphite filler loading on physical properties of high-density polyethylene composite. *Polymer Composites* **2012,** *33* (7), 1071-1076.
44. Bykova, I.; Weinhardt, V.; Kashkarova, A.; Lebedev, S.; Baumbach, T.; Pichugin, V.; Zaitsev, K.; Khlusov, I., Physical properties and biocompatibility of UHMWPE-derived materials modified by synchrotron radiation. *Journal of materials science. Materials in medicine* **2014,** *25* (8), 1843-1852.
45. Lippits, D. R.; Rastogi, S.; Talebi, S.; Bailly, C., Formation of Entanglements in Initially Disentangled Polymer Melts. *Macromolecules* **2006,** *39* (26), 8882-8885.
46. Huang, Y.-F.; Xu, J.-Z.; Zhang, Z.-C.; Xu, L.; Li, L.-B.; Li, J.-F.; Li, Z.-M., Melt processing and structural manipulation of highly linear disentangled ultrahigh molecular weight polyethylene. *Chemical Engineering Journal* **2017,** *315*, 132-141.
47. Mariano, M.; El Kissi, N.; Dufresne, A., Cellulose nanocrystals and related nanocomposites: Review of some properties and challenges. *Journal of Polymer Science Part B: Polymer Physics* **2014,** *52* (12), 791-806.
48. Xia, X.-C.; Yang, W.; Liu, Z.-Y.; Zhang, R.-Y.; Xie, D.-D.; Yang, M.-B., Strong shear-driven large scale formation of hybrid shish-kebab in carbon nanofiber reinforced polyethylene composites during the melt second flow. *Physical Chemistry Chemical Physics* **2016,** *18* (44), 30452-30461.
49. Koniuszewska, A. G.; Kaczmar, J. W., Application of polymer based composite materials in transportation. *Progress in Rubber Plastics and Recycling Technology* **2016,** *32* (1), 1-24.
50. Venkatraman, P.; Gohn, A. M.; Rhoades, A. M.; Foster, E. J., Developing high performance PA 11/cellulose nanocomposites for industrial-scale melt processing. *Composites Part B: Engineering* **2019,** *174*, 106988.

2.5 Supporting Information:

In situ dispersion and polymerization of polyethylene cellulose nanocrystal-based nanocomposites

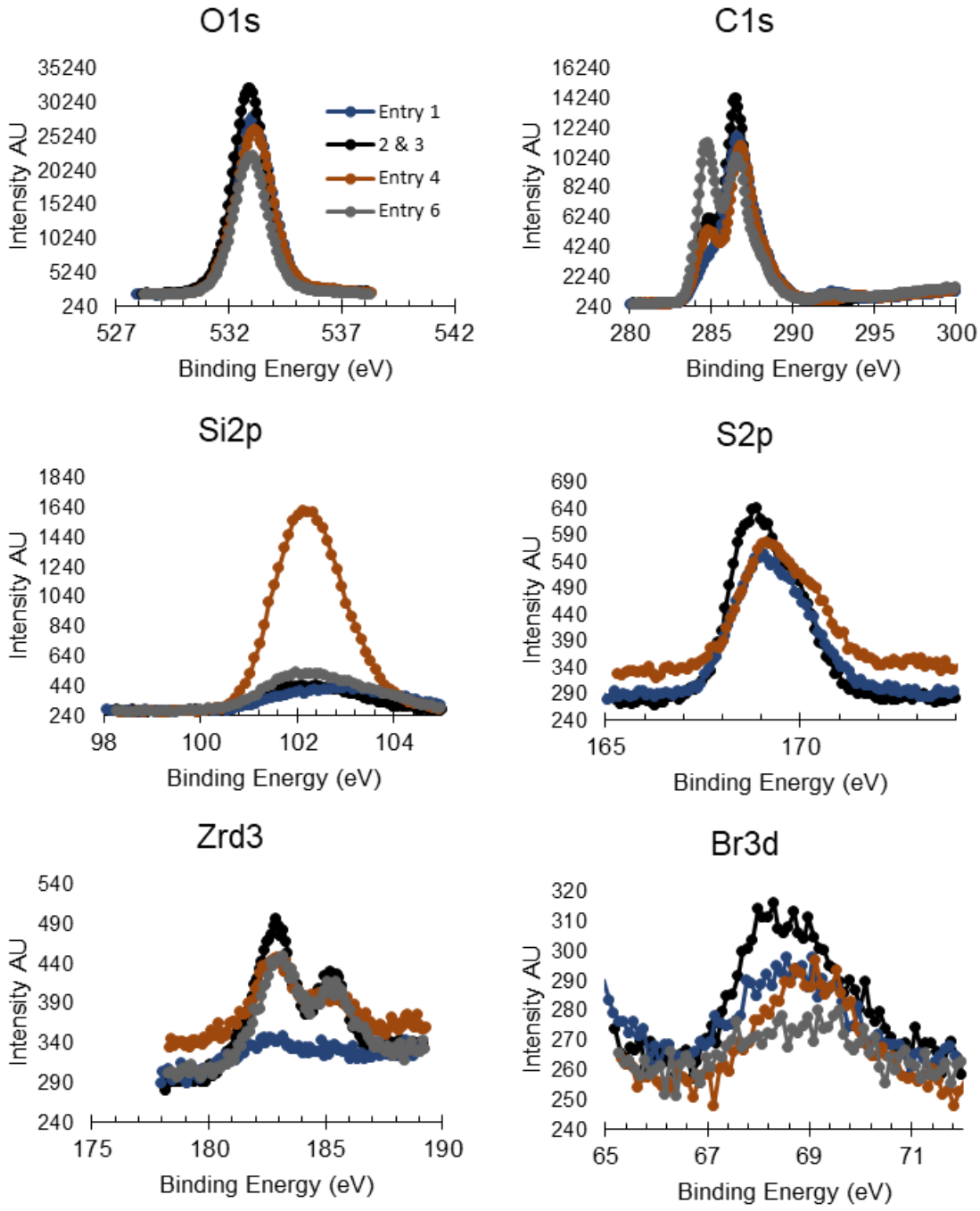

Figure S2.1: XPS data for Entries 1-4 and 6 show the elemental composition of the samples and verify that there is zirconium present on the surface of the functionalized CNCs.

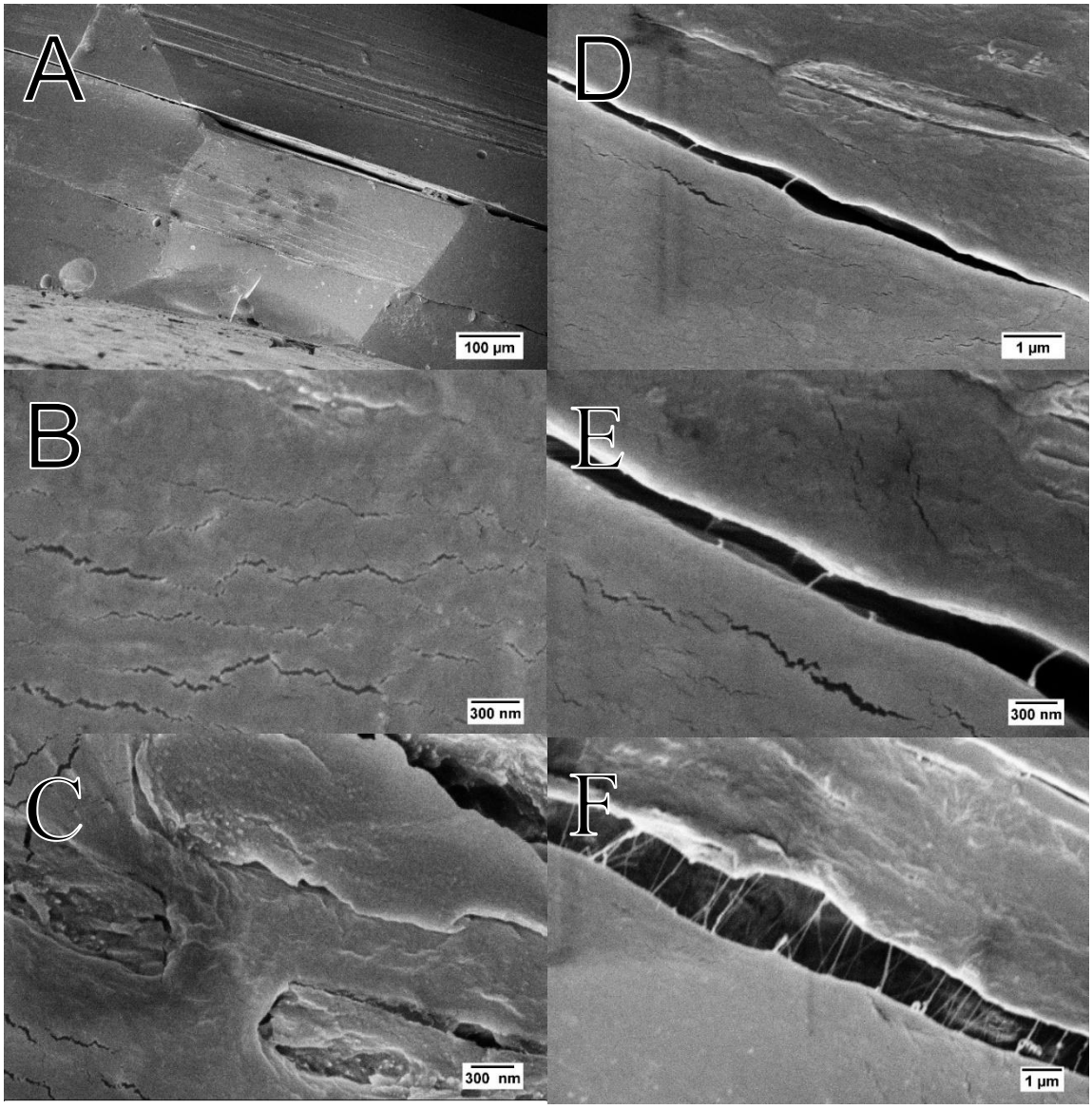

Figure S2.2: These additional SEM images showed little evidence of aggregation and dispersion. The SEM images above are of the crymicrotomed surface of Entry 3 (**Table 2.1)** 6 vol% CNCs. A) An overall view of the cryomicrotomed surface, B) the general surface of the polymer. C) A region that shows potential dispersion of sharp spikes. Images D, E, and F show thin spindles of fibrous materials that are likely too long to be CNCs within the polymer.

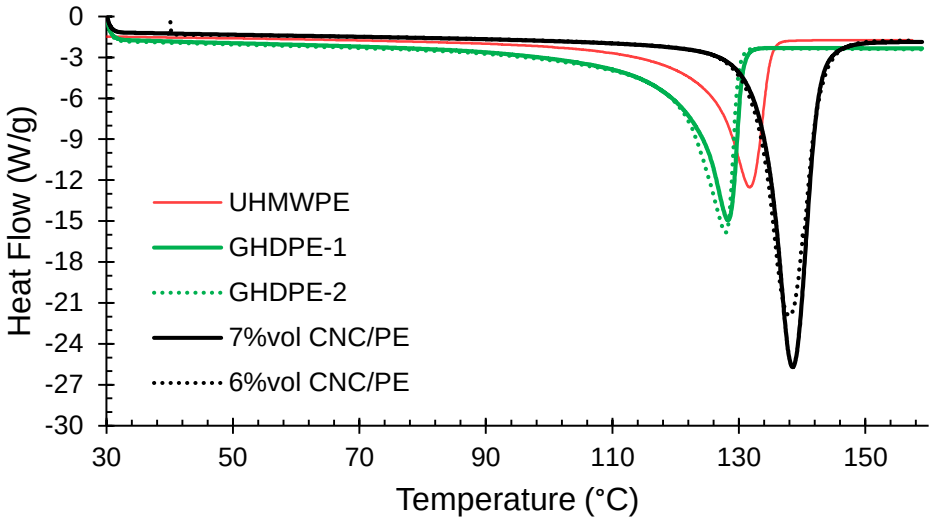

Figure S2.3: Shown above is the first heating on a DSC on CNC composite Entry 2, Entry 3, UHMWPE, GHDPE-1, and GHDPE-2 films (**Table 2.1**). The samples were heated at 10 °C min^{-1}. Melting points and crystallinity was measured using TA Universal Analysis software.

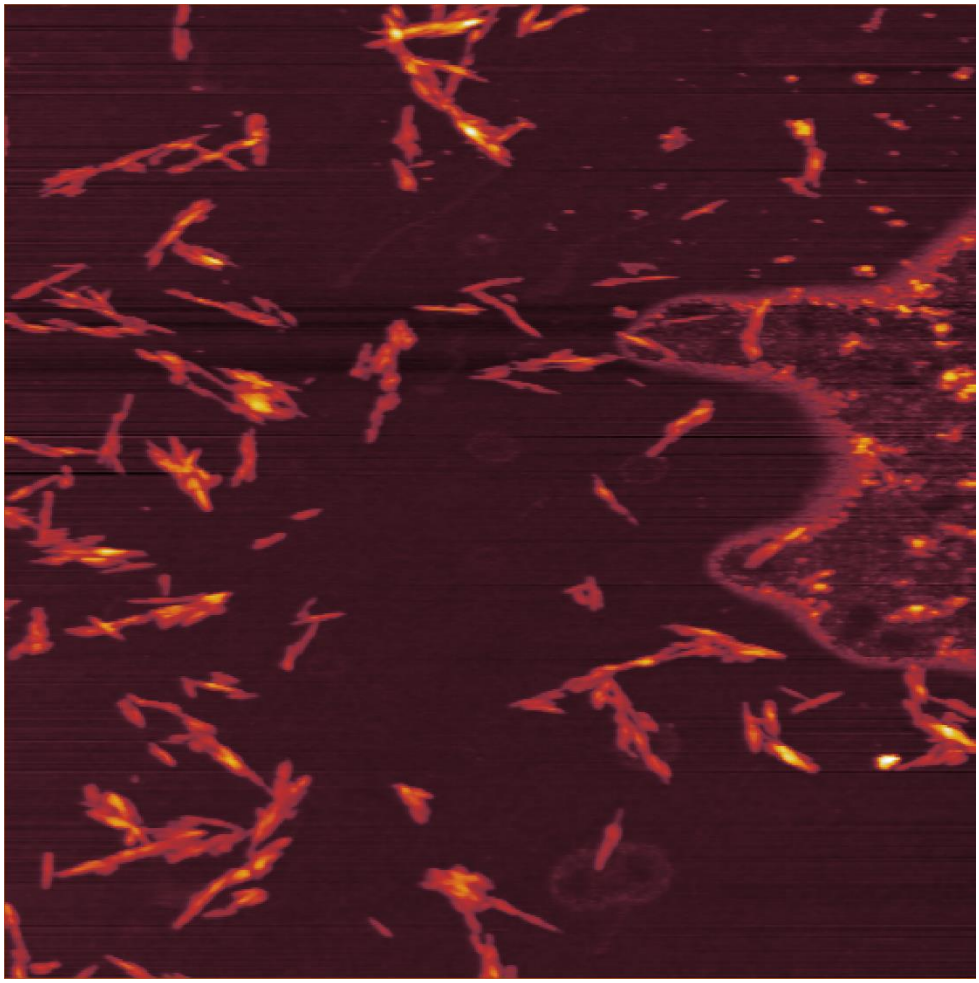

Figure S2.4: CNCs were measured using height and length to determine dimensions 90 ± 40 nm in length and 7 ± 2 nm in height using Gwyddion scanning probe microscopy software.

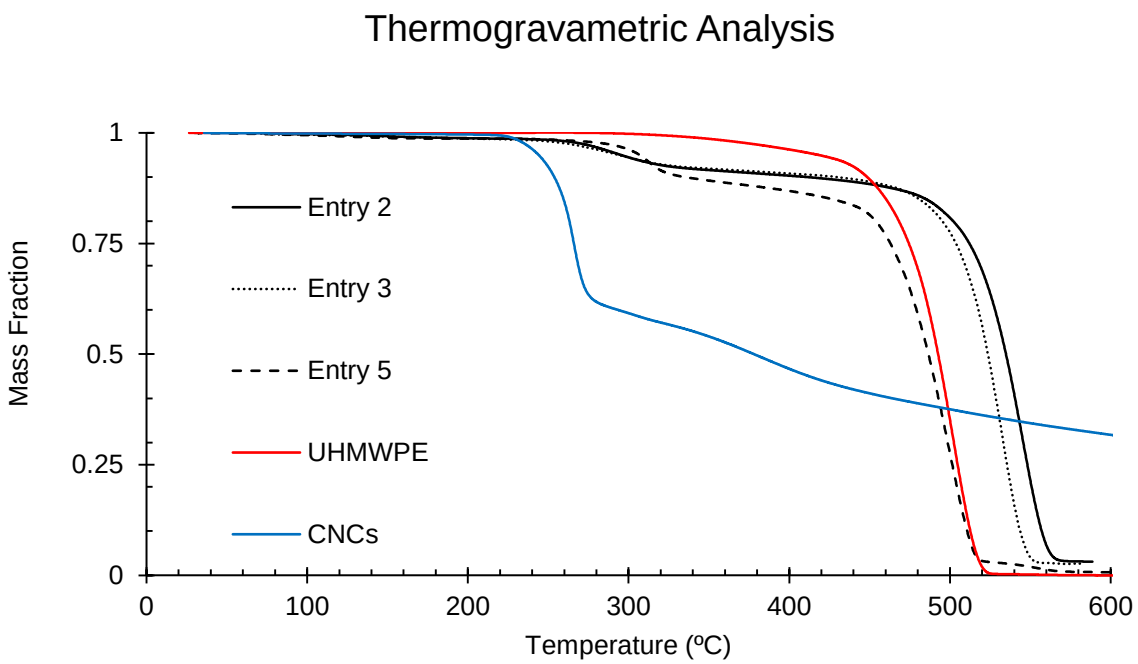

$$v_{CNCs} = \frac{0.95}{1.6} m_{CNCs} \quad (1)$$

$$m_{CNCs} = m_{200\,°C} - m_{375\,°C} + m_{575\,°C} m_{200°C} \quad (2)$$

Figure S2.5: Thermogravimetric analysis was performed on Entries 2, 3, 5, UHMWPE, and CNCs (**Table 2.1**). To approximate the amount of CNCs in the sample, equations assuming there was minimal CNC degradation in the flat areas were used to approximate the amount of CNCs in Entries 2, 3, and 5 as a volume fraction. The text *v* refers to volume fraction, *m* refers to mass fraction, the subscripts, temperatures, refers to the mass at which the temperature was taken, and 0.95[1] g·cm^{-1}and 1.6[2] g·cm^{-1} are approximate density values for polyethylene an CNCs respectively.

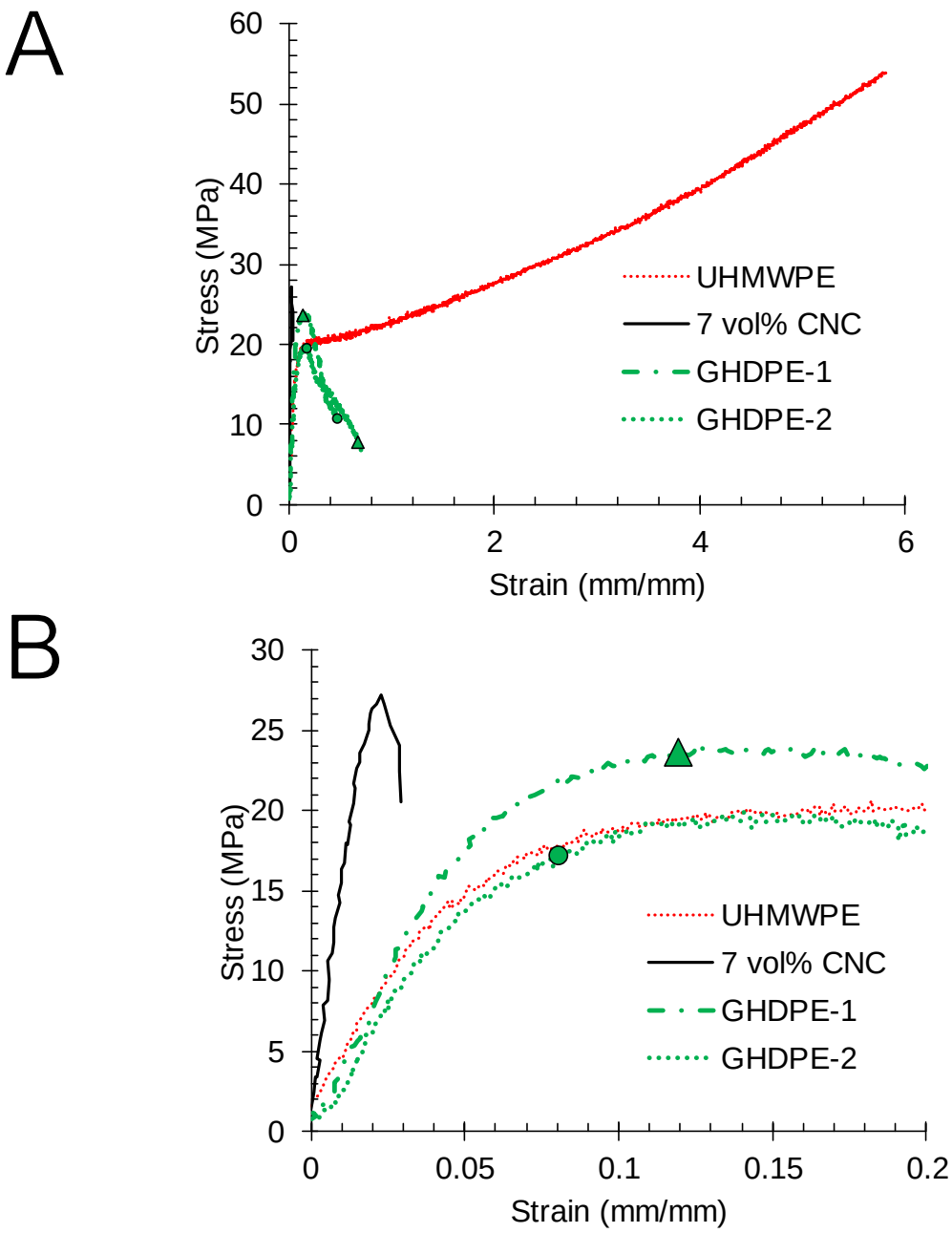

Figure S2.6: Tensile data with representative curves of the samples is presented as the full curves **A** and shorter curves that highlight yield strength and Young's Modulus **B**. GHDPE 1 and GHDPE 2 are differentiated with ▲(GHDPE-1) and ● (GHDPE-2).

References:

1. Lu, N.; Oza, S., A comparative study of the mechanical properties of hemp fiber with virgin and recycled high density polyethylene matrix. *Composites Part B: Engineering* **2013,** *45* (1), 1651-1656.
2. Moon, R. J.; Martini, A.; Nairn, J.; Simonsen, J.; Youngblood, J., Cellulose nanomaterials review: structure, properties and nanocomposites. *Chemical Society Reviews* **2011,** *40* (7), 3941-3994.

Chapter 3: Linear low-density polyethylene cellulose nanocrystal composites from *in-situ* polymerization mediated by an anchored metallocene catalyst

This work is presently under consideration for publication in *Polymer International*.

In this work I acknowledged the contributions of my fellow co-authors Sarita A. Hough, Kenneth Knott, Wei Lu, Paul A. Deck, and E. Johan Foster. All co-authors contributed with editing. Sarita A. Hough and Paul A. Deck synthesized the metallocene catalyst 1,1'-bis(bromodimethylsilyl)zirconocene dibromide, Kenneth Knott performed necessary NMR acquisition, and Wei Lu graciously provided GPC analysis. E. Johan Foster and Paul A. Deck contributed ideas and critical evaluation of this work.

Linear low-density polyethylene cellulose nanocrystal composites from *in-situ* polymerization mediated by an anchored metallocene catalyst

Keith D. Hendren, Sarita A. Hough, Kenneth Knott, Wei Lu, Paul A. Deck, and E. Johan Foster

Abstract:

Cellulose nanocrystals (CNCs) were functionalized with different loadings of metallocene catalyst and subjected to *in situ* polymerization with ethylene and 1-hexene to yield linear low-density polyethylene (LLDPE) polymer matrix composites (PMCs). CNC content was analyzed with thermogravimetric analysis (TGA), confirming that the PMCs varied in their CNC loadings from 3.6 wt% to 11.4 wt%. Differential scanning calorimetric (DSC), gel permeation chromatographic (GPC), and nuclear magnetic resonance spectroscopic (NMR) analyses revealed that the LLDPE (matrix) components of these PMCs shared similar physical properties. Dynamic mechanical analysis (DMA) showed a general increase in the storage modulus of the PMCs with increasing CNC content. These relative differences in storage modulus were even more evident at higher temperatures. Uniaxial tensile testing of the PMCs found a notable increase in Young's modulus between the 3.6 wt% CNC PMC (240 ± 50 MPa) and 11.4 wt% CNC PMC (391 ± 7 MPa), while the elongation at break decreased from the 3.6 wt% CNC PMC (400% ± 90%) to the 11.4 wt% CNC PMC (70% ± 10%). All PMCs showed similar yield strengths of ca. 10 MPa. These mechanical properties showed that the method of dispersing CNCs in LLDPE reported herein affords the highest moduli reported thus far in CNC-LLDPE PMCs. The ability of the catalyst to incorporate comonomer opens the window of application for these materials.

3.1 Introduction:

Nanomaterials, defined as materials that have at least one dimension in the nanoscale (0-100 nm), are often incorporated into polymers creating polymer matrix composites (PMCs). Reasons for creating PMCs can be to improve polymer properties including reinforcement, conductivity, antibacterial function, fluid transport, among others.[1] Nanomaterials are small enough (less than 1 μm) to provide significant reinforcement,[2] and they can be randomly oriented and reinforce a material equally in all directions.[3] Nanoparticles with strong attractive forces can interact with one another favorably leading to reinforcement even when the matrix and filler have different surface chemistry.[4] For example, hydrophobic rubber latex was significantly reinforced by interactions among dispersed hydrophilic cellulose nanocrystals (CNCs).[4] CNCs are an especially promising rod-shaped filler material having a high elastic modulus (110-220 MPa), low density (~1.6 g cm^3), high aspect ratios, and a tendency to reinforce materials in all directions unlike glass fibers or macroscopic cellulose fibers which tend to be highly directional.[3, 5]

Polyethylene (PE), the world's highest-volume polymer, is a low cost material with excellent chemical resistance.[6] However, both HDPE and LLDPE grades often suffer from a low modulus, which presents an opportunity to improve on this limitation by introducing filler materials such as mined clays and natural fibers.[7-9] Natural fibers are the most common bio-renewable filler added to HDPE and LLDPE creating PMCs which can be commercially used for decking boards.[7] However, a study found that more than 20 wt% natural fiber content was required to reinforce the LLDPE matrix.[10]

In contrast to natural fibers, studies have found that CNCs reinforce PE at filler loadings well below 20 wt%. PE variants that have been reinforced with CNCs include: low-density polyethylene (LDPE),[11-14] high density polyethylene (HDPE),[15] and linear low-density polyethylene (LLDPE).[12, 16] Creating CNCs-PE PMCs involves methods such as solvent casting with functional groups,[12] rollerblade or melt mixing unfunctionalized CNCs,[11, 16] rollerblade or melt mixing functional CNCs,[14, 17] or the solvent exchange or templating approach.[13]

An emerging approach toward incorporation of nanomaterials into polymer matrices is by polymerizing monomers near the surface of the nanomaterial.[15, 18-24] Our preliminary report described a new method to incorporate CNCs into an HDPE matrix to produce a PMC.[15] This was accomplished by covalently bonding a metallocene catalyst to the CNCs, washing to remove any small fraction of soluble catalyst, slurrying the metallocene-functionalized CNCs in toluene, adding a co-catalyst, and initiating polymerization by of the introduction of ethylene.[15] This method produced an CNC-HDPE PMC under mild experimental conditions (1 atm of ethylene and 50 °C), and mechanical testing showed an increase in Young's modulus of the HDPE due to the presence of well-dispersed CNCs.[15]

In the present study, we show that the CNC-LLDPE PMCs produced from *in situ* polymerization likewise have a higher Young's moduli than the previous leading method for producing CNC-LLDPE PMCs, which was solvent casting 2-ureido-4[1H]pyrimidinone (UPy) functionalized CNCs with LLDPE.[12] Additionally, the *in situ* polymerization PMCs have comparable mechanical properties compared to other LLDPE-

CNC PMCs that were functionalized with hydrophilic salts then mixed by twin screw extrusion (TSE).[16]

3.2 Experimental:

This section contains procedures that were performed to create the catalyst **1** functionalized CNCs (C1-CNCs) and the resulting CNC-LLDPE PMCs. This section also describes the procedures and instruments used to obtain analytical data.

3.2.1 Materials and Equipment:

Sodium bicarbonate, *tert*-butyl alcohol (TBA), 1,2,4-trichlorobenzene, chromium(III) acetylacetonate, modified methylalumoxane (MMAO-12, 7% solution in toluene), and a commercial LLDPE sample were purchased from Millipore Sigma. Research grade ethylene from Praxair was used without further purification. Aqueous CNC dispersions from sulfuric acid-hydrolyzed wood pulp were obtained from the University of Maine Forest Products laboratory and have dimensions of 90 ± 40 nm in length by 7 ± 2 nm in height.[15, 25] Methanol was purchased from Pharmco. Concentrated aqueous hydrochloric acid was purchased from Spectrum Chemicals. Tetrachloroethane-d_2 was purchased from Cambridge Isotope Laboratories. ACS grade toluene from Fisher Scientific was distilled from sodium and benzophenone ketyl under nitrogen. Hexanes of HPLC grade from Fisher Scientific and 1-hexene of 97% purity from Millipore Sigma were purified by distillation from calcium hydride (Alfa Aesar) under nitrogen. The anchoring catalyst 1,1'-bis(bromodimethylsilyl)zirconocene dibromide (catalyst **1**) was synthesized as previously described.[26]

3.2.2 CNC Aerogel Preparation:

A 60-mg mL^{-1} dispersion of CNCs in water was prepared as previously described.[15] A 500-mL Schlenk flask was charged with 10 mL of the CNC dispersion and 20 mL of *tert*-butyl alcohol. The mixture was stirred magnetically for 15 min, and then the stir bar was removed from the flask. The flask was sealed with a glass stopper. The mixture, contained in the sealed flask, was frozen using liquid nitrogen for 0.5 h. Then, the flask was removed from the liquid nitrogen bath, and a vacuum was applied to the flask immediately. The vacuum was applied using a vacuum pump capable of reaching an ultimate vacuum of 0.030 torr. We wanted to warm this flask slowly to room temperature to sublime/evaporate the solvents gradually, so our initial plan was to lower this flask immediately into a large Dewar flask at room temperature and cover the Dewar with foam insulation. However, this procedure resulted in reproducible cracking of the flasks, possibly from a change in the packing structure of the ice with an isothermal pressure change. A successful approach involved instead holding the flask at room temperature for 30 minutes under vacuum to undergo partial warming, and then lowering it into the Dewar flask, covering it with foam insulation, and continued subliming/evaporating of the solvents for 24 h. This procedure resulted in removal of all visible solvent, without incident. To ensure complete removal of the volatiles, the vacuum was applied continuously for another 24 h at room temperature (without insulating the flask) and for 24 h at 80 °C using an oil bath.[15, 27]

3.2.3 Catalyst Immobilization on CNC Aerogel:

To the 500 mL Schlenk flask containing the CNC aerogel, prepared as above, 40 mL of freshly distilled toluene was added. A stir bar was inserted, and the mixture was stirred at ambient temperature for 15 h to pulverize the CNC aerogel.

In a nitrogen glovebox, a 2-mL septum-sealed vial containing 10-20 mg of catalyst **1** was prepared. Freshly distilled toluene (1 mL) was added to the vial using a syringe affording a colorless solution. To each of four CNC aerogel/toluene aerogel slurries, a different amount of catalyst **1** solution was added by syringe. The catalyst-functionalized CNC aerogel samples are designated by the mass of catalyst in milligrams followed by the mass of the CNC aerogel in milligrams. Catalyst **1** functionalized CNCs (C1-CNCs) aerogels produced included 2_600, 4_600, 8_600, and 16_600. Thus, for example, the C1-CNCs indicated as 2_600 were prepared by adsorbing 2 mg of catalyst **1** onto 600 mg of CNC aerogel. These reactions of the CNC aerogels with catalyst **1** proceeded for 24 h at 30 °C; notably, we previously found that this reaction at room temperature during winter months produced inactive CNCs.

Wash cycles were used to remove of soluble catalyst from C1-CNCs. The C1-CNC slurries were combined with dry hexanes to produce a ca. 1:1 mixture of toluene to hexanes and poured into 50-mL centrifuge tubes. The addition of hexane seemed to cause the C1-CNCs to sink more easily to the base of the tubes. Slurries in conical tubes were centrifuged at 10,000 RPM for 20 min with an Eppendorf 5810 centrifuge equipped with an FA-45-6-30 rotor; a pellet formed, and the supernatant was discarded. The packed pellet was combined with 35-mL of dry hexanes, vortex-mixed at 3,000 RPM to expose more C1-CNC surface to fresh solvent, centrifuged at 10,000 RPM for 20 min, and decanted

removing the supernatant from the pellet. This washing procedure was repeated a total of three times. Finally, each C1-CNC sample was transferred to a dry 50-mL Schlenk flask as a slurry in 20 mL of hexanes and dried under vacuum (0.03 torr) at room temperature. The flasks containing resulting powders were transferred to a nitrogen glovebox and these CNC aerogel powders were transferred to storage tubes.

3.2.4 Polymerization from Catalyst 1 Functionalized CNC Aerogel:

For each polymerization a flame-dried 100-mL flask equipped with a magnetic stir bar was charged with a sample of C1-CNCs in a nitrogen glovebox and sealed with a rubber septum. The amount of C1-CNCs used was such that each of the four polymerizations used 0.67 mg of catalyst; addition of catalyst and C1-CNC content in each reaction is clarified in **Table 3.1**. Each flask charged with C1-CNCs was connected to a nitrogen inlet, and 48 mL of toluene was injected. The C1-CNC toluene slurry was stirred at 50 °C in an oil bath, and MMAO-12 solution (1 mL) and 1-hexene (1 mL) were added. Ethylene was added to the slurry by a needle piercing the septum. Excess ethylene was released via the nitrogen inlet of the flask into a mineral oil bubbler. The reaction was maintained under these conditions for 30 min. The reaction was quenched with 45 mL of methanol mixed with 5 mL of concentrated aqueous hydrochloric acid. The precipitated composite material was collected on a Buchner funnel and washed with 100 mL of methanol then 100 mL of aqueous sodium bicarbonate solution (1 $mg \cdot mL^{-1}$). The resulting materials were dried at 80 °C under vacuum.

Catalyst 1 CNC aerogel label	CNC aerogel (mg)	Catalyst 1 on CNC aerogel (mg)	C1-CNCs in reactor (mg)	Catalyst 1 in reactor (mg)
2_600	600	2	200	0.67
4_600	600	4	100	0.67
8_600	600	8	50	0.67
16_600	600	16	25	0.67

Table 3.1: Catalyst **1** functionalized CNC aerogels (C1-CNCs) were developed by adding catalyst **1** to a CNC aerogel.

3.2.4 Melt Processing CNC-LLDPE PMC Resins:

Dried CNC-LLDPE PMCs were processed using a Carver laboratory press maintained at 120 °C. Melt pressing was performed by first thermally relaxing the PMC resins by sandwiching each between Kapton sheets with 250-µm shims for 5 min at 1 metric ton and then pressing the films at 7 metric tons for 5 min. Each CNC-LLDPE PMC resins flowed to become a ca. 100 µm thick film. These CNC-LLDPE PMC films were removed from the press immediately and peeled free from the Kapton once cooled.

3.2.5 X-ray Photoelectron Spectroscopy (XPS):

Elemental surface compositions of the C1-CNC aerogels were analyzed using X-ray photoelectron spectroscopy (XPS) performed with a PHI VERSA Probe III scanning XPS microscope using an Al K-alpha source (1486.6 eV). Each analysis included high resolution scans for silicon, oxygen, carbon, zirconium, and bromine.

3.2.6 Nuclear Magnetic Resonance Spectroscopy (NMR):

Dried CNC-LLDPE PMC samples (250-300 mg) were added to 10-mm NMR tubes along with a mixture of 5 vol% tetrachloroethane-d_2 in 95 vol% 1,2,4-trichlorobenzene and 20 mg of chromium(III) acetylacetonate. The contents of each NMR tube were heated to 120 °C until the LLDPE portions of the PMC resins were dissolved. The dissolved LLDPE was characterized at 135 °C on a Bruker Avance III NMR system (^{13}C at 125 MHz). Each

sample received between 3,300 and 16,000 scans, with a relaxation time of 2 s. To ensure quantitative results inverse gated decoupling was used.

3.2.7 Thermogravimetric Analysis (TGA):

Degradation profiles of each of the CNC-LLDPE PMC resins, a C1-CNC aerogel sample (8_600), and a sample of commercial LLDPE (obtained from Millipore Sigma) were analyzed on a TA Instruments TGA Q50. Each of the samples were held isothermally at 80 °C for 20 minutes to remove residual water and then heated to 700 °C at a rate of 10 °C min^{-1}.

3.2.8 Differential Scanning Calorimetry (DSC):

Thermal properties were analyzed for CNC-LLDPE PMC resin samples of ca. 5 mg for each PMC with a TA Instruments DSC Q20. PMC samples were heated to 160 °C, cooled to –35 °C at 10 °C min^{-1} and heated to 160 °C at 10 °C min^{-1}. The enthalpy of melting (ΔH_m) and the peak melting temperature (T_m) were determined by using linear integration on the TA Instruments Universal Analysis software. The crystallinities of the LLDPE portion of the PMC samples were determined as the quotients of the ΔH_m for LLDPE (ΔH_{mLLDPE}) and the ΔH_m for purely crystalline PE (ΔH_{mPE}) as 290 J/g,[28] ($\Delta H_{mLLDPE} \cdot \Delta H_{mPE}^{-1}$). LLDPE masses in the PMCs were approximated by subtracting the CNC portion of the PMCs using TGA data and used in the DSC crystallinity measurements.

3.2.9 Gel Permeation Chromatography (GPC):

Molecular weight (M_w) and poly dispersity index were determined for each of the four C1-CNC PMCs using gel permeation chromatography (GPC). Each sample was dissolved in 1,2,4-trichlorobenzene while wrapped in a steel mesh to remove CNCs. LLDPE at a concentration of ca. 1 mg mL^{-1} were run on an EcoSEC high temperature GPC

system equipped with a Tosoh Dual-Flow refractive index detector, and the resulting data was processed by EcoSEC 8321GPC Analysis software. Three samples were run for each of the PMC resins.

3.2.10 Scanning Electron Microscopy (SEM):

Microstructures of each of the CNC-LLDPE PMC resins were observed with a Zeiss LEO scanning electron microscope (SEM). Prior to SEM analysis, PMC resins were coated with 3 nm of iridium using a LEICA ACE600 sputter coater. PMC resins were then analyzed using either the in-lens or secondary electron detectors with the electron beam operating at 3-5 keV.

3.2.11 Uniaxial Tensile Testing:

Uniaxial tensile tests were performed with dogbone shaped CNC-LLDPE PMC specimens that had a gauge length of 7 mm, a width of 3 mm, and a thickness of ca. 0.1 mm. The strain rate was set to 5 mm min^{-1} on a uniaxial Instron equipped with a 500-N load cell. In all, 3-4 samples were run for each CNC-LLDPE PMC film.

3.2.12 Dynamic Mechanical Analysis (DMA):

Single amplitude temperature sweeps were performed for each CNC-LLDPE PMC film with a TA Instruments DMA Q800 equipped with a tensile clamp. Rectangular samples were cut from ca. 100-µm thick PMC films to be 5 mm in width and greater than 18 mm in length so the that the distance between the tensile clamps could be set to 15 mm. The amplitude of the instrument was set to 20 µm, the frequency was set to 1 Hz, and the temperature ramp rate was set to 5 °C·min^{-1} from $^{-}$100 °C to mechanical failure of samples (typically ca. 120 °C).

3.3 Results and Discussion:

This section contains the analysis of data that was obtained from the above experimental procedures. This section also draws contrasts with previous studies and critically analyzes the resulting PMCs.

3.3.1 CNC Aerogel Functionalization:

CNC aerogels were formed by freeze-drying a dispersion of CNCs from a 2:1 mixture of *tert*-butanol to water. CNC dispersions freeze-dried from this mixture have been shown to afford a material with higher surface area than using a purely aqueous CNC dispersion.[27, 29] The *tert*-butanol water mixture was chosen to ensure that there would be adequate surface for catalyst loading onto the CNCs, and a CNC aerogel made from a more dilute dispersion of the CNCs in this mixture was previously used a support for catalyst **1**.[15] CNC aerogels were functionalized with catalyst **1** according to **Scheme 3.1a**. Analysis from XPS was used to confirm the presence of zirconium on the C1-CNC aerogel surfaces. The presence of zirconium and bromine was confirmed in low-resolution survey scans, but the average quantitative values we obtained for all aerogels of 0.03% for zirconium and 0.04% for bromine using higher-resolution scans were not sufficiently above the detection limits for zirconium or bromine to allow us to estimate Zr:Br ratios.[30] The significance of Zr:Br ratios in C1-CNC materials was described in our previous report.[15]

3.3.2 Olefin Polymerization from C1-CNCs:

C1-CNC aerogels were added to reaction flasks in amounts specified in **Table** 3.**1**. After the addition of toluene to the catalyst supported on the C1-CNCs, the catalyst was activated by MMAO-12. The active supported catalyst was then exposed to 1-hexene and ethylene initiating the polymerization, this is described in **Scheme 3.1b**. The chemical

depiction of catalyst anchoring show in **Scheme 3.1a** is intended to portray only the general concept that O-H bonds of the CNC surface are exchanged with Si-Br bonds of Catalyst **1** to afford covalent Si-O linkages between **1** and the CNC. Work is underway in our laboratories to understand the structure of the catalyst-support interface in more detail.

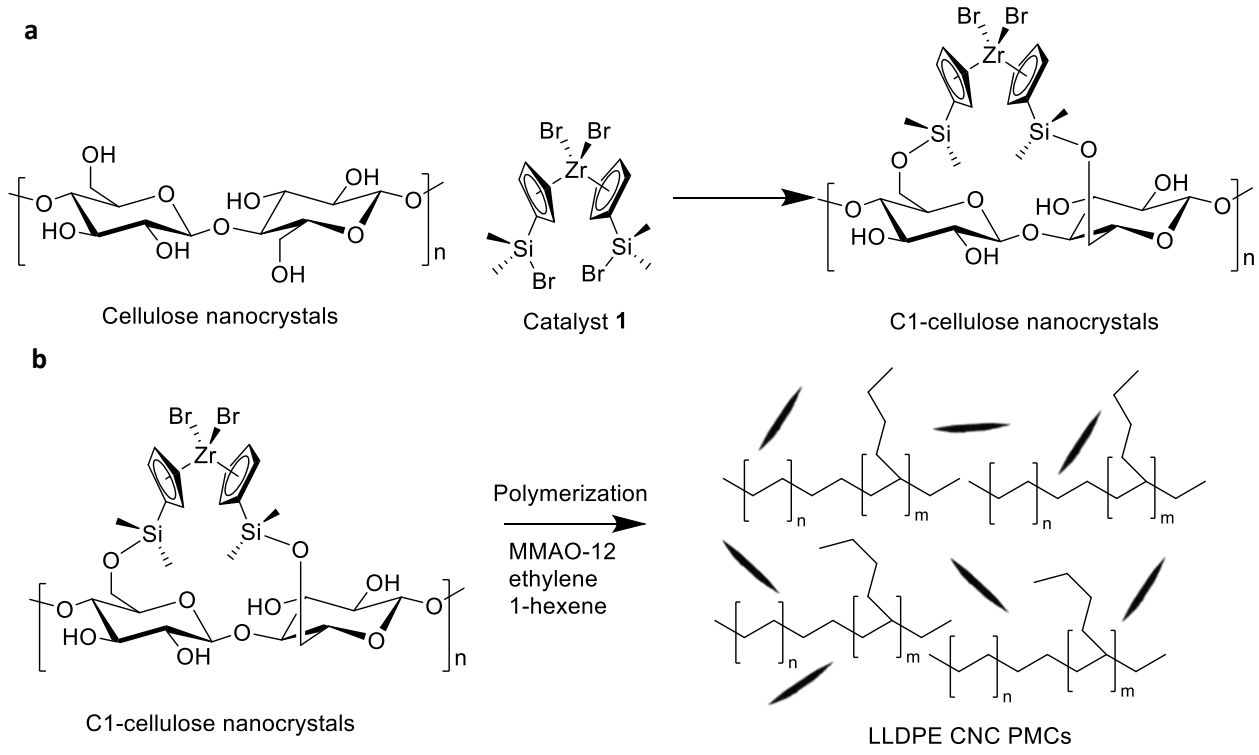

Scheme 3.1: a The attachment of the anchoring catalyst 1,1'-bis (bromodimethylsilyl)zirconocene dibromide (catalyst **1**) to the CNC was carried out under anhydrous conditions. **b** Catalyst **1** anchored on CNCs was activated by MMAO-12 and then ethylene and 1-hexene were added to initiate polymerization.

Activities of catalyst **1** for each of the C1-CNCs were calculated assuming that all of the catalyst **1** added was present on the surface of each C1-CNC aerogel and that all CNCs from the C1-CNC aerogels were incorporated into PMC resins. The mass of each of the CNC-LLDPE PMC resins generated are in **Table 3.2**. The activities of catalyst **1** were very similar for each C1-CNC, but the highest catalyst loading C1-CNC sample (16_600)

showed a decreased activity. The decrease in activity could be due to PE chains interfering with other sites, which could be described as a steric encumbrance effect or as a frustration of monomer diffusion.

C1-CNC aerogel label	C1-CNCs added to reactor (mg)	Mass of resin (g)	Activity of catalyst 1 ($kg_{PE}(mol_{Zr})^{-1}$)
2_600	200	1.53	2600
4_600	100	1.41	2600
8_600	50	1.38	2600
16_600	25	1.06	2000

Table 3.2: The above table shows the mass of each of the C1-CNC aerogels that were added to the reactor so that 0.67 mg of catalyst **1** was added to each reaction, the total mass of the PMC from the reactor (resin), and the resulting activity of the catalyst from each of the olefin polymerizations.

The resulting CNC-LLDPE PMCs from each polymerization from the C1-CNC aerogels resulted in similar looking resins and were somewhat soft white solids. Melt pressing the composites resulted in translucent films. CNC-LLDPE PMC films in which there were more CNCs in the reactor appeared somewhat less translucent and are depicted in **Figure S3.1**.

3.3.3 Thermogravimetric Analysis (TGA):

TGA data was used to approximate CNC content of the CNC-LLDPE PMCs using the C1-CNC aerogel (8_600) and MilliporeSigma LLDPE as references for degradation events **Figure 3.1a**. Sigma LLDPE underwent 1% degradation at 391 °C, whereas this temperature corresponded to 79% degradation for the C1-CNCs. As such, **Equation 1** was used to approximate the amount of CNCs present in each of the polymer samples ($\mathbf{m_{CNC}}$). The mass fraction of the composite at 391°C ($\mathbf{m_{391}}$) and subtracting it by the whole yielded the degraded CNC. The mass fraction of undegraded CNC was 21% of the degraded resin at 391 °C. The mass fraction of degraded LLDPE at 391 °C is 1%. Using these values, the amounts of CNCs were approximated and are presented in **Table 3.2**.

$$m_{CNC} = (1 - m_{391}) + (1 - m_{391})(0.21) - (m_{391})0.01 \quad (1)$$

3.3.4 Differential Scanning Calorimetry (DSC):

Thermal properties of each of the composite resins is presented as DSC thermograms. DSC analysis found that each of the CNC-LLDPE PMCs had a single endothermic event during the second heating cycle. This result implies that there was not a detectable amount of HDPE present in each sample or LLDPE with a significantly lower amount of 1-hexene. HDPE or a very low content 1-hexene LLDPE would be evidenced by a second melting event at a higher temperature. Each of the melting temperatures (T_m) for the PMCs were within 1 °C of 115 °C, and the crystalline contents of each of the CNC-LLDPE PMC resins were comparable. These results are summarized in **Table 3.3**. The mass of the CNCs found from the TGA results was used to calculate the mass of LLDPE in order to find the crystallinity of the PMCs.

Previous studies have also correlated molecular weight (M_w) and T_m with comonomer incorporation.[31] Accordingly, the T_m predicts that the LLDPE of each sample will have a molar of 1-hexene incorporation of less than 1.1% and a M_w of about 20 kDa to 100 kDa. Incorporation of greater than 1.7 mol% 1-hexene would likely have a lower melting point according to this data set.[31] Factors that could affect the melting point are a non-uniform distribution of comonomer, leading to a higher T_m, and high M_w could lead to a decrease in T_m.[31]

3.3.4 Nuclear Magnetic Resonance Spectroscopy (NMR):

Quantitative ^{13}C NMR was used to find the amount of 1-hexene in the LLDPE portion of the CNC-LLDPE PMCs, and the following analysis was adapted from previous works.[32-33] The amount of 1-hexene was quantified as the methyl group signal, the other

secondary and tertiary carbon signal was integrated, and the enchained 1-hexene was subtracted from the secondary tertiary carbon signal. The sum of the methyl carbons was found by integrating the peak at ca. 15 ppm and defining this integral as 1 using the Mestrelab MNova spectral analysis software. The sum of all the other carbons the methylene (-CH_2-) carbons and tertiary branch carbons (>CH-) was evaluated by integrating the region from 23 ppm to 40 ppm. The mols of ethylene was found by subtracting the secondary and tertiary carbon signal by 5, the defined remaining carbons in 1-hexene. This approach was validated by absence of the end groups alkene carbons (CH_3=CH_2) at 115-140 ppm. The results shown on **Table 3.3** show similar amounts of 1-hexene incorporation within each of the polymer samples, and the results from DSC affirm that the LLDPE components of the PMCs are similar. The NMR spectra are presented as **Figure S3.2**.

In order to have manageable relaxation times chromium(III) acetylacetonate was added to each of the PMC samples. ^{13}C NMR was chosen as previous work had been done allowing for the assignment of peaks. From this we were able to conclude that there were not runs of hexene due to the absence of peaks at 40-42 ppm. Concentrations of >250 mg in 4 mL or >60 mg mL^{-1} were used to increase signal. ^{13}C has more space between signals using (10-200ppm) relative to (0-10ppm) allowing for better peak separation especially because particulates are present in the spectra. Another concern is temperature, LLDPE samples did not dissolve at room temperature, so we used higher temperatures to solubilize the LLDPE.

The mechanical properties of the composites could be affected by changes in 1-hexene content. In a previous study of neat LLDPE materials, it was found that the yield

strength dramatically decreased with increasing 1-hexene content from ca. 10 MPa at 0.6-1.14 mol% 1-hexene to <5 MPa at >2.84 mol% 1-hexene.[34] Elongation at break was similar for samples between 0.6-3.52 mol% 1-hexene having values 1500-2000%.[34] The initial modulus (2-3% secant modulus) similar to Young's modulus was found to relate to the crystalline content of the LLDPE, but the initial modulus was between 40 and 70 MPa and decreased with increasing 1-hexene content.[34] Strain hardening, however was quite different for those samples having higher 1-hexene content.[34] From this information it seems likely that the elongation at break was not affected, but the yield strengths and Young's modulus of the PMCs may be affected.

The concentration of 1-hexene was found to be nearly constant throughout the reaction, assuming that negligible amounts of 1-hexene was evaporated during the reaction. This assumes that the compositional homogeneity of the LLDPE was not affected by changes in 1-hexene concentration. The amount of 1-hexene before and after the reaction was calculated from the resulting NMR data and the mass of each CNC-LLDPE PMC sample. This approximation assumes the mass of 1-hexene ($\mathbf{m_{1\text{-}hexene}}$) in each PMC was calculated by using **Equation 2**. The mass of LLDPE ($\mathbf{m_{LLDPE}}$) was approximated as the difference between the mass of the PMC resin minus the mass of CNCs added to the reactor. Each PMC was near 6 wt% 1-hexene and each reaction consumed ca. 10 wt% of the total 1-hexene. The change concentration in 1-hexene of the reactor was only from 2 vol% to about 1.7 vol%.

$$\boldsymbol{m_{1-hexene} = m_{LLDPE} \frac{M_{w,1-hexene} \times mol\%_{1-hexene}}{M_{w,1-hexene} \times mol\%_{1-hexene} + mol\%_{ethylene} \times MM_{w,ethylene}}} \quad (2)$$

C1-CNC Aerogel	CNC content (wt%)	Crystallinity	Peak T_m (°C)	1-hexene content
2_600	11.4	39%	115	1.6%
4_600	5.8	34%	115	1.9%
8_600	4.4	35%	115	2.3%
16_600	3.6	41%	116	1.6%

Table 3.3: The table denotes CNC content of PMCs, crystallinity of LLDPE portion of PMCs, peak melting point of PMCs, and 1-hexene content of PMCs.

3.3.5 Gel Permeation Chromatography (GPC):

PMC samples analyzed by gel permeation chromatography showed similar molecular weight in terms of both weight (M_w) and number averages (M_n), and the PDIs of the PMCs are lower than the PDIs typical of Ziegler-Natta catalyst polyethylenes (**Table 3.4**). A clear highlight of this data is that the 11.4 wt% CNC and 3.4 wt% CNC samples have the same M_w and only moderately differ in terms of M_n. Importantly, each of these LLDPE samples are not radically different from one another and have M_w differences that should reflect similar LLDPE portion of the PMCs.

C1-CNC PMC	M_n (kDa)	M_w (kDa)	PDI
2_600	42	129	3.09
4_600	34	138	4.04
8_600	41	170	4.12
16_600	23	128	5.60

Table 3.4: This table shows the M_w, the number average M_n, and the PDI for each of the polymer samples. Subsequent runs of each sample had variability of less than 1%.

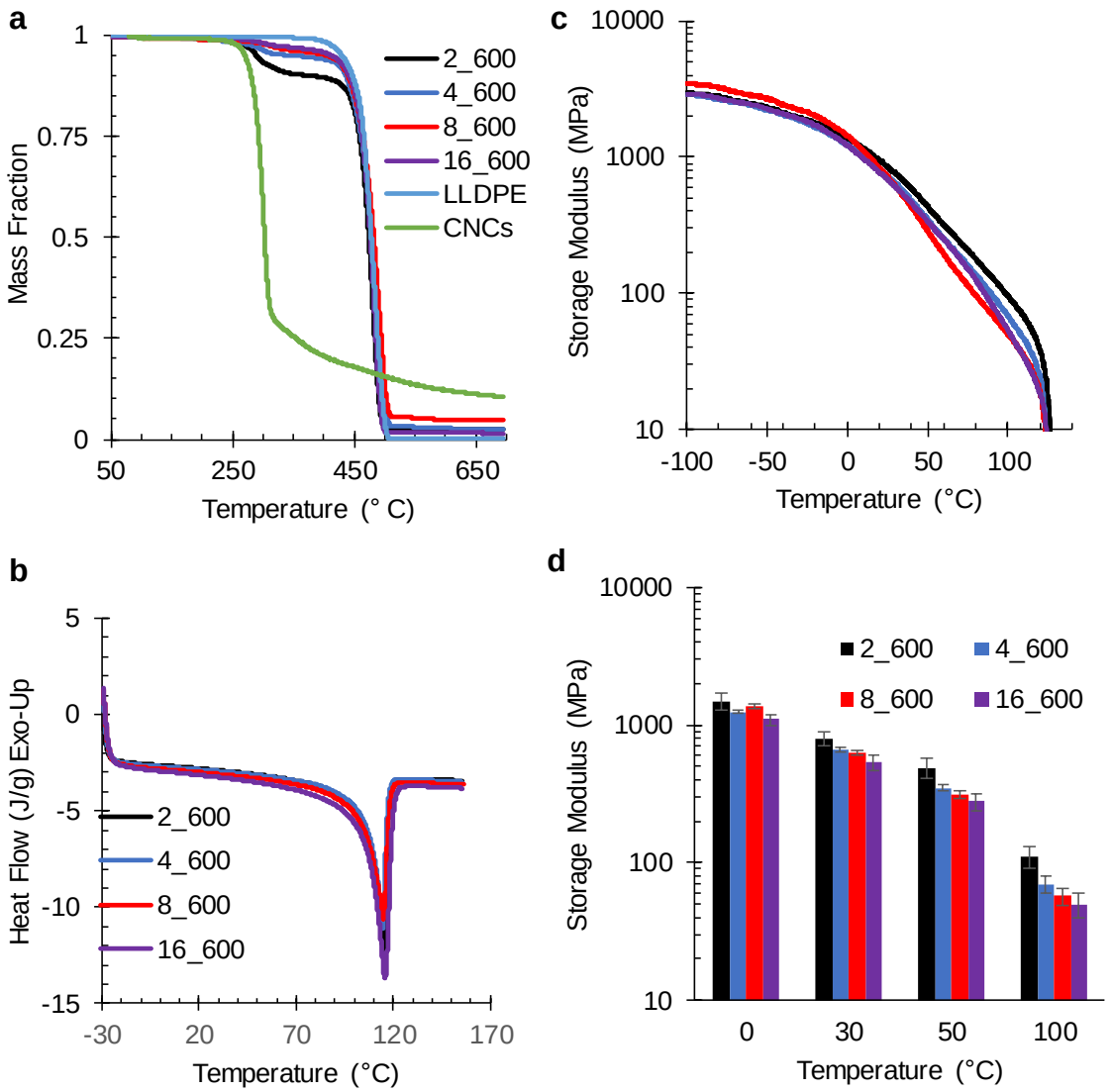

Figure 3.1: (a) Thermograms of LLDPE-CNC polymer matrix composites (PMCs) from four different C1-CNC catalyst loadings, commercial LLDPE, and native CNC material, were used to estimate CNC incorporation in the PMC samples. (**b)** DSC traces showing that the LLDPE matrix component of CNC-LLDPE PMCs have comparable fractional crystallinity. (**c**) and (**d**) DMA was data used to study the effect of CNC concentration on the storage moduli of corresponding CNC-LLDPE PMCs. Relation of catalyst loading to CNC content in PMCs is present on **Table 3.3**.

3.3.6 Dynamic Mechanical Analysis (DMA):

Temperature sweeps performed by DMA of each CNC-LLDPE PMC samples showed a clear trend of having greater average storage moduli with increasing CNC

content, which, in turn, results from decreased loading of metallocene onto the CNC (see Table 3.3) Analysis of the leathery region of the DMA curves shows that the CNCs may act as physical crosslinks inhibiting segmental motion of the LLDPE chains within the PMCs, and the relative difference between each PMC is exceptionally evident at 100 °C (**Figure 3.1c**). However, all of these PMCs materials seem to have similar processing temperatures as there is a clear point of mechanical failure at ca. 120 °C as shown in **Figure 3.1c**.

3.3.7 Uniaxial Tensile Testing:

The uniaxial tensile data from the CNC-LLDPE PMCs was evaluated for changes in Young's modulus, elongation at break, and yield strength. Each PMC showed a definite trend of increasing Young's modulus, a metric for reinforcement, with increased CNC loading. The largest difference in Young's modulus was between the 11.4 wt% CNC PMC with a Young's modulus of 391 ± 7 MPa versus the 3.6 wt% CNC PMC with a Young's modulus of 240 ± 50 MPa. The elongation at break however, did not follow the typical trend of decreasing with increasing filler loading. The composites had yield strengths of 10-11 MPa that did not vary significantly. Values of elongation at break were insignificant with the 11.4 wt% CNC PMC had a value of (70% ± 10%) and the 5.8 wt% CNC PMC had (60% ± 30%), while the 4.4 wt% CNC PMC (850% ± 60%) and the 3.6 wt% (400% ± 90%) CNC PMC had much greater elongation at break values. Tensile data is presented in **Figure 3.2, Table S3.1,** and as representative curves in **Figure S3.3**.

An interesting feature of the curves (**Figure S3.3**) is the strain hardening that the 4.4 wt% CNC PMC and 3.6 wt% CNC PMC undergo. The 3.6 wt% PMC undergoes little strain hardening deformation having effectively the same yield strength and stress at break

ca. 10 MPa. The 4.4 wt% CNC PMC however undergoes a much more pronounced strain hardening the yield strength is 10 ± 2 MPa and the strain at break is 18 ± 3 MPa. The strain hardening of 1-hexene LLDPE has been shown to occur at a faster rate with increased 1-hexene content.[34] The lower crystallinity allows for the polymer to become crystalline while being strained. It also seems that an effective percolation of the CNCs occurs between the PMCs of 4.4 wt% CNC and 5.8 wt% CNCs, where there is a dramatic decrease in elongation at break. The percolation threshold for the CNCs is estimated to be between 2.7-7.8 vol% and assuming the LLDPE has a density of 0.90 g cm^{-1} and the CNCs have a density of 1.6 g cm^{-1} the PMCs are 2.6 vol% and 3.4 vol% CNC respectively. This estimate uses the lower and upper bound aspect ratios (50/9) and (130/5) and assumes the percolation threshold, *volume fraction=(0.7/aspect ratio),* is true for aspect ratios below 30.

The resulting mechanical properties from C1-CNCs used to make LLDPE-CNC PMCs look favorable when compared the previous work[12] on modified 2-ureido -4[1H]pyrimidone (UPy) modified CNCs used to make CNC-LLDPE PMCs. In comparison, C1-CNC PMCs had greater Young's modulus at similar filler loadings, but the C1-CNCs were not able to maintain the elongation at break values >100% with high fillers loadings.[12] Another previous work that combined modified CNCs in LLDPE by melt mixing to make PMCs showed similar mechanical properties at similar filler loadings.[16] These results showed Young's modulus values of neat pure at ca. 100 MPa and vales of ca. 200 MPa for 3 wt% unmodified CNCs in LLDPE , 3 wt% N,N -dialkyl-3-methoxyazetidinium salt modified CNCs, and 3 wt% 1,1'-dihexyl-3-methoxyazetidnium chloride modified CNCs.[16] Data from these studies is presented in **Table S3.1**.

In an effort to compare C1-CNC LLDPE PMCs to those in literature,[12, 16] a point of reference for a commercial 1-octene LLDPE was established with a Young's modulus of ca. 140 MPa[35] that is similar to the LLDPEs used in the previous studies.[12, 16] Additionally, the T_m obtained from commercial 1-octene LLDPE is (ca. 115 °C) and that value is the T_m obtained from the C1-CNC LLDPE PMCs. The commercial 1-hexene LLDPE had a higher melting point[36] and was not used for this comparison, but the C1-CNC LLDPE with 11.4 % CNC loading had a greater Young's modulus (391 ± 7 MPa) that commercial 1-hexene LLDPEs (ca. 300 MPa).[36] A previous study that graphed 1-hexene incorporation and melting point suggests that these commercial 1-hexene LLDPEs (T_m ca. 125 °C) contain less than 0.4 mol% 1-hexene.[31]

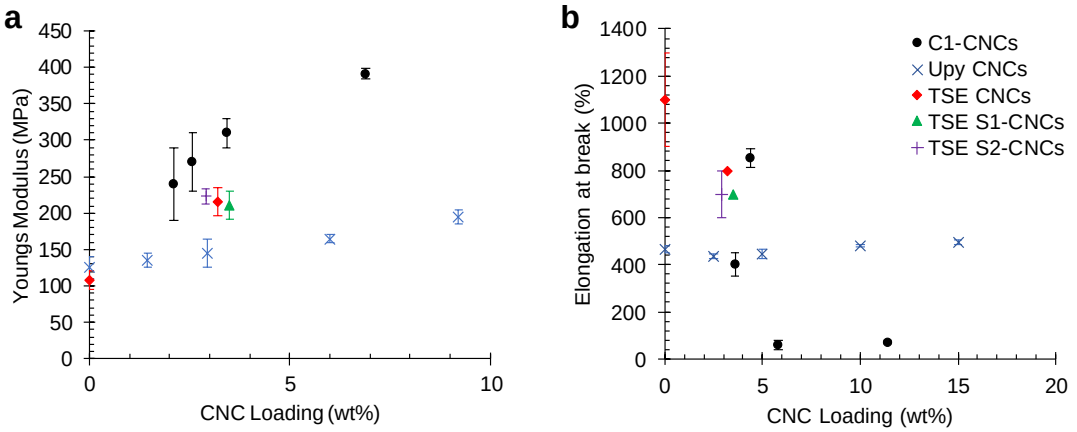

Figure 3.2: Tensile data Young's modulus **a** and **b** elongation at break of C1-CNC LLDPE PMCs were compared with tensile data from other studies. The symbols are represented as C1-CNC PMCs ●, UPy modified CNC PMCs X,[11] twin screw extruded (TSE) CNC PMCs ♦,[16] TSE N,N -dialkyl-3-methoxyazetidinium salt (S1) modified CNC PMCs ▲,[16] and 1,1'-dihexyl-3-methoxyazetidnium chloride (S2) modified CNC PMCs +.[16]

3.3.8 Imaging:

Optical photographs were taken of the pressed films (**Figure S3.2**). SEM imaging of the C1-CNC aerogels found that they were flaky structures, and they do not seem distinct

from the structures that were previously analyzed (**Figure S3.3**).[15] The images of the polymer materials taken as a dried unprocessed resin show an interesting cracking dendritic pattern. This dendritic pattern is different from the documented fragmentation of silica gel, which clearly shows the origin for polymerization.[37-38] A study that has polymerized ethylene from carbon nanotubes (CNTs) shows a channel of PE holding a CNT.[39] The channels in the CNC-LLDPE are near that scale and could be representative of a network of CNCs in the PMC. It is difficult to prove that the polymerization originated from the C1-CNCs (**Figure 3.3**). The distribution of this structure throughout each PMC is worthy of further study. The main limitation of SEM is the lack of contrast between CNCs and the LLDPE, but SEM can be used to find interesting structure with a height contrast as shown in these images (**Figure 3.3**).

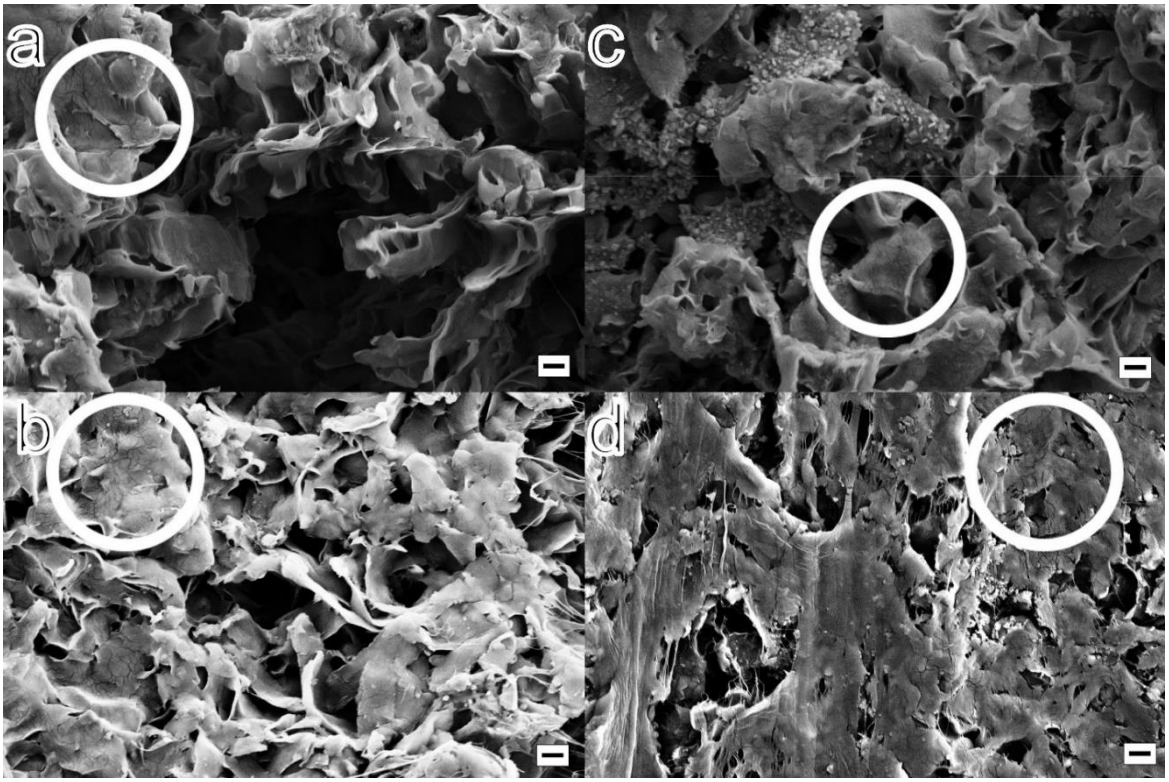

Figure 3.3: SEM micrographs were taken at 10 kX magnification and show dark structures that are fanning outward highlighted in white circles. The images correspond to: **a** 11.4 wt% CNC PMC, **b** 5.8 wt% CNC PMC, **c** 4.4 wt% CNC PMC, and **d** 3.6 wt% CNC PMC. Scale bars are 1 µm.

3.4 Conclusions:

We were able to incorporate CNCs in LLDPE in a manner that is scalable and include These C1-CNC PMCs have shown an increased Young's modulus with increasing CNC loading, suggesting that the CNCs are taking a large share of the load from applied stresses. The composites have also shown good translucency and elongation at break implying that there is not significant aggregation in the PMC leading to premature tearing. The C1-CNC PMCs presented here have the highest Young's moduli at their respective loadings of CNC, relative to other CNC-LLDPE PMCs. The increased Young's modulus could lead to applications of advanced composite materials where the scale of reinforcement begins at the nanoscale and more macroscopic material are added.[1]

This study is the first to analyze the mechanical properties of a LLDPE-CNC PMC polymerized from the surface of a nanomaterial. An alternative method of which has achieved good results uses an anchored co-catalyst to attract a metallocene to polymerize ethylene therefrom separating the nanofiller.[21, 40] The use of a LLDPE comonomer such as 1-hexene or 1-octene has to our knowledge was explored in an early pioneering study using non-cellulosic materials,[22] and later explored anchoring co-catalysts to carbon nanotubes.[41] We are hopeful that our positive result will continue the trend of researching filled LLDPE materials.

Acknowledgements:

I would like to thank Michael J. Bortner and Priya Venkatramen for their assistance in obtaining tensile data.

References:

1. Paul, D. R.; Robeson, L. M., Polymer nanotechnology: Nanocomposites. *Polymer* **2008,** *49* (15), 3187-3204.
2. Ma, J.; Zhang, L. Q.; Dai, J., Interface Modification and Characterization. In *Rubber Nanocomposites*, Thomas, S.; Stephen, R., Eds. 2010; pp 87-112.
3. Fornes, T. D.; Paul, D. R., Modeling properties of nylon 6/clay nanocomposites using composite theories. *Polymer* **2003,** *44* (17), 4993-5013.
4. Favier, V.; Cavaille, J. Y.; Canova, G. R.; Shrivastava, S. C., Mechanical percolation in cellulose whisker nanocomposites. *Polymer Engineering & Science* **1997,** *37* (10), 1732-1739.
5. Moon, R. J.; Martini, A.; Nairn, J.; Simonsen, J.; Youngblood, J., Cellulose nanomaterials review: structure, properties and nanocomposites. *Chemical Society Reviews* **2011,** *40* (7), 3941-3994.
6. Sastri, V. R., 6 - Commodity Thermoplastics: Polyvinyl Chloride, Polyolefins, and Polystyrene. In *Plastics in Medical Devices (Second Edition)*, Sastri, V. R., Ed. William Andrew Publishing: Oxford, 2014; pp 73-120.
7. Fernandes, E. M.; Mano, J. F.; Reis, L. R., 5. Polyethylene Composites with Lignocellulosic Material. In *Polyethylene-Based Blends, Composites and Nanocomposites*, Visakh, P. M.; Morlanes, M. J. M., Eds. John Wiley & Sons: 2015.
8. Rives, V.; Labajos, F. M.; Herrero, M., 6. Double layered hydroxides as nanofillers of composites and nanocomposite materials based on polyethylene. In *Polyethylene-Based Blends, Composites and Nanocomposites*, Visakh, P. M.; Morlanes, M. J. M., Eds. John Wiley & Sons: 2015.

9. Selke, S. E.; Hernandez, R. J., Packaging: Polymers for Containers. In *Encyclopedia of Materials: Science and Technology*, Buschow, K. H. J.; Cahn, R. W.; Flemings, M. C.; Ilschner, B.; Kramer, E. J.; Mahajan, S.; Veyssière, P., Eds. Elsevier: Oxford, 2001; pp 6646-6652.
10. Raj, R. G.; Kokta, B. V., Linear Low-Density Polyethylene Filled with Silane-Coated Wood Fibers. In *High-Tech Fibrous Materials*, American Chemical Society: 1991; Vol. 457, pp 102-113.
11. Sapkota, J.; Natterodt, J. C.; Shirole, A.; Foster, E. J.; Weder, C., Fabrication and Properties of Polyethylene/Cellulose Nanocrystal Composites. *Macromolecular Materials and Engineering* **2017,** *302* (1), 1600300-n/a.
12. Natterodt, J. C.; Sapkota, J.; Foster, E. J.; Weder, C., Polymer Nanocomposites with Cellulose Nanocrystals Featuring Adaptive Surface Groups. *Biomacromolecules* **2017,** *18* (2), 517-525.
13. Sapkota, J.; Jorfi, M.; Weder, C.; Foster, E. J., Reinforcing poly (ethylene) with cellulose nanocrystals. *Macromolecular rapid communications* **2014,** *35* (20), 1747-1753.
14. Junior de Menezes, A.; Siqueira, G.; Curvelo, A. A. S.; Dufresne, A., Extrusion and characterization of functionalized cellulose whiskers reinforced polyethylene nanocomposites. *Polymer* **2009,** *50* (19), 4552-4563.
15. Hendren, K. D.; Baughman, T. W.; Deck, P. A.; Foster, E. J., In situ dispersion and polymerization of polyethylene cellulose nanocrystal-based nanocomposites. *Journal of Applied Polymer Science* **2020,** *137* (13), 48500.
16. Borjesson, M.; Sahlin, K.; Bernin, D.; Westman, G., Increased thermal stability of nanocellulose composites by functionalization of the sulfate groups on cellulose nanocrystals with azetidinium ions. *Journal of Applied Polymer Science* **2018,** *135* (10), 10.
17. Nagalakshmaiah, M.; El Kissi, N.; Dufresne, A., Ionic Compatibilization of Cellulose Nanocrystals with Quaternary Ammonium Salt and Their Melt Extrusion with Polypropylene. *Acs Applied Materials & Interfaces* **2016,** *8* (13), 8755-8764.
18. Kaminsky, W., Zirconocene catalysts for olefin polymerization. *Catalysis Today* **1994,** *20* (2), 257-271.
19. Funck, A.; Kaminsky, W., Polypropylene carbon nanotube composites by in situ polymerization. *Composites Science and Technology* **2007,** *67* (5), 906-915.
20. Kaminsky, W.; Funck, A.; Klinke, C., In-situ Polymerization of Olefins on Nanoparticles or Fibers by Metallocene Catalysts. *Topics in Catalysis* **2008,** *48* (1), 84.
21. Kaminsky, W., Metallocene Based Polyolefin Nanocomposites. *Materials* **2014,** *7* (3), 1995-2013.
22. Alexandre, M.; Martin, E.; Dubois, P.; Garcia-Marti, M.; Jérôme, R., Use of metallocenes in the polymerization-filling technique with production of polyolefin-based composites. *Macromolecular rapid communications* **2000,** *21* (13), 931-936.
23. Alexandre, M.; Martin, E.; Dubois, P.; Marti, M. G.; Jérôme, R., Polymerization-Filling Technique: An Efficient Way To Improve the Mechanical Properties of Polyethylene Composites. *Chemistry of Materials* **2001,** *13* (2), 236-237.
24. Hees, T.; Zhong, F.; Rudolph, T.; Walther, A.; Mülhaupt, R., Nanocellulose Aerogels for Supporting Iron Catalysts and In Situ Formation of Polyethylene Nanocomposites. *Advanced Functional Materials* **2017,** *27* (11), 1605586-n/a.

25. Hendren, K. D.; Higgins, M. A.; Long, B. K.; Foster, E. J., Cellulose nanocrystal-reinforced poly(5-triethoxysilyl-2-norbornene) composites. *Polymer Chemistry* **2020,** *11* (2), 433-438.
26. Deck, P. A.; Fisher, T. S.; Downey, J. S., Boron−Silicon Exchange Reactions of Boron Trihalides with Trimethylsilyl-Substituted Metallocenes. *Organometallics* **1997,** *16* (6), 1193-1196.
27. Shamskar, K. R.; Heidari, H.; Rashidi, A., Preparation and evaluation of nanocrystalline cellulose aerogels from raw cotton and cotton stalk. *Industrial Crops and Products* **2016,** *93*, 203-211.
28. Hatakeyama, T.; Liu, Z., *Handbook of Thermal Analysis*. John Wiley and Sons, Inc: Chichester, 1998.
29. De France, K. J.; Hoare, T.; Cranston, E. D., Review of Hydrogels and Aerogels Containing Nanocellulose. *Chemistry of Materials* **2017,** *29* (11), 4609-4631.
30. Shard, A. G., Detection limits in XPS for more than 6000 binary systems using Al and Mg Kα X-rays. *Surface and Interface Analysis* **2014,** *46* (3), 175-185.
31. Alamo, R. G.; Mandelkern, L., The crystallization behavior of random copolymers of ethylene. *Thermochimica Acta* **1994,** *238*, 155-201.
32. Randall, J. C., A review of high resulution liquid ^{13}Carbon nuclear magnetic resonance characerizations of ethylene-based polymers. *Journal of Macromolecular Science, Part C* **1989,** *29* (2-3), 201-317.
33. Hsieh, E. T.; Randall, J. C., Ethylene-1-butene copolymers. 1. Comonomer sequence distribution. *Macromolecules* **1982,** *15* (2), 353-360.
34. Kennedy, M. A.; Peacock, A. J.; Failla, M. D.; Lucas, J. C.; Mandelkern, L., Tensile Properties of Crystalline Polymers: Random Copolymers of Ethylene. *Macromolecules* **1995,** *28* (5), 1407-1421.
35. SABIC, SABIC Supeer 8115: Metallocene linear low-density polyethylene. Revision 20181012, 2018.
36. SABIC, SABIC Supeer 7118: Metallocene linear low-density polyethylene. Revision 20181012, 2018.
37. McDaniel, M. P., Chapter 3 - A Review of the Phillips Supported Chromium Catalyst and Its Commercial Use for Ethylene Polymerization. In *Advances in Catalysis*, Gates, B. C.; Knözinger, H., Eds. Academic Press: 2010; Vol. 53, pp 123-606.
38. Zheng, X.; Smit, M.; Chadwick, J. C.; Loos, J., Fragmentation Behavior of Silica-Supported Metallocene/MAO Catalyst in the Early Stages of Olefin Polymerization. *Macromolecules* **2005,** *38* (11), 4673-4678.
39. Bahuleyan, B. K.; Atieh, M. A.; De, S. K.; Jabarulla Khan, M.; Al-Harthi, M. A., Easy one-pot method to control the morphology of polyethylene/carbon nanotube nanocomposites using metallocene catalysts. *Journal of Polymer Research* **2012,** *19* (2), 9744.
40. Bonduel, D.; Mainil, M.; Alexandre, M.; Monteverde, F.; Dubois, P., Supported coordination polymerization: a unique way to potent polyolefin carbon nanotube nanocomposites. *Chemical Communications* **2005,** (6), 781-783.
41. Toti, A.; Giambastiani, G.; Bianchini, C.; Meli, A.; Bredeau, S.; Dubois, P.; Bonduel, D.; Claes, M., Tandem Action of Early− Late Transition Metal Catalysts for the Surface Coating of Multiwalled Carbon Nanotubes with Linear Low-Density Polyethylene. *Chemistry of Materials* **2008,** *20* (9), 3092-3098.

3.5 Supporting Information

Linear low-density polyethylene cellulose nanocrystal composites from *in-situ* polymerization mediated by an anchored metallocene catalyst

The figures presented are organized in terms of CNC content. The C1-CNCs which were used to create these composites correspond to the following CNC contents 11.4 wt% CNC is 2_600, 5.8 wt% CNC is 4_600, 4.4 wt% CNC is 8_600, and 3.6 wt% CNC is 16_600. This is summarized in **Table 3.3**.

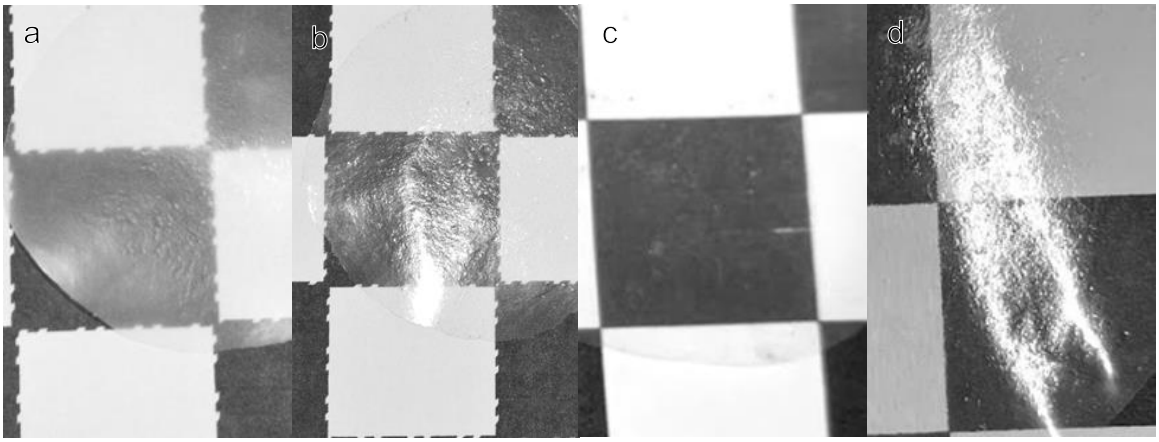

Figure S3.1: Images shown are films of each of the pressed CNC-LLDPE PMC resins. The resins correspond to **a** 11.4 wt% CNC (2_600), **b** 5.8 wt% CNC (4_600), **c** 4.4 wt% CNC (8_600), and **d** 3.6 wt% CNC (16_600). Each of the images labeled with CNC content from TGA data and the C1-CNC aerogel which they are made from.

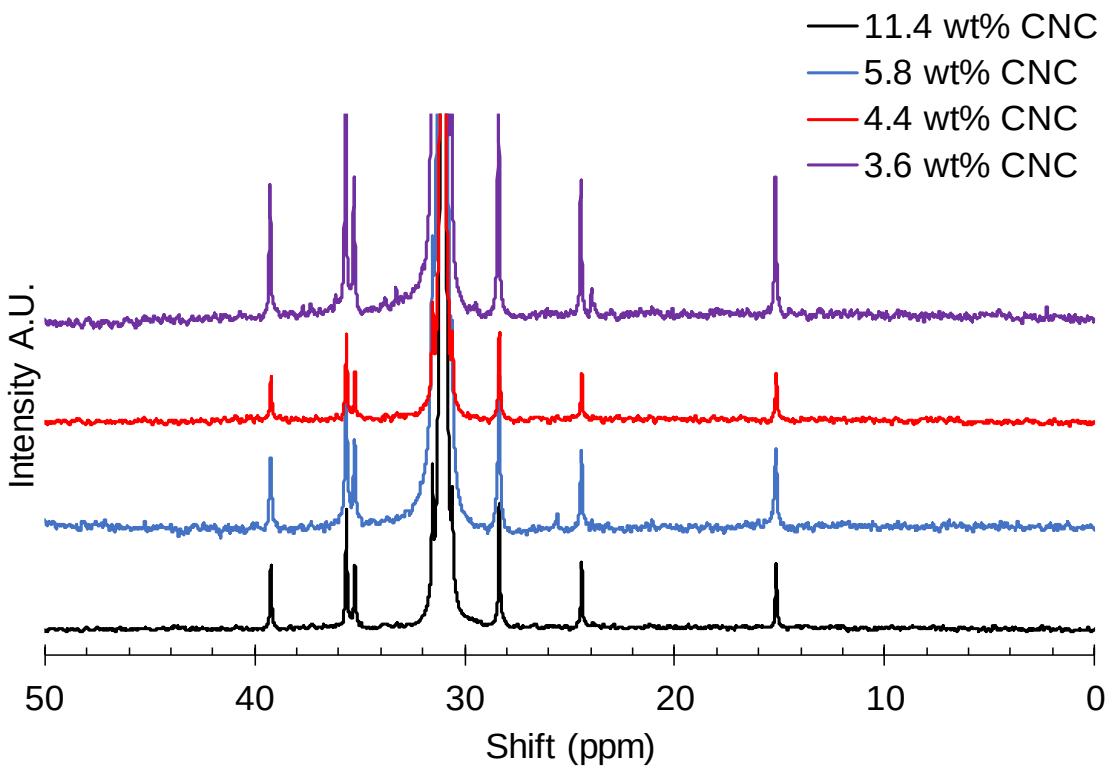

Figure S3.2: Spectra of ^{13}C NMR of each of the PMC samples were used to quantify the mol% of 1-hexene within the LLDPE portion of each PMC scans for each of the samples were PMC 2_600 (11.4 wt%) 3392 scans, PMC 4_600 (5.8 wt%) 16000, PMC 8_600 (4.4 wt% CNC) 6848, and PMC 16_600 (3.6 wt% CNC) 14592.

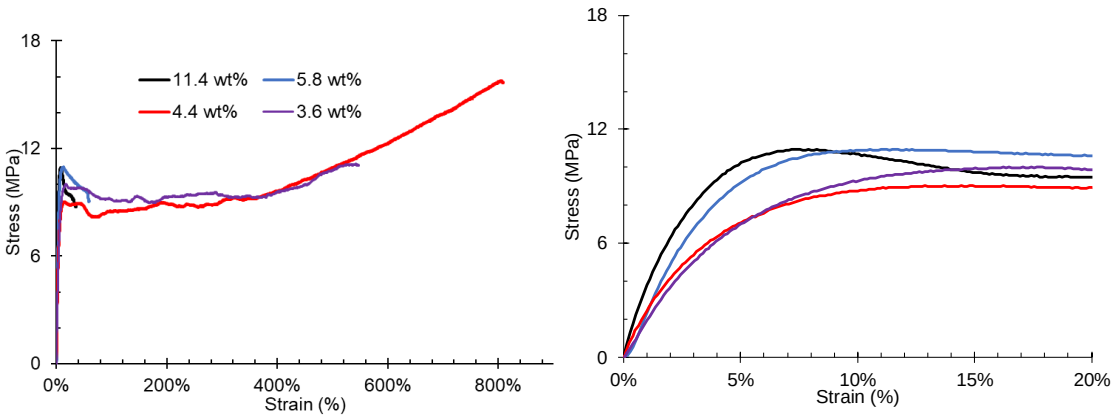

Figure S3.3: Above are representative stress-strain curves for the C1-CNC LLDPE PMCs arranged by mass fraction of CNC. The curves are **a**, the full stress strain curve and **b,** a truncated stress strain curve showing differences in Young's moduli.

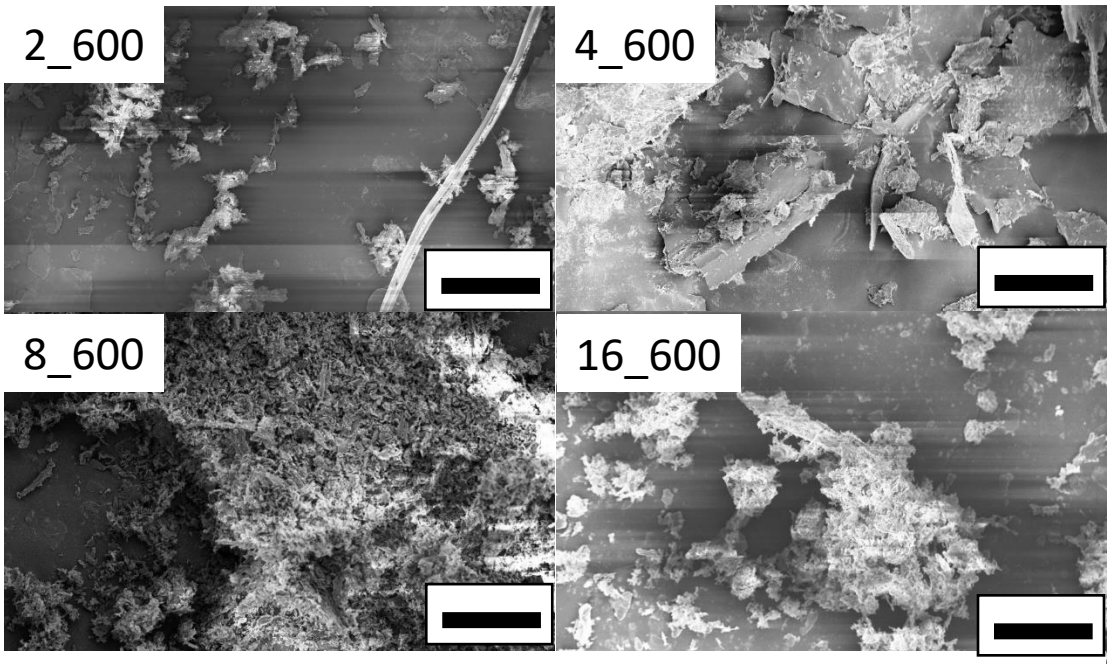

Figure S3.4: SEM Images of aerogels show flakey structure that was exhibited in all samples. The Images were taken at 3-5 keV with the in-lens or secondary electron detectors at 500x magnification. The scale bar is 100 µm.

CNCs	CNCs (wt%)	Young's Modulus (MPa)	Yield Strength (MPa)	Elongation at Break (%)
C1-CNCs 16_600	3.6	240 ± 50	11 ± 3	400 ± 90
C1-CNCs 8_600	4.4	270 ± 40	10 ± 2	850 ± 60
C1-CNCs 4_600	5.8	310 ± 20	10.8 ± 0.9	60 ± 30
C1-CNCs 2_600	11.4	391 ± 7	11 ± 1	70 ± 10
Natterodt et al.[1] UPy CNCs	0	125 ± 15	8.7 ± 0.9	465 ± 40
Natterodt et al.[1] UPy CNCs	2.5	135 ± 10	9.5 ± 0.2	435 ± 65
Natterodt et al.[1] UPy CNCs	5	145 ±20	9.9 ± 0.6	445 ± 50
Natterodt et al.[1] UPy CNCs	10	165 ± 5	10 ± 0.5	480 ± 30
Natterodt et al.[1] UPy CNCs	15	195 ± 10	13 ± 0.5	495 ± 15
Borjesson et al.[2] no CNCs	0	108 ± 13	-	1100 ± 200
Borjesson et al.[2] CNCs	3.2	216 ± 19	-	800 ± 0
Borjesson et al.[2]† S1-CNCs	3.5	211 ± 19	-	700 ± 0
Borjesson et al.[2]‡ S2-CNCs	2.9	223 ± 11	-	700 ± 100

Table S3.1: This table shows tensile data from CNC-LLDPE PMCs from C1-CNCs and those available from literature. S1-CNCs are functionalized with N,N-dialkyl-3-methoxyazetidinium salt and S2-CNCs are functionalized with 1,1'-dihexyl-3-methoxyazetidniumchloride salt.

References:

1. Natterodt, J. C.; Sapkota, J.; Foster, E. J.; Weder, C., Polymer Nanocomposites with Cellulose Nanocrystals Featuring Adaptive Surface Groups. *Biomacromolecules* **2017,** *18* (2), 517-525.
2. Borjesson, M.; Sahlin, K.; Bernin, D.; Westman, G., Increased thermal stability of nanocellulose composites by functionalization of the sulfate groups on cellulose nanocrystals with azetidinium ions. *Journal of Applied Polymer Science* **2018,** *135* (10), 10.

Chapter 4: Functionalization of cellulose nanocrystal composite materials for reverse osmosis applications

This chapter is part of a collaboration with Stephen A. Martin and Ethan D. Smith, and this work is a follow-up to the publication from the collaborative document "Functionalized Cellulose Nanocrystal Nanocomposites Membranes with Controlled Interfacial Transport for Improved Reverse Osmosis Performance." The following research is in preparation for a larger potential publication with Ethan D. Smith, Stephen A. Martin and E. Johan Foster. In the following chapters, I recognize the ideas, editing, and guidance from the coauthors Ethan D. Smith, Stephen A. Martin and E. Johan Foster.

Functionalization of cellulose nanocrystals for reverse osmosis applications

Keith D. Hendren, Ethan D. Smith, Stephen M. Martin, and E. Johan Foster

Abstract:

Cellulose nanocrystals (CNCs) with novel functionalization groups on the surfaces were developed for use in reverse osmosis (RO) membranes to investigate changes in RO membrane performance. Tertiary amine CNCs (ACNCs) were developed by coupling (2,2,6,6-tetramethylpiperidin-1-yl)oxyl (TEMPO) oxidized CNCs (TCNCs) with the known 1-ethyl-3-(3-dimethylaminopropyl)carbodiimide (EDC) coupling followed by a reaction with 3-(dimethylamino)-1-propylamine. Zwitterionic CNCs (ZCNCs) were subsequently developed from a reaction of ACNCs with β-propiolactone. The presence of nitrogen on the surfaces of the tertiary ACNCs and ZCNCs was verified by X-ray photoelectron spectroscopy (XPS). The presence of the second carboxylic groups afforded by β-propiolactone was verified by Fourier transform infrared spectroscopy (FTIR) at 1730 cm^{-1}. Functional groups were quantified by conductometric titration of the CNCs, and it was found that there were 1060 mmol kg^{-1} of carboxylic acid groups for TCNCs, 520 mmol kg^{-1} of amines for ACNCs, and 240 mmol kg^{-1} of zwitterions for ZCNCs.

4.1 Introduction:

There is a global demand for desalination technologies as both sources of seawater and brackish water are used as feed sources of freshwater. It is estimated that each person requires approximately 1000 m^3 per year of freshwater.[1] Arid and sub-humid regions of the world typically use more groundwater reserves than are replenished, and it is estimated that about 35% of the world's population suffers from having insufficient water resources.[2] Reverse osmosis (RO) is a pressure driven membrane technology that is used globally to

remove dissolved salts from water. It has two primary branches of application which accomplish the same goal, the desalination of sea water and the desalination of brackish water sources.[3]

RO membranes, a prominent technology, have undergone some refinement. RO began with cellulose acetate membranes and moved towards more efficient polyamide (PA) membranes. The current technology is crosslinked PA membranes.[4] Each new RO membrane technology improved salt rejection and/or water flux. Newer RO membrane technologies have focused on the addition of filler materials to further improve flux of water, resistance to biofouling, or mechanical stability.[5] Some porous nanoparticles are believed to provide nanochannel within the membrane that is small enough to reject salt ions but large enough to allow water to pass through improving flux.[6]

Cellulose nanocrystals (CNCs) are nanoscale cellulose filler material with dimensions that are smaller than membrane materials typically ca. 5-10 nm in width and 50-200 nm in length.[7-8] A previous study fabricated CNC-PA membranes using the vacuum filtration method and the monomer dispersion method.[9] It was found that the as received CNCs and the TEMPO oxidized CNCs (TCNCs) did not improve the RO membranes decreasing flux but maintaining salt rejection. Using the monomer dispersion method to fabricate as received CNC PA membranes resulted in increased flux in the RO membranes but slightly decreased salt rejection. In contrast, the monomer dispersion method with the TCNCs lead to increases in flux for all TCNC loadings from 0.05 wt% TCNC to 0.5 wt% TCNC in PA, while maintaining salt rejection. The result was that at the largest TCNC loading (0.5 wt% TOCN) the average flux of this composite was twice that of the control

membrane 10.9 ± 2.1 $Lm^{-2}h^{-1}$(LMH) compared to 4.1 ± 0.7 LMH, and the salt rejection of the composite was also slightly increased from 97.5% ± 0.3% to 99.0% ± 0.4%.[9]

From the favorable result of having increased flux in TCNC PA RO membranes it was concluded that the surface interaction of the TCNCs with the PA was more favorable than that of the as received CNCs.[9] It was ascribed this to the increased hydrogen bonding between the carboxylic acid groups on the TCNCs and the amine groups on the PA polymer. The interfacial interaction may have led to the development of nanochannels that allowed for increased flux of the water through the membrane, but the nanochannels were small enough to reject the salts.[9] The other conclusion was that the TCNCs dispersed well in the monomer dispersion method and poorly with the vacuum filtration method.[9]

Another study created membranes capable of even greater salt rejection and flux utilizing zwitterionic carbon nanotubes (CNTs) imbedded within a PA membrane.[6] This study found the addition of zwitterionic CNTs to PA membranes increased the flux by a factor of four going from 11.6 LMH to 48.8 LMH with similar or better salt rejection when 20 wt% of CNTs were added to the desalination membrane. It was concluded that water flowed through the CNTs as though it was a straw, and the zwitterionic groups present at ends of CNTs rejected dissolved salts. The charge of the zwitterionic groups was believed to reject ions effectively acting as a "gatekeeper" for charged salt species.[6]

The following is a report of the functionalization of CNCs to have tertiary amine terminal groups (TCNC) as well as CNCs with zwitterionic groups (ZCNC). ACNC were developed by coupling TCNCs with 1-ethyl-3-(3-dimethylaminopropyl)carbodiimide (EDC) and a subsequent reaction with 3-(dimethylamino)-1-propylamine. ZCNC were developed by the ring opening reaction of β-propiolactone and ACNCs. Ideally, the

resulting functionalized filler material will exhibit a good interface with the PA resulting in a RO membrane having nanochannels.[10] Additionally, the known resistance to biofouling of zwitterionic groups could make the addition of such particles even more enduring.[11-12]

4.2 Experimental:

This section details the methods used to develop the novel CNC surface chemistries (ACNCs) and (ZCNCs), the materials used, and the instruments used.

4.2.1 Materials:

Deionized water was obtained from Sybron Barnstead water purification system was used at ≥16.7 MΩ-cm. Ethyl acetate, acetone, sodium bromide (NaBr), tetrahydrofuran (THF), potassium chloride, and sodium hydroxide (NaOH) were purchased from Fisher Scientific. 4-dimethyl amino pyridine (DMAP) was purchased from Tokyo Chemical Industry, and β-propiolactone 97% purity was purchased from Beantown Chemical. Concentrated hydrochloric acid (HCl) was purchased from Spectrum Chemicals, and 1-ethyl-3-(3-dimethylaminopropyl)carbodiimide (EDC) was purchased from Creosalus. Dimethyl formamide (DMF), 2,2,6,6-tetramethylpiperidin-1-yl)oxyl (TEMPO), 3-(dimethylamino)-1-propylamine, and sodium chlorite (NaClO) solution (10-15%) were purchased from Millipore Sigma. Dialysis tubing was purchased from Fisher Education. Wood CNCs, isolated with sulfuric acid, were purchased from the University of Maine Forest Products Laboratory as an 11.8 wt% aqueous slurry and were previously characterized.[9] The centrifuge used was an Eppendorf 5810 equipped with a FA-45-6-30 capable of utilizing six 50-mL centrifuge tubes.

4.2.2 TEMPO Oxidation of CNCs (TCNCs):

CNC oxidation with TEMPO free-radical is based on previous protocols at an increased scale.[13,14] In a two-liter beaker 200 g of 11.8 wt% aqueous CNC slurry was combined with 1373 mL of deionized water. The mixture was homogenized by vigorous stirring on a 90 °C hot plate for 30-min intervals followed by 10-min intervals of sonication in a Branson sonication bath; these mixing methods were repeated until the mixture was visibly well mixed. In a separate beaker 650 mg of TEMPO free radical, 7.02 g of NaBr, and 400 mL of deionized water were combined and stirred until the solids dissolved (ca. 45 min). The solution of TEMPO, NaBr, and water was added to the CNC dispersion, and 109.4 mL of NaClO solution was added immediately after. The dropwise addition of 0.5 M NaOH solution over 3 h was used to keep the pH at 10. The reaction was terminated by the addition of 80 mL of ethanol. The TCNC dispersion was poured into dialysis tubes and dialyzed against deionized water for one week changing the dialysis water daily. The TCNCs dispersion was concentrated by rotary evaporation at 200 mbar and 90 °C to a final

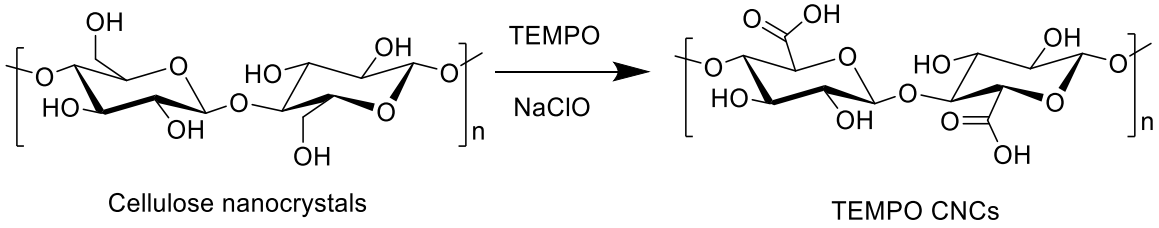

Figure 4.1: The reaction scheme shows converting as received CNCs to TCNCs and utilizes TEMPO and NaClO.

concentration of 19.1 mg mL^{-1}; this concentration was determined by evaporating 1 mL of TCNC dispersion onto an aluminum dish and taking the difference of the mass of the aluminum dish and the mass of the aluminum dish with dried TCNC dispersion. The reaction is shown in **Figure 4.1**.

4.2.3 Development of Tertiary Amine CNCs (ACNCs):

ACNCs were developed from adapting two protocols utilizing EDC coupling to attach primary amines to carboxylic acids forming amide linkages.[15-16] TCNC as an aqueous dispersion (150 mL) was added to each of two 1000-mL beakers, and 600 mL of acetone was slowly added without disturbing the aqueous phase. This biphasic mixture was allowed to stand quiescently for ca. 12 h. The top layer, consisting of mostly acetone and water, was decanted leaving a moist gel at the base. This gel, as 35-mL aliquots, was centrifuged at 10,000 RPM for 20 min in 50-mL centrifuge tubes and the supernatant liquid was decanted. After the supernatant was decanted, each pellet was combined with 35 mL of fresh acetone, vortex mixed at 3,000 RPM for ca. 2 min, centrifuged (10,000 RPM for 20 min), and discarding the supernatant; this washing procedure was repeated three times. All washed TCNC pellets were added to a media bottle containing 225 mL of DMF. The DMF and TCNC slurry was homogenized with an IKA Turrex homogenizer for 10 min operating at 5,000 PRM followed by bath sonication in for 1 h. DMF TCNC mixture was then rotary evaporated for 1 h at 200 mbar and 90 °C to remove residual acetone, and a 1-mL aliquot was dried on an aluminum plate to determine the concentration to be 9.8 mg mL^{-1}.

In order to attach a primary amine to the TCNCs, a previous protocol was followed but at a greater scale; the TCNC DMF mixture (203 mL) was diluted by adding 280 mL of DMF and stirred. The reagents EDC (58.8 g, 25 eq) and DMAP (37.3 g, 25 eq) were added to the TCNC DMF mixture and stirred for 30 min generating a frothy yellow mixture. The reactant 3-(dimethylamino)-1-propylamine (50 mL, 25 eq) was added and the mixture

became translucent; the reaction proceeded for 18 h at room temperature. The reaction is shown in **Figure 4.2**. The resulting ACNC product was evenly transferred into two large beakers, and while the products were stirred vigorously, the slow addition of 500 mL of ethyl acetate to each beaker cause some of the content to settle.

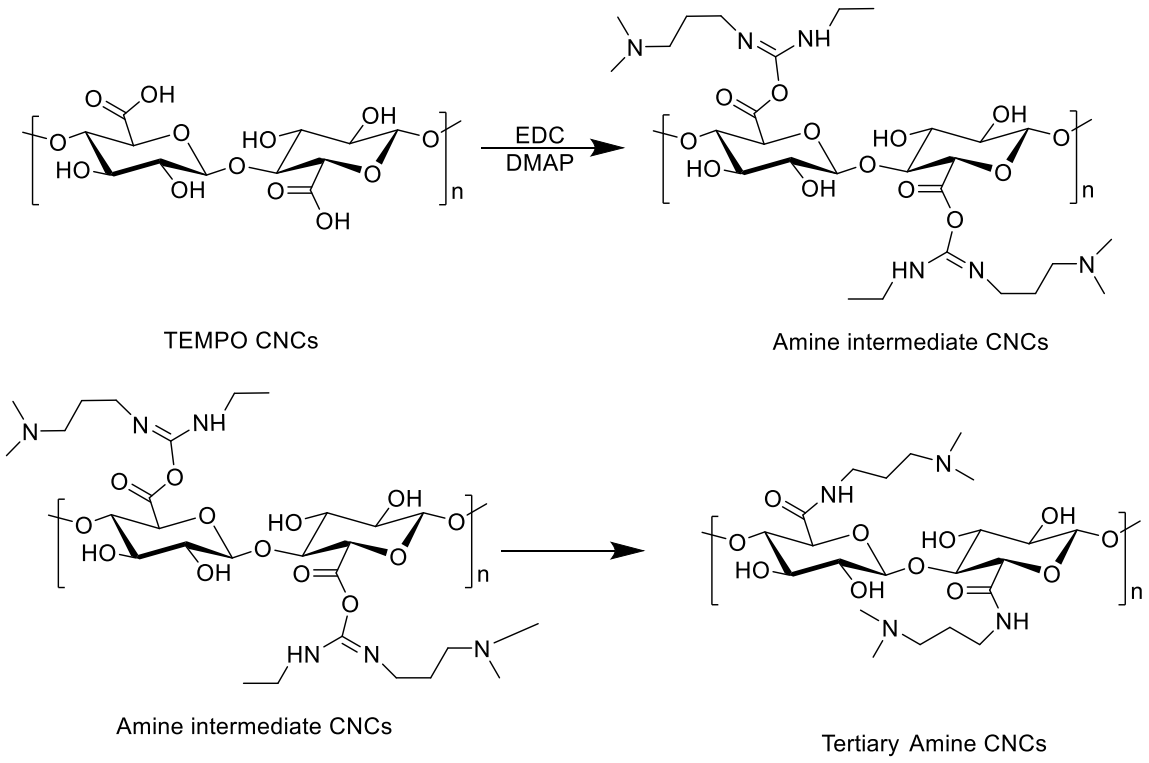

Figure 4.2: The reaction scheme shows converting TCNCs to ACNCs utilizing EDC coupling and an amide linkage with 3-(dimethylamino)-1-propylamine.

The ACNCs slurry was centrifuged (10,000 RPM for 20 min), the supernatant was discarded. Then the washing procedure began with the addition of 35 mL of fresh ethyl acetate, the pellet was vortex mixed at 3,000 RPM for ca. 2 min, centrifuged (10,000 RPM for 20 min), and the supernatant was discarded; this washing cycle was repeated three times. The same washing procedure was performed three times using 35 mL of deionized water instead of ethyl acetate. All resulting CNC pellets were combined with 250 mL of

deionized water and homogenized with the Turrex mixer for 10 min at 5,000 RPM and bath sonicated overnight. CNCs were dialyzed for four days against deionized water changing the dialysis water daily. The ACNCs dispersion was diluted to 500 mL with deionized water, and this dispersion was combined with a second batch of ACNC dispersion that was produced in the same manner at $5/6^{th}$ scale dispersed in 225 mL of deionized water. The resulting aqueous dispersion of ACNCs was found to be 3.6 mg mL^{-1} by evaporating 1 mL of dispersion on an aluminum dish.

4.2.4 Development of Zwitterionic CNCs (ZCNCs):

ZCNCs were developed based on previous methods used for developing zwitterionic CNTs and zwitterionic poly(carboxybetaine methacrylate).[10, 17] The procedure begins with a solvent exchange from water to THF, and this was accomplished by combining one-part (380 mL) of ACNC dispersion in water and three-parts THF and mixing. The ACNCs, water, and THF mixture was centrifuged (10,000 RPM, 20 min), the supernatant was discarded, and the pellets were combined into two centrifuge tubes. The ACNCs were combined 35 mL of fresh THF, vortex mixed for 3,000 RPM for ca. 2 min, centrifuged (10,000 RPM, 20 min), and the supernatant was discarded. The lids of the 50-mL centrifuge tubes were changed to septum modified lids. The ACNCs pellets were combined with 35 mL of anhydrous THF (CaH_2 distilled), vortex mixed (3,000 RPM, ca. 2 min) then centrifuged at 2,000 RPM for 30 min, the supernatant was decanted by syringe, dry THF was added (35 mL), and this washing process was performed three times.

The washed ACNC pellets were combined with 230 mL of dry THF by pouring under purge into a flame dried 250-mL flask in a cooling bath at 0 °C. The suspension of ACNCs in THF was stirred and equilibrated for 1 h and then β-propiolactone (0.56 mL,

1.1 eq) was injected into the flask. The reaction persisted at 0 °C for 4 h, and the reaction continued for another 16 h at 15 °C. The reaction is shown in **Figure 5.3**. The product was

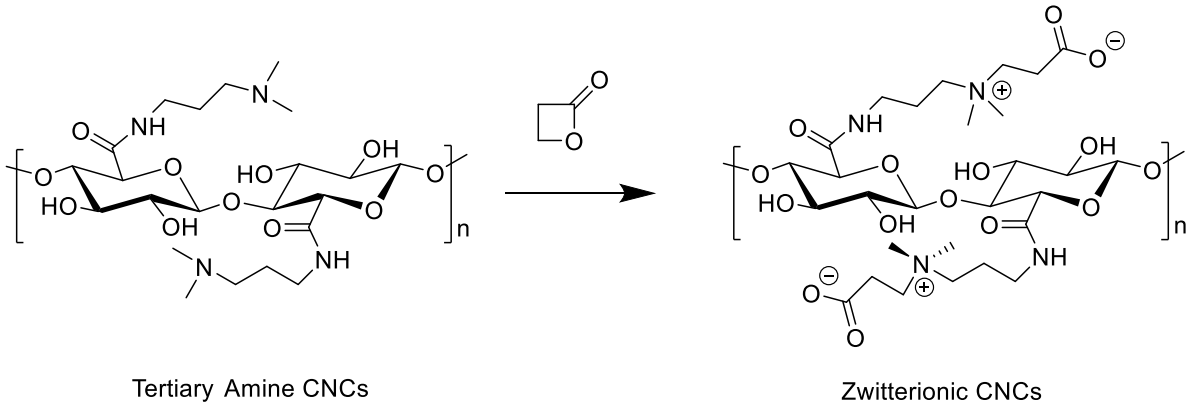

Figure 4.3: The reaction scheme shows converting ACNCs to ZCNCs utilizing β-propiolactone ring opening.

centrifuged (10,000 RPM, 20 min), the supernatant was decanted, 35 mL of dry THF was added, the tube was vortex mixed (3,000 RPM ca. 2 min), and the supernatant was discarded. The ZCNC pellet was then added to 70 mL of deionized water, vortex mixed (3,000 RPM, ca. 2 min), bath sonicated for 10 min, and dialyzed for 4 days changing dialysis water daily. The mixture was diluted to 500 mL and the dispersion of ZCNCs was found to be 2.1 mg mL^{-1} by evaporating 1 mL of dispersion on an aluminum dish.

4.2.5 X-ray photoelectron spectroscopy (XPS):

Samples in respective dispersions were solvent exchanged with THF, by the addition of 2-5 mL of aqueous CNC suspension to 30-33 mL of THF. This CNC mixture was centrifuged (10,000 RPM, 20 min), the supernatant was discarded, 35 mL of THF was added, this mixture was centrifuged a second time, and the supernatant was discarded. The centrifuge tubes were uncapped, and the CNC pellets dried at room temperature under air. These CNC pellets were analyzed on a PHI Versa Probe III scanning XPS microscope using monochromatic Al K-α X-ray source (1486.6 eV). Binding energies were referenced

to C-C peak at 284.8 eV. Survey scans were done as a 280-eV pass energy (1.0 eV step$^{-1)}$ for 5 sweeps. High resolution spectra for carbon, nitrogen, and oxygen were done at 26-eV pass energies (0.1 eV step^{-1}), for 20, 60, and 10 sweeps respectively.

4.2.6 Fourier Transform Infrared spectroscopy (FTIR):

The CNC pellets prepared for XPS were also used for FTIR analysis. CNC samples were evaluated on a Thermo Scientific Nicolet iS 7 for 32 scans in the 4000-600 cm^{-1} region after subtracting the background spectrum from each sample spectrum.

4.2.7 Conductometric Titrations:

From each aqueous dispersion of CNCs, TCNCs, ACNCs, and ZCNCs 50 mg of CNCs was added to 50-mL beakers. To these beakers 5 mL of 0.01 M KCl solution was added, the mixtures were then diluted to 29 mL with deionized water, the pH was adjusted to 2 with ca. 0.4 mL of 1 M HCl, and the final volume was adjusted to 30 mL with deionized water. The initial conductivity was recorded and 200-µL aliquots of 0.05 M NaOH were added, and 20-µL aliquots of NaOH were added below ca. 1600 µS to increase the graph resolution.

4.3 Results and Discussion:

This section details the results that were obtained in the experimental section and conclusions that can be drawn from these results.

4.3.1 Development of ACNCs and ZCNCs:

Chemistry used to oxidize CNCs to obtain TCNCs is commonly performed, therefore this section will focus on the development of ACNCs and ZCNCs. The EDC coupling is a system used to create bulky intermediates that will selectively form amide linkages when in the presence of primary amines. This reaction pathway selectivity for

primary amines is evident as EDC has a tertiary amine group. This reaction pathway has been previously utilized generating both aliphatic terminal CNCs[18] and CNCs with *boc*-protected primary amines that can be hydrolyzed to become CNCs with terminal primary amines.[15]

The ZCNC chemistry has not been previously performed, and this is the first attempt we are aware of to have positive and negative charges on CNC surfaces in close proximity. The presented chemistry is largely adapted from previous publications that used β-propiolactone in either dry acetone or dry THF. These reactions were done at either 15 °C or room temperature for 4 h; the reaction scheme presented used 0 °C for 4 h and 15 °C for 16 h. These temperatures were chosen to first to ensure that the most selective groups present would could react with β-propiolactone and then to ensure that all β-propiolactone had reacted. The increased reaction time at a higher temperature was done in the interest of safety as β-propiolactone is toxic.

4.3.2 X-ray photoelectron spectroscopy (XPS):

XPS was used to analyze the amount of nitrogen on the surface of the ACNCs and ZCNCs. The spectra showed that there was 2-3% nitrogen content for both ACNCs and ZCNCs. Both spectra have two peaks present in the high-resolution nitrogen scans for both the ACNCs and ZCNCs (**Figure 5.4**). The peak at ca. 400 eV was assigned to be the amide nitrogen ($O=C-NR_2$) and the amine nitrogen (NR_3) in our sytem.[19] The other nitrogen peak at ca. 403 eV is difficult to assign, as many nitrogen species share common areas and the resolution of XPS is notoriously poor. The peak at ca. 403 eV is most likely due to a nitrogen species carrying a charge as either an ammonium salt ($HNR_3^+Cl^-$) or a quaternary amine nitrogen in the case of the ZCNCs (NR_4^+).[20]

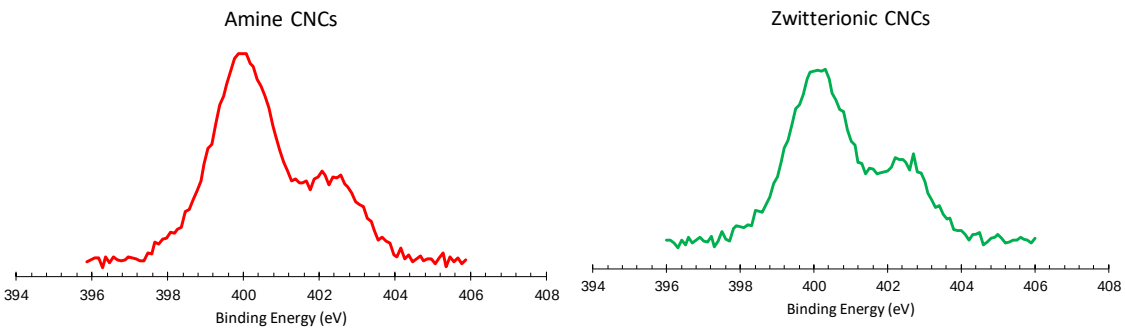

Figure 4.4: XPS high resolution spectra of ACNCs and ZCNCs show peaks at binding energy ca. 400 peak and a peak at ca. 403.

4.3.4 Fourier Transform Infrared Spectroscopy (FTIR):

The FTIR spectrum of the TCNCs shows that there is a peak indicative of carbonyl groups at ca. 1600 cm^{-1} (**Figure 4.5**). In the ACNC FTIR spectrum the carboxylic acid carbonyl (C=O) peak at 1600 cm^{-1} is somewhat muted, and there are not clear indicators of amine being added to ACNCs N-H at ca. 3400 cm^{-1}, C-H at ca. 1600 cm^{-1}, or the C-N 1300 cm^{-1}. This could be attributed in large part to the poor resolution of FTIR spectra. The ZCNCs FTIR spectrum shows a second carboxylic acid peak at ca. 1730 cm^{-1}; this peak supports the proposed reaction of reaction of β-propiolactone with the ACNCs forming a tertiary amine. The rest of the spectrum does not seem to imply that residual imides or carbodiimide (ca. 2130 cm^{-1}) are present from residual EDC.

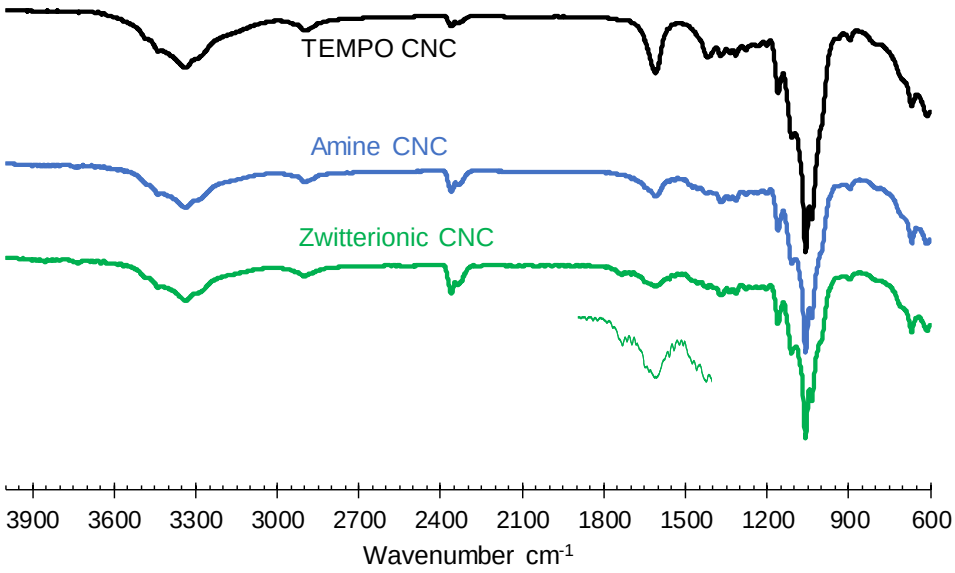

Figure 4.5: FTIR spectra of TCNCs, ACNCs, and ZCNCs show is a notable suppression of the carboxylic acid peak for ACNCs and ZCNCs at ca. 1600 cm^{-1} and ca. 1730 cm^{-1}. The green line below the ZCNCs highlights the carboxylic acid peak at ca. 1730 cm^{-1}.

4.3.5 Conductometric Titration:

Conductometric titrations were used to find the number of acidic groups in the TCNC, ACNC, and ZCNC dispersions (**Figure 4.6**). The first region of each curve is where the strong acid and base are forming NaCl, the conductivity is decreasing as the hydronium (OH^-) ions are being consumed to form water (H_2O) and the Na^+ ions, which do not contribute to the conductivity as much the hydronium ions. The second region of each curve, the flat region is where the carboxylic acid groups (COOH) are being deprotonated (COO^-), nothing is contributing to the conductivity of the solution as the ion pair COO^- Na^+ does not dissociate well. The last region of the curve, the increasing region is where the ammonium ion (NR_3H^+) with the counter chlorine ion (Cl^-) is being deprotonated and

contributing NaCl to the solution. In addition, the strong base allows Na^+ ions and OH^- ions to further increase the conductivity of the solution.

The mmol kg^{-1} of acidic groups for the TCNCs, ACNCs, and ZCNCs was found as the number of millimoles of NaOH for the flat region of the curve over the mass of CNCs ($mmols_{NaOH} \div kg_{CNCs}$). The as received CNC were found to have 80 mmol kg^{-1}. The TCNCs were found to have 1060 mmol·kg^{-1}, the ACNCs were found to have 540 mmol·kg^{-1}, and the ZCNCs were found to have 760 mmol·kg^{-1}. Because the tertiary amine groups did not contribute to the flat region of the curve, the difference between the TCNCs and ACNCs represents the number of ACNC groups 520 mmol kg^{-1}. The number of acidic groups added to the ACNCs is the difference in the conductivity of the ACNCs and ZCNCs, therefore the number of added carboxylic acids 220 mmol·kg^{-1}; thus, there are 220 mmol·kg^{-1} of zwitterionic groups on the ZCNCs.

A major drawback of using conductimetric titration is that large amounts of material (ca. 250-mg) are consumed using auto-titrators. We instead chose to do this manually using only 50 mg instead. This allowed for most of the CNCs to be allocated for composite membrane preparation as opposed to conductometric titration.

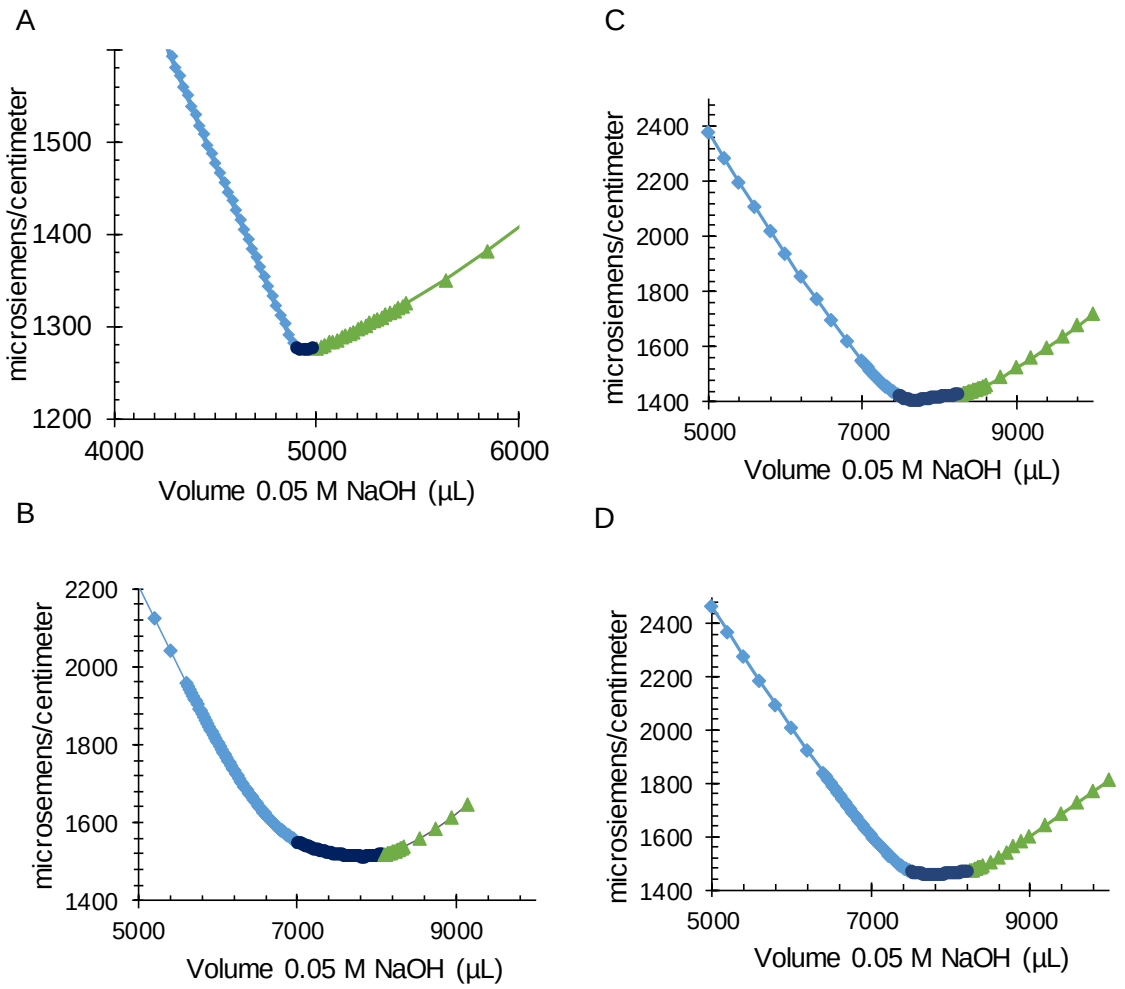

Figure 4.6: Conductometric titrations of CNCs (**A**), TCNCs (**B**), ACNCs (**C**), and ZCNCs (**D**) show the conductivity of the solution as NaOH is added. The light blue region (♦) represent the acidic region where HCl is present, the dark blue region (●) represents the flat region of the curve and the number of acidic groups on the CNCs, and the green ▲ region represents the alkaline region of the curve, where NaOH is present.

4.4 Conclusions:

The results show that there was a definite change in composition from the TCNCs, ACNCs, and with the ZCNCs. The FTIR analysis along with the results from the conductometric titration is sufficient to conclude that the functionalization of as received CNCs happened as indicated in **Figure 4.1**. The reaction with the TCNCs with 3-

(dimethylamino)-1-propylamine mediated by EDC coupling was characterized with XPS and FTIR. The XPS characterization of the ACNCs showed an increase in the amount of nitrogen as well as binding energies (400 eV and 403 eV) that could be explained as amides, amines, and ammonium salts. The FTIR characterization showed there were no peaks that indicated residual reactants from the EDC coupling and the carboxylic acid peak at 1600 cm^{-1} was suppressed. The FTIR spectrum of the ZCNCs also had the suppressed carboxylic acid peak at 1600 cm^{-1} but had a second carboxylic acid peak at 1730 cm^{-1}.

Finding functional groups on CNCs in small quantities is typically difficult. However, we believed that the tertiary amine functional groups are on the ACNCs and that the zwitterionic groups are present on the ZCNCs. We look forward to the eventual testing of these ZNCs for the intended application of RO membranes.

References:

1. Rogers, P., Facing the Freshwater CRISIS. *Scientific American* **2008,** *299* (2), 46-53.
2. Wada, Y.; van Beek, L. P. H.; van Kempen, C. M.; Reckman, J. W. T. M.; Vasak, S.; Bierkens, M. F. P., Global depletion of groundwater resources. *Geophysical Research Letters* **2010,** *37* (20).
3. Greenlee, L. F.; Lawler, D. F.; Freeman, B. D.; Marrot, B.; Moulin, P., Reverse osmosis desalination: Water sources, technology, and today's challenges. *Water Research* **2009,** *43* (9), 2317-2348.
4. Kucera, J., Introduction and History of Development. In *Reverse Osmosis*, Kucera, J., Ed. 2010; pp 1-13.
5. Fritzmann, C.; Löwenberg, J.; Wintgens, T.; Melin, T., State-of-the-art of reverse osmosis desalination. *Desalination* **2007,** *216* (1), 1-76.
6. Chan, W.-F.; Chen, H.-y.; Surapathi, A.; Taylor, M. G.; Shao, X.; Marand, E.; Johnson, J. K., Zwitterion Functionalized Carbon Nanotube/Polyamide Nanocomposite Membranes for Water Desalination. *ACS Nano* **2013,** *7* (6), 5308-5319.
7. Sacui, I. A.; Nieuwendaal, R. C.; Burnett, D. J.; Stranick, S. J.; Jorfi, M.; Weder, C.; Foster, E. J.; Olsson, R. T.; Gilman, J. W., Comparison of the properties of cellulose nanocrystals and cellulose nanofibrils isolated from bacteria, tunicate, and wood processed using acid, enzymatic, mechanical, and oxidative methods. *ACS Appl Mater Interfaces* **2014,** *6* (9), 6127-38.

8. Moon, R. J.; Martini, A.; Nairn, J.; Simonsen, J.; Youngblood, J., Cellulose nanomaterials review: structure, properties and nanocomposites. *Chemical Society Reviews* **2011,** *40* (7), 3941-3994.
9. Smith, D. E.; Hendren, D. K.; Haag, V. J.; Foster, J. E.; Martin, M. S., Functionalized Cellulose Nanocrystal Nanocomposite Membranes with Controlled Interfacial Transport for Improved Reverse Osmosis Performance. *Nanomaterials* **2019,** *9* (1).
10. Surapathi, A.; Chen, H.-y.; Marand, E.; Karl Johnson, J.; Sedlakova, Z., Gas sorption properties of zwitterion-functionalized carbon nanotubes. *Journal of Membrane Science* **2013,** *429*, 88-94.
11. Yu, H. Y.; Yan, C. F.; Yao, J. M., Fully biodegradable food packaging materials based on functionalized cellulose nanocrystals/poly(3-hydroxybutyrate-co-3-hydroxyvalerate) nanocomposites. *Rsc Advances* **2014,** *4* (104), 59792-59802.
12. Shao, Q.; Jiang, S., Molecular Understanding and Design of Zwitterionic Materials. *Advanced Materials* **2015,** *27* (1), 15-26.
13. Hendren, K. D.; Baughman, T. W.; Deck, P. A.; Foster, E. J., In situ dispersion and polymerization of polyethylene cellulose nanocrystal-based nanocomposites. *Journal of Applied Polymer Science* **2020,** *137* (13), 48500.
14. Saito, T.; Isogai, A., TEMPO-mediated oxidation of native cellulose. The effect of oxidation conditions on chemical and crystal structures of the water- insoluble fractions. *Biomacromolecules* **2004,** *5*.
15. Way, A. E.; Hsu, L.; Shanmuganathan, K.; Weder, C.; Rowan, S. J., pH-Responsive Cellulose Nanocrystal Gels and Nanocomposites. *Acs Macro Letters* **2012,** *1* (8), 1001-1006.
16. Cudjoe, E. Cellulose Nanocrystals and Related Polymer Nanocomposites. Case Western Reserve University, 2017.
17. Zhang, Z.; Chen, S. F.; Jiang, S. Y., Dual-functional biomimetic materials: Nonfouling poly(carboxybetaine) with active functional groups for protein immobilization. *Biomacromolecules* **2006,** *7* (12), 3311-3315.
18. Dagnon, K. L.; Way, A. E.; Carson, S. O.; Silva, J.; Maia, J.; Rowan, S. J., Controlling the Rate of Water-Induced Switching in Mechanically Dynamic Cellulose Nanocrystal Composites. *Macromolecules* **2013,** *46* (20), 8203-8212.
19. Zorn, G.; Liu, L.-H.; Árnadóttir, L.; Wang, H.; Gamble, L. J.; Castner, D. G.; Yan, M., X-ray Photoelectron Spectroscopy Investigation of the Nitrogen Species in Photoactive Perfluorophenylazide-Modified Surfaces. *The Journal of Physical Chemistry C* **2014,** *118* (1), 376-383.
20. Wei, X. L.; Fahlman, M.; Epstein, A. J., XPS Study of Highly Sulfonated Polyaniline. *Macromolecules* **1999,** *32* (9), 3114-3117.

Chapter 5: Cellulose nanocrystal-reinforced poly(5-triethoxysilyl-2-norbornene) composites

This Chapter is adapted from the publication: “Cellulose nanocrystal-reinforced poly(5-triethoxysilyl-2-norbornene) composites” in the journal Polymer Chemistry with permission from the Royal Society of Chemistry.

I recognize the contribution of Morgan A. Higgins, as co-first author of this publication, sharing equal responsibility of fabrication, characterization, ideas, and data analysis. I recognize that the coauthors Brian K. Long and E. Johan Foster, contributed ideas, data analysis, document refinement, and document editing.

Cellulose nanocrystal-reinforced poly(5-triethoxysilyl-2-norbornene) composites

Keith D. Hendren, Morgan A. Higgins, Brian K. Long, and E. Johan Foster

Abstract:

We demonstrate the reinforcement of a previously inaccessible norbornene-silane with a stiff, bio-based nanofiller. Poly(5-triethoxysilyl-2-norbornene) (PTESN), a glassy and thermally stable polymer, was combined with cellulose nanocrystals (CNCs) and solvent cast from toluene to form reinforced materials. Composite films showed excellent translucency and no visible aggregation, which was supported by scanning electron micrographs that showed no signs of CNC aggregation within the polymer matrix. Reinforcement was evident at moderate of 5 wt% CNC loading, showing a statistically significant enhancement for both Young's modulus (540 MPa vs 970 MPa) and storage modulus at 25 °C (400 MPa vs 1200 MPa). We suspect that there is a strong interaction between the polymer and CNC filler based upon the increase of thermal degradation temperature of the CNCs increasing, for example from 278 °C to 295 °C at 10 wt% CNCs. These interactions were probed via solid-state NMR, which suggests that no covalent bonding occurs between the triethoxylsilyl substituents of the polymer and the CNCs. We therefore hypothesize that hydrogen bonding interactions between PTESN and CNCs are responsible for the increased thermal stability and reinforcement of the polymer material.

5.1 Introduction:

Alkoxysilane-functionalized vinyl-addition polynorbornenes are an intriguing polymer class whose high molecular weight homopolymers were only recently accessed via careful catalyst selection (**Figure 5.1**).[1-2] The prototypical vinyl-addition homopolymer poly(5-triethoxysilyl-2-norbornene) (PTESN) was

preceded by other polymers with similar functionality, but that were made via ring opening metathesis polymerization (ROMP) to yield either rubbery[2] and glassy polynorbornenes[3] bearing trimethoxysilane or triethoxysilane pendant groups. However, PTESN films made via vinyl-addition are frequently more mechanically robust than their analogous ROMP polymers, which are often rubbery and exhibit tacky character.[2]

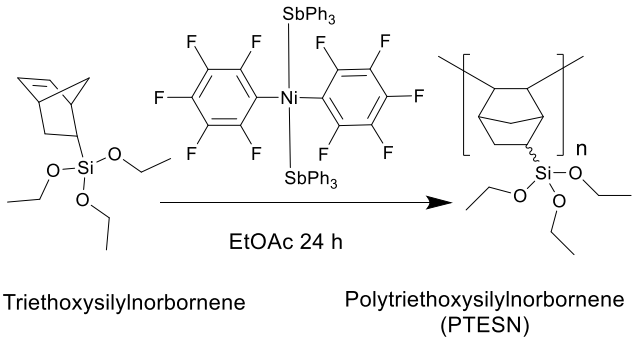

Figure 5.1: Vinyl-addition reaction scheme shows PTESN synthesis with the catalyst trans-[Ni(C_6F_5)$_2$($SbPh_3$)$_2$].

Cellulose nanocrystals (CNCs) are a unique filler material that has been previously incorporated into a wide variety of polymer matrices for reinforcement, through many different techniques such as solvent exchange,[4] melt mixing,[5] solvent casting,[6] and surface modification of CNCs.[6] CNCs are most commonly made into composite materials by dispersion into polar organic solvents, into which the polymer can also be dissolved and cast.[7] Another interesting and successful strategy of composite fabrication with CNCs and latex has been the emulsifying of the polymer into water and allowing the emulsified particles to interact with CNC particles.[8] Strategies for the incorporation of CNCs into a polymer matrix depend on the chemistry and morphology of the polymer.[9]

PTESN was previously characterized and shown to have moderate mechanical properties, making it an ideal prototype to expand the mechanical properties of this material

class.[10] Therefore, reinforcement of this and other alkoxysilane substituted, vinyl-addition polynorbornenes will ultimately allow this class of materials to be used in much broader range of applications. As such, (CNCs) were chosen as an additive, as they possess an uncommon filler property of being largely transparent when well dispersed in addition to reinforcing polymer matrices.[11] Ideally, unfunctionalized CNCs are utilized in order to maximize hydrogen bonding interactions between CNCs and reinforce the host polymer. This reinforcement is generally more prevalent at higher CNC concentrations, as percolation networks can be formed under such conditions.[8]

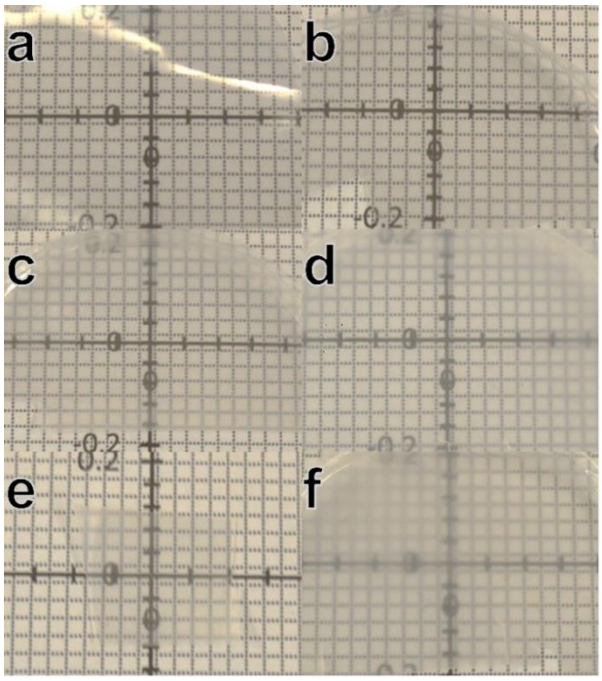

Figure 5.2: Optical photographs are arranged in order of increasing CNC content: **5.2a** PTESN, **5.2b** 1-CNC-PTESN, **5.2c** 5-CNC-PTESN, **5.2d** 10-CNC-PTESN, **5.2e** 15-CNC-PTESN, and **5.2f** 20-CNC-PTESN.

Previous efforts to reinforce alkoxysilane-bearing polymers using CNCs have focused on acrylate-based polymers and used CNCs as a platform for crosslinking.[12-19] Vinyl-addition polynorbornenes discussed here are distinct from those silane containing

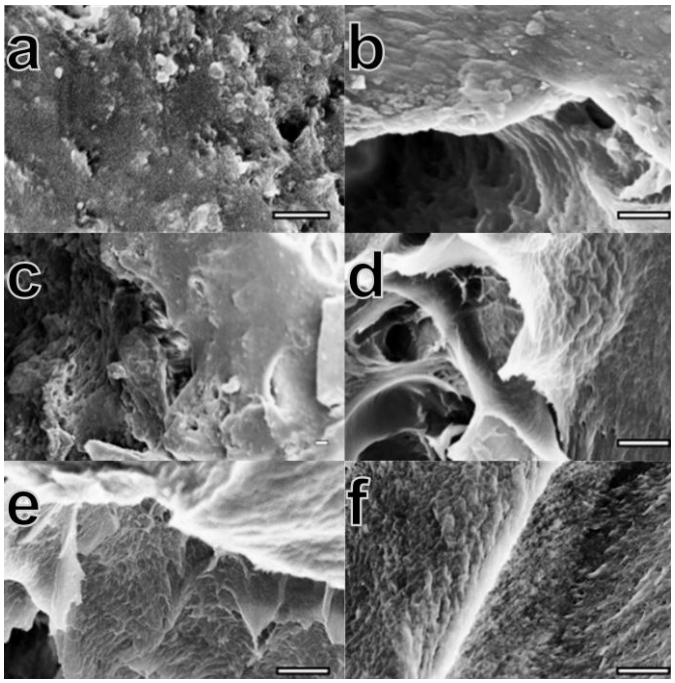

Figure 5.3: SEM micrographs are arranged in order of increasing CNC content. **5.3a** PTESN, **5.3b** 1-CNC-PTESN, and **5.3c** 5-CNC-PTESN, **5.3d** 10-CNC-PTESN, **5.3e** 15-CNC-PTESN, and **5.3f** 20-CNC-PTESN. All scale bars are 1 µm.

polymers that were combined with CNCs, such as trialkoxysilane functionalized polyacrylates, as they have a bicyclic backbone and form a rigid polymer without a need to use a crosslinking platform. Herein we show that we can easily fabricate CNC-PTESN composites that are dispersed by simple solvent casting from toluene. Confirmation of minimal aggregation was obtained from scanning electron microscope (SEM) and transmission electron microscope (TEM) imaging. Even at CNC concentrations as high as 20 wt% in PTESN (20-CNC-PTESN), TEM showed only very small as clusters of CNC aggregates. The dispersion was made more evident with mechanical reinforcement of the matrix polymer at high concentrations of filler loadings, illustrated by increases in the storage and Young's modulus, implying reinforcement from filler-filler and filler-matrix interactions. This work uses a novel polymer-filler system to study silane-OH interactions.

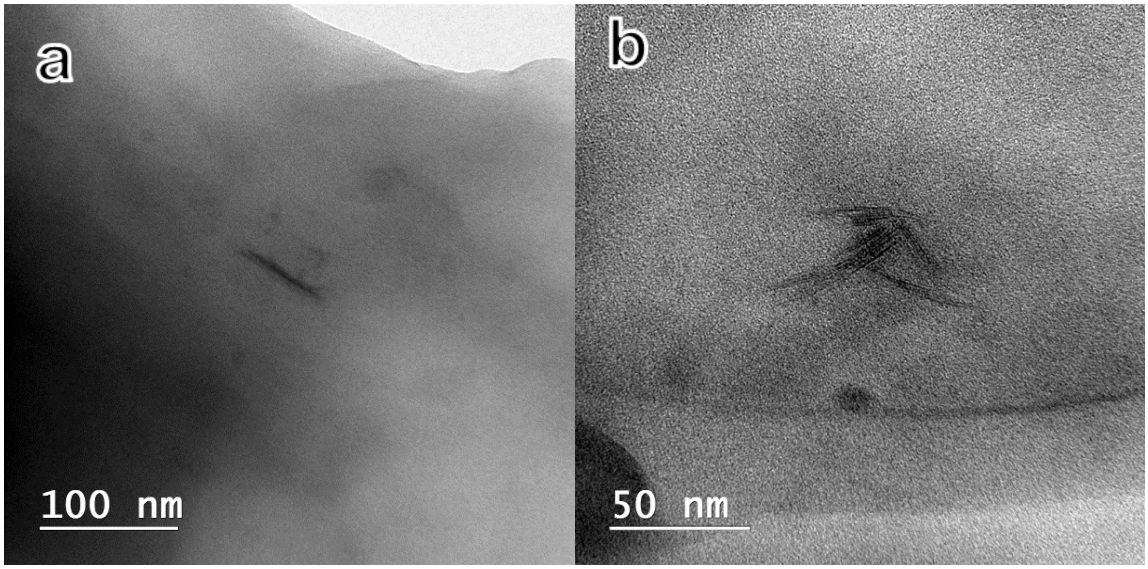

Figure 5.4: TEM images of 20-CNC-PTESN show occasional nanoscale aggregation of CNCs in PTESN composite films. The findings of occasional minor aggregation from images **5.4a** and **5.4b** suggest good dispersion.

5.2 Results & Discussion:

The PTESN-CNC composite materials described herein are denoted as "#-CNC-PTESN" wherein the "#" represents the wt% of CNCs dispersed in the composite material. Typically, dispersion of CNCs into a polymer matrix from solvent casting requires a polar organic solvent. However, as we will show, we found that CNCs could be readily dispersed in a PTESN matrix using toluene, a nonpolar solvent that fails to disperse unfunctionalized CNCs[20] without the aid of a surfactant.[21] These polymer solutions with CNCs could then be readily cast to yield CNC-PTESN composite films with apparent optical transparency when pressed against a field and possessing no macroscopically visible clusters or aggregates (**Figure 5.2**), despite toluene being a poor CNC dispersing solvent.[20] However, as expected the randomly oriented nanoparticles scatter visible light. Observation with polarized optical microscopy did not show significant birefringence diagnostic of a liquid crystalline phase. SEM imaging used to examine the fracture surface of the composites

found an absence of CNC aggregation on a 1-10 μm scale within cast films, suggesting that negligible amounts of CNC clusters were present at this scale. Further, the presence of nanosized features in PTESN **Figure 5.3a** made it exceedingly difficult to confirm the presence of dispersed CNCs in the other polymer films **Figures 5.3b-5.3f**. TEM imaging of these composite films did reveal the presence of some small clusters of aggregated CNCs within the polymer matrix (**Figure 5.4**). However, it should be noted that TEM imaging of individual CNCs within a carbon-based polymer matrix is exceedingly difficult[22] as the width of CNCs approach the resolution and contrast limits of TEM. This makes smaller clusters or individual CNCs difficult to image using this technique. As such, the lack of aggregated species on the macroscopic scale (**Figure 5.2**) and the lack of significant aggregation via TEM imaging (**Figure 5.4**) suggest that there is a good dispersion of CNCs within the matrix, though the authors acknowledge this is not definitive proof of ideal CNC dispersion.

The DMA data indicates that storage modulus E' is increased at CNC concentrations as low as 5 wt%, and steadily increases as a function of CNC loading percent starting at an initial value of 400 MPa for PTESN and ending with a value of 1200 MPa for PTESN-20-CNC at 25 °C (**Table S1**). It should be noted that the applications available for a polymer with a storage modulus of 1200 MPa are significantly broader than those applicable to non-reinforced PTESN, thereby opening the use of these nanocomposites to a broader audience.

Representative tan δ curves (**Figure 5.5**) show a shift in the glass transition temperature of the composite material indicating strong interactions between filler and matrix.[23] Further, broadening is observed which has been ascribed to the loss of mobility

of the polymer chains through the possible mechanisms of friction from filler particle interactions, filler polymer motion at filler interface, or a change in polymer properties at filler interface.[23-24]

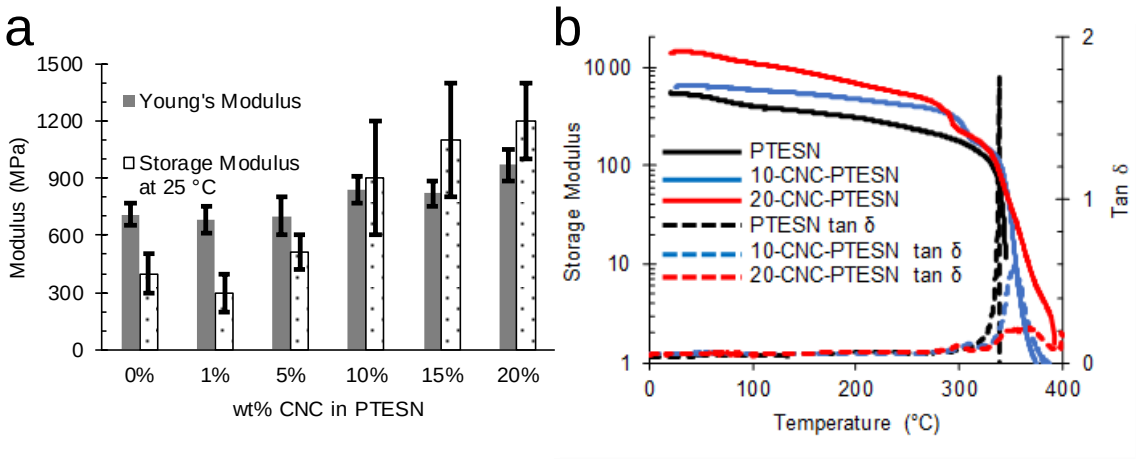

Figure 5.5: PTESN CNC composites were tested with dynamic mechanical analysis (DMA) and tensile testing. Reinforcement from increased stiffness (E' and E) is presented on bar graph **5.5a** and DMA traces show the increase in storage modulus (E') with increasing CNC content **5.5b**.

Young's modulus increases as CNC loading is increased, and significant enhancements are observed at 5 wt% CNC loading increasing from the neat polymer at 540 MPa to 700 MPa and further increased for 20-CNC-PTESN to 970 MPa. The strain at break and toughness have a trend of decreasing toughness and elongation at break with increased CNC loading. In contrast there is not a clear trend with the change in maximum tensile stress as the experimental error of the neat PTESN and 1-CNC-PTESN. Data from **Table S5.2** and representative curves (**Figure S5.3**) show these trends.

Thermal gravimetric analysis of these composites revealed an increase in the thermal degradation temperature of the CNCs °C 15-CNC-PTESN, and 283 °C for the 20-CNC-PTESN sample (**Figure 5.6**). Notably 1-CNC-PTESN and 5-CNC-PTESN do not have a clear degradation event associated with CNCs. Previous studies have hypothesized

that there is an increase in thermal stability of cellulose composite materials when there are favorable interactions between the filler and matrix arising from van der Waals interactions and hydrogen bonding, and a decrease in thermal stability upon aggregation of the cellulose filler.23 Application of this relationship could correspond to a 10-CNC-PTESN that is well dispersed and thermally stabilized and for 15-CNC-PTESN and 20-CNC-PTESN samples approach the onset of aggregation for the material. Data for all TGA traces is available as **Figure S5.4**.

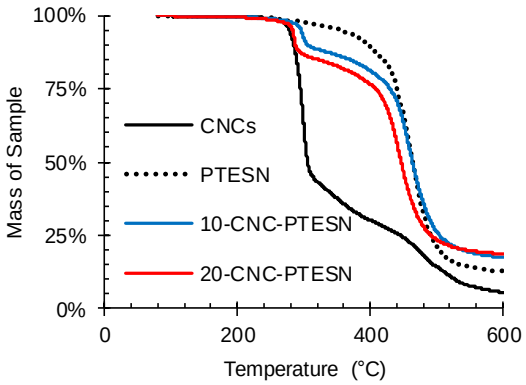

Figure 5.6: Thermogravimetric analysis of neat CNCs, 10-CNC-PTESN, 20-CNC-PTESN, and PTESN show that the CNCs have increased thermal stability when combined with PTESN. The 5 wt% loss for neat CNCs is ca. 278 °C, 10-CNC-PTESN is ca. 295 °C, and 20-CNC-PTESN is ca. 283 °C, and PTESN is 354 °C.

Previous polymers that have been able to increase the degradation temperature of CNCs include polyvinyl alcohol,[25] polyfuryl alcohol (PFA),[26] and γ-aminopropyltrimethoxysilane (APS) functionalized CNCs in polyurethane.[15] Interestingly, the PFA-CNC composite showed great thermal stability and its (C-O-C) backbone is analogous to PTESN's pendant groups (Si-O-C) as only being able to accept hydrogen bonds. Additionally, APS functionalized CNCs mixed with polyurethane are interesting as

the trimethoxysilane functional groups on the CNCs may have similar interactions as the CNC-PTESN composite system studied herein.

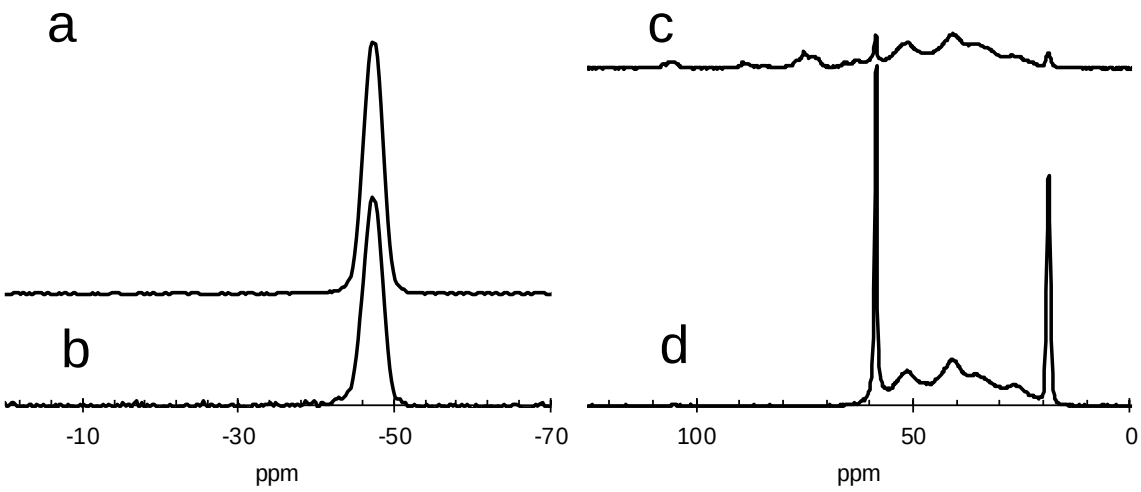

Figure 5.7: Solid-State NMR spectra of PTESN and 20-CNC-PTESN are shown with the number of scans noted in parenthesis. The ^{29}Si NMR spectra for **5.7a)** neat PTESN (2000) is **5.7a)** and **5.7b)** is 20-CNC-PTESN (32000). The ^{13}C spectra of neat CNCs is **5.7c)** (8000) and **5.7d)** is 20-CNC-PTESN (8000).

To better understand how and why we are able to readily disperse CNCs in a PTESN matrix using a typically poor performing solvent, toluene, we looked to a previous study that explained favorable interactions between alkoxysilane molecules and cellulose fibers.[13] This study suggested that alkoxysilane groups are subject to reactions with alcohols and adventitious water to form silanol groups (Si-OH). Furthermore, previous studies have shown that cellulose may form covalent bonds with these pendant side groups (Si-O-cellulose) and residual moisture may lead to possible siloxane linkages (Si-O-Si) under similar conditions.[13, 27] In our study, solid-state NMR (^{29}Si and ^{13}C) was employed to interrogate both the PTESN and 20-CNC-PTESN systems (**Figure 5.7**).

The ^{29}Si NMR spectra for PTESN and 20-CNC-PTESN are shown in **Figure 5.7** in which both samples showed only a single resonance indicating that there is no detectable amount of hydrolysis (Si-OH) or etherification reactions (Si-O-Si) occurring. Previous

studies that have found additional peaks further upfield ca. 7-9 ppm for self-condensed (Si-O-Si) etherification bonds and hydrolysis (Si-OH).[13, 27] These studies were unable to directly detect the presence of (Si-O-) groups bonded to cellulose as there likely not an appreciable change in chemical shift. The solid-state ^{13}C spectrum of the 20-CNC-PTESN, has peaks are similar to previous ^{13}C spectra of the neat polymer[1] with expected peaks from cellulose.[28] Although this is not conclusive, as we believe the number of reactions, if any are occurring, are below the detection limit of NMR, and we do not discount the possibility of hydrolysis reactions. Although water was not directly added to the system, atmospheric water did have ample opportunity to react with the PTESN and 20-CNC-PTESN, however, there is no evidence of hydrolysis occurring in **Figure 5.7**. As water is more reactive than primary ether species (C-OH) we believe that (Si-O-CNC) linkages are unlikely.

Hydrolysis reactions creating (Si-OH) groups would likely improve interactions between the CNCs and the pendant groups, which would then act as strong hydrogen bond acceptors and donors for the numerous hydroxyls displayed on the CNCs. The significant reinforcement observed indicates that some advantageous interactions between the polymer and filler are present and based upon the spectral data collected we hypothesize that hydrogen bonding between the CNCs and the Si-O-R moieties, with or without water, are the most likely sources of these favourable interactions.

5.3 Experimental:

5.3.1 Materials:

The catalyst trans-[$Ni(C_6F_5)_2(SbPh_3)_2$] and monomer 5-triethoxysilyl-2-norbornene were synthesized according to literature procedures.[1, 10] Ethyl acetate (EtOAc) was dried over CaH_2 and degassed via three freeze-pump-thaw cycles. All polymerizations were conducted in a glovebox under air-free conditions unless otherwise noted. Solution-state NMR spectroscopy was conducted using a Varian Mercury Vx 300 MHz instrument and referenced to residual solvent. Wood CNCs hydrolyzed from sulfuric acid with 0.94% sulfur content by weight and dimensions of 90 ± 40 nm by 7 ± 2 nm (**Figure S5.5**) were obtained from the University of Maine Forest Products Laboratory and dried overnight at 50 °C under high vacuum before use.

5.3.2 Synthesis of poly(triethoxysilylnorbornene) (PTESN):

Polymerizations were conducted using a modified literature procedure.[1, 10] In a typical polymerization, the catalyst *trans*-[$Ni(C_6F_5)_2(SbPh_3)_2$] (0.011 g, 10 μmol) was added to a stirred solution of ethyl acetate (EtOAc) (4 mL) and the monomer 5-triethoxysilyl-2-norbornene (2.56 g, 10 mmol). The polymerization was stirred for 24 h, then diluted with additional EtOAc (6 mL) and precipitated into excess methanol (**Figure 5.1**). The resultant polymer was isolated via vacuum filtration and dried *in vacuo* to yield PTESN (1.359 g, 53.1%, Mn 227 kg/mol, and Đ 2.18), which was characterized by NMR (**Figure S5.1**) and GPC (**Figure S5.2**). The dispersity agrees with the ranges previously published for vinyl-addition polymerizations.[1]

5.3.3 Gel Permeation Chromatography (GPC):

Molecular weight data for PTESN was measured using a Tosoh EcoSEC GPC operating at 40 °C in THF and molecular weight values are reported relative to polystyrene standards.

5.3.4 Fabrication of CNC-reinforced PTESN films:

CNCs were dried by heating at 50 °C under vacuum for 12-24 h. PTESN (0.5 g) was dissolved in toluene (10 mL) and pushed through 0.45 μm PTFE syringe filter into a clean vial. The dried CNCs (1-20 wt%) were added to the polymer solution, capped, and the resultant suspension stirred for 48 h. The suspension was then deposited onto a levelled Teflon casting dish, covered with aluminum foil, and the solvent slowly evaporated for 5 days. Recovered samples are referenced using the #-CNC-PTESN format in which # represents the wt% of CNCs relative to PTESN.

5.3.5 Dynamic Mechanical Analysis:

Dynamic mechanical analysis was conducted using a TA Instruments Q800 DMA using a film tension clamp and a temperature ramp from room temperature to 400 °C at 0.1% strain, 1 Hz, and a heating rate of 5 °C/min. Tested films were cut into rectangular coupons that were ca. 5 mm in width, 15 mm in length, and ca. 150 μm thick.

5.3.6 Tensile Testing:

Tensile tests were run on an Instron 5943 with a strain rate of 1 mm/min. The sample dimensions of the dog bone specimens were ca. 110 μm thick and 3.5 mm wide with a gauge length of ca. 15 mm.

5.3.7 Scanning Electron Microscopy:

PTESN and all CNC-PTESN composite films were fractured by bending the films to a 180° angle and gently pulling the two pieces apart. Films were placed on aluminum SEM holders on double stick carbon tape and oriented into a beach chair configuration and coated with 5 nm of iridium in a Leica Sputter Coater. Images of the fractured surface were taken using a Zeiss Leo Gemini SEM In-lens detector.

5.3.8 Transmission Electron Microscopy:

The 20-CNC-PTESN composite film was mounted on an SEM holder with folded single sided copper tape and coated with 5 nm of iridium using a Leica sputter coater. The sample was flipped, and the other side coated with another 5 nm of iridium. The sample was then embedded in epoxy and cut into 125 nm sections using a Diatome diamond knife on an RMC microtome with water at room temperature. Sample was retrieved from the microtome using the perfect loop method and a 300 mesh Peclo formvar coated lacey grid, which was then imaged using a JEOL 2100 TEM.

5.3.9 Solid State NMR:

Solid state ^{13}C and ^{29}Si NMR spectra were collected using a Bruker III 600 MHz NMR at 2000-32000 scans to analyze samples for a silyl ether reaction that may have taken place. Created films were ground in a Spex Cryomill for three 3 min cycles with a 1 min rest in between milling times. The ^{29}Si spectra (**Figures 5.7a-b**) correspond to PTESN and 20-CNC-PTESN. The 20-CNC-PTESN sample was chosen as it is the most likely to have a split peak in the ^{29}Si spectra indicating a possible hydrolysis or etherification reaction.[27] The neat PTESN sample was chosen as the control. The corresponding ^{13}C NMR (**Figure**

5.7 c-d) were present to verify agreement with the ^{29}Si NMR and note deviations from previous ^{13}C NMR scans of the monomeric species.[1]

5.3.10 Thermogravimetric Analysis:

Thermogravimetric analysis (TGA) was carried out on a TA Instruments Q10 with a temperature ramp of 10 °C min^{-1} from room temperature to 1000 °C in nitrogen atmosphere for all composite samples. The raw CNC sample was equilibrated to 80 °C and held isothermally for 20 minutes to drive off residual moisture. The data from the TGA were then taken from the base weight at 80 °C and plotted in **Figure 5.6** in the relevant temperature range 80-600 °C.

5.4 Conclusions:

Novel reinforced composites of PTESN and CNCs were cast from toluene. Though toluene is typically a poor solvent for CNC dispersion, we have shown that if PTESN is used as a polymer matrix, good CNC dispersion may be realized on both the macroscopic and nanoscopic scales. This is evidenced by the mechanical reinforcement observed through both tensile and DMA results, which show significant improvements at 5 wt% loading.[22] The higher thermal degradation temperature of the CNC as composites, as compared to the neat CNCs, suggests CNCs in contact with alkoxysilanes can be melt processed into a variety of other silanes, opening these fillers up to use in a much larger variety of applications. This indicates the reported methods should allow lower melting point polymers of this type to be processed by extrusion, melt mixing and other conventional means leading to a new class of thermally stable CNC composite materials.

Conflicts of interest:

The authors declare no conflict of interests.

Acknowledgements:

The authors would like to acknowledge Christopher Winkler for operation of the JEOL 2100 TEM.

References:

1. Gmernicki, K. R.; Hong, E.; Maroon, C. R.; Mahurin, S. M.; Sokolov, A. P.; Saito, T.; Long, B. K., Accessing Siloxane Functionalized Polynorbornenes via Vinyl-Addition Polymerization for CO2 Separation Membranes. *ACS Macro Letters* **2016,** *5* (7), 879-883.
2. Sundell, B. J.; Lawrence Iii, J. A.; Harrigan, D. J.; Vaughn, J. T.; Pilyugina, T. S.; Smith, D. R., Alkoxysilyl functionalized polynorbornenes with enhanced selectivity for heavy hydrocarbon separations. *RSC Advances* **2016,** *6* (57), 51619-51628.
3. Bermeshev, M. V.; Syromolotov, A. V.; Starannikova, L. E.; Gringolts, M. L.; Lakhtin, V. G.; Yampolskii, Y. P.; Finkelshtein, E. S., Glassy Polynorbornenes with Si–O–Si Containing Side Groups. Novel Materials for Hydrocarbon Membrane Separation. *Macromolecules* **2013,** *46* (22), 8973-8979.
4. Sapkota, J.; Jorfi, M.; Weder, C.; Foster, E. J., Reinforcing poly (ethylene) with cellulose nanocrystals. *Macromolecular rapid communications* **2014,** *35* (20), 1747-1753.
5. Sapkota, J.; Natterodt, J. C.; Shirole, A.; Foster, E. J.; Weder, C., Fabrication and Properties of Polyethylene/Cellulose Nanocrystal Composites. *Macromolecular Materials and Engineering* **2017,** *302* (1), 1600300-n/a.
6. Biyani, M. V.; Foster, E. J.; Weder, C., Light-Healable Supramolecular Nanocomposites Based on Modified Cellulose Nanocrystals. *ACS Macro Letters* **2013,** *2* (3), 236-240.
7. Natterodt, J. C.; Sapkota, J.; Foster, E. J.; Weder, C., Polymer Nanocomposites with Cellulose Nanocrystals Featuring Adaptive Surface Groups. *Biomacromolecules* **2017,** *18* (2), 517-525.
8. Favier, V.; Cavaille, J. Y.; Canova, G. R.; Shrivastava, S. C., Mechanical percolation in cellulose whisker nanocomposites. *Polymer Engineering & Science* **1997,** *37* (10), 1732-1739.
9. Chakrabarty, A.; Teramoto, Y., Recent Advances in Nanocellulose Composites with Polymers: A Guide for Choosing Partners and How to Incorporate Them. *Polymers* **2018,** *10* (5).
10. Belov, N.; Nikiforov, R.; Starannikova, L.; Gmernicki, K. R.; Maroon, C. R.; Long, B. K.; Shantarovich, V.; Yampolskii, Y., A detailed investigation into the gas permeation properties of addition-type poly(5-triethoxysilyl-2-norbornene). *European Polymer Journal* **2017,** *93*, 602-611.
11. Moon, R. J.; Martini, A.; Nairn, J.; Simonsen, J.; Youngblood, J., Cellulose nanomaterials review: structure, properties and nanocomposites. *Chemical Society Reviews* **2011,** *40* (7), 3941-3994.
12. Elmabrouk, A. B.; Wim, T.; Dufresne, A.; Boufi, S., Preparation of poly(styrene-co-hexylacrylate)/cellulose whiskers nanocomposites via miniemulsion polymerization. *Journal of Applied Polymer Science* **2009,** *114* (5), 2946-2955.

13. Mabrouk, A. B.; Salon, M. C. B.; Magnin, A.; Belgacem, M. N.; Boufi, S., Cellulose-based nanocomposites prepared via mini-emulsion polymerization: Understanding the chemistry of the nanocellulose/matrix interface. *Colloids and Surfaces A: Physicochemical and Engineering Aspects* **2014,** *448*, 1-8.
14. Yue, L.; Maiorana, A.; Khelifa, F.; Patel, A.; Raquez, J. M.; Bonnaud, L.; Gross, R.; Dubois, P.; Manas-Zloczower, I., Surface-modified cellulose nanocrystals for biobased epoxy nanocomposites. *Polymer* **2018,** *134*, 155-162.
15. Kargarzadeh, H.; Sheltami, R. M.; Ahmad, I.; Abdullah, I.; Dufresne, A., Cellulose nanocrystal: A promising toughening agent for unsaturated polyester nanocomposite. *Polymer* **2015,** *56*, 346-357.
16. Ladhar, A.; Ben Mabrouk, A.; Arous, M.; Boufi, S.; Kallel, A., Dielectric properties of nanocomposites based on cellulose nanocrystals (CNCs) and poly(styrene-co-2-ethyl hexylacrylate) copolymer. *Polymer* **2017,** *125*, 76-89.
17. Ladhar, A.; Arous, M.; Boufi, S.; Kallel, A., Molecular dynamics of poly(styrene-co-2-ethyl hexylacrylate) copolymer/cellulose nanocrystals nanocomposites investigated by dielectric relaxation spectroscopy: Effect of the silane content. *Journal of Molecular Liquids* **2016,** *224*, 515-525.
18. Yang, J.; Han, C.-R.; Duan, J.-F.; Ma, M.-G.; Zhang, X.-M.; Xu, F.; Sun, R.-C.; Xie, X.-M., Studies on the properties and formation mechanism of flexible nanocomposite hydrogels from cellulose nanocrystals and poly(acrylic acid). *Journal of Materials Chemistry* **2012,** *22* (42), 22467-22480.
19. Yang, J.; Han, C.-R.; Duan, J.-F.; Ma, M.-G.; Zhang, X.-M.; Xu, F.; Sun, R.-C., Synthesis and characterization of mechanically flexible and tough cellulose nanocrystals–polyacrylamide nanocomposite hydrogels. *Cellulose* **2013,** *20* (1), 227-237.
20. Peng, S. X.; Chang, H.; Kumar, S.; Moon, R. J.; Youngblood, J. P., A comparative guide to controlled hydrophobization of cellulose nanocrystals via surface esterification. *Cellulose* **2016,** *23* (3), 1825-1846.
21. Heux, L.; Chauve, G.; Bonini, C., Nonflocculating and Chiral-Nematic Self-ordering of Cellulose Microcrystals Suspensions in Nonpolar Solvents. *Langmuir* **2000,** *16* (21), 8210-8212.
22. Foster, E. J.; Moon, R. J.; Agarwal, U. P.; Bortner, M. J.; Bras, J.; Camarero-Espinosa, S.; Chan, K. J.; Clift, M. J. D.; Cranston, E. D.; Eichhorn, S. J.; Fox, D. M.; Hamad, W. Y.; Heux, L.; Jean, B.; Korey, M.; Nieh, W.; Ong, K. J.; Reid, M. S.; Renneckar, S.; Roberts, R.; Shatkin, J. A.; Simonsen, J.; Stinson-Bagby, K.; Wanasekara, N.; Youngblood, J., Current characterization methods for cellulose nanomaterials. *Chemical Society Reviews* **2018,** *47* (8), 2609-2679.
23. Dufresne, A., *Nanocellulose: from nature to high performance tailored materials*. Walter de Gruyter GmbH & Co KG: 2017.
24. Bendahou, A.; Kaddami, H.; Dufresne, A., Investigation on the effect of cellulosic nanoparticles' morphology on the properties of natural rubber based nanocomposites. *European Polymer Journal* **2010,** *46* (4), 609-620.
25. Cho, M.-J.; Park, B.-D., Tensile and thermal properties of nanocellulose-*reinforced poly(vinyl alcohol) nanocomposites. *J. Ind. Eng. Chem.* **2011,** *17* (1), 36-40.
26. Pranger, L.; Tannenbaum, R., Biobased Nanocomposites Prepared by In Situ Polymerization of Furfuryl Alcohol with Cellulose Whiskers or Montmorillonite Clay. *Macromolecules* **2008,** *41* (22), 8682-8687.

27. Salon, M.-C. B.; Gerbaud, G.; Abdelmouleh, M.; Bruzzese, C.; Boufi, S.; Belgacem, M. N., Studies of interactions between silane coupling agents and cellulose fibers with liquid and solid-state NMR. *Magnetic Resonance in Chemistry* **2007,** *45* (6), 473-483.
28. Kono, H.; Yunoki, S.; Shikano, T.; Fujiwara, M.; Erata, T.; Takai, M., CP/MAS 13C NMR Study of Cellulose and Cellulose Derivatives. 1. Complete Assignment of the CP/MAS 13C NMR Spectrum of the Native Cellulose. *Journal of the American Chemical Society* **2002,** *124* (25), 7506-7511.

5.5 Supporting Information:

Cellulose Nanocrystal-Reinforced Poly(5-triethoxysilyl-2-norbornene) Composites

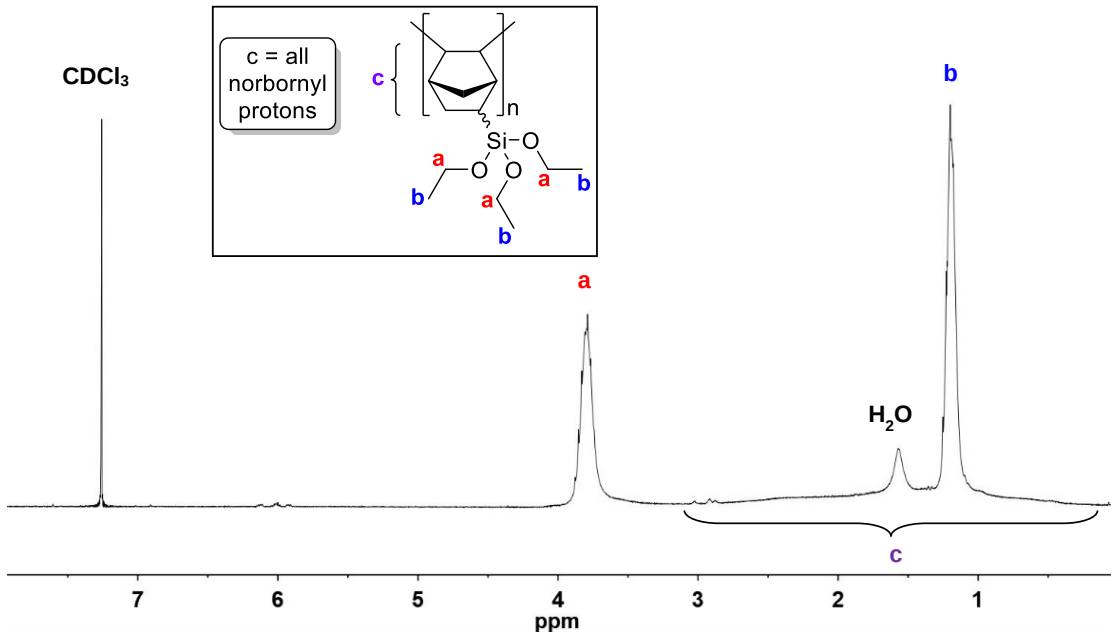

Figure S5.1: Above is an ^{1}H-NMR spectrum of poly(5-triethoxysilyl-2-norbornene) (PTESN).

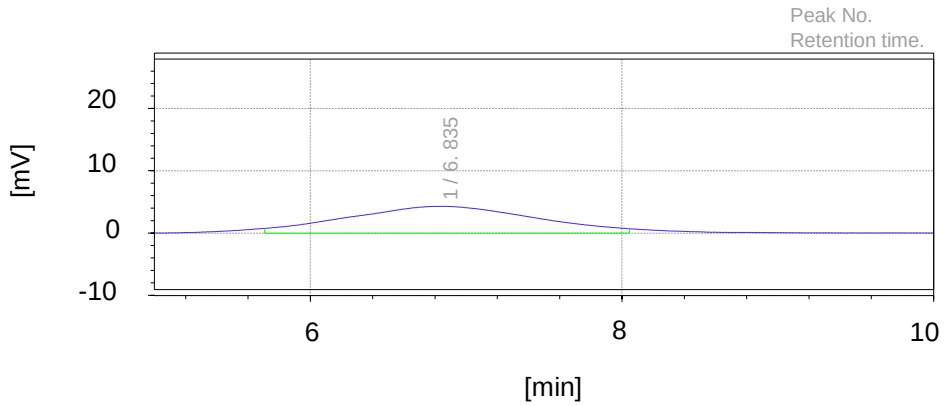

Result of molecular weight calculation (RI)

Peak 1 Valley Peak					
	[min]	[mV]	[mol]	Mn	226,900
Peak start	5.707	0.738	4,150,000	Mw	495,000
Peak top	6.835	4.306	316,300	Mz	1,131,000
Peak end	8.048	0.679	50,670	Mz+1	2,005,000
				Mv	495,000
Height [mV]			4.309	Mp	305,000
Area [mV*sec]			358.2	Mz/Mw	2.29
Area% [%]			100	Mw/Mn	2.18
[eta]			495000	Mz+1/Mw	4.06

Figure S5.2: A GPC trace of PTESN is shown.

Table S5.1: DMA data of PTESN CNC composites at select temperatures is below.

Temperature °C	Storage Modulus (MPa)					
	0-CNCs	1-CNC	5-CNC	10-CNC	15-CNC	20-CNC
25	400 ± 100	300 ± 100	510 ± 90	900 ± 300	1100 ± 300	1200 ± 200
50	400 ± 100	300 ± 100	510 ± 80	900 ± 300	1100 ± 300	1100 ± 200
100	320 ± 70	300 ± 100	460 ± 50	822 ± 200	900 ± 200	900 ± 200
200	310 ± 3	600 ±100	320 ± 10	570 ± 80	520 ± 100	600 ±100
300	174 ± 4	120 ± 40	170 ± 20	230 ± 40	170 ± 30	200 ±30

Table S5.2. Tensile data of PTESN CNC composites is denoted below.

Sample	Young's Modulus (MPa)	Maximum Tensile Stress (MPa)	Strain at break (%)	Toughness kJ m^{-3}
PTESN	540 ± 50	12 ± 4	5 ± 2	230 ± 70
1-CNC-PTESN	600 ± 200	15 ± 4	3 ± 2	310 ± 260
5-CNC-PTESN	700 ± 100	12.0 ± 0.7	2.1 ± 0.4	140 ± 30
10-CNC-PTESN	840 ± 70	13 ± 1	1.9 ± 0.2	130 ± 20
15-CNC-PTESN	820 ± 70	10 ± 2	1.6 ± 0.2	80 ± 20
20-CNC-PTESN	970 ± 80	12 ± 1	1.5 ± 0.2	80 ± 30

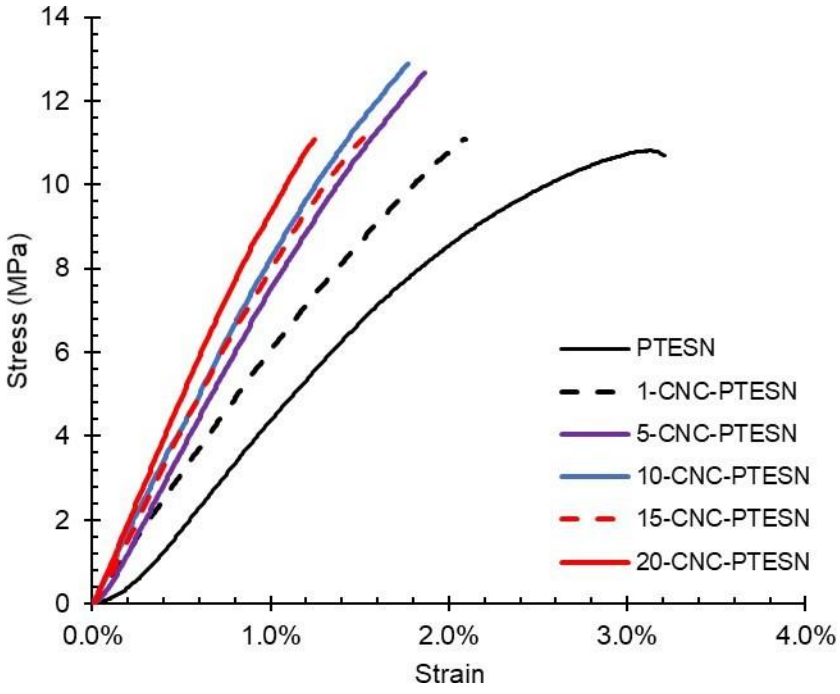

Figure S5.3: Representative tensile plots from PTESN CNC composites are shown.

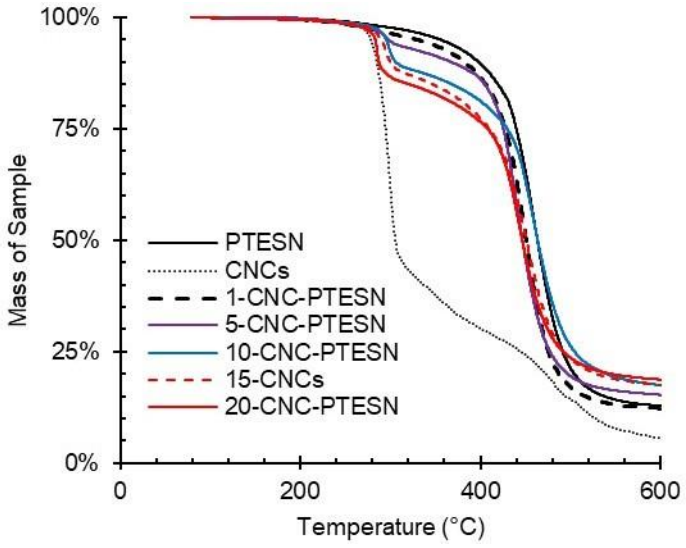

Figure S5.4: Thermogravimetric traces for PTESN, 1-CNC-PTESN, 5-CNC-PTESN, 10-CNC-PTESN, 15-CNC-PTESN, and 20-CNC-PTESN are shown.

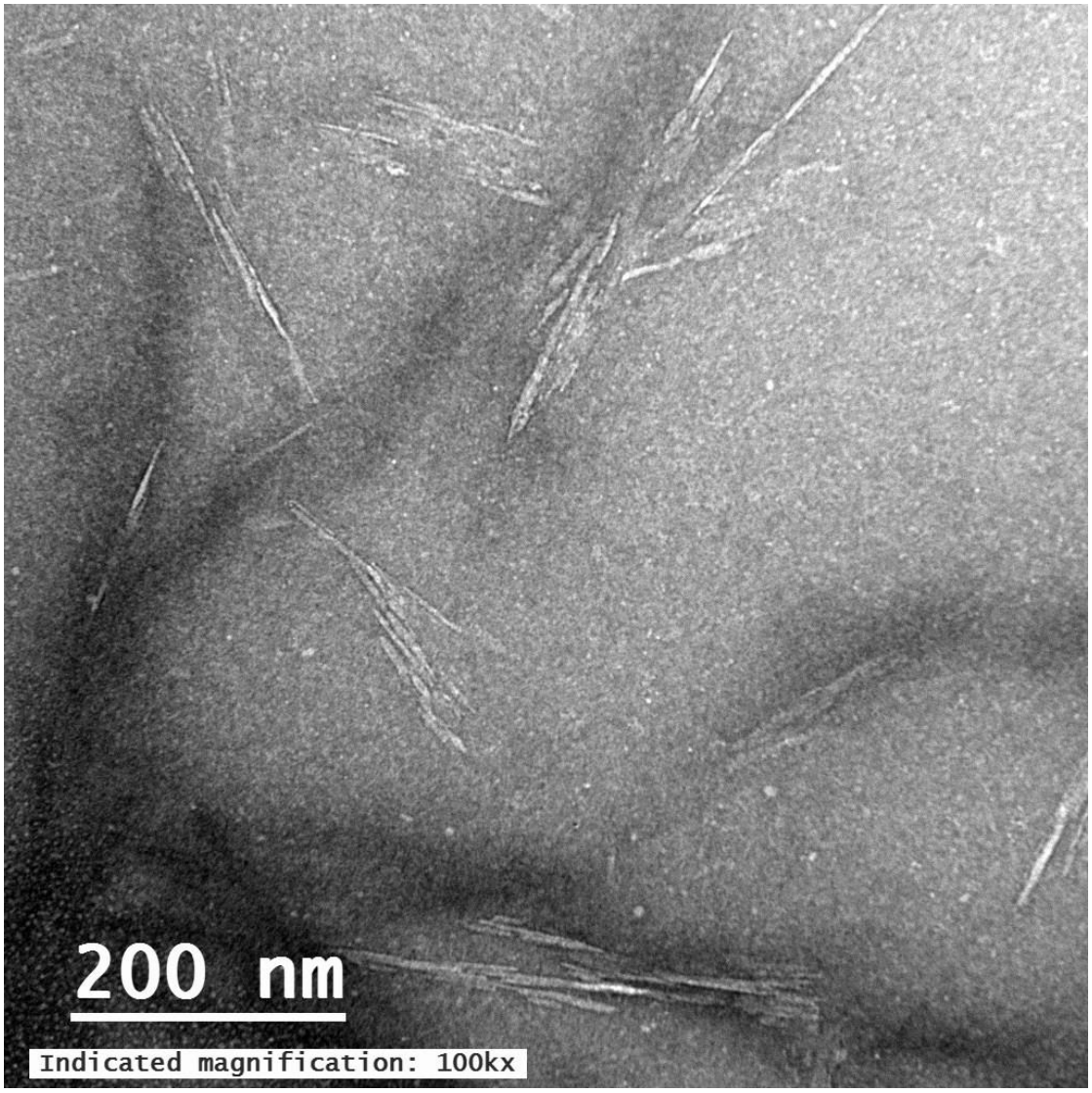

Figure S5.5: TEM Micrograph shows University of Maine CNCs. CNCs have dimensions of 90 ± 40 and 7 ± 2. Image was taken on JEOL 2100 TEM. Photo credit Rose Roberts and Kelly Stinson Bagby.

Chapter 6: Conclusions and Outlook

This chapter takes information from chapters 1-5 to draw reasonable conclusions and future steps to further this research.

Conclusions and outlook:

The challenges overcome in this work were the incorporation of cellulose nanocrystals (CNCs) into hydrophobic polymer matrices and the functionalization of CNCs with the catalyst 1,1'-bis(bromodimethylsilyl)zirconocene (catalyst **1**), tertiary amine groups (ACNC), and CNCs with zwitterionic groups (ZCNCs).

The unfavorable interactions of hydrophobic to disperse hydrophilic CNCs into hydrophobic polymer matrices was overcome in a high molecular weight unsubstituted polyethylene (PE) in chapter 2 of this work. The CNCs were functionalized by a reaction with the anchoring catalyst (catalyst **1**). These catalyst functionalized CNCs (C1-CNCs) were separated by the subsequent polymerization of ethylene from the active catalyst on the C1-CNC surfaces. This work was subsequently built upon in chapter 3, where C1-CNCs were used in conjunction with ethylene and 1-hexene making a linear low-density polyethylene (LLDPE) polymer matrix composite (PMC). The LLDPE PMC had physical properties such as melting point close to those of existing commercial LLDPEs but a greater Young's modulus. These LLDPE materials could likely be substituted into existing LLDPE technologies and used for advanced composite materials.

In chapter 2 and chapter 3 there was a substantial increase in the Young's modulus of the polymer when combined with C1-CNCs to form a PMC. The straight chain PE at a high molecular weight had a Young's modulus that was 10% better than existing robust PEs we referenced. The CNC-LLDPE PMC materials showed a two-fold increase in Young's modulus between 3.6 wt% CNC PMC and 11.4 wt% CNC PMCs. The primary accomplishment from each of these chapters was the easy incorporation of the CNCs into

the PE/LLDPE, and because of the low cost and known versatility of PE this technology, this process could be used to make stiffer PE/LLDPE products.

The even greater potential benefit of this CNC/PE PMC technology lies in what could be accomplished with the functional groups on CNCs. It is established that PE is a very inert polymer, and even incorporation of additives can be challenging and require an intense mixing process. Using the C1-CNCs that are going to be added to the PE, there is a possibility to add other functional groups to the CNCs before catalyst **1** is added to the surface of the CNCs. A useful application would be attaching dyes that are compatible with cellulose to have the dispersed CNCs color the PMC material. A challenge with this approach would be the reaction with the anchoring catalyst on the dye functionalized CNCs surface, and a second roadblock could be a reaction between the dye and the methylalumoxane co-catalyst.

The incorporation of CNCs into poly(5-triethoxysilyl-2-norbornene) (PTESN) was accomplished by solvent casting. The result was a mechanically robust PMC that had improved stiffness when compared to the neat PTESN material. The reinforced polymer result is both stiffer and more thermally stable, but the vehicle for application in this system is even greater than that for the PE/CNC PMCs. The PTESN was generated by using a catalyst capable of polymerizing cyclic alkenes without the need for methylalumoxane. This corresponds to the polymerization of custom polynorbornenes being possible to the extent that they do not poison the polymerizing catalyst. Custom polynorbornene combined with functional CNCs could lead to interesting combinations and designer PMCs that can have more complicated functionalities than the PE/CNC PMCs.

The ACNCs and ZCNCs have potential applications as membrane materials. Chapter 4 discussed at length the features of the zwitterionic CNCs and how they could be used for membrane applications. The ZCNCs also fill a unique role in that they feature hydrophilic groups. The large amount of both positive and negative charges on the ZCNC surface could be useful for water retaining applications. Although most prominent water retaining application are present in the biological fields where charged polysaccharides like heparin are common.

In this work I have presented new methods for incorporating CNCs into hydrophobic polymer materials, and the functionalization of CNC surfaces with various species. These materials are a contribution to research and industry as intermediate steps. These technologies can be used to ideally overcome the faults (such as the unreactive nature) that some hydrophobic polymers have. Thus, I propose that the mixing methods presented in these chapters and the functionalization chapter 3, can be used to further research and scientific end goals by providing avenues for novel composite materials.

Appendix A:

Below is a list of acronyms and abbreviations used in the appendix.

Headings:
Volume percentage of CNC: (vol%); Value (V); Deviation from mean as presented (D); Ultimate tensile strength: σ_u; Tensile strength at yield: σ_y; and Maximum tensile strength or unspecified tensile strength: σ_t.

Cellulose Sources:
Microcrystalline cellulose (MCC), Husk of *Xanthoceras sorbifolia* bunge: plant (XSB)

CNC Modifications and hydrolysis:
Hydrobromic acid: (HBr), Acetic anhydride: (AcO_2), Sulfuric acid: (H_2SO_4), Hydrochloric acid: (HCl), Phosphoric acid: (H_3PO_4), Formic acid: (HCOOH), Compatibilizer: (CMPTBLZR)

Polymers:
Poly(vinyl alcohol) (PVA), Poly(vinyl acetate): (PVAc), Polyurethane: (PU), Waterborne Polyurethane: (PU-W), Poly(acrylic acid): PAA, Electro spun: (E-Spun), Polycaprolactone: (PCL), Hydroxyethyl cellulose: (HEC), Water borne epoxy: (Epoxy-W), Poly(ethylene glycol diacrylate): PEGDA, Aligned: (Ⅲ), Unaligned: (#), Poly(3-hydroxybutyrate-co-3-hydroxyvalerate): (PHB-co-PHV), Poly(vinyl pyrrolidone): (PVP), Rollerblade mix: (RBM), Poly(glycerol-co-succinate-co-maleate): (PGSMA), Poly(propylene oxide): PPO, Poly(ethylene oxide): PEO, Poly (hydroxybuterate): PHB, Unsaturated Polyester Resin: (UPR) , PBAT Poly(butylene-adipate-terthalate), Poly(sulfone): (PSU), Telechelic poly(ethylene-co-butylene):PEB, PSA-co-PDM: Poly(sebacic acid-co-poly-D-mannitol), Poly(ethylene oxide epichlorohydrin): (PEO-EPI), Cellulose acetate (CA), Cellulose acetate butyrate: (CAB), Acrylonitrile butadiene styrene: (ABS)

Processing Methods:
Melt Mixing (MM), Twin Screw Extrusion: (TSE), Polymerization reaction: (P-RXN), Organogel/templating solvent exchange method: (O/T-SE), Compatibilizer: (CMPTBLZR), Crosslink: (X-link)

Reagents and additives:
Silver: (Ag), Nanoparticles: (NP), Isophorone Diisocyanate: (IDPI), Polyether-based triol: (PE-triol), Diphenylmethane diisocyanate: (MDI), Dicumyl peroxide: (DCP), Maleic anhydride (MA), Maleic acid (MA-OH), Dubecco's phosphate buffer saline (DPBS).

Data was extracted from tables, or graphs using Fiji ImageJ. Volume percentages were found using CNC density[1] 1.6 g cm^{-3} and the polymer density from the publication, manufacturer, or engineering handbooks.[2-3]

R	CNC, Source, Hydrolysis, Modification	Method	Matrix	CNC	Young's Modulus (MPa)		Strain at Break (%)		Strength (MPa)			
				vol%	V	D	V	D	σ_u	σ_y	σ_t	D
[4]	Cotton, H2SO4	Cast	PVA	0.00	20	2	-	-	-	-	-	-
[4]	Cotton, H2SO4	Cast	PVA	0.75	21	5	-	-	-	-	-	-
[4]	Cotton, H2SO4	Cast	PVA	1.50	23	2	-	-	-	-	-	-
[4]	Potato Peel H2SO4	Cast	PVA	0.75	27	1	-	-	-	-	-	-
[4]	Potato Peel H2SO4	Cast	PVA	1.50	30.8	0.8	-	-	-	-	-	-
[4]	Cotton, H2SO4	Cast	PVA	0.00	330	40	-	-	-	-	-	-
[4]	Cotton, H2SO4	Cast	PVA	0.75	360	40	-	-	-	-	-	-
[4]	Cotton, H2SO4	Cast	PVA	1.50	390	30	-	-	-	-	-	-
[4]	Potato Peel H2SO4	Cast	PVA	0.75	400	20	-	-	-	-	-	-
[4]	Potato Peel H2SO4	Cast	PVA	1.50	460	40	-	-	-	-	-	-
[5]	Cotton, H2SO4	Cast	PVA	0.00	1300	200	-	-	-	-	-	-
[5]	Cotton, H2SO4	Cast	PVA:PAA 90:10	0.00	1600	300	-	-	-	-	-	-
[5]	Cotton, H2SO4	Cast	PVA	11.60	1400	-	-	-	-	-	-	-
[5]	Cotton, H2SO4	Cast	PVA:PAA 80:10	7.63	2200	400	-	-	-	-	-	-
[5]	Cotton, H2SO4	Cast	PVA:PAA 70:10	15.68	2100	400	-	-	-	-	-	-
[6]	Cotton, H2SO4	E-Spun Mats (Ⅲ)	PVA	0.00	87	5	-	-	-	-	5.3	0.2
[6]	Cotton, H2SO4	E-Spun Mats (Ⅲ)	PVA	2.25	110	4	-	-	-	-	6.7	0.6
[6]	Cotton, H2SO4	E-Spun Mats (Ⅲ)	PVA	3.77	124	8	-	-	-	-	7.3	0.9
[6]	Cotton, H2SO4	E-Spun Mats (Ⅲ)	PVA	7.63	160	10	-	-	-	-	8.6	0.3
[6]	Cotton, H2SO4	E-Spun Mats (Ⅲ)	PVA	11.60	190	20	-	-	-	-	10.7	0.9
[6]	Cotton, H2SO4	E-Spun Mats (Ⅲ)	PVA	0.00	64	5	-	-	-	-	4.1	0.3
[6]	Cotton, H2SO4	E-Spun Mats (#)	PVA	2.25	81	6	-	-	-	-	5.1	0.5
[6]	Cotton, H2SO4	E-Spun Mats (#)	PVA	3.77	87	10	-	-	-	-	5.6	0.6
[6]	Cotton, H2SO4	E-Spun Mats (#)	PVA	7.63	111	4	-	-	-	-	6.6	0.4
[6]	Cotton, H2SO4	E-Spun Mats (#)	PVA	11.60	134	6			-	-	7.9	0.1
[7]	Cotton, H2SO4	MM (TSE)	PVAc	0.00	2200	800	5	1	-	-	31	2
[7]	Cotton, H2SO4	MM (TSE)	PVAc	3.77	1900	400	29	3	-	-	18	3
[7]	Cotton, H2SO4	MM (TSE)	PVAc	7.63	2100	700	11	2	-	-	16	1
[7]	Cotton, H2SO4	MM (TSE)	PVAc	0.00	1700	400	60	30	-	-	15	3
[7]	Cotton, H2SO4	MM (TSE)	PVAc	3.77	900	100	160	30	-	-	17	2
[7]	Cotton, H2SO4	MM (TSE)	PVAc	7.63	1800	200	140	20	-	-	20	1
[8]	Cotton, H2SO4	Cast	PVA	0.00	210	20	250	10	-	-	25	4
[8]	Cotton, H2SO4 0.1 Ag particles	Cast	PVA	0.75	750	40	230	10	-	-	46	1
[8]	Cotton H2SO4, 0.1 Ag particles	Cast	PVA	0.75	780	40	210	20	-	-	48	3

R	CNC, Source, Hydrolysis, Modification	Method	Matrix	CNC	Young's Modulus (MPa)		Strain at Break (%)		Strength (MPa)			
				vol%	V	D	V	D	σ_u	σ_y	σ_t	D
[8]	Cotton H2SO4, 0.1 Ag particles	Cast	PVA	0.75	790	50	225	4	-	-	45	2
[8]	Cotton H2SO4, 0.5 Ag particles	Cast	PVA	0.75	550	30	240	20	-	-	47	3
[8]	Cotton H2SO4, 0.5 Ag particles	Cast	PVA	0.75	630	40	200	20	-	-	43	2
[8]	Cotton H2SO4, 0.5 Ag particles	Cast	PVA	0.75	560	20	270	10	-	-	49	1
[9]	Cotton H2SO4	Cast	PVA	0.00	950	90	140	50	-	-	30	4
[9]	Cotton H2SO4	Cast	PVA	0.75	1100	100	100	20	-	-	31.5	0.7
[10]	Cotton, H2SO4	E-Spun	PVA	0.00	162	-	25	-	-	-	6.9	-
[10]	Cotton, H2SO4	E-Spun	PVA	2.2	171	-	14	-	-	-	10.3	-
[11]	Wood, H2SO4	Cast	PVA	0.00	3200	300	0.5	0.4	-	-	95	9
[11]	Wood, H2SO4	Cast	PVA	0.80	3600	100	0.5	0.2	-	-	98	8
[11]	Wood, H2SO4	Cast	PVA	1.59	3900	100	0.5	0.3	-	-	109	4
[11]	Wood, H2SO4	Cast	PVA	2.4	3900	100	0.4	0.2	-	-	111	2
[11]	Wood, H2SO4	Cast	PVA	3.20	3900	200	0.3	0.2	-	-	103	4
[11]	Wood, H2SO4	Cast	PVA	4.01	3600	300	0.2	0.1	-	-	101	5
[12]	Red seaweed, H2SO4	Cast	PVA	3.77	-	-	-	-	-	-	22.9	0.9
[12]	Red seaweed, H2SO4	Cast	PVA	3.77	-	-	-	-	-	-	24.2	0.4
[12]	Red seaweed, H2SO4	Cast	PVA	3.77	-	-	-	-	-	-	25	3
[13]	Wood, H2SO4	F-Spin	PVA	0.00	3190	70	30	4	-	-	90	30
[13]	Wood, H2SO4	F-Spin	PVA	3.77	3400	500	17	6	-	-	150	20
[13]	Wood, H2SO4	F-Spin	PVA	7.63	4000	1000	13	8	-	-	190	30
[13]	Wood, H2SO4	F-Spin	PVA	11.60	6000	1000	15	7	-	-	230	30
[13]	Wood, H2SO4	F-Spin	PVA	15.68	5000	900	9	7	-	-	180	40
[13]	Wood, H2SO4, Drawn Fiber	F-Spin	PVA	0.00	5100	600	23	8	-	-	110	40
[13]	Wood, H2SO4, Drawn Fiber	F-Spin	PVA	3.77	8000	2000	14	6	-	-	170	40
[13]	Wood, H2SO4, Drawn Fiber	F-Spin	PVA	7.63	12000	2000	10	7	-	-	220	30
[13]	Wood, H2SO4, Drawn Fiber	F-Spin	PVA	11.60	15100	900	10	2	-	-	270	60
[13]	Wood, H2SO4, Drawn Fiber	F-Spin	PVA	15.68	13900	800	6	3	-	-	240	30
[13]	Wood, H2SO4, As Spun	F-Spin	PVA	3.77	7000	1000	17	9	-	-	150	40
[13]	Wood, H2SO4, As Spun	F-Spin	PVA	7.63	9600	500	11	5	-	-	210	20
[13]	Wood, H2SO4, As Spun	F-Spin	PVA	11.60	14000	1000	10	9	-	-	270	40
[13]	Wood, H2SO4, As Spun	F-Spin	PVA	15.68	1300	2000	5	5	-	-	260	50
[13]	Wood, H2SO4, Drawn Fiber	F-Spin	PVA	3.77	9000	2000	12	5	-	-	190	40
[13]	Wood, H2SO4, Drawn Fiber	F-Spin	PVA	7.63	13000	3000	7	7	-	-	240	60
[13]	Wood, H2SO4, Drawn Fiber	F-Spin	PVA	11.60	19000	10000	5	4	-	-	320	40

R	CNC, Source, Hydrolysis, Modification	Method	Matrix	CNC	Young's Modulus (MPa)		Strain at Break (%)		Strength (MPa)			
				vol%	V	D	V	D	σ_u	σ_y	σ_t	D
[13]	Wood, H2SO4, Drawn Fiber	F-Spin	PVA	15.68	16000	2000	4	3	-	-	300	30
[14]	paper sludge, H2SO4	Cast	PVA	0.00	199	0	240	0	-	-	25	0
[14]	paper sludge, H2SO4	Cast	PVA	0.75	250	70	260	90	-	-	29	6
[14]	paper sludge, H2SO4	Cast	PVA	2.25	250	70	310	70	-	-	34	3
[14]	paper sludge, H2SO4	Cast	PVA	3.77	200	100	250	50	-	-	28	5
[15]	Red Algae, H2SO4	Cast	PVA	0.00	930	80	90	6	-	-	37	3
[15]	Red Algae, H2SO4	Cast	PVA	0.75	1320	70	74	7	-	-	47	2
[15]	Red Algae, H2SO4	Cast	PVA	2.25	1800	100	64	7	-	-	67	4
[15]	Red Algae, H2SO4	Cast	PVA	3.77	2260	90	55	6	-	-	82	3
[15]	Red Algae, H2SO4	Cast	PVA	6.07	2900	100	42	7	-	-	94	4
[16]	Cotton, unknown hydrolysis	Cast	PVA	0.00	32.3	0.6	0.61	-	-	-	117	3
[16]	Cotton, unknown hydrolysis	Cast	PVA	0.37	26.7	0.6	1.4	-	-	-	98	2
[16]	Cotton, unknown hydrolysis	Cast	PVA	0.75	14	1	10.8	-	-	-	104	2
[16]	Cotton, unknown hydrolysis	Cast	PVA	1.12	19.8	0.9	5.6	-	-	-	105	3
[16]	Cotton, unknown hydrolysis	Cast	PVA	1.50	20	1	7.2	-	-	-	119	3
[16]	Cotton, unknown hydrolysis	Cast	PVA	3.01	30.8	1	8.9	-	-	-	132	3
[16]	Cotton, unknown hydrolysis	Cast	PVA	4.53	39.9	0.8	1.1	-	-	-	150	3
[16]	Cotton, unknown hydrolysis	Cast	PVA	0.00	0.117	0	36	-	-	-	25.9	0.1
[16]	Cotton, unknown hydrolysis	Cast	PVA	0.37	0.556	0	34	-	-	-	41	0.1
[16]	Cotton, unknown hydrolysis	Cast	PVA	0.75	0.565	0	42	-	-	-	50.7	0.1
[16]	Cotton, unknown hydrolysis	Cast	PVA	1.12	0.729	0	40	-	-	-	47.1	0.1
[16]	Cotton, unknown hydrolysis	Cast	PVA	1.50	2.5	0	36	-	-	-	59	0.1
[16]	Cotton, unknown hydrolysis	Cast	PVA	3.01	3.2	0	33	-	-	-	62.6	0.1
[16]	Cotton, unknown hydrolysis	Cast	PVA	4.53	3.7	0	35	-	-	-	64.4	0.1
[16]	Cotton, unknown hydrolysis	Cast	PVA	0.00	9.6	0.4	21.6	-	-	-	54	1
[16]	Cotton, unknown hydrolysis	Cast	PVA	0.37	6.2	0.4	18.3	-	-	-	58.3	0.9
[16]	Cotton, unknown hydrolysis	Cast	PVA	0.75	9.8	0.2	19.1	-	-	-	82.7	0.9
[16]	Cotton, unknown hydrolysis	Cast	PVA	1.12	9.6	0.8	17.1	-	-	-	82.3	1.6
[16]	Cotton, unknown hydrolysis	Cast	PVA	1.50	15	1	11.9	-	-	-	96	3
[16]	Cotton, unknown hydrolysis	Cast	PVA	3.01	24.6	0.6	5.1	-	-	-	103	2
[16]	Cotton, unknown hydrolysis	Cast	PVA	4.53	25.8	1	1.1	-	-	-	136	3

R	CNC, Source, Hydrolysis, Modification	Method	Matrix	CNC	Young's Modulus (MPa)		Strain at Break (%)		Strength (MPa)			
				vol%	V	D	V	D	σ_u	σ_y	σ_t	D
[17]	Cotton, H2SO4	Cast	80:20 PVA:PCL	0.00	11	1	490	20	-	12.8	-	0.5
[17]	Cotton, H2SO4	Pickering Emulsion	80:20 PVA:PCL	3.77	4050	50	37	5	-	65	-	6
[17]	Cotton, H2SO4	Pickering emulsion	80:20 PVA:PCL	7.63	3050	4	19	2	-	67	-	5
[17]	Cotton, H2SO4	Cast	80:20 PVA:PCL	7.63	3.5	0.2	400	20	-	7.3	-	0.8
[17]	Cotton, H2SO4	Pickering emulsion	80:20 PVA:PCL	15.68	2910	30	2.5	0.5	-	28	-	2
[17]	Cotton, H2SO4	Cast	60:40 PVA:PCL	0.00	2.8	0.3	620	20	-	7.1	-	0.9
[17]	Cotton, H2SO4	Pickering emulsion	60:40 PVA:PCL	3.77	1640	60	2.1	0.5	-	25	-	1
[17]	Cotton, H2SO4	Pickering emulsion	60:40 PVA:PCL	7.63	2640	40	2.8	0.3	-	46	-	6
[17]	Cotton, H2SO4	Cast	60:40 PVA:PCL	7.63	1.9	0.3	550	20	-	5.8	-	0.6
[17]	Cotton, H2SO4	Pickering emulsion	60:40 PVA:PCL	15.68	2220	40	1.6	0.4	-	23.5	-	0.9
[17]	Cotton, H2SO4	E-Spun	PVA	0.00	38	2	77	7	-	-	7.5	0.4
[17]	Cotton, H2SO4	E-Spun Ⅲ	PVA	7.63	185	4	88	7	-	-	10.3	0.3
[17]	Cotton, H2SO4	E-Spun Ⅲ	PVA	19.87	343	7	30	3	-	-	6.5	0.1
[17]	Cotton, H2SO4	E-Spun Ⅲ	PVA	42.65	236	5	8.1	0.9	-	-	2.79	0.02
[17]	Cotton, H2SO4	E-Spun Ⅲ	PVA	7.63	850	10	20	4	-	-	8.3	0.3
[17]	Cotton, H2SO4	E-Spun Ⅲ	PVA	19.87	431	7	3.1	8	-	-	4	0.2
[17]	Cotton, H2SO4	E-Spun Ⅲ	PVA	42.65	17	2	2.9	0.3	-	-	0.4	0.03
[17]	Cotton, H2SO4	E-Spun core sheath CNC inside	PVA	7.63	115	2	110	10	-	-	8.8	0.3
[17]	Cotton, H2SO4	E-Spun core sheath CNC inside	PVA	7.63	840	10	38	6	-	-	6.8	0.3
[18]	Plant (XSB), H2SO4	Cast	PVA &.5% Graphene nanoplatelet	0.00	2200	500	70	30	-	-	83	4
[18]	Plant (XSB), H2SO4	Cast	PVA &.4% Graphene nanoplatelet	0.07	2500	600	190	70	-	-	93	6
[18]	Plant (XSB), H2SO4	Cast	PVA &.1% Graphene nanoplatelet	0.30	2800	400	150	70	-	-	100	10
[19]	Bacteria, H2SO4	Cast	PVA	0.00	280	20	-	-	-	-	38	2
[19]	Bacteria, H2SO4	Cast	PVA	0.75	370	20	-	-	-	-	41	1
[19]	Bacteria, H2SO4	Cast	PVA	2.25	460	40	-	-	-	-	44	2
[19]	Bacteria, H2SO4	Cast	PVA	3.77	380	20	-	-	-	-	40	3
[20]	Cotton, H2SO4, PU Graft	Reaction& Cast	WPU	0.00	1.7	0.2	1050	30	-	-	4.4	0.2
[20]	Cotton, H2SO4, PU Graft	Reaction& Cast	WPU	1.51	5	1	1270	40	-	-	6	1
[20]	Cotton, H2SO4, PU Graft	Reaction& Cast	WPU	3.03	23	2	1360	60	-	-	7.5	0.8

R	CNC, Source, Hydrolysis, Modification	Method	Matrix	CNC	Young's Modulus (MPa)		Strain at Break (%)		Strength (MPa)			
				vol%	V	D	V	D	σ_u	σ_y	σ_t	D
[20]	Cotton, H2SO4, PU Graft	Reaction& Cast	WPU	4.57	41	2	1030	30	-	-	9	1
[20]	Cotton, H2SO4, PU Graft	Reaction& Cast	WPU	6.12	56	4	830	30	-	-	9.4	0.5
[20]	Cotton, H2SO4, PU Graft	Reaction& Cast	WPU	7.69	107	6	630	10	-	-	9.7	0.6
[21]	Eucalyptus, H2SO4	Cast	WPU	0.00	1200	100	380	20	-	-	5.4	0.2
[21]	Eucalyptus, H2SO4	Cast	WPU	0.15	2400	100	360	20	-	-	6	0.3
[21]	Eucalyptus, H2SO4	Cast	WPU	0.38	2400	200	386	9	-	-	8.1	0.5
[21]	Eucalyptus, H2SO4	Cast	WPU	0.75	2300	100	370	20	-	-	12.2	0.5
[21]	Eucalyptus, H2SO4	Cast	WPU	1.51	2800	100	360	20	-	-	9.6	0.8
[21]	Eucalyptus, H2SO4	Cast	WPU	2.27	3100	400	350	10	-	-	8	0.5
[21]	Eucalyptus, H2SO4	Cast	WPU	3.03	4800	100	300	20	-	-	8.1	0.3
[21]	Eucalyptus, H2SO4	Cast	WPU	3.80	3400	300	300	20	-	-	6.6	0.3
[22]	Cotton, H2SO4, Polymer grafting	Cast	PU	0.00	8.2	0.9	750	30	-	-	8	1
[22]	Cotton, H2SO4, Polymer grafting	Cast	PU	0.38	41	3	110	60	-	-	27	2
[22]	Cotton, H2SO4, Polymer grafting	Cast	PU	0.75	42	3	62	5	-	-	62	5
[22]	Cotton, H2SO4, Polymer grafting	Cast	PU	3.80	45	2	50	7	-	-	50	7
[23]	Cotton H2SO4	Cast	PU	0.00	178	3	880	50	-	-	32	1
[23]	Cotton H2SO4	Cast	PU	0.75	218	5	650	30	-	-	22	1
[23]	Cotton H2SO4	Cast	PU	2.27	247	9	750	40	-	-	26	1
[23]	Cotton H2SO4	Cast	PU	3.80	296	9	570	30	-	-	18	1
[23]	Cotton H2SO4	Cast	PU	7.69	340	10	540	20	-	-	17	1
[23]	Cotton H2SO4	Cast	PU	0.00	199	4	210	20	-	-	20	1
[23]	Cotton H2SO4	Cast	PU	0.75	279	4	102	9	-	-	17.3	0.6
[23]	Cotton H2SO4	Cast	PU	2.27	311	6	90	10	-	-	17	1
[23]	Cotton H2SO4	Cast	PU	3.80	329	9	58	9	-	-	16	1
[23]	Cotton H2SO4	Cast	PU	7.69	359	9	70	10	-	-	16.1	0.9
[24]	Cotton H2SO4	Cast & Coating	PU Wool	0.00	-	-	71	2	-	-	18.7	0.8
[24]	Cotton H2SO4	Cast & Coating	PU + Wool	0.15	-	-	71	2	-	-	19.2	0.3
[24]	Cotton H2SO4	Cast & Coating	PU + Wool	0.30	-	-	70	3	-	-	21.5	0.5
[24]	Cotton H2SO4	Cast & Coating	PU + Wool	0.45	-	-	68.7	0.6	-	-	20.8	0.4
[24]	Cotton H2SO4	Cast & Coating	PU + Wool	0.60	-	-	68	1	-	-	21.1	0.1
[24]	Cotton H2SO4	Cast & Coating	PU + Wool	0.75	-	-	68	2	-	-	21.5	0.5
[24]	Cotton H2SO4	Cast & Coating	PU + Wool	0.00	-	-	52	1	-	-	10.7	0.1
[24]	Cotton H2SO4	Cast & Coating	PU + Wool	0.15	-	-	51	1	-	-	1.7	0.4
[24]	Cotton H2SO4	Cast & Coating	PU + Wool	0.30	-	-	54	3	-	-	10.9	0.25

R	CNC, Source, Hydrolysis, Modification	Method	Matrix	CNC	Young's Modulus (MPa)		Strain at Break (%)		Strength (MPa)			
				vol%	V	D	V	D	σ_u	σ_y	σ_t	D
[24]	Cotton H2SO4	Cast & Coating	PU + Wool	0.45	-	-	54	2	-	-	10.9	0.2
[24]	Cotton H2SO4	Cast & Coating	PU + Wool	0.60	-	-	53	3	-	-	11	0.4
[24]	Cotton H2SO4	Cast & Coating	PU + Wool	0.75	-	-	52	2	-	-	10.99	0.07
[25]	Cotton, H2SO4, Polymer grafting	Cast	PU	0.00	0.8	0.3	-	-	-	-	0.13	0.02
[25]	Cotton, H2SO4, Polymer grafting	Cast	PU	3.80	1.7	0.3	-	-	-	-	0.23	0.02
[25]	Cotton, H2SO4, Polymer grafting	Cast	PU	7.69	2.9	0.3	-	-	-	-	0.38	0.02
[25]	Cotton, H2SO4, Polymer grafting	Cast	PU	11.69	4	0.3	-	-	-	-	0.49	0.03
[26]	H2SO4, cotton, AcO2	Cast	PU	0.00	0.9	0.01	209	2	-	-	2.95	0.01
[26]	H2SO4, cotton, AcO2	Cast	PU	3.80	1.6	0.01	297	8	-	-	6.53	0.01
[26]	H2SO4, cotton, AcO2	Cast	PU	7.69	2.6	0.01	443	5	-	-	6.23	0.01
[26]	H2SO4, cotton, AcO2	Cast	PU	11.69	8.235	0.9	325	1	-	-	6.65	0.01
[26]	H2SO4, cotton, AcO2	Cast	PU	15.79	12.02	0.3	280	10	-	-	8.63	0.05
[26]	H2SO4, cotton, AcO2	Cast	PU	20.00	42.95	4	210	10	-	-	10.44	0.05
[27]	Eucalyptus (wood), H2SO4	Cast	PU	0.00	6	0.7	690	30	-	-	1.5	0.5
[27]	Eucalyptus (wood), H2SO4	Cast	PU	0.75	37	7	635	9	-	-	4.5	0.5
[27]	Eucalyptus (wood), H2SO4	RXN with pre-polymer	PU	0.75	64	2	430	20	-	-	5.8	0.6
[27]	Eucalyptus, H2SO4, Polymer grafting	RXN with monomer	PU	0.75	23	4	410	20	-	-	3.03	-
[28]	Wood, H2SO4	IDPI & PE-triol P-RXN	PU	0.00	3400	600	160	20	-	-	4	1
[28]	Wood, H2SO4	IDPI & PE-triol P-RXN	PU	0.75	3800	100	176	9	-	-	4.9	0.4
[28]	Wood, H2SO4	IDPI & PE-triol P-RXN	PU	3.80	5600	900	160	20	-	-	5	1
[28]	wood, H2SO4, IDPI	IDPI & PE-triol P-RXN	PU	0.75	4000	100	200	20	-	-	7	0.6
[28]	wood, H2SO4, IDPI	IDPI & PE-triol P-RXN	PU	3.80	8600	400	190	20	-	-	14	2
[29]	Wood, H2SO4	Cast	WPU	0.00	17	4	1300	200	-	-	10	2
[29]	Wood, H2SO4	Cast	WPU	0.68	22	1	1200	300	-	-	10	2
[29]	Wood, H2SO4	Cast	WPU	2.04	32	3	800	100	-	-	10	3
[29]	Wood, H2SO4	Cast	WPU	3.43	68	9	600	200	-	-	14	3
[29]	Wood, H2SO4	Cast	WPU	6.98	140	31	170	60	-	-	13	1
[30]	Eucalyptus, H2SO4,	Cast	PU	0.00	1.5	0.2	431	88	-	-	3.1	0.2
[30]	Eucalyptus, H2SO4,	Cast	PU	0.08	1.5	0.2	517	98	-	-	3.7	0.5
[30]	Eucalyptus, H2SO4,	Cast	PU	0.23	1.4	0.1	509	69	-	-	3.6	0.2
[30]	Eucalyptus, H2SO4,	Cast	PU	0.38	1.6	0.2	527	130	-	-	3.7	0.4
[30]	Eucalyptus, H2SO4,	Cast	PU	0.75	1.4	0.1	616	59	-	-	4.1	0.2

R	CNC, Source, Hydrolysis, Modification	Method	Matrix	CNC	Young's Modulus (MPa)		Strain at Break (%)		Strength (MPa)			
				vol%	V	D	V	D	σ_u	σ_y	σ_t	D
[30]	Eucalyptus, H2SO4,	Cast	PU	2.27	1.5	0.1	517	21	-	-	3.4	0.2
[30]	Eucalyptus, H2SO4,	Cast	PU	3.03	1.5	0.1	589	35	-	-	3.8	0.2
[30]	Eucalyptus, H2SO4,	Cast	PU	3.80	1.8	0.2	368	31	-	-	3.1	0.1
[30]	Eucalyptus (wood), MDI oleyl alcohol	Cast	PU	0.08	1.4	0.1	633	69	-	-	3.7	0.1
[30]	Eucalyptus, wood, MDI oleyl alcohol	Cast	PU	0.23	1.5	0.2	470	103	-	-	3.3	0.2
[30]	Eucalyptus, wood, MDI oleyl alcohol	Cast	PU	0.38	1.5	0.1	544	68	-	-	3.4	0.2
[30]	Eucalyptus, wood, MDI oleyl alcohol	Cast	PU	0.75	1.4	0.1	698	55	-	-	3.8	0.2
[30]	Eucalyptus, wood, MDI oleyl alcohol	Cast	PU	2.27	1.8	0.1	517	80	-	-	3.7	0.2
[30]	Eucalyptus, wood, MDI oleyl alcohol	Cast	PU	3.03	2.2	0.3	421	71	-	-	3.3	0.2
[30]	Eucalyptus, wood, MDI oleyl alcohol	Cast	PU	3.80	2.3	0.2	472	25	-	-	3.4	0.1
[31]	Cotton, Phosphoric acid	Cast	PU	0.00	42	0.8	635	15	-	-	-	-
[31]	Cotton, Phosphoric acid	RBM	PU	3.80	60	5	515	25	-	-	-	-
[31]	Cotton, Phosphoric acid	RBM	PU	7.69	72	3	320	5	-	-	-	-
[31]	Cotton, Phosphoric acid	RBM	PU	11.69	90	10	335	20	-	-	-	-
[32]	Ramie, H2SO4	Cast & 2x E-beam radiation	PU-A	0.00	2330	-	-	-	-	-	30	10
[32]	Ramie, H2SO4	Cast & E-beam radiation	PU-A	0.75	1840	-	-	-	-	-	39	8
[32]	Ramie, H2SO4	Cast & 2x E-beam radiation	PU-A	0.75	2140	-	-	-	-	-	35	1
[32]	Ramie, H2SO4	Cast & UV radiation	PU-A	0.00	1300	-	-	-	-	-	24	7
[32]	Ramie, H2SO4	Cast & UV radiation	PU-A	0.75	1760	-	-	-	-	-	23	4
[33]	Wood H2SO4	Cast & Curing	PU	0.00	1050	50	16	2	18	-	-	1
[33]	Wood H2SO4	Cast & Curing	PU	0.19	1230	20	31	1	26	-	-	1
[33]	Wood H2SO4	Cast & Curing	PU	0.38	1300	20	30	3	25	-	-	1
[33]	Wood H2SO4	Cast & Curing	PU	0.56	1010	10	43	2	27	-	-	1
[33]	Wood H2SO4	Cast & Curing	PU	0.75	1130	10	36	4	29			1
[34]	Sisal fiber, H2SO4	Cast	PU-W	0.00	17	1	1400	200	-	-	11.7	0.9
[34]	Sisal fiber, H2SO4	Cast	PU-W	0.75	17.7	0.8	1160	70	-	-	8.8	0.6
[34]	Sisal fiber, H2SO4	Cast	PU-W	2.27	18	2	1200	200	-	-	10	1

R	CNC, Source, Hydrolysis, Modification	Method	Matrix	CNC	Young's Modulus (MPa)		Strain at Break (%)		Strength (MPa)			
				vol%	V	D	V	D	σ_u	σ_y	σ_t	D
[34]	Sisal fiber, H2SO4	Cast	PU-W	3.80	35	2	600	100	-	-	7.2	0.9
[34]	Sisal fiber, H2SO4	Cast	PU-W	7.69	35	3	700	100	-	-	7.7	0.5
[35]	MCC, H2SO4	Cast	PU	0.00	10.7	0.9	36	4	-	-	2.2	0.3
[35]	MCC, H2SO4	Cast	PU	0.38	7	1	41	2	-	-	1.8	0.9
[35]	MCC, H2SO4	Cast	PU	0.75	40	10	20	5	-	-	4	1
[35]	MCC, H2SO4	Cast	PU	1.51	3.1	0.2	43	2	-	-	1.1	0.2
[36]	Wood, H2SO4	Cast	PU	0.00	100	20	-	-	-	-	2.1	0.2
[36]	Wood, H2SO4	Cast	PU	0.38	300	20	-	-	-	-	2.5	0.3
[36]	Wood, H2SO4	Cast	PU	0.75	300	30	-	-	-	-	3	0.2
[36]	Wood, H2SO4	Cast	PU	1.13	360	30	-	-	-	-	3.2	0.3
[36]	Wood, H2SO4	Cast	PU	1.51	400	30	-	-	-	-	2.8	0.3
[36]	Wood, H2SO4, MA	Cast	PU	0.38	390	30	-	-	-	-	3.6	0.3
[36]	Wood, H2SO4, MA	Cast	PU	0.75	400	5	-	-	-	-	4.24	0.09
[36]	Wood, H2SO4, MA	Cast	PU	1.13	500	40	-	-	-	-	3.5	0.2
[36]	Wood, H2SO4, MA	Cast	PU	1.51	600	30	-	-	-	-	3	0.3
[36]	Bacteria, H2SO4	Cast	PU	0.38	380	30	-	-	-	-	3.5	0.4
[36]	Bacteria, H2SO4	Cast	PU	0.75	393	9	-	-	-	-	3.8	0.4
[36]	Bacteria, H2SO4	Cast	PU	1.13	410	23	-	-	-	-	4.1	0.5
[36]	Bacteria, H2SO4	Cast	PU	1.51	470	23	-	-	-	-	4.4	0.3
[36]	Bacteria, H2SO4, MA	Cast	PU	0.38	440	20	-	-	-	-	4	0.2
[36]	Bacteria, H2SO4, MA	Cast	PU	0.75	460	20	-	-	-	-	4.5	0.1
[36]	Bacteria, H2SO4, MA	Cast	PU	1.13	450	20	-	-	-	-	5.3	0.2
[36]	Bacteria, H2SO4, MA	Cast	PU	1.51	470	30	-	-	-	-	5.9	0.2
[37]	Cotton, H2SO4	Cast	SMPU	0.00	1.7	0.1	12.3	0.4	-	-	20	1
[37]	Cotton, H2SO4	Cast	SMPU	3.80	2.13	0.03	15	3	-	-	24	2
[37]	Cotton, H2SO4, Au NP 0.15 wt%	Cast	SMPU	3.80	2.3	0.1	17	3	-	-	24	3
[37]	Cotton, H2SO4, Au NP .35 wt%	Cast	SMPU	3.80	2.2	0.3	18.4	0.3	-	-	23	2
[37]	Cotton, H2SO4, Au NP .5 wt%	Cast	SMPU	3.80	2.1	0.4	17	2	-	-	21	3
[38]	Cotton H2SO4	Cast	PLA	0.00	2500	200	2	0.3	-	-	33	3
[38]	Cotton H2SO4	Cast	PLA	1.56	2900	100	1.4	0.1	-	-	32	2
[38]	Cotton H2SO4	Cast	PLA	3.92	2700	300	1.3	0.1	-	-	27	3
[38]	Cotton H2SO4	Cast	PLA	7.93	2900	300	1	0.1	-	-	24	3
[38]	Cotton, H2SO4, Casein	Cast	PLA	1.56	3000	100	1.9	0.3	-	-	33	1
[38]	Cotton, H2SO4, Casein	Cast	PLA	3.92	3200	100	1	0.1	-	-	28	3
[38]	Cotton, H2SO4, Casein	Cast	PLA	7.93	3500	100	0.8	0.1	-	-	25	2
[39]	MCC, H2SO4	MM	PLA	43.66	-	-	-	-	-	-	42	4

R	CNC, Source, Hydrolysis, Modification	Method	Matrix	CNC	Young's Modulus (MPa)		Strain at Break (%)		Strength (MPa)			
				vol%	V	D	V	D	σ_u	σ_y	σ_t	D
[39]	MCC, H2SO4	MM	PLA 1% MA-OH	43.66	-	-	-	-	-	-	46	4
[39]	MCC, H2SO4	MM	PLA 3% MA-OH	43.66	-	-	-	-	-	-	48	4
[39]	MCC, H2SO4	MM	PLA 5% MA-OH	43.66	-	-	-	-	-	-	43	3
[39]	MCC, H2SO4	MM	PLA 3% MA-OH 1% nanoclay	43.66	-	-	-	-	-	-	48	4
[39]	MCC, H2SO4	MM	PLA 3% MA-OH 2% nanoclay	43.66	-	-	-	-	-	-	48	2
[39]	MCC, H2SO4	MM	PLA 3% MA-OH 3% nanoclay	43.66	-	-	-	-	-	-	49	4
[39]	MCC, H2SO4	MM	PLA 3% MA-OH 4% nanoclay	43.66	-	-	-	-	-	-	47	5
[40]	MCC, H2SO4	Cast	PLA	0.00	2330	80	2.9	0.1	-	-	25	1
[40]	MCC, H2SO4	Cast	PLA	0.08	2410	40	2.7	0.5	-	-	25	1
[40]	MCC, H2SO4	Cast	PLA	0.39	2560	60	2.7	0.6	-	-	27.8	0.8
[41]	Cotton, H2SO4, AcO2	Cast	PLA	0.00	2700	200	-	-	-	-	53	1.172
[41]	Cotton, H2SO4, AcO2	Cast	PLA	0.78	2800	200	-	-	-	-	57.9	0.9
[41]	Cotton, H2SO4, AcO2	Cast	PLA	1.56	2900	200	-	-	-	-	60	2
[41]	Cotton, H2SO4, AcO2	Cast	PLA	2.34	3200	200	-	-	-	-	66	2
[42]	Bacteria, H2SO4	Freeze drying	PLA	0.00	22	2	9	2	-	-	0.69	0.04
[42]	Bacteria, H2SO4	Freeze drying	PLA	3.92	37	2	7	3	-	-	1.02	0.04
[43]	Bamboo, H2SO4, Magnetic CNCs	Cast	PLA	0.00	550	50	30	5	21.3	-	-	0.9
[43]	Bamboo, H2SO4, Magnetic CNCs	Cast	PLA	0.78	1180	90	22	4	27	-	-	1
[43]	Bamboo, H2SO4, Magnetic CNCs	Cast ‖	PLA	1.56	1200	100	36	5	37	-	-	1
[43]	Bamboo, H2SO4, Magnetic CNCs	Cast ‖	PLA	2.34	1560	90	30	7	47	-	-	2
[43]	Bamboo, H2SO4, Magnetic CNCs	Cast =	PLA	0.78	690	50	60	10	40	-	-	2
[43]	Bamboo, H2SO4, Magnetic CNCs	Cast ‖	PLA	1.56	900	100	55	9	50	-	-	1
[43]	Bamboo, H2SO4, Magnetic CNCs	Cast ‖	PLA	2.34	1200	100	52	9	58	-	-	2
[43]	Bamboo, H2SO4, Magnetic CNCs	Cast ‖	PLA	0.78	600	40	80	20	44	-	-	2
[43]	Bamboo, H2SO4, Magnetic CNCs	Cast ‖	PLA	1.56	720	60	80	10	57	-	-	2
[43]	Bamboo, H2SO4, Magnetic CNCs	Cast ‖	PLA	2.34	1100	100	60	10	67	-	-	3
[44]	Bamboo, H2SO4	Extrusion	PLA	0.00	390	20	8.9	0.4	35.9	-	-	0.9
[44]	Bamboo, H2SO4	Extrusion	PLA	0.78	780	20	4.5	0.6	41.4	-	-	0.9
[44]	Bamboo, H2SO4, Radical Present	Extrusion	PLA	0.00	2110	70	2.1	0.1	42	-	-	0.6
[44]	Bamboo, H2SO4, Radical Present	Extrusion	PLA	0.78	2260	90	1.8	0.1	51	-	-	1
[44]	Bamboo, H2SO4, Radical Present	Extrusion	PLA	1.56	2400	100	1.8	0.1	47.3	-	-	0.9

R	CNC, Source, Hydrolysis, Modification	Method	Matrix	CNC	Young's Modulus (MPa)		Strain at Break (%)		Strength (MPa)			
				vol%	V	D	V	D	σ_u	σ_y	σ_t	D
[44]	Bamboo, H2SO4, Radical Present	Extrusion	PLA	2.34	2100	200	1.53	0.07	43	-	-	1
[44]	Bamboo, H2SO4, Radical & nonsoluable PLA&CNC removed by chloroform	Extrusion	PLA	0.00	1400	80	2.3	0.1	34	-	-	1
[44]	Bamboo, H2SO4, Radical & nonsoluable PLA&CNC removed by chloroform	Extrusion	PLA	1.05	1400	70	2.4	0.2	31	-	-	1
[44]	Bamboo, H2SO4, Radical & nonsoluable PLA&CNC removed by chloroform	Extrusion	PLA	2.60	1190	90	2.8	0.2	33.6	-	-	0.7
[44]	Bamboo, H2SO4, Radical & nonsoluable PLA&CNC removed by chloroform	Extrusion	PLA	4.04	930	70	2.3	0.2	30.4	-	-	0.7
[45]	MCC, H2SO4, Ag NP, & glucose	Cast	PLA:PBAT (4:1)	0.00	-	-	140	10	-	-	19	2
[45]	MCC, H2SO4, Ag NP, & glucose	Cast	PLA:PBAT (4:1)	0.78	-	-	25	4	-	-	20	2
[45]	MCC, H2SO4, Ag NP, & glucose	Cast	PLA:PBAT (4:1)	1.56	-	-	16	2	-	-	18	3
[45]	MCC, H2SO4, Ag NP, & glucose	Cast	PLA:PBAT (4:1)	3.13	-	-	12	2	-	-	15	1
[45]	MCC, H2SO4, Ag NP, & glucose	Cast	PLA:PBAT (4:1)	6.31	-	-	9	2	-	-	13	2
[46]	MCC, H2SO4	MM	PLA:PBS 30:70	0.00	22.1	-	227	-	32.7	-	44.5	-
[46]	MCC, H2SO4	MM	PLA:PBS 30:70	1.56	34.3	-	266	-	31.1	-	45.1	-
[46]	MCC, H2SO4, 0.2% DCP	MM	PLA:PBS 30:70	0.00	19.8	-	293	-	30.9	-	56.5	-
[46]	MCC, H2SO4, 0.2% DCP	MM	PLA:PBS 30:70	0.39	19.6	-	286	-	32.6	-	46.9	-
[46]	MCC, H2SO4, 0.2% DCP	MM	PLA:PBS 30:70	0.78	24.7	-	282	-	44.4	-	50	-
[46]	MCC, H2SO4, 0.2% DCP	MM	PLA:PBS 30:70	1.56	27.9	-	298	-	43.3	-	48.5	-
[47]	Cotton, H2SO4	TSE with peroxide X-linker (DCP)	PLA	0.00	-	-	13.05	-	41		-	-
[47]	Cotton H2SO4	TSE with peroxide X-linker (DCP)	PLA	0.78	-	-	15.84	-	48		-	-
[47]	Cotton, H2SO4, Peroxide Covalent Bonding	TSE with peroxide X-linker (DCP)	PLA	0.78	-	-	18.71	-	52		-	-
[47]	Cotton, H2SO4, Peroxide Covalent Bonding	TSE with peroxide X-linker (DCP)	PLA	1.56	-	-	17.21	-	50		-	-

R	CNC, Source, Hydrolysis, Modification	Method	Matrix	CNC	Young's Modulus (MPa)		Strain at Break (%)		Strength (MPa)			
				vol%	V	D	V	D	σ_u	σ_y	σ_t	D
[47]	Cotton HCl	TSE with peroxide X-linker (DCP)	PLA	0.00	-	-	13.06	-	42		-	-
[47]	Cotton HCl	TSE with peroxide X-linker (DCP)	PLA	0.78	-	-	13.89	-	48		-	-
[47]	Cotton HCl Peroxide Covalent Bonding	TSE with peroxide X-linker (DCP)	PLA	0.78	-	-	16.25	-	53		-	-
[47]	Cotton HCl Peroxide Covalent Bonding	TSE with peroxide X-linker (DCP)	PLA	1.56	-	-	16.08	-	48		-	-
[48]	Wood, H2SO4, PGSMA	Reactive Extrusion	PLA	0.00	2800	0	4	0			70	0.5
[48]	Wood, H2SO4, PGSMA	Reactive Extrusion	PLA:PGSMA 4:1	0.00	2900	200	32	23			51	3
[48]	Wood, H2SO4, PGSMA	Reactive Extrusion	PLA:PGSMA 4:2	0.16	2800	80	25	2.5			49	0.5
[48]	Wood, H2SO4, PGSMA	Reactive Extrusion	PLA:PGSMA 4:3	0.47	3000	100	16	6			56	1
[49]	Cotton, H2SO4, Triazine derivative	dry mixing powders	PLA	0.00	-	-	1.9	0.6	25	-	-	2
[49]	Cotton, H2SO4, Triazine derivative	dry mixing powders	PLA	0.78	-	-	2.9	0.5	44	-	-	2
[49]	Cotton, H2SO4, Triazine derivative	dry mixing powders	PLA	1.56	-	-	3.3	0.3	43	-	-	2
[49]	Cotton, H2SO4, Triazine derivative	dry mixing powders	PLA	2.34	-	-	3	0.3	39	-	-	2
[49]	Cotton, H2SO4, Triazine derivative	dry mixing powders	PLA	3.13	-	-	3.6	0.7	41	-	-	2
[49]	Cotton, H2SO4, Triazine derivative	dry mixing powders	PLA	3.92	-	-	3.3	0.3	39	-	-	2
[50]	Aspen, H2SO4	Melt Mixed	PLA	0.00	3700	600	7	1	64	-	-	2
[50]	Aspen, H2SO4	Melt Mixed	PLA	0.39	4300	500	11	2	61	-	-	3
[50]	Aspen, H2SO4	Melt Mixed	PLA	0.78	4200	400	12	1	63	-	-	3
[50]	Aspen, H2SO4	Melt Mixed	PLA	1.56	4200	400	13	1	63	-	-	3
[50]	Aspen, H2SO4	Melt Mixed	PLA	3.92	4500	500	11	2	59	-	-	2
[50]	High lignin, unknown source & hydrolysis	Melt Mixed	PLA	0.39	4100	200	8.2	0.7	60	-	-	1
[50]	High lignin, unknown source & hydrolysis	Melt Mixed	PLA	0.78	4800	900	12	1	58	-	-	3
[50]	High lignin, unknown source & hydrolysis	Melt Mixed	PLA	1.56	4800	600	12	1	58	-	-	4
[50]	High lignin, unknown source & hydrolysis	Melt Mixed	PLA	3.92	4600	700	11	1	56	-	-	3
[51]	MCC, Sonication	Cast PLA & MM TPU	PLA	0.00	2380	20	3.6	0.3	-	-	61.3	0.8

R	CNC, Source, Hydrolysis, Modification	Method	Matrix	CNC	Young's Modulus (MPa)		Strain at Break (%)		Strength (MPa)			
				vol%	V	D	V	D	σ_u	σ_y	σ_t	D
[51]	MCC, Sonication	Cast PLA & MM TPU	PLA:PU 4:1	0.00	1130	20	21	8	-	-	20	0.5
[51]	MCC, Sonication	Cast PLA & MM TPU	PLA:PU 4:2	0.78	1350	20	24	7	-	-	32	0.6
[51]	MCC, Sonication	Cast PLA & MM TPU	PLA:PU 4:3	2.34	1390	20	50	20	-	-	27	1
[51]	MCC, H2SO4, HCl (spherical)	Cast PLA & MM TPU	PLA:PU 4:4	0.78	1390	10	29	9	-	-	34	0.4
[51]	MCC, H2SO4, HCl (spherical)	Cast PLA & MM TPU	PLA:PU 4:5	2.34	1440	30	70	30	-	-	29	0.9
[51]	Wood, H2SO4 (rod shaped)	Cast PLA & MM TPU	PLA:PU 4:6	0.78	1430	10	22	5	-	-	31.5	0.7
[51]	Wood, H2SO4 (rod shaped)	Cast PLA & MM TPU	PLA:PU 4:7	2.34	1440	20	13	4	-	-	28	1
[52]	Bamboo H2SO4	Cast	PLA	0.00	410	20	9	4	-	-	12	1
[52]	Bamboo H2SO4	Cast	PLA	0.39	410	50	7	5	-	-	10.5	0.9
[52]	Bamboo H2SO4	Cast	PLA	0.78	300	30	12	4	-	-	10.2	0.3
[52]	Bamboo H2SO4	Cast	PLA	1.17	260	30	11	3	-	-	9.1	0.9
[52]	Bamboo H2SO4	Cast	PLA	1.56	350	80	9.6	0.9	-	-	10.5	0.6
[52]	Bamboo H2SO4	Cast	PLA	1.95	440	40	7	2	-	-	10	1
[52]	Bamboo H2SO4	Cast	PLA	2.34	320	30	7	1	-	-	10	1
[52]	Bamboo H2SO4	Cast	PLA	2.73	280	10	8.5	0.3	-	-	10.1	0.3
[52]	Bamboo H2SO4	Cast	PLA	3.13	260	5	3.6	0.4	-	-	7.5	0.5
[53]	Cotton, HCl	Cast & MM	PLA 19:1 (L:D)	0.00	1800	-	-	-	-	-	45*	-
[53]	Cotton, HCl	Cast & MM	PLA 19:1 (L:D)	0.78	1700	-	-	-	-	-	50*	-
[53]	Cotton, HCl	Cast & MM	PLA 19:1 (L:D)	2.34	1700	-	-	-	-	-	46*	-
[53]	Cotton, HCl	Cast & MM	PLA 19:1 (L:D)	3.92	1600	-	-	-	-	-	29*	-
[53]	Cotton, HCl	Cast & MM	PLA 19:1 (L:D)	7.93	1100	-	-	-	-	-	11*	-
[53]	Cotton, HCl, 1wt% Surfactant Decylamine	Cast & MM	PLA 19:1 (L:D)	0.78	1800	-	-	-	-	-	46*	-
[53]	Cotton, HCl, 1wt% Surfactant Decylamine	Cast & MM	PLA 19:1 (L:D)	2.34	1800	-	-	-	-	-	47*	-
[53]	Cotton, HCl, 1wt% Surfactant Decylamine	Cast & MM	PLA 19:1 (L:D)	3.92	1800	-	-	-	-	-	45*	-
[53]	Cotton, HCl, 1wt% Surfactant Decylamine	Cast & MM	PLA 19:1 (L:D)	7.93	1200	-	-	-	-	-	23*	-
[53]	Cotton, HCl, 1wt% Surfactant Decylamine	Cast & MM	PLA 19:1 (L:D)	0.78	1900	-	-	-	-	-	44*	-
[53]	Cotton, HCl, 1wt% Surfactant Decylamine	Cast & MM	PLA 19:1 (L:D)	2.34	1800	-	-	-	-	-	36*	-
[53]	Cotton, HCl, 1wt% Surfactant Decylamine	Cast & MM	PLA 19:1 (L:D)	3.92	1600	-	-	-	-	-	37*	-
[53]	Cotton, HCl, 1wt% Surfactant Decylamine	Cast & MM	PLA 19:1 (L:D)	7.93	900	-	-	-	-	-	25*	-

R	CNC, Source, Hydrolysis, Modification	Method	Matrix	CNC	Young's Modulus (MPa)		Strain at Break (%)		Strength (MPa)			
				vol%	V	D	V	D	σ_u	σ_y	σ_t	D
[54]	Wood, H2SO4, PLA Graft &PCL:PLA graft	Cast & injection molded	PLA	0.00	3900	300	8	4	-	-	58	1
[54]	Wood, H2SO4, PLA Graft &PCL:PLA graft	Cast & injection molded	PLA	1.95	3200	400	190	20	-	-	50.5	0.9
[54]	Wood, H2SO4, PLA Graft &PCL:PLA graft	Cast & injection molded	PLA	3.92	2700	300	210	20	-	-	44	0.3
[54]	Wood, H2SO4, PLA Graft &PCL:PLA graft	Cast & injection molded	PLA	7.93	2600	400	250	30	-	-	42	1
[54]	Wood, H2SO4, PLA graft	Cast & injection molded	PLA	1.95	3400	500	11.8	0.9	-	-	53	3
[54]	Wood, H2SO4, PLA graft	Cast & injection molded	PLA	3.92	3300	400	9	2	-	-	55.5	0.8
[55]	Ramie, H2SO4	MM	PLA	0.00	2000	200	3.5	0.4	-	-	40	7
[55]	Ramie, H2SO4	MM	PLA 10% imidazolium salt	0.00	1700	100	2.6	0.6	-	-	33	5
[55]	Ramie, H2SO4	MM	PLA 10% imidazolium salt	16.23	1900	200	2.4	0.5	-	-	31	10
[55]	Ramie, H2SO4	MM	PLA:PEG 9:1	0.00	2200	200	1.9	0.3	-	-	33	8
[55]	Ramie, H2SO4	MM	PLA:PEG 9:2	7.93	2200	500	1.6	0.4	-	-	15	4
[56]	MCC, H2SO4	PLA CNC-PA Core Shell E-Spin	PLA-PAN	0.00	600	100	6	1	-	-	1.5	0.3
[56]	MCC, H2SO4	PLA CNC-PA Core Shell E-Spin	PLA-PAN	3.92	900	100	6.2	0.7	-	-	4	1
[56]	MCC, H2SO4	PLA CNC-PA Core Shell E-Spin	PLA-PAN	7.93	700	100	9	2	-	-	3.2	0.9
[56]	MCC, H2SO4	PLA CNC-PA Core Shell E-Spin	PLA-PAN	12.03	700	100	10	1	-	-	2.9	0.4
[56]	Cotton, H2SO4	PLA CNC-PA Core Shell E-Spin	PLA-PAN	16.23	700	100	4.4	0.9	-	-	2	0.3
[56]	MCC, High Pressure Homogenization	PLA CNC-PA Core Shell E-Spin	PLA-PAN	3.92	500	100	17	2	-	-	4	1
[56]	MCC, High Pressure Homogenization	PLA CNC-PA Core Shell E-Spin	PLA-PAN	7.93	500	100	5	1	-	-	1.8	0.5
[56]	MCC, High Pressure Homogenization	PLA CNC-PA Core Shell E-Spin	PLA-PAN	12.03	900	100	6	1	-	-	2	1
[56]	MCC, High Pressure Homogenization	PLA CNC-PA Core	PLA-PAN	16.23	900	100	4.4	0.9	-	-	2.4	1

R	CNC, Source, Hydrolysis, Modification	Method	Matrix	CNC	Young's Modulus (MPa)		Strain at Break (%)		Strength (MPa)			
				vol%	V	D	V	D	σ_u	σ_y	σ_t	D
		Shell E-Spin										
[57]	Cotton, H2SO4	PLA CNC-PA Core Shell E-Spin	PC	0.00	1980	20	56	2	-	-	46.5	0.7
[57]	Cotton, H2SO4	Cast	PC	0.38	2040	20	46	3	-	-	48.1	0.7
[57]	Cotton, H2SO4	Cast	PC	0.76	2160	30	33	1	-	-	51.1	0.8
[57]	Cotton, H2SO4	Cast	PC	1.52	2360	30	23	2	-	-	55.6	0.5
[57]	Cotton, H2SO4	Cast	PC	2.29	2520	20	17	1	-	-	60.6	0.6
[57]	Cotton, H2SO4	Cast& Cure	PC	3.83	2500	20	16	1	-	-	60.2	0.7
[58]	Wood, H2SO4	Cast& Cure	W-Epoxy	0.00	2100	200	-	-	-	-	-	-
[58]	Wood, H2SO4	Cast& Cure	W-Epoxy	0.39	2200	100	-	-	-	-	-	-
[58]	Wood, H2SO4	Cast& Cure	W-Epoxy	1.57	2400	100	-	-	-	-	-	-
[58]	Wood, H2SO4	Cast& Cure	W-Epoxy	3.95	2600	100	-	-	-	-	-	-
[58]	Wood, H2SO4	Cast& Cure	W-Epoxy	7.99	3100	100	-	-	-	-	-	-
[58]	Wood, H2SO4	Cast& Cure	W-Epoxy	12.12	3600	200	-	-	-	-	-	-
[59]	Wood, H2SO4	Cast& Cure	Epoxy	0.00	1200	80	50	10	-	57	-	3
[59]	Wood, H2SO4	Cast& Cure	Epoxy	0.31	1400	40	12	2	-	65	-	2
[59]	Wood, H2SO4	Cast& Cure	Epoxy	0.95	1500	90	13	3	-	51	-	6
[59]	Wood, H2SO4	Cast& Cure	Epoxy	1.61	1400	100	17	4	-	53	-	5
[59]	Wood, H2SO4	Cast& Cure	Epoxy	0.00	2120	70	7.7	0.5	-	-	100	6
[59]	Wood, H2SO4	Cast& Cure	Epoxy	0.31	2300	100	7.4	0.6	-	-	107	5
[59]	Wood, H2SO4	Cast& Cure	Epoxy	0.44	2500	90	10.3	0.5	-	-	117	9
[59]	Wood, H2SO4	Cast& Cure	Epoxy	0.71	2500	200	8	1	-	-	101	4
[59]	Wood, H2SO4	Cast& Cure	Epoxy	0.91	2300	200	9	1	-	-	104	6
[59]	Wood, H2SO4	Cast& Cure	Epoxy	0.00	1400	200	9	1	-	-	106	9
[59]	Wood, H2SO4	Cast& Cure	Epoxy	0.31	1400	100	8	1	-	-	106	7
[59]	Wood, H2SO4	Cast& Cure	Epoxy	0.58	1950	40	8	1	-	-	118	8
[59]	Wood, H2SO4	Cast& Cure	Epoxy	0.95	1500	200	8	1	-	-	110	20
[59]	Wood, H2SO4	Cast& Cure	Epoxy	1.22	1800	300	9	1	-	-	110	6
[60]	MCC, H2SO4	Cast	Epoxy	0.00	300	10	7.1	0.4	-	-	29	1
[60]	MCC, H2SO4	Cast	Epoxy	0.39	540	30	9.8	0.1	-	-	2.5	0.1
[60]	MCC, H2SO4	Cast	Epoxy	0.78	630	30	11.1	0.6	-	-	2.5	0.1
[60]	MCC, H2SO4	Cast	Epoxy	1.57	700	40	12.4	0.6	-	-	3.2	0.2
[60]	MCC, H2SO4	Cast	Epoxy	3.15	700	30	13.9	0.7	-	-	3.1	0.2
[60]	MCC, H2SO4	Cast	Epoxy	6.36	800	40	15.2	0.8	-	-	3.6	0.2
[60]	MCC, TEMPO	Cast	Epoxy	0.00	1190	80	3.5	0.4	-	-	64	5
[60]	MCC, TEMPO	Cast & Cure	Epoxy	3.95	1300	200	1.4	0.2	-	-	33	6
[60]	MCC, TEMPO, Triblock of PEO&PPO (type 61)	Cast & Cure	Epoxy	3.95	1700	70	2.3	0.2	-	-	60	10

R	CNC, Source, Hydrolysis, Modification	Method	Matrix	CNC	Young's Modulus (MPa)		Strain at Break (%)		Strength (MPa)			
				vol%	V	D	V	D	σ_u	σ_y	σ_t	D
[60]	MCC, TEMPO, Triblock of PEO&PPO (type 61)	Cast & Cure	Epoxy	3.95	1400	100	1.8	0.3	-	-	50	10
[60]	MCC, TEMPO, Triblock of PEO&PPO (type 121)	Cast & Cure	Epoxy	0.00	1300	70	1.7	0.2	-	-	50	5
[60]	MCC, TEMPO, Triblock of PEO&PPO (type 121)	Cast & Cure	Epoxy	0.00	1200	80	1.8	0.1	-	-	50	5
[61]	Wood, H2SO4	Cast & Cure	W-Epoxy	0.00	-	-	-	-	-	-	30	10
[61]	Wood, H2SO4	Cast & Cure	W-Epoxy	0.00	-	-	-	-	-	-	27	4
[61]	Wood, H2SO4	Cast & Cure	W-Epoxy	3.95	-	-	-	-	-	-	48	6
[61]	Wood, H2SO4	Cast & Cure	W-Epoxy	3.95	-	-	-	-	-	-	45	9
[61]	Wood, H2SO4	Cast & Cure	W-Epoxy	7.99	-	-	-	-	-	-	36	2
[61]	Wood, H2SO4	Cast & Cure	W-Epoxy	7.99	-	-	-	-	-	-	50	10
[62]	Wood, H2SO4	Cast & Cure	Epoxy	0.00	2030	90	-	-	-	-	61	2
[62]	Wood, H2SO4	Cast & Cure	Epoxy	0.78	2100	40	-	-	-	-	44	3
[62]	Wood, H2SO4	Cast & Cure	Epoxy	3.95	2230	50	-	-	-	-	40	2
[62]	Wood, H2SO4, Triphenyl methyl	Cast & Cure	Epoxy	0.78	2200	200	-	-	-	-	49	4
[63]	Cotton, H2SO4	E-Spun	PAA (X-linked)	0.00	56	1	136	7	-	-	0.29	0.01
[63]	Cotton, H2SO4	E-Spun	PAA	3.65	188	4	126	6	-	-	0.68	0.03
[63]	Cotton, H2SO4	E-Spun	PAA	7.40	224	1	67	4	-	-	0.84	0.04
[63]	Cotton, H2SO4	E-Spun	PAA	11.26	1190	20	60	3	-	-	3.3	0.2
[63]	Cotton, H2SO4	E-Spun	PAA	15.23	1980	50	36	2	-	-	4.5	0.2
[63]	Cotton, H2SO4	E-Spun, X-linked	PAA	15.23	4300	400	17	1	-	-	16.7	0.8
[64]	MCC, H2SO4	Cast	PHB-co-PHV PEG CMPTBLZR	0.00	820	-	12.4	-	-	-	14.1	-
[64]	MCC, H2SO4	Cast	PHB-co-PHV PEG CMPTBLZR	1.53	1100	-	7.1	-	-	-	15.5	-
[64]	MCC, H2SO4	Cast	PHB-co-PHV PEG CMPTBLZR	3.86	1760		7.4	-	-	-	26.1	-
[64]	MCC, H2SO4	MM	PHB-co-PHV PEG CMPTBLZR	0.00	1630	30	6.2	0.7	-	-	28.93	0.3
[64]	MCC, H2SO4	MM	PHB-co-PHV PEG CMPTBLZR	1.53	1740	60	4	0.2	-	-	25.04	0.3
[64]	MCC, H2SO4	MM	PHB-co-PHV PEG CMPTBLZR	3.86	1920	70	3.4	0.5	-	-	24.88	0.4
[65]	MCC, HCl, HCOOH	Cast	PHB-co-PHV	0.00	900	100	8	0.7	-	-	13	1

R	CNC, Source, Hydrolysis, Modification	Method	Matrix	CNC	Young's Modulus (MPa)		Strain at Break (%)		Strength (MPa)			
				vol%	V	D	V	D	σ_u	σ_y	σ_t	D
[65]	MCC, HCl, HCOOH	Cast	PHB-co-PHV	7.81	1900	200	1.9	0.2	-	-	19	0.7
[65]	MCC, HCl, HCOOH, AgNP 0.17 wt%	Cast	PHB-co-PHV	7.67	1600	200	1.7	0.5	-	-	16.3	0.902
[65]	MCC, HCl, HCOOH, AgNP 0.34 wt%	Cast	PHB-co-PHV	7.54	1700	200	1.7	0.2	-	-	16.8	0.8
[65]	MCC, HCl, HCOOH, AgNP 0.51 wt%	Cast	PHB-co-PHV	7.40	1800	200	1.7	0.4	-	-	18.5	0.7
[65]	MCC, HCl, HCOOH, AgNP 0.68 wt%	Cast	PHB-co-PHV	7.27	1900	200	1.6	0.3	-	-	20	2
[65]	MCC, HCl, HCOOH, AgNP 0.85 wt%	Cast	PHB-co-PHV	7.13	2300	200	1.4	0.2	-	-	22	0.7
[65]	MCC, HCl, HCOOH, AgNP 1.7 wt%	Cast	PHB-co-PHV	6.46	3200	200	1.3	0.4	-	-	25	1
[66]	MCC, H2SO4	Cast	PEEK(S)	0.00	210	-	-	-	-	-	37.6	-
[66]	MCC, H2SO4	Cast	PEEK(S)	1.66	266	-	-	-	-	-	57.8	-
[66]	MCC, H2SO4	Cast	PEEK(S)	4.16	357	-	-	-	-	-	61.1	-
[66]	MCC, H2SO4	Cast	PEEK(S)	6.69	272	-	-	-	-	-	111.5	-
[66]	MCC, H2SO4	Cast	PEEK(S)	8.40	244	-	-	-	-	-	102.1	-
[66]	MCC, H2SO4	Cast	PEEK(S+)	0.00	271	-	-	-	-	-	12.8	-
[66]	MCC, H2SO4	Cast	PEEK(S+)	1.66	199	-	-	-	-	-	35.9	-
[66]	MCC, H2SO4	Cast	PEEK(S+)	4.16	337	-	-	-	-	-	56.7	-
[66]	MCC, H2SO4	Cast	PEEK(S+)	6.69	200	-	-	-	-	-	60.1	-
[66]	MCC, H2SO4	Cast	PEEK(S+)	8.40	313	-	-	-	-	-	35.3	-
[67]	Cotton, H2SO4	Cast & Cured	PSA-co-PDM 2:1	0.00	7.2	0.1	36	4	-	-	4.5	0.7
[67]	Cotton, H2SO4	Cast & Cured	PSA-co-PDM 2:2	0.63	11.1	0.6	26	3	-	-	5	1
[67]	Cotton, H2SO4	Cast & Cured	PSA-co-PDM 2:3	3.18	15	1	25	2	-	-	6	1
[67]	Cotton, H2SO4	Cast & Cured	PSA-co-PDM 2:4	6.49	32	3	23.4	0.1	-	-	9	2
[68]	Wood, H2SO4	Cast	PA 11	0.00	410	20	44	6	-	-	38	2
[68]	Wood, H2SO4	Cast	PA 11	0.75	440	30	55	3	-	-	41	2
[68]	Wood, H2SO4	Cast	PA 11	2.27	480	20	52	6	-	-	44	2
[68]	Wood, H2SO4	Cast	PA 11	3.80	540	30	35	3	-	-	43	3
[68]	Wood, H2SO4	Cast	PA 11	5.34	640	50	22	4	-	-	46	3
[68]	Wood, H2SO4, dodecanoic acid	Cast	PA 11	7.69	720	30	17	2	-	-	51	5
[68]	Wood, H2SO4, dodecanoic acid	Cast	PA 11	0.41	460	40	60	5	-	-	41	2
[68]	Wood, H2SO4, dodecanoic acid	Cast	PA 11		510	30	46	6	-	-	41	2
[68]	Wood, H2SO4, dodecanoic acid	Cast	PA 11	2.08	590	30	35	7	-	-	41	2
[68]	Wood, H2SO4, dodecanoic acid	Cast	PA 11	2.92	600	30	31	7	-	-	41	2
[68]	Wood, H2SO4, dodecanoic acid	Cast	PA 11	4.18	570	20	32	6	-	-	44	1

R	CNC, Source, Hydrolysis, Modification	Method	Matrix	CNC	Young's Modulus (MPa)		Strain at Break (%)		Strength (MPa)			
				vol%	V	D	V	D	σ_u	σ_y	σ_t	D
[68]	Wood, H2SO4, methyl laurate	Cast	PA 11	0.41	390	30	90	20	-	-	38	1
[68]	Wood, H2SO4, methyl laurate	Cast	PA 11	2.08	460	20	100	20	-	-	41	1
[68]	Wood, H2SO4, methyl laurate	Cast	PA 11	4.18	446	7	70	10	-	-	46	0.6
[68]	Wood, H2SO4	Cast	PA-co-PAA	0.00	2200	100	30	20	-	-	75	3
[68]	Wood, H2SO4	Cast	PA-co-PAA	3.80	2400	100	10	3	-	-	84	3
[68]	Wood, H2SO4	Cast	PA-co-PAA	7.60	2400	100	5.3	0.6	-	-	91	4
[68]	Wood, H2SO4	Cast	PA-co-PAA	15.70	3000	100	4	0.8	-	-	97	9
[68]	Wood, H2SO4	Cast	PA-co-PAA	24.20	3200	100	4.3	0.3	-	-	116	6
[68]	Wood, H2SO4	Cast	PA-co-PAA	33.20	3700	100	4.2	0.4	-	-	132	9
[69]	MCC, Hydrochloric, ZnO	E-Spun Mats	PHB-co-PHV	0.00	79	8	6.3	0.3	-	-	6.3	0.3
[69]	MCC, Hydrochloric, ZnO	E-Spun Mats	PHB-co-PHV	2.30	150	9	4.9	0.2	-	-	4.9	0.2
[69]	MCC, Hydrochloric, ZnO	E-Spun Mats	PHB-co-PHV	3.86	170	10	3.2	0.2	-	-	3.2	0.2
[69]	MCC, Hydrochloric, ZnO	E-Spun Mats	PHB-co-PHV	7.81	160	10	3.6	0.2	-	-	3.6	0.2
[69]	MCC, Hydrochloric, ZnO	E-Spun Mats	PHB-co-PHV	11.86	142	8	3.8	0.2	-	-	3.8	0.2
[69]	MCC, Hydrochloric, ZnO	Cast	PHB-co-PHV	0.00	52	5	10.7	0.6	-	-	12.6	0.7
[69]	MCC, Hydrochloric, ZnO	Cast	PHB-co-PHV	2.30	106	6	9.2	0.5	-	-	16.3	0.9
[69]	MCC, Hydrochloric, ZnO	Cast	PHB-co-PHV	3.86	124	7	7.1	0.4	-	-	24	1
[69]	MCC, Hydrochloric, ZnO	Cast	PHB-co-PHV	7.81	151	7	5.7	0.4	-	-	30	2
[69]	MCC, Hydrochloric, ZnO	Cast	PHB-co-PHV	11.86	149	8	4	0.4	-	-	28	1
[69]	MCC, Hydrochloric, ZnO	Cast	PHB-co-PHV	16.01	135	7	3.2	0.4	-	-	27	1
[70]	Cotton, H2SO4	Reaction hydrogel	H2O:PAA: PEDGA	0.13	0.011	3E-04	650	30	.073	-	-	0.003
[70]	Cotton, H2SO4	Reaction hydrogel	H2O:PAA: PEDGA	0.31	0.017	5E-04	960	30	.115	-	-	0.003
[70]	Cotton, H2SO4	Reaction hydrogel	H2O:PAA: PEDGA	0.63	0.022	6E-04	1390	50	.151	-	-	0.003
[70]	Cotton, H2SO4	Reaction hydrogel	H2O:PAA: PEDGA	0.94	0.027	7E-04	1250	50	.173	-	-	0.003
[70]	Cotton, H2SO4	Reaction hydrogel	H2O:PAA: PEDGA	1.26	0.03	8E-04	1020	40	.181	-	-	0.004
[70]	Cotton, H2SO4	Reaction hydrogel	H2O:PAA: PEDGA	0	0.007	2E-04	450	10	.035	-	-	0.002
[71]	Cotton, HCl	Cast	PHB-co-PHV	0.00	59	5	-	-	13	-	-	1

R	CNC, Source, Hydrolysis, Modification	Method	Matrix	CNC	Young's Modulus (MPa)		Strain at Break (%)		Strength (MPa)			
				vol%	V	D	V	D	σ_u	σ_y	σ_t	D
[71]	Cotton, HCl	Cast	PHB-co-PHV	3.86	183	8	-	-	28	-	-	1
[71]	Cotton, HCl	Cast	PHB-co-PHV	7.81	220	10	-	-	31	-	-	2
[71]	Cotton, HCl, HCOOH	Cast	PHB-co-PHV	3.86	180	10	-	-	29	-	-	1
[71]	Cotton, HCl, HCOOH	Cast	PHB-co-PHV	7.81	210	9	-	-	31	-	-	2
[71]	Cotton, HCl, Citrate	Cast	PHB-co-PHV	3.86	220	10	-	-	33	-	-	0.5
[71]	Cotton, HCl, Citrate	Cast	PHB-co-PHV	7.81	250	10	-	-	35	-	-	5
[72]	Wood, H2SO4	F-Spun draw ratio 10	PA-co-PMA	0.00	14500	900	8.9	0.5	-	-	650	60
[72]	Wood, H2SO4	F-Spun draw ratio 10	PA-co-PMA	0.72	15700	700	8	1	-	-	610	70
[72]	Wood, H2SO4	F-Spun draw ratio 10	PA-co-PMA	3.65	18000	1000	8.8	0.5	-	-	730	90
[72]	Wood, H2SO4	F-Spun draw ratio 10	PA-co-PMA	7.40	19000	2000	9.5	0.9	-	-	700	100
[73]	Wood, H2SO4	Cast + extrusion	ABS	0.00	3300	200	9	1	-	-	32	2
[73]	Wood, H2SO4	Cast + extrusion	ABS	0.47	4500	200	6	1	-	-	37	2
[73]	Wood, H2SO4	Cast + extrusion	ABS	0.14	4400	200	4.1	0.6	-	-	34	1
[73]	Wood, H2SO4	Cast + extrusion	ABS	2.37	4200	200	3.8	0.5	-	-	34	1
[73]	Wood, H2SO4	Cast + extrusion	ABS	4.79	4400	200	3.3	0.5	-	-	35	1
[74]	Cotton H2SO4	Cast	PHB-co-PHV	0.00	1200	100	-	-	-	-	27	5
[74]	Cotton H2SO4	Cast	PHB-co-PHV	0.38	1500	200	-	-	-	-	27	5
[74]	Cotton H2SO4	Cast	PHB-co-PHV	0.92	1800	200	-	-	-	-	34	7
[74]	Cotton H2SO4	Cast	PHB-co-PHV	1.53	1900	200	-	-	-	-	36	4
[74]	Cotton H2SO4	Cast	PHB-co-PHV	1.76	1900	200	-	-	-	-	36	5
[74]	Cotton H2SO4	Cast	PHB-co-PHV	2.23	1700	200	-	-	-	-	31	2
[74]	Cotton H2SO4	Cast	PHB-co-PHV	2.54	1700	100	-	-	-	-	31	5
[74]	Cotton H2SO4	Cast	PHB-co-PHV	2.77	1800	200	-	-	-	-	26	5
[74]	Cotton H2SO4	Cast	PHB-co-PHV	3.23	1700	200	-	-	-	-	27	8
[74]	Cotton H2SO4	Cast	PHB-co-PHV	3.55	1800	400	-	-	-	-	19	7
[75]	Cotton H2SO4 + X linking	Cast	PMVE-co-MA, PEG	18.64	90	60	310	20	-	-	2.3	0.8
[75]	Cotton H2SO4 + X linking	Cast	PMVE-co-MA, PEG	40.74	190	60	230	20	-	-	4.2	0.2
[75]	Cotton H2SO4 + X linking	Cast	PMVE-co-MA, PEG	67.35	2300	100	120	2	-	-	4	0.1
[75]	Cotton H2SO4 + X linking	Cast	PMVE-co-MA, PEG	100.00	3900	800	105	0	-	-	4	2
[75]	Cotton H2SO4 + X linking	Cast	PMVE-co-MA, PEG	67.35	14300	3000	106	2	-	-	36.8	5

R	CNC, Source, Hydrolysis, Modification	Method	Matrix	CNC	Young's Modulus (MPa)		Strain at Break (%)		Strength (MPa)			
				vol%	V	D	V	D	σ_u	σ_y	σ_t	D
[75]	Cotton H2SO4 + X linking	Cast	PMVE-co-MA, PEG	67.35	8700	900	116	4	-	-	8.5	3
[75]	Cotton H2SO4 + X linking	Cast	PMVE-co-MA, PEG	67.35	2300	100	120	2	-	-	4	0.05
[76]	Cotton, H2SO4	Cast	PHB-co-PHV	0.00	55	6	19	2	-	-	13	1
[76]	Cotton, H2SO4	Cast	PHB-co-PHV	0.76	86	7	17	2	-	-	15	1
[76]	Cotton, H2SO4	Cast	PHB-co-PHV	2.30	140	10	13	2	-	-	24	1
[76]	Cotton, H2SO4	Cast	PHB-co-PHV	3.86	170	10	9	2	-	-	28.8	0.8
[76]	Cotton, H2SO4	Cast	PHB-co-PHV	7.81	196	9	6	2	-	-	31.1	0.8
[76]	Cotton, H2SO4	Cast	PHB-co-PHV	11.86	193	7	5	2	-	-	31	1
[76]	Cotton, H2SO4	Cast	PHB-co-PHV	16.01	190	6	5	1	-	-	31	1
[77]	Cotton, H2SO4	Free Radical P-RXN	PA:PbA	0.00	0.03	0.02	-	-	-	-	-	-
[77]	Cotton, H2SO4	Free Radical P-RXN	PA:PbA	8.28	0.04	0.02	-	-	-	-	-	-
[77]	Cotton, H2SO4	Free Radical P-RXN	PA:PbA	16.88	0.04	0.02	-	-	-	-	-	-
[77]	Cotton, H2SO4	Free Radical P-RXN	PA:PbA	44.83	0.08	0.07	-	-	-	-	-	-
[77]	Cotton H2SO4 Glycosidal Methacrylate	Free Radical P-RXN	PA	8.28	0.11	0.08	-	-	-	-	-	-
[77]	Cotton H2SO4 Glycosidal Methacrylate	Free Radical P-RXN	PA	16.88	0.12	0.01	-	-	-	-	-	-
[77]	Cotton H2SO4 Glycosidal Methacrylate	Free Radical P-RXN	PA	44.83	0.33	0.08	-	-	-	-	-	-
[78]	MCC, HCl, HCOOH, Ag NP	Cast	PHB-co-PHV	0.00	60	6	11	1	-	-	13	2
[78]	MCC, HCl, HCOOH, Ag NP	Cast	PHB-co-PHV	0.76	100	10	8.2	0.8	-	-	16	2
[78]	MCC, HCl, HCOOH, Ag NP	Cast	PHB-co-PHV	2.30	130	10	6.6	0.6	-	-	21	2
[78]	MCC, HCl, HCOOH, Ag NP	Cast	PHB-co-PHV	3.86	150	10	5.5	0.5	-	-	24	2
[78]	MCC, HCl, HCOOH, Ag NP	Cast	PHB-co-PHV	7.81	180	10	5	0.7	-	-	31	2
[78]	MCC, HCl, HCOOH, Ag NP	Cast	PHB-co-PHV	11.86	180	10	4	0.5	-	-	29	2
[78]	MCC, HCl, HOOH	Cast	PHB-co-PHV	0.00	8	5	12	1	-	-	14	1
[78]	MCC, HCl, HOOH	Cast	PHB-co-PHV	0.76	118	6	10	1	-	-	17	1
[78]	MCC, HCl, HOOH	Cast	PHB-co-PHV	2.30	160	10	9	1	-	-	24	1
[78]	MCC, HCl, HOOH	Cast	PHB-co-PHV	3.86	180	10	7	1	-	-	27.9	0.9
[78]	MCC, HCl, HOOH	Cast	PHB-co-PHV	7.81	209	8	6.2	0.8	-	-	32	1
[78]	MCC, HCl, HOOH	Cast	PHB-co-PHV	11.86	219	7	6	1	-	-	33	1

R	CNC, Source, Hydrolysis, Modification	Method	Matrix	CNC	Young's Modulus (MPa)		Strain at Break (%)		Strength (MPa)			
				vol%	V	D	V	D	σ_u	σ_y	σ_t	D
[78]	MCC, HCl, HOOH	Cast	PHB-co-PHV	16.01	229	6	5.3	0.8	-	-	35	1
[79]	None	Cast	Pea starch glycerol (70:30)	0.00	-	-	30	3	4.1	-	-	0.3
[79]	Variable Hydrolysis time 4-hr	Cast	Pea starch glycerol (70:30)	9.43	-	-	41	2	7.7	-	-	0.5
[79]	Variable Hydrolysis time 8-hr	Cast	Pea starch glycerol (70:30)	9.43	-	-	61	6	7.9	-	-	0.5
[79]	Variable Hydrolysis time 12-hr	Cast	Pea starch glycerol (70:30)	9.43	-	-	58	6	6.1	-	-	0.3
[79]	Variable Hydrolysis time 16-hr	Cast	Pea starch glycerol (70:30)	9.43	-	-	57	8	5.8	-	-	0.6
[79]	Variable Hydrolysis time 24-hr	Cast	Pea starch glycerol (70:30)	9.43	-	-	55	6	5.8	-	-	0.5
[80]	Wood, H2SO4	E-Spun Mats	Silk Fibers	0.00	310	40	10.8	0.4	-	-	9	3
[80]	Wood, H2SO4	E-Spun Mats	Silk Fibers	0.81	420	80	9.9	0.3	-	-	15	3
[80]	Wood, H2SO4	E-Spun Mats	Silk Fibers	1.63	620	70	7.6	0.3	-	-	19	3
[80]	Wood, H2SO4	E-Spun Mats	Silk Fibers	2.45	1040	70	5.2	0.6	-	-	26	3
[80]	Wood, H2SO4	E-Spun Mats	Silk Fibers	3.27	1200	100	4.8	0.9	-	-	37	4
[81]	Wood, H2SO4	Cast	Silk Fibers	0.00	820	60	90	10	-	-	20	1
[81]	Wood, H2SO4	Cast	Silk Fibers	2.45	1070	80	80	10	-	-	23	3
[81]	Wood, H2SO4	Cast	Silk Fibers	4.93	1400	100	63	8	-	-	28	2
[81]	Wood, H2SO4	Cast	Silk Fibers	7.44	1950	40	53	7	-	-	33	2
[81]	Wood, H2SO4	Cast	Silk Fibers	9.97	2110	70	32	7	-	-	36	1
[81]	Wood, H2SO4	Cast	Silk Fibers	12.54	2050	90	11	3	-	-	33	2
[82]	Cotton H2SO4	Cast	HBr	0.00	400	300	17	6	-	-	12	5
[82]	Cotton H2SO4	Cast	HBr	31.91	4100	900	1.8	0.5	-	-	29	3
[82]	Cotton H2SO4	Cast	HBr	46.54	5100	400	1.2	0.6	-	-	40	6
[82]	Cotton H2SO4	Cast	HBr	58.44	8000	2000	0.595	0.3	-	-	48	5
[83]	Rice husk, H2SO4	Cast	1:2 Cassava starch glycerol	0.00	100	30			-	-	4.1	0.5
[83]	Rice husk, H2SO4	Cast	1:2 Cassava starch glycerol	1.88	210	30	-	-	-	-	5.1	0.5
[83]	Rice husk, H2SO4	Cast	1:2 Cassava starch glycerol	3.76	250	30	-	-	-	-	5.6	0.6
[83]	Rice husk, H2SO4	Cast	1:2 Cassava starch glycerol	5.65	260	30	-	-	-	-	6.1	0.5

R	CNC, Source, Hydrolysis, Modification	Method	Matrix	CNC	Young's Modulus (MPa)		Strain at Break (%)		Strength (MPa)			
				vol%	V	D	V	D	σ_u	σ_y	σ_t	D
[83]	Rice husk, H2SO4	Cast	1:2 Cassava starch glycerol	7.54	250	30	-	-	-	-	5.3	0.9
[83]	Rice husk, H2SO4	Cast	1:2 Cassava starch glycerol	9.43	220	20	-	-	-	-	5.3	0.6
[84]	MCC, H2SO4	Template	CAB	0.00	1300	100	5	2	-	-	29	5
[84]	MCC, H2SO4	Template	CAB	2.36	1450	40	6.2	0.3	-	-	40	1
[84]	MCC, H2SO4	Template	CAB	4.75	1820	10	5	2	-	-	43	2
[85]	Sugarcane, H2SO4, Pectin	Ball Milling	Starch 3d@50%RH	0.00	29	2	17	3	-	-	1.8	0.2
[85]	Sugarcane, H2SO4, Pectin	Ball Milling	Starch 3d@50%RH	0.94	49	5	14	3	-	-	2.7	0.4
[85]	Sugarcane, H2SO4, Pectin	Ball Milling	Starch 3d@50%RH	4.70	107	6	9	2	-	-	4.6	0.6
[85]	Sugarcane, H2SO4, Pectin	Ball Milling	Starch 3d@50%RH	9.43	112	9	8	3	-	-	4.5	0.5
[85]	Sugarcane, H2SO4, Pectin	Ball Milling	Starch 3d@50%RH	14.20	130	20	8	0.6	-	-	4.9	0.5
[86]	Kenaf, H2SO4	Cast	K-Careegan + Glycerol	0.00	770	-	-	-	-	-	23.6	-
[86]	Kenaf, H2SO4	Cast	K-Careegan + Glycerol	1.72	820	-	-	-	-	-	29	-
[86]	Kenaf, H2SO4	Cast	K-Careegan + Glycerol	3.44	1370	-	-	-	-	-	37.4	-
[86]	Kenaf, H2SO4	Cast	K-Careegan + Glycerol	5.18	950	-	-	-	-	-	35.2	-
[86]	Kenaf, H2SO4	Cast	K-Careegan + Glycerol	6.93	920	-	-	-	-	-	30.4	-
[87]	Rice, H2SO4	Cast	Starch	0.00	330	50	33	3	-	-	10	0.5
[87]	Rice, H2SO4	Cast	Starch	0.02	530	40	21	3	-	-	13.9	0.9
[87]	Rice, H2SO4	Cast	Starch	4.48	500	30	23	2	-	-	14	2
[87]	Rice, H2SO4	Cast	Starch	8.57	900	50	4.2	0.2	-	-	26.8	0.8
[87]	Rice, H2SO4	Cast	Starch	12.33	900	50	3.6	0.4	-	-	26	1
[88]	Wood, H2SO4	F-Spin (as spun)	CAB	0.00	933	9	21	3	-	-	20.9	0.9
[88]	Wood, H2SO4	F-Spin (as spun)	CAB	1.57	1470	50	7	2	-	-	27	1
[88]	Wood, H2SO4	F-Spin (as spun)	CAB	7.99	1770	30	6	2	-	-	25.8	0.3
[88]	Wood, H2SO4	F-Spin (drawn)	CAB	0.00	1480	50	4.1	0.4	-	-	31	3
[88]	Wood, H2SO4	F-Spin (drawn)	CAB	1.57	1500	50	3.2	0.3	-	-	26	1
[88]	Wood, H2SO4	F-Spin (drawn)	CAB	7.99	2200	100	2.3	0.5	-	-	30	4
[89]	Wood, H2SO4	W-Spin draw ratio 1	Silk	0.00	8600	900			-	-	190	10
[89]	Wood, H2SO4	W-Spin draw ratio 2	Silk	0.00	13400	600	-	-	-	-	350	20
[89]	Wood, H2SO4	W-Spin draw ratio 3	Silk	0.00	15000	1000	-	-	-	-	450	20

R	CNC, Source, Hydrolysis, Modification	Method	Matrix	CNC	Young's Modulus (MPa)		Strain at Break (%)		Strength (MPa)			
				vol%	V	D	V	D	σ_u	σ_y	σ_t	D
[89]	Wood, H2SO4	W-Spin draw ratio 1	Silk	0.81	9300	600	-	-	-	-	220	20
[89]	Wood, H2SO4	W-Spin draw ratio 2	Silk	0.81	17000	2000	-	-	-	-	420	20
[89]	Wood, H2SO4	W-Spin draw ratio 3	Silk	0.81	24000	3000	-	-	-	-	560	30
[89]	Wood, H2SO4	W-Spin draw ratio 1	Silk	2.45	12000	1000	-	-	-	-	280	20
[89]	Wood, H2SO4	W-Spin draw ratio 2	Silk	2.45	20000	1000	-	-	-	-	460	30
[89]	Wood, H2SO4	W-Spin draw ratio 3	Silk	2.45	25000	2000	-	-	-	-	660	40
[89]	Wood, H2SO4	W-Spin draw ratio 1	Silk	4.10	15000	3000	-	-	-	-	320	20
[89]	Wood, H2SO4	W-Spin draw ratio 2	Silk	4.10	22000	1000	-	-	-	-	570	40
[89]	Wood, H2SO4	W-Spin draw ratio 3	Silk	4.10	29000	3000	-	-	-	-	740	40
[89]	Wood, H2SO4	W-Spin draw ratio 1	Silk	5.76	11000	800	-	-	-	-	300	20
[89]	Wood, H2SO4	W-Spin draw ratio 2	Silk	5.76	18000	2000	-	-	-	-	460	30
[89]	Wood, H2SO4	W-Spin draw ratio 3	Silk	5.76	25000	3000	-	-	-	-	690	30
[90]	Cotton H2SO4	Cast	PLA	0.00	270	300	16	4	-	-	37	2
[90]	Cotton H2SO4	Cast + annealing at 80 °C	PLA	0.00	2600	200	70	60	-	-	26	2
[90]	Cotton H2SO4	Cast + annealing at 120 °C	PLA	0.00	3100	200	14	0	-	-	28	2
[90]	Cotton H2SO4	Cast + annealing at 140 °C	PLA	0.00	2800	500	2	0	-	-	32	7
[90]	Cotton H2SO4	Cast	PLA	1.56	2500	100	4	0	-	-	47	3
[90]	Cotton H2SO4	Cast + annealing at 80 °C	PLA	1.56	1000	300	200	100	-	-	17	5
[90]	Cotton H2SO4	Cast + annealing at 120 °C	PLA	1.56	3400	400	3	1	-	-	43	6
[90]	Cotton H2SO4	Cast + annealing at 140 °C	PLA	1.56	1400	300	16	6	-	-	19	4
[90]	Cotton H2SO4	Cast	PLA	7.93	2800	200	1.2	0.3	-	-	33	9
[90]	Cotton H2SO4	Cast + annealing at 80 °C	PLA	7.93	3500	100	1.8	0.2	-	-	24.7	0.4
[90]	Cotton H2SO4	Cast + annealing at 120 °C	PLA	7.93	3800	300	1.8	0	-	-	28	2
[90]	Cotton H2SO4	Cast + annealing at 140 °C	PLA	7.93	4000	200	1.4	0	-	-	33	4
[90]	Cotton H2SO4	Cast	PLA	13.70	3700	300	1.2	0.2	-	-	42	3
[90]	Cotton H2SO4	Cast + annealing at 80 °C	PLA	13.70	4000	300	1.6	0.1	-	-	27.9	0
[90]	Cotton H2SO4	Cast + annealing at 120 °C	PLA	13.70	4100	200	1.2	0	-	-	28.1	0.9

R	CNC, Source, Hydrolysis, Modification	Method	Matrix	CNC	Young's Modulus (MPa)		Strain at Break (%)		Strength (MPa)			
				vol%	V	D	V	D	σ_u	σ_y	σ_t	D
[90]	Cotton H2SO4	Cast + annealing at 140 °C	PLA	13.70	4100	900	0.7	0.2	-	-	27.7	0.9
[91]	Wood, H2SO4	Cast	None	100	5800	100	0.7	0.1	-	-	35	7
[91]	Wood, H2SO4	Cast	PLA	96.80	4500	300	1.1	0.3	-	-	30	3
[91]	Wood, H2SO4	Cast	PLA	93.64	3000	1000	1.8	0.5	-	-	29	7
[91]	Wood, H2SO4	Cast	PLA	87.46	2000	2000	1.7	0.3	-	-	19	9
[92]	Palm, Mechanical Separation	Cast	PLA	0.00	3880	70	98	5	-	-	16.5	0.5
[92]	Palm, Mechanical Separation	Cast	PLA	0.78	4700	100	31	7	-	-	22.9	0.8
[92]	Palm, Mechanical Separation	Cast	PLA	2.34	4980	80	30	8	-	-	30.6	0.7
[92]	Palm, Mechanical Separation	Cast	PLA	3.92	5190	80	29	4	-	-	24	0.6
[93]	bamboo, H2SO4, cellulose I	Cast	PLA	0.00	560	20	38	2	-	-	21.3	0.4
[93]	bamboo, H2SO4, cellulose I	Cast	PLA	0.78	620	20	18	2	-	-	26.2	0.5
[93]	bamboo, H2SO4, cellulose I	Cast	PLA	1.56	700	30	16	2	-	-	35	0.4
[93]	bamboo, H2SO4, cellulose I	Cast	PLA	2.34	800	40	14	1	-	-	23.8	0.6
[93]	bamboo, H2SO4, cellulose II	Cast	PLA	0.78	920	10	12	2	-	-	33.6	0.9
[93]	bamboo, H2SO4, cellulose II	Cast	PLA	1.56	1150	40	9	2	-	-	37	1
[93]	bamboo, H2SO4, cellulose II	Cast	PLA	2.34	840	50	8	2	-	-	25.7	0.4
[93]	bamboo, H2SO4, cellulose II	Cast	PLA	0.78	940	30	8	2	-	-	36.8	1
[93]	bamboo, H2SO4, cellulose II	Cast	PLA	1.56	900	60	5	2	-	-	30.3	0.5
[93]	bamboo, H2SO4, cellulose II	Cast	PLA	2.34	740	50	4	1	-	-	30.6	0.7
[94]	Cotton HCl	MM	CA	0.00	560	10	23	1	-	43	-	3
[94]	Cotton HCl	Cast & MM	CA	4.10	537	9	23.1	0.5	-	36	-	1
[94]	Cotton HCl	Cast & MM	CA	8.28	580	10	20.9	0.6	-	35.7	-	0.4
[94]	Cotton HCl	Cast & MM	CA	12.54	630	20	17	0.7	-	36.8	-	0.7
[94]	Cotton HCl	MM	CA	4.10	540	10	20.9	0.5	-	38.6	-	0.5
[94]	Cotton HCl	MM	CA	8.28	550	10	19	0.7	-	35.6	-	0.4
[94]	Cotton HCl	MM	CA	12.54	560	20	16.2	0.6	-	37	-	0.6
[95]	MCC, H2SO4	MM	Starch	0.00	240	20	20	2	3.1	-	-	0.3
[95]	Cotton, H2SO4	MM	Starch	0.81	520	30	15	1	5.1	-	-	0.4
[95]	Cotton, H2SO4	MM	Starch	2.45	1300	100	10	1	8.1	-	-	0.8
[95]	Cotton, H2SO4	MM	Starch	4.10	2300	100	6.5	0.8	9.8	-	-	0.7
[95]	Cotton, H2SO4	MM	Starch	5.76	3300	200	5	0.4	10.8	-	-	0.8
[95]	Cotton, H2SO4	MM	Starch	7.44	4200	300	4	0.4	11	-	-	1
[96]	Cotton, Unknown	Cast	soy protein isolate, glycerol, & ethylene	0.00	21	2	10		-	-	3.1	0.4

R	CNC, Source, Hydrolysis, Modification	Method	Matrix	CNC	Young's Modulus (MPa)		Strain at Break (%)		Strength (MPa)			
				vol%	V	D	V	D	σ_u	σ_y	σ_t	D
			diglycidyl ether									
[96]	Cotton, Unknown	Cast	soy protein isolate, glycerol, & ethylene diglycidyl ether	1.04	48	2	3		-	-	4.8	0.2
[96]	Cotton, Unknown, (3-aminopropyl) triethoxysilane	Cast	soy protein isolate, glycerol, & ethylene diglycidyl ether	1.04	66	4	4		-	-	5.6	0.2
[97]	Tunicin, H2SO4	Cast	Wood CNCs	0.00	9100	500	0.36	0.1	-	-	32.9	5
[97]	Tunicin, H2SO4	Cast	Wood CNCs	1.00	13200	1700	0.47	0.09	-	-	48.42	5.8
[97]	Tunicin, H2SO4	Cast	Wood CNCs	5.00	15500	1600	0.62	0.08	-	-	74.2	10.6
[97]	Tunicin, H2SO4	Cast	Wood CNCs	10.00	16700	1800	0.74	0.09	-	-	109.7	8.5
[97]	Tunicin, H2SO4	Cast	Wood CNCs	30.00	20200	900	1.07	0.1	-	-	138	4.3
[97]	Tunicin, H2SO4	Cast	Wood CNCs	60.00	21400	1200	0.76	0.1	-	-	122.3	12.6
[97]	Tunicin, H2SO4	Cast	Wood CNCs	100	20500	1900	0.7	0.05	-	-	132.3	10
[98]	Cotton, H2SO4	Cast	Chitosan Xylan 1:2	0.00	-	-	-	-	-	-	4.9	0.36
[98]	Cotton, H2SO4	Cast	Chitosan Xylan 1:3	4.00	-	-	-	-	-	-	-	-
[98]	Cotton, H2SO4	Cast	Chitosan Xylan 1:4	12.00	-	-	-	-	-	-	16.04	0.22
[98]	Cotton, H2SO4	Cast	Chitosan Xylan 1:5	16.00	-	-	-	-	-	-	12.76	0.24
[99]	Wood H2SO4	Cast & X-linking	Alginate	0.00	292	-	9.66	-	9.66	-	-	-
[99]	Wood H2SO4	Cast & X-linking	Alginate	10.00	349	-	24.4	-	24.4	-	-	-
[99]	Wood H2SO4	Cast & X-linking	Alginate	30.00	361	-	18.7	-	18.7	-	-	-
[99]	Wood H2SO4	Cast & X-linking	Alginate	50.00	133	-	3.4	-	3.4	-	-	-
[99]	Wood H2SO4	Cast & X-linking	Alginate	70.00	425	-	8.5	-	8.5	-	-	-
[99]	Wood, H2SO4, TEMPO	Cast & X-linking	Alginate	10.00	397	-	33	-	33	-	-	-
[99]	Wood, H2SO4, TEMPO	Cast & X-linking	Alginate	30.00	437	-	21.8	-	21.8	-	-	-
[99]	Wood, H2SO4, TEMPO	Cast & X-linking	Alginate	50.00	233	-	4.5	-	4.5	-	-	-
[99]	Wood, H2SO4, TEMPO	Cast & X-linking	Alginate	70.00	277	-	7.3	-	7.3	-	-	-
[99]	Wood, H2SO4	Cast & X-linking	Alginate 37°C+wet	0.00	49.7	-	37.4	-	3.4	-	-	-
[99]	Wood, H2SO4	Cast & X-linking	Alginate 37°C+wet	10.00	23.2	-	51.5	-	3.2	-	-	-
[99]	Wood, H2SO4	Cast & X-linking	Alginate 37°C+wet	30.00	53.3	-	41	-	6.3	-	-	-
[99]	Wood, H2SO4	Cast & X-linking	Alginate 37°C+wet	50.00	38.9	-	31.1	-	3.9	-	-	-
[99]	Wood, H2SO4	Cast & X-linking	Alginate 37°C+wet	70.00	8.17	-	17.6	-	2.1	-	-	-

R	CNC, Source, Hydrolysis, Modification	Method	Matrix	CNC	Young's Modulus (MPa)		Strain at Break (%)		Strength (MPa)			
				vol%	V	D	V	D	σ_u	σ_y	σ_t	D
[99]	Wood, Sulfuric acid TEMPO	Cast & X-linking	Alginate 37°C+wet	10.00	25.3	-	33.6	-	2	-	-	-
[99]	Wood, Sulfuric acid TEMPO	Cast & X-linking	Alginate 37°C+wet	30.00	30.2	-	22.6	-	1	-	-	-
[99]	Wood, Sulfuric acid TEMPO	Cast & X-linking	Alginate 37°C+wet	50.00	41.6	-	21.4	-	1.5	-	-	-
[99]	Wood, Sulfuric acid TEMPO	Cast & X-linking	Alginate 37°C+wet	70.00	16.8	-	26.7	-	0.3	-	-	-
[99]	Wood, H2SO4	Cast & X-linking	Alginate 37 °C DPBS	0.00	20.2	-	31.4	-	3.6	-	-	-
[99]	Wood, H2SO4	Cast & X-linking	Alginate 37 °C DPBS	10.00	10.4	-	38.6	-	1.7	-	-	-
[99]	Wood, H2SO4	Cast & X-linking	Alginate 37 °C DPBS	30.00	6.2	-	19.8	-	0.9	-	-	-
[99]	Wood, H2SO4	Cast & X-linking	Alginate 37 °C DPBS	50.00	15.8	-	12	-	0.1	-	-	-
[99]	Wood, H2SO4	Cast & X-linking	Alginate 37 °C DPBS	70.00	16.6	-	9.5	-	1.5	-	-	-
[99]	Wood, H2SO4, TEMPO	Cast & X-linking	Alginate 37 °C DPBS	10.00	76	-	33	-	11.1	-	-	-
[99]	Wood, H2SO4, TEMPO	Cast & X-linking	Alginate 37 °C DPBS	30.00	35	-	30.8	-	5.1	-	-	-
[99]	Wood, H2SO4, TEMPO	Cast & X-linking	Alginate 37 °C DPBS	50.00	16	-	23.9	-	1.8	-	-	-
[99]	Wood, H2SO4, TEMPO	Cast & X-linking	Alginate 37 °C DPBS	70.00	2.1	-	23.2	-	0.3	-	-	-
[100]	Cotton, H2SO4	Cast	Paperboard	0.00	900	150	1.5	0.3	-	-	9	2
[100]	Cotton, H2SO4	Cast	Paperboard + 15% PHB	0.00	1120	70	1.6	0.2	-	-	12.6	0.9
[100]	Cotton, H2SO4	Cast	Paperboard + 15% PHB	3.76	1100	100	1.7	0.3	-	-	10	1
[101]	Wood, H2SO4	TSE & Cast	Collagen (bovine tendon)	0.00	3700	400	3.6	-	-	-	-	-
[101]	Wood, H2SO4	TSE & Cast	Collagen (bovine tendon)	0.81	3800	200	3.76	-	-	-	-	-
[101]	Wood, H2SO4	TSE & Cast	Collagen (bovine tendon)	1.63	3900	200	4.3	-	-	-	-	-
[101]	Wood, H2SO4	TSE & Cast	Collagen (bovine tendon)	2.45	4000	200	4.47	-	-	-	-	-
[101]	Wood, H2SO4	TSE & Cast	Collagen (bovine tendon)	3.27	4300	200	4.74	-	-	-	-	-
[101]	Wood, H2SO4	TSE & Cast	Collagen (bovine tendon)	4.10	4700	300	3.52	-	-	-	-	-
[101]	Wood, H2SO4	TSE & Cast	Collagen (bovine tendon)	4.93	5100	300	2.19	-	-	-	-	-
[101]	Wood, H2SO4	TSE & Cast	Collagen (bovine tendon)	5.76	5100	300	1.56	-	-	-	-	-
[102]	Cotton, H2SO4	Cast	10:1 Starch:PVA	0.00	-	-	61	6	-	-	4.2	0.4
[102]	Cotton, H2SO4	Cast	10:1 Starch:PVA	2.82	-	-	66	6	-	-	2.8	0.2
[102]	Cotton, H2SO4	Cast	10:1 Starch:PVA	4.70	-	-	65	5	-	-	4.2	0.6
[102]	Cotton, H2SO4	Cast	10:1 Starch:PVA	6.59	-	-	70	1	-	-	4.2	0.3

R	CNC, Source, Hydrolysis, Modification	Method	Matrix	CNC	Young's Modulus (MPa)		Strain at Break (%)		Strength (MPa)			
				vol%	V	D	V	D	σ_u	σ_y	σ_t	D
[102]	Cotton, H2SO4	Cast	10:1 Starch:PVA	9.43	-	-	58	2	-	-	4.6	0.4
[102]	Cotton, H2SO4	Cast	10:1 Starch:PVA	14.20	-	-	53	4	-	-	3.8	0.4
[102]	Cotton, H2SO4	Cast	10:1 Starch:PVA	18.99	-	-	41	5	-	-	3.5	0.7
[103]	Ramie, HCl	Cast	Soy Protein Isolate	0.00	-	-	200	20	-	-	6.3	0.2
[103]	Ramie, HCl, Aldehyde Oxidation	Cast	Soy Protein Isolate	4.25	-	-	140	20	-	-	8.8	0.7
[103]	Ramie, HCl, Aldehyde Oxidation	Cast	Soy Protein Isolate	2.12	-	-	220	20	-	-	9	1
[103]	Ramie, HCl, Aldehyde Oxidation	Cast	Soy Protein Isolate	4.25	-	-	220	7	-	-	10.9	0.6
[103]	Ramie, HCl, Aldehyde Oxidation	Cast	Soy Protein Isolate	6.40	-	-	180	20	-	-	12.6	0.3
[103]	Ramie, HCl, Aldehyde Oxidation	Cast	Soy Protein Isolate	8.57	-	-	150	20	-	-	14	2
[104]	Algae, HBr	Cast	10:3 Starch: Glycerol	0.00	150	50	36	8	-	-	9.2	0.8
[104]	Algae, HBr	Cast	10:3 Starch: Glycerol	0.94	700	100	13	9	-	-	16	2
[104]	Algae, HBr	Cast	10:3 Starch: Glycerol	2.82	180	40	17	0.2	-	-	16	0.9
[104]	Algae, HBr	Cast	10:3 Starch: Glycerol	4.70	170	60	18.6	0.7	-	-	12.6	0.8
[105]	MCC, H2SO4	E-Spun Mat	CA	0.00	70	10	5.4	0.2	-	-	1.4	0.2
[105]	MCC, H2SO4	E-Spun Mat	CA	8.28	10	20	9.7	0.5	-	-	0.7	0.1
[105]	MCC, H2SO4	E-Spun Mat	CA	0.00	180	10	12.9	0.2	-	-	6.8	0.6
[105]	MCC, H2SO4	E-Spun Mat	CA	8.28	20	10	40	-	-	-	1.3	0.2
[106]	Sweet potato, H2SO4, Carboxymethyl CNCs	Cast	Starch (Cassava)	0.00	-	-	25	1	-	-	3.6	0.8
[106]	Sweet potato, H2SO4, Carboxymethyl CNCs	Cast	Starch (Cassava)	2.85	-	-	19	1	-	-	10.4	0.5
[106]	Sweet potato, H2SO4, Carboxymethyl CNCs	Cast	Starch (Cassava)	4.27	-	-	12	1	-	-	11.3	0.9
[106]	Sweet potato, H2SO4, Carboxymethyl CNCs	Cast	Starch (Cassava)	5.70	-	-	10.8	0.6	-	-	21.8	0.9
[106]	Sweet potato, H2SO4, Carboxymethyl CNCs	Cast	Starch (Cassava)	7.14	-	-	8.7	0.3	-	-	22.5	0.9
[106]	Sweet potato, H2SO4	Cast	Starch (Cassava)	2.85	-	-	10	1	-	-	11.8	0.8
[106]	Sweet potato, H2SO4	Cast	Starch (Cassava)	4.27	-	-	7.9	0.6	-	-	15.6	0.9
[106]	Sweet potato, H2SO4	Cast	Starch (Cassava)	5.70	-	-	8.6	0.4	-	-	10.8	0.8

R	CNC, Source, Hydrolysis, Modification	Method	Matrix	CNC	Young's Modulus (MPa)		Strain at Break (%)		Strength (MPa)			
				vol%	V	D	V	D	σ_u	σ_y	σ_t	D
[106]	Sweet potato, H2SO4	Cast	Starch (Cassava)	7.14	-	-	10.5	0.4	-	-	5.6	0.5
[107]	Rice, H2SO4	Cast	Starch (Cassava) (2:1 glycerol)	0.00	13	2	-	-	-	-	2.5	0.1
[107]	Rice, H2SO4	Cast	Starch (Cassava) (2:1 glycerol)	1.63	33	6	-	-	-	-	3.3	0.1
[107]	Rice, H2SO4	Cast	Starch (Cassava) (2:1 glycerol)	3.27	36	5	-	-	-	-	3.25	0.08
[107]	Rice, H2SO4	Cast	Starch (Cassava) (2:1 glycerol)	4.93	56	4	-	-	-	-	3.78	0.03
[107]	Rice, H2SO4	Cast	Starch (Cassava) (2:1 glycerol)	6.60	41	5	-	-	-	-	3.57	0.03
[107]	Rice, H2SO4	Cast	Starch (Cassava) (2:1 glycerol)	8.28	40	5	-	-	-	-	3.5	0.2
[108]	Coconut, H2SO4	Cast	Manioc Starch glycerol 4:1	0.00	-	-	26	5	-	-	3.2	0.5
[108]	Coconut, H2SO4	Cast	Manioc Starch glycerol 4:1	7.51	-	-	24	2	-	-	3.7	0.7
[108]	Coconut, H2SO4	Cast	Manioc Starch glycerol 4:1	13.98	-	-	17.5	0.8	-	-	4.4	0.3
[108]	Coconut, H2SO4	Cast	Manioc Starch glycerol 4:1	19.60	-	-	25	3	-	-	3.8	0.9
[108]	Coconut, H2SO4	Cast	Potato Starch 4:1 glycerol	0.00	-	-	31	4	-	-	4.1	0.2
[108]	Coconut, H2SO4	Cast	Potato Starch 4:1 glycerol	7.51	-	-	24	4	-	-	8.2	0.5
[108]	Coconut, H2SO4	Cast	Potato Starch 4:1 glycerol	13.98	-	-	27	4	-	-	5.4	0.2
[108]	Coconut, H2SO4	Cast	Potato Starch 4:1 glycerol	19.60	-	-	30	1	-	-	4.1	0.6
[109]	Cotton, H2SO4	Cast	PMMA	0	1240	60	10.2	0.2	-	-	1240	60
[109]	Cotton, H2SO4	Cast	PMMA	0.38	1270	30	10.6	0.2	-	-	1270	30
[109]	Cotton, H2SO4	Cast	PMMA	0.76	1340	50	10.8	0.3	-	-	1340	50
[109]	Cotton, H2SO4	Cast	PMMA	2.30	1360	80	8.9	0.6	-	-	1360	80
[109]	Cotton, H2SO4	Cast	PMMA	3.86	1300	100	5	0.5	-	-	1300	100
[109]	Cotton, H2SO4, MA-OH	Cast	PMMA	0.38	1300	40	12.7	0.3	-	-	1300	40
[109]	Cotton, H2SO4, MA-OH	Cast	PMMA	0.76	1380	20	14.3	0.4	-	-	1380	20
[109]	Cotton, H2SO4, MA-OH	Cast	PMMA	2.30	1420	50	16.9	0.7	-	-	1420	50

R	CNC, Source, Hydrolysis, Modification	Method	Matrix	CNC	Young's Modulus (MPa)		Strain at Break (%)		Strength (MPa)			
				vol%	V	D	V	D	σ_u	σ_y	σ_t	D
[109]	Cotton, H2SO4, MA-OH	Cast	PMMA	3.86	1490	40	22.3	0.9	-	-	1490	40
[109]	Cotton, H2SO4, MA-OH	Cast	PMMA	0.38	1480	60	11.5	0.7	-	-	1480	60
[109]	Cotton, H2SO4, MA-OH	Cast	PMMA	0.76	1590	30	16.8	0.9	-	-	1590	30
[109]	Cotton, H2SO4, MA-OH	Cast	PMMA	2.30	1450	90	7.3	0.7	-	-	1450	90
[109]	Cotton, H2SO4, MA-OH	Cast	PMMA	3.86	1510	70	9.1	1	-	-	1510	70
[110]	MCC, H2SO4	MM + (Premix TSE)	LLDPE	0	108	13	11	2	-	-	25	4
[110]	MCC, H2SO4	MM + (Premix TSE)	LLDPE	1.86	216	19	8	0	-	-	18	1
[110]	MCC, H2SO4, *1,1*-diethy-*3*-*hydroxyazetidinium chloride*	MM + (Premix TSE)	LLDPE	2.04	211	19	7	0	-	-	14	1
[110]	MCC, H2SO4, *1,10*-diethyl-*3*-*hydroxyazetidinium chloride*	MM + (Premix TSE)	LLDPE	1.68	223	11	7	1	-	-	15	1
[111]	Wood, H2SO4, Toluene Diisocyanate, Maleated PP	Extrusion	PP	0	5200	200	1.5	0.3	-	-	37.4	0.2
[111]	Wood, H2SO4, Toluene Diisocyanate, Maleated PP	Extrusion	PP 1% Maleated PP	0	5220	80	1.5	0.4	-	-	36.5	0.8
[111]	Wood, H2SO4, Toluene Diisocyanate, Maleated PP	Extrusion	PP 3% Maleated PP	0	5200	300	1.2	0.2	-	-	33.8	0.6
[111]	Wood, H2SO4, Toluene Diisocyanate, Maleated PP	Extrusion	PP	0.57	5400	300	1.2	0.1	-	-	33.1	0.5
[111]	Wood, H2SO4, Toluene Diisocyanate, Maleated PP	Extrusion	PP 1% Maleated PP	0.57	5000	300	1.4	0.3	-	-	36.9	0.3
[111]	Wood, H2SO4, Toluene Diisocyanate, Maleated PP	Extrusion	PP 3% Maleated PP	0.57	4800	200	1.2	0.1	-	-	36.2	0.7
[111]	Wood, H2SO4, Toluene Diisocyanate, Maleated PP	Extrusion	PP	2.91	5200	300	1.2	0.2	-	-	33.7	0.4
[111]	Wood, H2SO4, Toluene Diisocyanate, Maleated PP	Extrusion	PP 1% Maleated PP	2.91	4800	100	1.3	0.2	-	-	33.2	0.4
[111]	Wood, H2SO4, Toluene Diisocyanate, Maleated PP	Extrusion	PP 3% Maleated PP	2.91	5000	300	1.2	0.1	-	-	36.6	0.4
[111]	Wood, H2SO4, Toluene Diisocyanate, Maleated PP	Extrusion	PP	5.94	5300	200	1.5	0.4	-	-	33.6	0.5

R	CNC, Source, Hydrolysis, Modification	Method	Matrix	CNC	Young's Modulus (MPa)		Strain at Break (%)		Strength (MPa)			
				vol%	V	D	V	D	σ_u	σ_y	σ_t	D
[111]	Wood, H2SO4, Toluene Diisocyanate, Maleated PP	Extrusion	PP 1% Maleated PP	5.94	4800	300	1	0.1	-	-	33.3	0.7
[111]	Wood, H2SO4, Toluene Diisocyanate, Maleated PP	Extrusion	PP 3% Maleated PP	5.94	4900	400	1.07	0.07	-	-	33.4	0.4
[111]	Wood, H2SO4, Toluene Diisocyanate, Maleated PP	Premix Hot Toluene + Extrusion	PP 1% Maleated PP	0.57	5700	500	1.9	0.4	-	-	30.9	0.5
[111]	Wood, H2SO4, Toluene Diisocyanate, Maleated PP	Premix Hot Toluene + Extrusion	PP 1% Maleated PP	1.73	5800	300	1.6	0.1	-	-	32.1	0.3
[111]	Wood, H2SO4, Toluene Diisocyanate, Maleated PP	Premix Hot Toluene + Extrusion	PP 1% Maleated PP	2.91	6000	600	1.3	0.2	-	-	32.83	0.09
[111]	Wood, H2SO4, Toluene Diisocyanate, Maleated PP	Premix Hot Toluene + Extrusion	PP 1% Maleated PP	5.94	6300	400	1.2	0.2	-	-	32.2	0.6
[111]	Wood, H2SO4, Toluene Diisocyanate, Maleated PP	Premix Hot Toluene + Extrusion	PP 0% Maleated PP	2.91	4800	300	1.2	0.1	-	-	30.1	0.4
[111]	Wood, H2SO4, Toluene Diisocyanate, Maleated PP	Premix Hot Toluene + Extrusion	PP 1% Maleated PP	2.91	6000	700	1.2	0.2	-	-	36.9	0.1
[111]	Wood, H2SO4, Toluene Diisocyanate, Maleated PP	Premix Hot Toluene + Extrusion	PP 3% Maleated PP	2.91	5700	400	1	0.1	-	-	37.6	0.3
[111]	Wood, H2SO4, Toluene Diisocyanate, Maleated PP	Premix Hot Toluene + Extrusion	PP 5% Maleated PP	2.91	6500	400	0.95	0.09	-	-	38.9	0.5
[111]	Wood, H2SO4, Toluene Diisocyanate, Maleated PP	Premix Hot Toluene + Extrusion	PP 7% Maleated PP	2.91	6000	600	0.94	0.06	-	-	37.2	0.4
[112]	kenaf, H2SO4	Cast	κ-carrageenan	0	790	100	-	-	-	-	23	1
[112]	kenaf, H2SO4	Cast	κ-carrageenan	1.88	900	100	-	-	-	-	29	3
[112]	kenaf, H2SO4	Cast	κ-carrageenan	3.76	1340	90	-	-	-	-	39	3
[112]	kenaf, H2SO4	Cast	κ-carrageenan	5.65	1100	100	-	-	-	-	36	4
[112]	kenaf, H2SO4	Cast	κ-carrageenan	7.54	950	100	-	-	-	-	30	3
[113]	Cotton, H2SO4, TEMPO	Cast	PS	0	1900	200	1.9	0.1	22.3	-	-	0.5
[113]	Cotton, H2SO4, TEMPO	Cast	PS	1.99	1300	300	1.4	0.2	24	-	-	1

R	CNC, Source, Hydrolysis, Modification	Method	Matrix	CNC	Young's Modulus (MPa)		Strain at Break (%)		Strength (MPa)			
				vol%	V	D	V	D	σ_u	σ_y	σ_t	D
[113]	Cotton, H2SO4, TEMPO & stearyl trimethyl ammonium chloride	Cast	PS	1.99	3100	300	2.7	0.1	27.1	-	-	0.9
[113]	Cotton, H2SO4, TEMPO & stearyl trimethyl ammonium chloride	Cast	PS	1.99	2600	400	2.5	0.2	30	-	-	1
[113]	Cotton, H2SO4, TEMPO & stearyl trimethyl ammonium chloride	Cast	PS	1.99	2800	200	2.4	0.1	29.6	-	-	0.7
[114]	MCC, H2SO4	Cast	PVP	0	120	-	5.5	-	6.6	-	-	-
[114]	MCC, H2SO4	Cast	PVP	3.47	132	-	7.4	-	9.7	-	-	-
[114]	MCC, H2SO4	Cast	PVP	6.69	413	-	4.2	-	17.2	-	-	-
[114]	MCC, H2SO4	Cast	PVP	14.39	457	-	6.9	-	31.8	-	-	-
[114]	MCC, H2SO4	Cast	PVP	22.24	1284	-	3	-	38.4	-	-	-
[114]	MCC, H2SO4	Cast	PVP	24.37	1755	-	2.5	-	43.8	-	-	-
[114]	MCC, H2SO4	Cast	PVP	34.15	1216	-	2.1	-	25.3	-	-	-
[115]	Cotton, H2SO4	Cast	PEO	2.36	41	-	3.06	-	-	-	0.101	-
[115]	Cotton, H2SO4	Cast	PEO	6.9589	43	-	3.49	-	-	-	0.16	-
[115]	Cotton, H2SO4	Cast	PEO	10.96	57	-	4.88	-	-	-	0.188	-
[115]	Cotton, H2SO4	Cast	PEO	15.06	66	-	4.14	-	-	-	0.218	-
[115]	Cotton, H2SO4	Cast	PEO	20.13	79	-	4.14	-	-	-	0.2	-
[115]	Cotton, H2SO4	Cast	PEO	28.94	101	-	3.61	-	-	-	0.115	-
[115]	Cotton, H2SO4	Cast	PEO	39.18	37	-	4.14	-	-	-	0.097	-
[115]	Cotton, H2SO4	Cast	PEO	49.05	64	-	3.39	-	-	-	0.106	-
[115]	Cotton, H2SO4	Cast	PEO	56.29	45	-	3.72	-	-	-	0.083	-
[116]	Wood, H2SO4, Tannic acid	Cured Hydrogels	PAA	0	0.006	5E-04	500	20	-	-	0.059	0.002
[116]	Wood, H2SO4, Tannic acid	Cured Hydrogels	PAA	0.08	0.032	0.001	1080	40	-	-	0.12	0.003
[116]	Wood, H2SO4, Tannic acid	Cured Hydrogels	PAA	0.23	0.045	0.001	1600	40	-	-	0.186	0.004
[116]	Wood, H2SO4, Tannic acid	Cured Hydrogels	PAA	0.46	0.049	0.002	2950	50	-	-	0.257	0.004
[116]	Wood, H2SO4, Tannic acid	Cured Hydrogels	PAA	0.61	0.05	0.002	2770	50	-	-	0.309	0.004
[116]	Wood, H2SO4, Tannic acid	Cured Hydrogels	PAA	0.76	0.064	0.002	1740	40	-	-	0.347	0.004
[116]	Wood, H2SO4, Tannic acid	Cured Hydrogels	PAA	1.15	0.078	0.002	1570	40	-	-	0.38	0.005
[117]	Cotton, H2SO4, UPy	Cast	LDPE	0	98	6	65	15	-	5.8	-	0.9
[117]	Cotton, H2SO4, UPy	Cast	LDPE	1.46	140	17	26	8	-	7	-	0.5

R	CNC, Source, Hydrolysis, Modification	Method	Matrix	CNC	Young's Modulus (MPa)		Strain at Break (%)		Strength (MPa)			
				vol%	V	D	V	D	σ_u	σ_y	σ_t	D
[117]	Cotton, H2SO4, UPy	Cast	LDPE	2.95	160	20	19	7	-	7.4	-	0.6
[117]	Cotton, H2SO4, UPy	Cast	LDPE	6.03	205	20	13	3	-	7.6	-	0.5
[117]	Cotton, H2SO4, UPy	Cast	LDPE	9.25	232	41	7.5	1.2	-	7.8	-	0.5
[117]	Cotton, H2SO4, UPy	Cast	LLDPE	0	125	15	465	40	-	8.7	-	0.9
[117]	Cotton, H2SO4, UPy	Cast	LLDPE	1.45	135	10	435	65	-	9.5	-	0.2
[117]	Cotton, H2SO4, UPy	Cast	LLDPE	2.93	145	20	445	50	-	9.9	-	0.2
[117]	Cotton, H2SO4, UPy	Cast	LLDPE	6.00	165	5	480	30	-	10	-	0.5
[117]	Cotton, H2SO4, UPy	Cast	LLDPE	9.20	195	10	495	15	-	13	-	0.5
[117]	Cotton, H2SO4, UPy	Cast	PEO-EPI	0	0.7	0.1	265	35	-	0.23	-	0.008
[117]	Cotton, H2SO4, UPy	Cast	PEO-EPI	2.18	1.5	0.4	135	25	-	0.24	-	0.006
[117]	Cotton, H2SO4, UPy	Cast	PEO-EPI	4.37	3	0.8	75	22	-	0.27	-	0.005
[117]	Cotton, H2SO4, UPy	Cast	PEO-EPI	8.80	4.4	0.9	40	13	-	0.28	-	0.009
[117]	Cotton, H2SO4, UPy	Cast	PEO-EPI	13.30	5	1.2	35	8	-	0.34	-	0.11
[118]	Cotton, H2SO4	Premix & RBM	LDPE	0	102	7	77	10	-	-	6.1	0.3
[118]	Cotton, H2SO4	Premix & RBM	LDPE	2.95	125	13	35	10	-	-	7.1	0.5
[118]	Cotton, H2SO4	Premix & RBM	LDPE	6.03	148	15	18	2	-	-	8.1	0.5
[118]	Cotton, H2SO4	Premix & RBM	LDPE	9.25	166	9	13	2	-	-	7.8	0.2
[118]	Cotton, H2SO4	RBM	LDPE	6.03	118	11	16	4	-	-	7.3	0.6
[119]	Tunicin, H2SO4	O/T-SE	LDPE	0	385	35	180	30	-	-	12.1	3.3
[119]	Tunicin, H2SO4	O/T-SE	LDPE	0.6	790	60	52	12	-	-	19.9	2.7
[119]	Tunicin, H2SO4	O/T-SE	LDPE	1.3	850	45	33	5.3	-	-	24.8	3.1
[119]	Tunicin, H2SO4	O/T-SE	LDPE	2.5	900	140	17	4	-	-	22.3	1.9
[119]	Tunicin, H2SO4	O/T-SE	LDPE	3.3	915	50	14	3	-	-	25.9	0.3
[119]	Tunicin, H2SO4	O/T-SE	LDPE	4.7	1174	172	7	0.2	-	-	24.3	2.5
[119]	Tunicin, H2SO4	O/T-SE	LDPE	6.4	1506	70	6.7	0.2	-	-	33.7	3
[119]	Tunicin, H2SO4	O/T-SE	LDPE	7.6	1595	90	5.9	1	-	-	39.5	2.6
[120]	Tunicin, UPy	Cast	t-PEB	0	13	4	51.5	3.6	-	-	1.6	-
[120]	Tunicin, UPy	Cast	t-PEB	5.88	62	5	18.9	0.9	-	-	2.3	0.7
[120]	Tunicin, UPy	Cast	t-PEB	9.03	103	6	8.2	0.5	-	-	3.6	0.1
[120]	Tunicin, UPy	Cast	t-PEB	12.33	158	25	6	1	-	-	4.4	0.5
[121]	Wood, H2SO4	Cast	PEO (35K)	0	220	30	-	-	-	-	-	-
[121]	Wood, H2SO4	Cast	PEO (35K)	0.76	250	40	-	-	-	-	-	-
[121]	Wood, H2SO4	Cast	PEO (35K)	2.67	320	20	-	-	-	-	-	-
[121]	Wood, H2SO4	Cast	PEO (35K)	5.78	360	50	-	-	-	-	-	-
[121]	Wood, H2SO4	Cast	PEO (35K)	7.75	410	30	-	-	-	-	-	-

R	CNC, Source, Hydrolysis, Modification	Method	Matrix	CNC	Young's Modulus (MPa)		Strain at Break (%)		Strength (MPa)			
				vol%	V	D	V	D	σ_u	σ_y	σ_t	D
[121]	Wood, H2SO4	Cast	PEO (100K)	0	248	9	-	-	-	-	-	-
[121]	Wood, H2SO4	Cast	PEO (100K)	0.76	320	6	-	-	-	-	-	-
[121]	Wood, H2SO4	Cast	PEO (100K)	2.67	379	9	-	-	-	-	-	-
[121]	Wood, H2SO4	Cast	PEO (100K)	5.78	400	20	-	-	-	-	-	-
[121]	Wood, H2SO4	Cast	PEO (100K)	7.75	400	30	-	-	-	-	-	-
[122]	Alfa, H2SO4	Cast	κ-carrageenan	0	1520	40	27	4	-	-	48	7
[122]	Alfa, H2SO4	Cast	κ-carrageenan	0.88	1960	70	21	2	-	-	70	18
[122]	Alfa, H2SO4	Cast	κ-carrageenan	2.63	2230	80	18	3	-	-	87	4
[122]	Alfa, H2SO4	Cast	κ-carrageenan	4.40	2710	70	16	3	-	-	99	6
[122]	Alfa, H2SO4	Cast	κ-carrageenan	7.07	3090	70	13	3	-	-	118	5
[123]	MCC, H2SO4	MM TSE	PBS	0	317	4	365	4	-	-	-	-
[123]	MCC, H2SO4, AcO2	MM TSE	PBS	2.27	373	4	-	-	-	-	-	-
[123]	MCC, H2SO4, butyric anhydride	MM TSE	PBS	2.27	434	3	335	3	-	-	-	-
[123]	MCC, H2SO4, caprotic anhydride	MM TSE	PBS	2.27	350	4	-	-	-	-	-	-
[123]	MCC, H2SO4, butyric anhydride	MM TSE	PBS	0.38	382	4	354	4	-	-	-	-
[123]	MCC, H2SO4, butyric anhydride	MM TSE	PBS	0.75	399	11	342	4	-	-	-	-
[123]	MCC, H2SO4, butyric anhydride	MM TSE	PBS	3.79	424	4	309	5	-	-	-	-
[123]	MCC, H2SO4, butyric anhydride	MM TSE	PBS	5.34	347	4	286	4	-	-	-	-
[124]	Cotton, H2SO4	MM	HDPE	0	1130	90	11	1	-	-	20.1	0.3
[124]	Cotton, H2SO4	MM	HDPE	0.30	1230	20	6.5	1	-	-	21.1	0.3
[124]	Cotton, H2SO4	MM	HDPE	0.91	1260	20	5	1	-	-	21.5	0.5
[124]	Cotton, H2SO4	MM	HDPE	1.52	1220	40	4.6	0.5	-	-	20.1	0.6
[124]	Cotton, H2SO4	MM	HDPE	3.06	1210	20	4.1	0.9	-	-	20	0.5
[124]	Cotton H2SO4 PEO CMPTBLZR	MM	HDPE	0.30	1470	30	9.2	0.1	-	-	23.8	0.5
[124]	Cotton H2SO4 PEO CMPTBLZR	MM	HDPE	0.91	1520	50	8.4	0.4	-	-	24.8	0.5
[124]	Cotton H2SO4 PEO CMPTBLZR	MM	HDPE	1.52	1440	30	7.8	0.1	-	-	23.9	0.4
[124]	Cotton H2SO4 PEO CMPTBLZR	MM	HDPE	3.06	1310	30	7.4	0.5	-	-	22	1
[125]	Wood, H2SO4	P-RXN	PBS	0	690	30	230	20	-	-	42.1	0.7
[125]	Wood, H2SO4	P-RXN	PBS	0.075	680	20	450	20	-	-	66	2
[125]	Wood, H2SO4	P-RXN	PBS	0.225	751	9	275	1	-	-	61.1	0.7
[125]	Wood, H2SO4	P-RXN	PBS	0.376	830	10	360	20	-	-	54	1

R	CNC, Source, Hydrolysis, Modification	Method	Matrix	CNC	Young's Modulus (MPa)		Strain at Break (%)		Strength (MPa)			
				vol%	V	D	V	D	σ_u	σ_y	σ_t	D
[125]	Wood, H2SO4	P-RXN	PBS	0.752	900	20	8	1	-	-	41	1
[126]	MCC, H2SO4	Cast (slow)	PEO	87.19	5500	500	1.8	0.4	-	-	48	8
[126]	MCC, H2SO4	Cast (slow)	PEO	75.16	3900	900	2.3	0.6	-	-	20	4
[126]	MCC, H2SO4	Cast (slow)	PEO	63.83	2000	400	2.5	0.6	-	-	10	4
[126]	MCC, H2SO4	Cast (slow)	PEO	53.15	2800	600	1.9	0.5	-	-	16	6
[127]	Wood, H2SO4	TSE	PBAT with graft MA	0	50	2	164	9	-	-	16.1	0.3
[127]	Wood, H2SO4	TSE	PBAT with graft MA	0.63	57	2	157	6	-	-	16.3	0.3
[127]	Wood, H2SO4	TSE	PBAT with graft MA	1.90	76.1	0.5	100	20	-	-	17.4	0.1
[127]	Wood, H2SO4	TSE	PBAT with graft MA	3.84	86	1	88	3	-	-	18.6	0.2
[127]	Wood, H2SO4	TSE	PBAT with graft MA	5.82	108	5	80	4	-	-	19.7	0.4
[128]	abaca plant H2SO4	Sonicated in PEGDA/H2O & Printed	PEGDA	0	25	1	2.3	0.8	-	-	26	1
[128]	abaca plant H2SO4	Sonicated in PEGDA/H2O & Printed	PEGDA	0.21	26.8	0.9	4.8	1	-	-	26.6	0.7
[128]	abaca plant H2SO4	Sonicated in PEGDA/H2O & Printed	PEGDA	0.35	27	1	1.9	0.8	-	-	28	1
[128]	abaca plant H2SO4	Sonicated in PEGDA/H2O & Printed	PEGDA	0.63	26.8	0.8	1.7	0.5	-	-	26	0.6
[128]	abaca plant H2SO4	Sonicated in PEGDA/H2O & Printed	PEGDA	0.84	26	2	3.2	1	-	-	26	2
[129]	Unknown	Pre-polymer mix & 3-D Printing	PMMA (uncured)	0	670	20	10	1	-	-	36.1	0.5
[129]	unknown	Pre-polymer mix & 3-D Printing	PMMA (uncured)	0.08	670	10	9	2	-	-	36.3	0.3
[129]	unknown	Pre-polymer mix & 3-D Printing	PMMA (uncured)	0.38	670	20	8	2	-	-	35.8	0.2
[129]	unknown	Pre-polymer mix & 3-D Printing	PMMA (uncured)	0.75	630	20	4.7	0.5	-	-	33	0.4
[129]	unknown	Pre-polymer mix & 3-D Printing	PMMA (cured)	0	1180	40	2.9	0.3	-	-	79	3
[129]	unknown	Pre-polymer mix & 3-D Printing	PMMA (cured)	0.075	1260	50	3.05	0.09	-	-	85	1

R	CNC, Source, Hydrolysis, Modification	Method	Matrix	CNC	Young's Modulus (MPa)		Strain at Break (%)		Strength (MPa)			
				vol%	V	D	V	D	σ_u	σ_y	σ_t	D
[129]	unknown	Pre-polymer mix & 3-D Printing	PMMA (cured)	0.38	1260	10	2.8	0.1	-	-	94.5	0.5
[129]	unknown	Pre-polymer mix & 3-D Printing	PMMA (cured)	0.75	1230	20	2.4	0.2	-	-	67	2
[130]	Cotton, H2SO4	Cast	PSU	0	700	200	-	-	-	-	-	-
[130]	Cotton, H2SO4	Cast	PSU	0.39	700	400	-	-	-	-	-	-
[130]	Cotton, H2SO4	Cast	PSU	0.78	1000	300	-	-	-	-	-	-
[130]	Cotton, H2SO4	Cast	PSU	3.13	1600	500	-	-	-	-	-	-
[130]	Cotton, H2SO4	Cast	PSU	5.51	1900	300	-	-	-	-	-	-
[130]	Cotton, H2SO4	Cast	PSU	8.74	800	200	-	-	-	-	-	-
[131]	Wood, H2SO4	MM	PCL	0	186	9	-	-	-	16.5	-	0.3
[131]	Wood, H2SO4	MM	PCL	0.36	190	10	-	-	-	17.2	-	0.7
[131]	Wood, H2SO4	MM	PCL	0.72	200	10	-	-	-	18	-	1
[131]	Wood, H2SO4	MM	PCL	3.65	220	10	-	-	-	16	-	1
[131]	Wood, H2SO4	MM & Foaming	PCL	0	100	10	-	-	-	7.1	-	0.5
[131]	Wood, H2SO4	MM & Foaming	PCL	0.36	120	20	-	-	-	7.4	-	0.7
[131]	Wood, H2SO4	MM & Foaming	PCL	0.72	130	10	-	-	-	8.5	-	0.8
[131]	Wood, H2SO4	MM & Foaming	PCL	3.65	170	20	-	-	-	12	-	1
[132]	Cotton H2SO4	cast pre-polymer low X-linking	PSA-co-PDM	0.63	2.1	0.5	150	30	2.3	2.3	-	0.02
[132]	Cotton H2SO4	cast pre-polymer low X-linking	PSA-co-PDM	3.18	3	0.3	170	20	4.6	4.6	-	0.6
[132]	Cotton H2SO4	cast pre-polymer low X-linking	PSA-co-PDM	6.49	6	0.7	120	20	5.6	5.6	-	0.4
[132]	Cotton H2SO4	cast pre-polymer high X-linking	PSA-co-PDM	0	54	3	41	7	7	7.0	-	0.6
[132]	Cotton H2SO4	cast pre-polymer high X-linking	PSA-co-PDM	0.63	55	2	94	14	13.2	13.2	-	2
[132]	Cotton H2SO4	cast pre-polymer high X-linking	PSA-co-PDM	3.18	130	20	80	10	20.1	20.1	-	3
[132]	Cotton H2SO4	cast pre-polymer high X-linking	PSA-co-PDM	6.49	100	10	37	6	19.4	19.4	-	2
[133]	Kenaf H2SO4	Solution Cast	κ-carrageenan	0	800	100	19.4	0.6	-	-	23	2
[133]	Kenaf H2SO4	Solution Cast	κ-carrageenan	1.75	900	100	18.3	0.7	-	-	29	3

R	CNC, Source, Hydrolysis, Modification	Method	Matrix	CNC	Young's Modulus (MPa)		Strain at Break (%)		Strength (MPa)			
				vol%	V	D	V	D	σ_u	σ_y	σ_t	D
[133]	Kenaf H2SO4	Solution Cast	κ-carrageenan	3.52	100	100	17.1	0.6	-	-	37	2
[133]	Kenaf H2SO4	Solution Cast	kappa-carrageenan	5.29	1110	90	19.6	0.7	-	-	35	3
[133]	Kenaf H2SO4	Solution Cast	κ-carrageenan	7.07	950	80	17	0.6	-	-	30	3
[134]	Kenaf H2SO4	Cast (styrene) & Curing	UPR	0	820	50	-	-	-	-	30	4
[134]	Kenaf H2SO4	Cast (styrene) & Curing	UPR	1.51	840	10	-	-	-	-	31	4
[134]	Kenaf H2SO4	Cast (styrene) & Curing	UPR	3.03	790	40	-	-	-	-	35	1
[134]	Kenaf, H2SO4, N-(baminoethyl)-g-aminopropyltrimethoxysilane	Cast (styrene) & Curing	UPR	4.57	740	30	-	-	-	-	27	2
[134]	Kenaf, H2SO4, N-(baminoethyl)-g-aminopropyltrimethoxysilane	Cast (styrene) & Curing	UPR	1.51	900	30	-	-	-	-	38	2
[134]	Kenaf, H2SO4, N-(baminoethyl)-g-aminopropyltrimethoxysilane	Cast (styrene) & Curing	UPR	3.03	900	30	-	-	-	-	36	4
[134]	Kenaf, H2SO4, N-(baminoethyl)-g-aminopropyltrimethoxysilane	Cast (styrene) & Curing	UPR	4.57	800	20	-	-	-	-	29	4
[135]	Cotton, H2SO4, carbon black to CNC 2:1	Coagulation with H2SO4	Natural Rubber Latex	2.7	4	1	510	50	-	-	2.1	0.1
[135]	Cotton, H2SO4, carbon black to CNC 2:2	Coagulation with H2SO4	Natural Rubber Latex	5.3	6	1	570	50	-	-	3.6	0.2
[135]	Cotton, H2SO4, carbon black to CNC 2:3	Coagulation with H2SO4	Natural Rubber Latex	8	17	9	450	70	-	-	5.1	0.7
[135]	Cotton, H2SO4, carbon black to CNC 2:4	Coagulation with H2SO4	Natural Rubber Latex	11	23	9	440	60	-	-	7.4	0.6
[135]	Cotton, H2SO4, carbon black to CNC 2:5	Coagulation with H2SO4	Natural Rubber Latex	16	100	20	150	50	-	-	6	1
[136]	Unknown	MM	PP	0	1040	60	610	60	-	-	28	3
[136]	Wood, H2SO4	MM	PP	2.91	1170	80	22	4	-	-	27	1
[136]	Wood, H2SO4	MM CMPTBLZR 15wt% added	PP	0	1310	30	200	100	-	-	24	1
[136]	Premixed 3:1 ratio CMPTBLZR:CNC	MM	PP	2.91	1400	60	30	10	-	-	23	1

R	CNC, Source, Hydrolysis, Modification	Method	Matrix	CNC	Young's Modulus (MPa)		Strain at Break (%)		Strength (MPa)			
				vol%	V	D	V	D	σ_u	σ_y	σ_t	D
[136]	Premixed 3:1 ratio solution mixed CMPTBLZR:CNC	MM	PP	2.91	1530	30	35	6	-	-	28.5	0.7
[137]	Wood, H2SO4	Pulverizing & MM	LDPE	0	160	5	500	30	-	-	10	0.3
[137]	Wood, H2SO4	Pulverizing & MM	LDPE	6.00	270	10	460	30	-	-	13	1
[137]	Wood, H2SO4	Pulverizing & MM	PP	0	910	50	740	40	-	-	32.0	0.7
[137]	Wood, H2SO4	Pulverizing & MM	PP	5.91	1830	70	12	3	-	-	38	1
[138]	Cotton H2SO4	E-Spun	PS	0	-	-	60	5	-	-	0.15	0.05
[138]	Cotton H2SO4	E-Spun	PS	0.66	-	-	56	4	-	-	0.18	0.04
[138]	Cotton H2SO4	E-Spun	PS	1.99	-	-	15	6	-	-	0.27	0.06
[138]	Cotton H2SO4	E-Spun	PS	3.34	-	-	29	3	-	-	0.30	0.03
[138]	Cotton H2SO4	E-Spun	PS	4.71	-	-	25	3	-	-	0.40	0.02
[139]	Cotton H2SO4	Cast	PEG	75	560	90	2.3	0.2	-	-	13	2
[139]	Cotton H2SO4	Cast	PEG	63.64	500	100	2.6	0.2	-	-	13	2
[139]	Cotton H2SO4	Cast	PEG	52.94	200	100	4	0.2	-	-	9	1
[139]	Cotton H2SO4	Cast	PEG	42.86	200	200	4.6	0.5	-	-	11	3
[140]	Corn, H2SO4	E-Spun Mats	PVP (40:360k) (1:1)	0	N.R	N.R	9.1	0.2	2.3	-	-	0.2
[140]	Corn, H2SO4	E-Spun Mats	PVP (40:360k) (1:1)	1.57	N.R	N.R	2.7	0.2	2.9	-	-	0.2
[140]	Corn, H2SO4	E-Spun Mats	PVP (40:360k) (1:1)	3.15	N.R	N.R	3.25	0.2	3.1	-	-	0.1
[140]	Corn H2SO4 AgNO3 (0.34%)	E-Spun Mats	PVP (40:360k) (1:1)	3.15	N.R	N.R	2.5	0.3	2.8	-	-	0.3
[141]	Wood H2SO4	MM	PP	0	180	60	40	6	-	20	-	4
[141]	Wood H2SO4	MM	PP	1.73	320	50	15	4	-	14	-	1
[141]	Wood, H2SO4, Quaternary Ammonium Salt	MM	PP	0.57	200	20	330	20	-	14	-	2
[141]	Wood, H2SO4, Quaternary Ammonium Salt	MM	PP	1.73	230	40	110	30	-	13	-	2
[141]	Wood, H2SO4, Quaternary Ammonium Salt	MM	PP	3.50	230	60	350	20	-	14	-	2
[141]	Wood, H2SO4, Quaternary Ammonium Salt	MM	PP	5.94	280	60	12	7	-	7.7	-	0.9
[142]	Cotton H2SO4	MM	PBAT	0	38.9	-	927	-	11	6	-	-
[142]	Cotton H2SO4	MM	PBAT	0.39	104	-	505	-	9.2	6.9	-	-
[142]	Cotton H2SO4	MM	PBAT	0.79	93.5	-	416	-	9	6.4	-	-
[142]	Cotton H2SO4	MM	PBAT	1.19	95.3	-	415	-	8.8	6.5	-	-
[142]	Cotton H2SO4	MM	PBAT	1.58	99.6	-	348	-	8.5	6.4	-	-

R	CNC, Source, Hydrolysis, Modification	Method	Matrix	CNC	Young's Modulus (MPa)		Strain at Break (%)		Strength (MPa)			
				vol%	V	D	V	D	σ_u	σ_y	σ_t	D
[142]	Cotton H2SO4, AcO2	MM	PBAT	0.39	120	-	558	-	9.7	6.9	-	-
[142]	Cotton H2SO4, AcO2	MM	PBAT	0.79	113	-	446	-	9	6.9	-	-
[142]	Cotton H2SO4, AcO2	MM	PBAT	1.19	105	-	375	-	8.6	6.9	-	-
[142]	Cotton H2SO4, AcO2	MM	PBAT	1.58	94.2	-	312	-	8.3	6.9	-	-

References

1. Moon, R. J.; Martini, A.; Nairn, J.; Simonsen, J.; Youngblood, J., Cellulose nanomaterials review: structure, properties and nanocomposites. *Chemical Society Reviews* **2011,** *40* (7), 3941-3994.
2. Mark, J. E., *Polymer Data Handbook*. Oxford University Press: 2009.
3. Wypych, G., Handbook of Polymers (2nd Edition). ChemTec Publishing: 2016.
4. Chen, D.; Lawton, D.; Thompson, M. R.; Liu, Q., Biocomposites reinforced with cellulose nanocrystals derived from potato peel waste. *Carbohydrate Polymers* **2012,** *90* (1), 709-716.
5. Pakzad, A.; Simonsen, J.; Yassar, R. S., Elastic properties of thin poly(vinyl alcohol)-cellulose nanocrystal membranes. *Nanotechnology* **2012,** *23* (8).
6. Lee, J.; Deng, Y. L., Increased mechanical properties of aligned and isotropic electrospun PVA nanofiber webs by cellulose nanowhisker reinforcement. *Macromolecular Research* **2012,** *20* (1), 76-83.
7. Mathew, A. P.; Gong, G.; Bjorngrim, N.; Wixe, D.; Oksman, K., Moisture Absorption Behavior and Its Impact on the Mechanical Properties of Cellulose Whiskers-Based Polyvinylacetate Nanocomposites. *Polymer Engineering and Science* **2011,** *51* (11), 2136-2142.
8. Fortunati, E.; Luzi, F.; Puglia, D.; Terenzi, A.; Vercellino, M.; Visai, L.; Santulli, C.; Torre, L.; Kenny, J. M., Ternary PVA nanocomposites containing cellulose nanocrystals from different sources and silver particles: Part II. *Carbohydrate Polymers* **2013,** *97* (2), 837-848.
9. Montes, S.; Carrasco, P. M.; Ruiz, V.; Cabanero, G.; Grande, H. J.; Labidi, J.; Odriozola, I., Synergistic reinforcement of poly(vinyl alcohol) nanocomposites with cellulose nanocrystal-stabilized graphene. *Composites Science and Technology* **2015,** *117*, 26-31.
10. Zhao, X. J.; Zheng, H. Z.; Qu, D.; Jiang, H. J.; Fan, W.; Sun, Y. Y.; Xu, Y., A supramolecular approach towards strong and tough polymer nanocomposite fibers. *Rsc Advances* **2018,** *8* (19), 10361-10366.
11. Tanpichai, S.; Oksman, K., Crosslinked poly(vinyl alcohol) composite films with cellulose nanocrystals: Mechanical and thermal properties. *Journal of Applied Polymer Science* **2018,** *135* (3), 11.

12. Singh, S.; Gaikwad, K. K.; Lee, Y. S., Antimicrobial and antioxidant properties of polyvinyl alcohol bio composite films containing seaweed extracted cellulose nano-crystal and basil leaves extract. *International Journal of Biological Macromolecules* **2018,** *107*, 1879-1887.
13. Shrestha, S.; Montes, F.; Schueneman, G. T.; Snyder, J. F.; Youngblood, J. P., Effects of aspect ratio and crystal orientation of cellulose nanocrystals on properties of poly(vinyl alcohol) composite fibers. *Composites Science and Technology* **2018,** *167*, 482-488.
14. Risnasari, I.; Febrianto, F.; Wistara, N. J.; Sadiyo, S.; Nikmatin, S.; Teramoto, Y.; Lee, S. H.; Jang, J. H.; Hidayat, W.; Kim, N. H., Characterization of cellulose nanocrystal with cellulose II polymorph from primary sludge and its application to PVA nanocomposites. *Wood Sci. Technol.* **2018,** *52* (2), 555-565.
15. El Achaby, M.; Kassab, Z.; Aboulkas, A.; Gaillard, C.; Barakat, A., Reuse of red algae waste for the production of cellulose nanocrystals and its application in polymer nanocomposites. *International Journal of Biological Macromolecules* **2018,** *106*, 681-691.
16. Jahan, Z.; Niazi, M. B. K.; Gregersen, O. W., Mechanical, thermal and swelling properties of cellulose nanocrystals/PVA nanocomposites membranes. *J. Ind. Eng. Chem.* **2018,** *57*, 113-124.
17. Lu, Y.; Huang, J.; Ge, L. L.; Xie, W. Y.; Wu, D. F., Selective localization of cellulose nanocrystals in the biodegradable poly (vinyl alcohol)/poly(epsilon-caprolactone) blend composites prepared by Pickering emulsions. *Polymer* **2018,** *156*, 136-147.
18. Liu, Y. Y.; Liu, D. Y.; Sui, G. X., Effects of Cellulose Nanowhiskers on the Properties of Poly(Vinyl Alcohol)/Graphene Nanoplatelets Nanocomposites. *Polymer Composites* **2017,** *38*, E98-E107.
19. Lam, N. T.; Saewong, W.; Sukyai, P., Effect of varying hydrolysis time on extraction of spherical bacterial cellulose nanocrystals as a reinforcing agent for poly(vinyl alcohol) composites. *Journal of Polymer Research* **2017,** *24* (5).
20. Cao, X. D.; Habibi, Y.; Lucia, L. A., One-pot polymerization, surface grafting, and processing of waterborne polyurethane-cellulose nanocrystal nanocomposites. *Journal of Materials Chemistry* **2009,** *19* (38), 7137-7145.
21. Gao, Z. Z.; Peng, J.; Zhong, T. H.; Sun, J.; Wang, X. B.; Yue, C., Biocompatible elastomer of waterborne polyurethane based on castor oil and polyethylene glycol with cellulose nanocrystals. *Carbohydrate Polymers* **2012,** *87* (3), 2068-2075.
22. Pei, A. H.; Malho, J. M.; Ruokolainen, J.; Zhou, Q.; Berglund, L. A., Strong Nanocomposite Reinforcement Effects in Polyurethane Elastomer with Low Volume Fraction of Cellulose Nanocrystals. *Macromolecules* **2011,** *44* (11), 4422-4427.
23. Saralegi, A.; Rueda, L.; Martin, L.; Arbelaiz, A.; Eceiza, A.; Corcuera, M. A., From elastomeric to rigid polyurethane/cellulose nanocrystal bionanocomposites. *Composites Science and Technology* **2013,** *88*, 39-47.
24. Zhao, Q.; Sun, G.; Yan, K. L.; Zhou, A. J.; Chen, Y. X., Novel bio-antifelting agent based on waterborne polyurethane and cellulose nanocrystals. *Carbohydrate Polymers* **2013,** *91* (1), 169-174.
25. Park, S. H.; Oh, K. W.; Kim, S. H., Reinforcement effect of cellulose nanowhisker on bio-based polyurethane. *Composites Science and Technology* **2013,** *86*, 82-88.

26. Lin, S.; Huang, J.; Chang, P. R.; Wei, S. W.; Xu, Y. X.; Zhang, Q. X., Structure and mechanical properties of new biomass-based nanocomposite: Castor oil-based polyurethane reinforced with acetylated cellulose nanocrystal. *Carbohydrate Polymers* **2013,** *95* (1), 91-99.
27. Wu, G. M.; Liu, D.; Liu, G. F.; Chen, J.; Huo, S. P.; Kong, Z. W., Thermoset nanocomposites from waterborne bio-based epoxy resin and cellulose nanowhiskers. *Carbohydrate Polymers* **2015,** *127*, 229-235.
28. Girouard, N. M.; Xu, S. H.; Schueneman, G. T.; Shofner, M. L.; Meredith, J. C., Site-Selective Modification of Cellulose Nanocrystals with Isophorone Diisocyanate and Formation of Polyurethane-CNC Composites. *Acs Applied Materials & Interfaces* **2016,** *8* (2), 1458-1467.
29. Buffa, J. M.; Mondragon, G.; Corcuera, M. A.; Eceiza, A.; Mucci, V.; Aranguren, M. I., Physical and mechanical properties of a vegetable oil based nanocomposite. *European Polymer Journal* **2018,** *98*, 116-124.
30. Prataviera, R.; Pollet, E.; Bretas, R. E. S.; Avérous, L.; Lucas, A. A., Nanocomposites based on renewable thermoplastic polyurethane and chemically modified cellulose nanocrystals with improved mechanical properties. *Journal of Applied Polymer Science* **2018,** *135* (45), 46736.
31. Nicharat, A.; Shirole, A.; Foster, E. J.; Weder, C., Thermally activated shape memory behavior of melt-mixed polyurethane/cellulose nanocrystal composites. *Journal of Applied Polymer Science* **2017,** *134* (27), 45033.
32. Furtak-Wrona, K.; Kozik-Ostrowka, P.; Jadwiszczak, K.; Maigret, J. E.; Aguie-Beghin, V.; Coqueret, X., Polyurethane acrylate networks including cellulose nanocrystals: a comparison between UV and EB- curing. *Radiation Physics and Chemistry* **2018,** *142*, 94-99.
33. Kong, X. H.; Wolodko, J.; Zhao, L. Y.; Curtis, J. M., The preparation and characterization of polyurethane reinforced with a low fraction of cellulose nanocrystals. *Progress in Organic Coatings* **2018,** *125*, 207-214.
34. Mondragon, G.; Santamaria-Echart, A.; Hormaiztegui, M. E. V.; Arbelaiz, A.; Pena-Rodriguez, C.; Mucci, V.; Corcuera, M.; Aranguren, M. I.; Eceiza, A., Nanocomposites of Waterborne Polyurethane Reinforced with Cellulose Nanocrystals from Sisal Fibres. *J. Polym. Environ.* **2018,** *26* (5), 1869-1880.
35. Mucci, V. L.; Ivdre, A.; Buffa, J. M.; Cabulis, U.; Stefani, P. M.; Aranguren, M. I., Composites made from a soybean oil biopolyurethane and cellulose nanocrystals. *Polymer Engineering and Science* **2018,** *58* (2), 125-132.
36. Yuwawech, K.; Wootthikanokkhan, J.; Wanwong, S.; Tanpichai, S., Polyurethane/esterified cellulose nanocrystal composites as a transparent moisture barrier coating for encapsulation of dye sensitized solar cells. *Journal of Applied Polymer Science* **2017,** *134* (45).
37. Hu, Z. J.; Fu, S. Y.; Tang, A. M., Fabrication of Light-triggered AuNP/CNC/SMP Nano-Composites. *Bioresources* **2017,** *12* (1), 1982-1990.
38. Gu, J.; Catchmark, J. M., Polylactic acid composites incorporating casein functionalized cellulose nanowhiskers. *J. Biol. Eng.* **2013,** *7* (1), 10.
39. Hong, J.; Kim, D. S., Preparation and physical properties of polylactide/cellulose nanowhisker/nanoclay composites. *Polymer Composites* **2013,** *34* (2), 293-298.

40. Lee, J. H.; Park, S. H.; Kim, S. H., Preparation of cellulose nanowhiskers and their reinforcing effect in polylactide. *Macromolecular Research* **2013,** *21* (11), 1218-1225.
41. Lee, J. H.; Park, S. H.; Kim, S. H., Surface Modification of Cellulose Nanowhiskers and Their Reinforcing Effect in Polylactide. *Macromolecular Research* **2014,** *22* (4), 424-430.
42. Luo, H. L.; Xiong, G. Y.; Li, Q. P.; Ma, C. Y.; Zhu, Y.; Guo, R. S.; Wan, Y. Z., Preparation and properties of a novel porous poly(lactic acid) composite reinforced with bacterial cellulose nanowhiskers. *Fibers and Polymers* **2014,** *15* (12), 2591-2596.
43. Dhar, P.; Kumar, A.; Katiyar, V., Magnetic Cellulose Nanocrystal Based Anisotropic Polylactic Acid Nanocomposite Films: Influence on Electrical, Magnetic, Thermal, and Mechanical Properties. *Acs Applied Materials & Interfaces* **2016,** *8* (28), 18393-18409.
44. Dhar, P.; Tarafder, D.; Kumar, A.; Katiyar, V., Thermally recyclable polylactic acid/cellulose nanocrystal films through reactive extrusion process. *Polymer* **2016,** *87*, 268-282.
45. Ma, P. M.; Jiang, L.; Yu, M. M.; Dong, W. F.; Chen, M. Q., Green Antibacterial Nanocomposites from Poly(lactide)/Poly(butylene adipate-co-terephthalate)/Nanocrystal Cellulose Silver Nanohybrids. *Acs Sustainable Chemistry & Engineering* **2016,** *4* (12), 6417-6426.
46. Zhang, X. Z.; Zhang, Y., Reinforcement effect of poly(butylene succinate) (PBS)-grafted cellulose nanocrystal on toughened PBS/polylactic acid blends. *Carbohydrate Polymers* **2016,** *140*, 374-382.
47. Dhar, P.; Kumar, M. R.; Bhasney, S. M.; Bhagabati, P.; Kumar, A.; Katiyar, V., Sustainable Approach for Mechanical Recycling of Poly(lactic acid)/Cellulose Nanocrystal Films: Investigations on Structure-Property Relationship and Underlying Mechanism. *Ind. Eng. Chem. Res.* **2018,** *57* (43), 14493-14508.
48. Brown, E.; Abdelwahab, M.; Valerio, O.; Misra, M.; Mohanty, A. K., In Situ Cellulose Nanocrystal-Reinforced Glycerol-Based Biopolyester for Enhancing Poly(lactic acid) Biocomposites. *ACS Omega* **2018,** *3* (4), 3857-3867.
49. Yin, Y. Y.; Zhao, L. N.; Jiang, X.; Wang, H. B.; Gao, W. D., Cellulose nanocrystals modified with a triazine derivative and their reinforcement of poly(lactic acid)-based bionanocomposites. *Cellulose* **2018,** *25* (5), 2965-2976.
50. Wei, L. Q.; Agarwal, U. P.; Matuana, L.; Sabo, R. C.; Stark, N. M., Performance of high lignin content cellulose nanocrystals in poly(lactic acid). *Polymer* **2018,** *135*, 305-313.
51. Shakouri, Z.; Nazockdast, H., Microstructural development and mechanical performance of PLA/TPU blends containing geometrically different cellulose nanocrystals. *Cellulose* **2018,** *25* (12), 7167-7188.
52. Qian, S. P.; Zhang, H. H.; Yao, W. C.; Sheng, K. C., Effects of bamboo cellulose nanowhisker content on the morphology, crystallization, mechanical, and thermal properties of PLA matrix biocomposites. *Compos. Pt. B-Eng.* **2018,** *133*, 203-209.
53. Orellana, J. L.; Wichhart, D.; Kitchens, C. L., Mechanical and Optical Properties of Polylactic Acid Films Containing Surfactant-Modified Cellulose Nanocrystals. *J. Nanomater.* **2018**, 12.

54. Muiruri, J. K.; Liu, S. L.; Teo, W. S.; Kong, J. H.; He, C. B., Highly Biodegradable and Tough Polylactic Acid-Cellulose Nanocrystal Composite. *Acs Sustainable Chemistry & Engineering* **2017,** *5* (5), 3929-3937.
55. Mariano, M.; Pilate, F.; de Oliveira, F. B.; Khelifa, F.; Dubois, P.; Raquez, J. M.; Dufresne, A., Preparation of Cellulose Nanocrystal-Reinforced Poly(lactic acid) Nanocomposites through Noncovalent Modification with PLLA-Based Surfactants. *ACS Omega* **2017,** *2* (6), 2678-2688.
56. Jalvo, B.; Mathew, A. P.; Rosal, R., Coaxial poly(lactic acid) electrospun composite membranes incorporating cellulose and chitin nanocrystals. *Journal of Membrane Science* **2017,** *544*, 261-271.
57. Xu, W. N.; Qin, Z. Y.; Yu, H. Y.; Liu, Y. N.; Liu, N.; Zhou, Z.; Chen, L., Cellulose nanocrystals as organic nanofillers for transparent polycarbonate films. *Journal of Nanoparticle Research* **2013,** *15* (4), 8.
58. Xu, S. H.; Girouard, N.; Schueneman, G.; Shofner, M. L.; Meredith, J. C., Mechanical and thermal properties of waterborne epoxy composites containing cellulose nanocrystals. *Polymer* **2013,** *54* (24), 6589-6598.
59. Peng, S. X.; Moon, R. J.; Youngblood, J. P., Design and characterization of cellulose nanocrystal-enhanced epoxy hardeners. *Green Mater.* **2014,** *2* (4), 193-205.
60. Emami, Z.; Meng, Q. K.; Pircheraghi, G.; Manas-Zloczower, I., Use of surfactants in cellulose nanowhisker/epoxy nanocomposites: effect on filler dispersion and system properties. *Cellulose* **2015,** *22* (5), 3161-3176.
61. Girouard, N.; Schueneman, G. T.; Shofner, M. L.; Meredith, J. C., Exploiting colloidal interfaces to increase dispersion, performance, and pot-life in cellulose nanocrystal/waterborne epoxy composites. *Polymer* **2015,** *68*, 111-121.
62. Fox, D. M.; Kaufman, N.; Woodcock, J.; Davis, C. S.; Gilman, J. W.; Shields, J. R.; Davis, R. D.; Matko, S.; Zammarano, M., *Epoxy Composites Using Wood Pulp Components as Fillers*. Intech Europe: Rijeka, 2016; p 199-215.
63. Lu, P.; Hsieh, Y. L., Cellulose nanocrystal-filled poly(acrylic acid) nanocomposite fibrous membranes. *Nanotechnology* **2009,** *20* (41), 9.
64. Jiang, L.; Morelius, E.; Zhang, J. W.; Wolcott, M.; Holbery, J., Study of the Poly(3-hydroxybutyrate-co-3-hydroxyvalerate)/Cellulose Nanowhisker Composites Prepared by Solution Casting and Melt Processing. *J. Compos Mater.* **2008,** *42* (24), 2629-2645.
65. Zhang, H.; Yu, H. Y.; Wang, C.; Yao, J. M., Effect of silver contents in cellulose nanocrystal/silver nanohybrids on PHBV crystallization and property improvements. *Carbohydrate Polymers* **2017,** *173*, 7-16.
66. Wei, Y. C.; Shang, Y. B.; Ni, C. J.; Zhang, H. Y.; Li, X. B.; Liu, B. J.; Men, Y. F.; Zhang, M. Y.; Hu, W., Modified nanocrystal cellulose/fluorene-containing sulfonated poly(ether ether ketone ketone) composites for proton exchange membranes. *Applied Surface Science* **2017,** *416*, 996-1006.
67. Sonseca, A.; Menes, O.; Gimenez, E., A comparative study of the mechanical, shape-memory, and degradation properties of poly(lactic acid) nanofiber and cellulose nanocrystal reinforced poly(mannitol sebacate) nanocomposites. *Rsc Advances* **2017,** *7* (35), 21869-21882.
68. Peng, S. X.; Shrestha, S.; Youngblood, J. P., Crystal structure transformation and induction of shear banding in Polyamide 11 by surface modified Cellulose Nanocrystals. *Polymer* **2017,** *114*, 88-102.

69. Abdalkarim, S. Y. H.; Yu, H. Y.; Wang, D. C.; Yao, J. M., Electrospun poly(3-hydroxybutyrate-co-3-hydroxy-valerate)/cellulose reinforced nanofibrous membranes with ZnO nanocrystals for antibacterial wound dressings. *Cellulose* **2017,** *24* (7), 2925-2938.
70. Yang, J.; Han, C. R., Mechanically Viscoelastic Properties of Cellulose Nanocrystals Skeleton Reinforced Hierarchical Composite Hydrogels. *Acs Applied Materials & Interfaces* **2016,** *8* (38), 25621-25630.
71. Yu, H. Y.; Yao, J. M., Reinforcing properties of bacterial polyester with different cellulose nanocrystals via modulating hydrogen bonds. *Composites Science and Technology* **2016,** *136*, 53-60.
72. Chang, H. B.; Chien, A. T.; Liu, H. C.; Wang, P. H.; Newcomb, B. A.; Kumar, S., Gel Spinning of Polyacrylonitrile/Cellulose Nanocrystal Composite Fibers. *ACS Biomater. Sci. Eng.* **2015,** *1* (7), 610-616.
73. Ma, L. B.; Zhang, Y.; Meng, Y. J.; Anusonti-Inthra, P.; Wang, S. Q., Preparing cellulose nanocrystal/acrylonitrile-butadiene-styrene nanocomposites using the master-batch method. *Carbohydrate Polymers* **2015,** *125*, 352-359.
74. Ten, E.; Bahr, D. F.; Li, B.; Jiang, L.; Wolcott, M. P., Effects of Cellulose Nanowhiskers on Mechanical, Dielectric, and Rheological Properties of Poly(3-hydroxybutyrate-co-3-hydroxyvalerate)/Cellulose Nanowhisker Composites. *Ind. Eng. Chem. Res.* **2012,** *51* (7), 2941-2951.
75. Goetz, L.; Foston, M.; Mathew, A. P.; Oksman, K.; Ragauskas, A. J., Poly(methyl vinyl ether-co-maleic acid)-Polyethylene Glycol Nanocomposites Cross-Linked In Situ with Cellulose Nanowhiskers. *Biomacromolecules* **2010,** *11* (10), 2660-2666.
76. Yu, H. Y.; Qin, Z. Y.; Liu, Y. N.; Chen, L.; Liu, N.; Zhou, Z., Simultaneous improvement of mechanical properties and thermal stability of bacterial polyester by cellulose nanocrystals. *Carbohydrate Polymers* **2012,** *89* (3), 971-978.
77. Atifi, S.; Su, S. X.; Hamad, W. Y., Mechanically tunable nanocomposite hydrogels based on functionalized cellulose nanocrystals. *Nord. Pulp Paper Res. J.* **2014,** *29* (1), 95-104.
78. Yu, H. Y.; Sun, B.; Zhang, D. Z.; Chen, G. Y.; Yang, X. Y.; Yao, J. M., Reinforcement of biodegradable poly(3-hydroxybutyrate-co-3-hydroxyvalerate) with cellulose nanocrystal/silver nanohybrids as bifunctional nanofillers. *J. Mat. Chem. B* **2014,** *2* (48), 8479-8489.
79. Chen, Y.; Liu, C. H.; Chang, P. R.; Cao, X. D.; Anderson, D. P., Bionanocomposites based on pea starch and cellulose nanowhiskers hydrolyzed from pea hull fibre: Effect of hydrolysis time. *Carbohydrate Polymers* **2009,** *76* (4), 607-615.
80. Huang, J.; Liu, L.; Yao, J. M., Electrospinning of Bombyx mori Silk Fibroin Nanofiber Mats Reinforced by Cellulose Nanowhiskers. *Fibers and Polymers* **2011,** *12* (8), 1002-1006.
81. Li, R. J.; Zhang, Y. H.; Zhu, L. J.; Yao, J. M., Fabrication and characterization of silk fibroin/poly(ethylene glycol)/cellulose nanowhisker composite films. *Journal of Applied Polymer Science* **2012,** *124* (3), 2080-2086.
82. Hossain, K. M. Z.; Jasmani, L.; Ahmed, I.; Parsons, A. J.; Scotchford, C. A.; Thielemans, W.; Rudd, C. D., High cellulose nanowhisker content composites through cellosize bonding. *Soft Matter* **2012,** *8* (48), 12099-12110.

83. Johar, N.; Ahmad, I., Morphological, thermal, and mechanical properties of starch biocomposite films reinforced by cellulose nanocrystals from rice husks. *Bioresources* **2012,** *7* (4), 5469-5477.
84. Siqueira, G.; Mathew, A. P.; Oksman, K., Processing of cellulose nanowhiskers/cellulose acetate butyrate nanocomposites using sol–gel process to facilitate dispersion. *Composites Science and Technology* **2011,** *71* (16), 1886-1892.
85. Moreira, F. K. V.; Marconcini, J. M.; Mattoso, L. H. C., Solid state ball milling as a green strategy to improve the dispersion of cellulose nanowhiskers in starch-based thermoplastic matrices. *Cellulose* **2012,** *19* (6), 2049-2056.
86. Zakuwan, S. Z.; Ahmad, I.; Ramli, N., Preparation of Hybrid Nano Biocomposite kappa-Carrageenan/Cellulose Nanocrystal/Nanoclay. In *2013 Ukm Fst Postgraduate Colloquium*, Murad, A.; Yen, C. C.; Ismail, E. S.; Maskat, M. Y.; Noorani, M. S. M.; Ibrahim, N.; Karim, N.; Yahya, R.; Khalid, R. M.; Ismail, W. R.; Ling, W. S.; Ibrahim, Z., Eds. Amer Inst Physics: Melville, 2013; Vol. 1571, pp 738-743.
87. Agustin, M. B.; Ahmmad, B.; Alonzo, S. M. M.; Patriana, F. M., Bioplastic based on starch and cellulose nanocrystals from rice straw. *J. Reinf. Plast. Compos.* **2014,** *33* (24), 2205-2213.
88. Hooshmand, S.; Aitomaki, Y.; Skrifvars, M.; Mathew, A. P.; Oksman, K., All-cellulose nanocomposite fibers produced by melt spinning cellulose acetate butyrate and cellulose nanocrystals. *Cellulose* **2014,** *21* (4), 2665-2678.
89. Liu, L.; Yang, X. G.; Yu, H. Y.; Ma, C.; Yao, J. M., Biomimicking the structure of silk fibers via cellulose nanocrystal as beta-sheet crystallite. *Rsc Advances* **2014,** *4* (27), 14304-14313.
90. Camarero-Espinosa, S.; Boday, D. J.; Weder, C.; Foster, E. J., Cellulose Nanocrystal Driven Crystallization of Poly(D,L-lactide) and Improvement of the Thermomechanical Properties. *Journal of Applied Polymer Science* **2015,** *132* (10), 11.
91. Bardet, R.; Belgacem, N.; Bras, J., Flexibility and Color Monitoring of Cellulose Nanocrystal Iridescent Solid Films Using Anionic or Neutral Polymers. *Acs Applied Materials & Interfaces* **2015,** *7* (7), 4010-4018.
92. Haafiz, M. K. M.; Hassan, A.; Khalil, H.; Khan, I.; Inuwa, I. M.; Islam, M. S.; Hossain, M. S.; Syakir, M. I.; Fazita, M. R. N., Bionanocomposite based on cellulose nanowhisker from oil palm biomass-filled poly(lactic acid). *Polymer Testing* **2015,** *48*, 133-139.
93. Dhar, P.; Tarafder, D.; Kumar, A.; Katiyar, V., Effect of cellulose nanocrystal polymorphs on mechanical, barrier and thermal properties of poly(lactic acid) based bionanocomposites. *Rsc Advances* **2015,** *5* (74), 60426-60440.
94. Leite, L. S. F.; Battirola, L. C.; da Silva, L. C. E.; Goncalves, M. D., Morphological investigation of cellulose acetate/cellulose nanocrystal composites obtained by melt extrusion. *Journal of Applied Polymer Science* **2016,** *133* (44), 10.
95. Tabassi, N.; Moghbeli, M. R.; Ghasemi, I., Thermoplastic starch/cellulose nanocrystal green composites prepared in an internal mixer. *Iran. Polym. J.* **2016,** *25* (1), 45-57.
96. Zhang, S. F.; Xia, C. L.; Dong, Y. M.; Yan, Y. T.; Li, J. Z.; Shi, S. Q.; Cai, L. P., Soy protein isolate-based films reinforced by surface modified cellulose nanocrystal. *Industrial Crops and Products* **2016,** *80*, 207-213.

97. Natarajan, B.; Krishnamurthy, A.; Qin, X.; Emiroglu, C. D.; Forster, A.; Foster, E. J.; Weder, C.; Fox, D. M.; Keten, S.; Obrzut, J.; Gilman, J. W., Binary Cellulose Nanocrystal Blends for Bioinspired Damage Tolerant Photonic Films. *Advanced Functional Materials* **2018,** *28* (26), 1800032.
98. Bao, Y. P.; Zhang, H.; Luan, Q.; Zheng, M. M.; Tang, H.; Huang, F. H., Fabrication of cellulose nanowhiskers reinforced chitosan-xylan nanocomposite films with antibacterial and antioxidant activities. *Carbohydrate Polymers* **2018,** *184*, 66-73.
99. Smyth, M.; M'Bengue, M.-S.; Terrien, M.; Picart, C.; Bras, J.; Foster, E. J., The effect of hydration on the material and mechanical properties of cellulose nanocrystal-alginate composites. *Carbohydrate Polymers* **2018,** *179*, 186-195.
100. Seoane, I. T.; Manfredi, L. B.; Cyras, V. P., Bilayer biocomposites based on coated cellulose paperboard with films of polyhydroxybutyrate/cellulose nanocrystals. *Cellulose* **2018,** *25* (4), 2419-2434.
101. Long, K. Y.; Cha, R. T.; Zhang, Y. P.; Li, J. J.; Ren, F. P.; Jiang, X. Y., Cellulose nanocrystals as reinforcements for collagen-based casings with low gas transmission. *Cellulose* **2018,** *25* (1), 463-471.
102. Noshirvani, N.; Hong, W. Y. J.; Ghanbarzadeh, B.; Fasihi, H.; Montazami, R., Study of cellulose nanocrystal doped starch-polyvinyl alcohol bionanocomposite films. *International Journal of Biological Macromolecules* **2018,** *107*, 2065-2074.
103. Xie, D. Y.; Qian, D.; Song, F.; Wang, X. L.; Wang, Y. Z., A Fully Biobased Encapsulant Constructed of Soy Protein and Cellulose Nanocrystals for Flexible Electromechanical Sensing. *Acs Sustainable Chemistry & Engineering* **2017,** *5* (8), 7063-7070.
104. Sucaldito, M. R.; Camacho, D. H., Characteristics of unique HBr-hydrolyzed cellulose nanocrystals from freshwater green algae (Cladophora rupestris) and its reinforcement in starch -based film. *Carbohydrate Polymers* **2017,** *169*, 315-323.
105. Nair, S. S.; Mathew, A. P., Porous composite membranes based on cellulose acetate and cellulose nanocrystals via electrospinning and electrospraying. *Carbohydrate Polymers* **2017,** *175*, 149-157.
106. Ma, X. H.; Cheng, Y. J.; Qin, X. L.; Guo, T.; Deng, J.; Liu, X., Hydrophilic modification of cellulose nanocrystals improves the physicochemical properties of cassava starch-based nanocomposite films. *Lwt-Food Science and Technology* **2017,** *86*, 318-326.
107. Kargarzadeh, H.; Johar, N.; Ahmad, I., Starch biocomposite film reinforced by multiscale rice husk fiber. *Composites Science and Technology* **2017,** *151*, 147-155.
108. Cerqueira, J. C.; Penha, J. D.; Oliveira, R. S.; Guarieiro, L. L. N.; Melo, P. D.; Viana, J. D.; Machado, B. A. S., Production of biodegradable starch nanocomposites using cellulose nanocrystals extracted from coconut fibers. *Polimeros-Ciencia E Tecnologia* **2017,** *27* (4), 320-329.
109. Wang, W.; Liang, T.; Zhang, B.; Bai, H.; Ma, P.; Dong, W., Green functionalization of cellulose nanocrystals for application in reinforced poly(methyl methacrylate) nanocomposites. *Carbohydrate Polymers* **2018,** *202*, 591-599.
110. Borjesson, M.; Sahlin, K.; Bernin, D.; Westman, G., Increased thermal stability of nanocellulose composites by functionalization of the sulfate groups on cellulose nanocrystals with azetidinium ions. *Journal of Applied Polymer Science* **2018,** *135* (10), 10.

111. Gwon, J. G.; Cho, H. J.; Lee, D.; Choi, D. H.; Lee, S.; Wu, Q. L.; Lee, S. Y., Physicochemical and Mechanical Properties of Polypropylene-cellulose Nanocrystal Nanocomposites: Effects of Manufacturing Process and Chemical Grafting. *Bioresources* **2018,** *13* (1), 1619-1636.
112. Zakuwan, S. Z.; Ahmad, I., Synergistic Effect of Hybridized Cellulose Nanocrystals and Organically Modified Montmorillonite on kappa-Carrageenan Bionanocomposites. *Nanomaterials* **2018,** *8* (11), 14.
113. Yin, Y. Y.; Hong, Z. Z.; Tian, X. Z.; Zhu, Q. Y.; Jiang, X.; Wang, H. B.; Gao, W. D., Cellulose nanocrystals modified with quaternary ammonium salts and its reinforcement of polystyrene. *Polym. Bull.* **2018,** *75* (5), 2151-2166.
114. Voronova, M.; Rubleva, N.; Kochkina, N.; Afineevskii, A.; Zakharov, A.; Surov, O., Preparation and Characterization of Polyvinylpyrrolidone/Cellulose Nanocrystals Composites. *Nanomaterials* **2018,** *8* (12).
115. Surov, O. V.; Voronova, M. I.; Afineevskii, A. V.; Zakharov, A. G., Polyethylene oxide films reinforced by cellulose nanocrystals: Microstructure-properties relationship. *Carbohydrate Polymers* **2018,** *181*, 489-498.
116. Shao, C. Y.; Wang, M.; Meng, L.; Chang, H. L.; Wang, B.; Xu, F.; Wang, J.; Wan, P. B., Mussel-Inspired Cellulose Nanocomposite Tough Hydrogels with Synergistic Self-Healing, Adhesive, and Strain-Sensitive Properties. *Chemistry of Materials* **2018,** *30* (9), 3110-3121.
117. Natterodt, J. C.; Sapkota, J.; Foster, E. J.; Weder, C., Polymer Nanocomposites with Cellulose Nanocrystals Featuring Adaptive Surface Groups. *Biomacromolecules* **2017,** *18* (2), 517-525.
118. Sapkota, J.; Natterodt, J. C.; Shirole, A.; Foster, E. J.; Weder, C., Fabrication and Properties of Polyethylene/Cellulose Nanocrystal Composites. *Macromolecular Materials and Engineering* **2017,** *302* (1), 1600300-n/a.
119. Sapkota, J.; Jorfi, M.; Weder, C.; Foster, E. J., Reinforcing poly (ethylene) with cellulose nanocrystals. *Macromolecular rapid communications* **2014,** *35* (20), 1747-1753.
120. Biyani, M. V.; Foster, E. J.; Weder, C., Light-Healable Supramolecular Nanocomposites Based on Modified Cellulose Nanocrystals. *ACS Macro Letters* **2013,** *2* (3), 236-240.
121. Reid, M. S.; Stimpson, T. C.; Niinivaara, E.; Villalobos, M.; Cranston, E. D., Comparing Soft Semicrystalline Polymer Nanocomposites Reinforced with Cellulose Nanocrystals and Fumed Silica. *Ind. Eng. Chem. Res.* **2018,** *57* (1), 220-230.
122. El Achaby, M.; Kassab, Z.; Barakat, A.; Aboulkas, A., Alfa fibers as viable sustainable source for cellulose nanocrystals extraction: Application for improving the tensile properties of biopolymer nanocomposite films. *Industrial Crops and Products* **2018,** *112*, 499-510.
123. He, Y. Y.; Zhu, J.; Wang, W. T.; Ni, H. T., Surface modification of cellulose nanocrystals with different acid anhydrides for improved dispersion in poly(butylene succinate). *Rsc Advances* **2018,** *8* (67), 38305-38314.
124. Inai, N. H.; Lewandowska, A. E.; Ghita, O. R.; Eichhorn, S. J., Interfaces in polyethylene oxide modified cellulose nanocrystal - polyethylene matrix composites. *Composites Science and Technology* **2018,** *154*, 128-135.
125. Kim, T.; Jeon, H.; Jegal, J.; Kim, J. H.; Yang, H. C.; Park, J.; Oh, D. X.; Hwang, S. Y., Trans crystallization behavior and strong reinforcement effect of cellulose nanocrystals

on reinforced poly(butylene succinate) nanocomposites. *Rsc Advances* **2018,** *8* (28), 15389-15398.
126. Yao, K.; Meng, Q.; Bulone, V.; Zhou, Q., Flexible and Responsive Chiral Nematic Cellulose Nanocrystal/Poly(ethylene glycol) Composite Films with Uniform and Tunable Structural Color. *Advanced Materials* **2017,** *29* (28).
127. Rahimi, S. K.; Aeinehvand, R.; Kim, K.; Otaigbe, J. U., Structure and Biocompatibility of Bioabsorbable Nanocomposites of Aliphatic-Aromatic Copolyester and Cellulose Nanocrystals. *Biomacromolecules* **2017,** *18* (7), 2179-2194.
128. Palaganas, N. B.; Mangadlao, J. D.; de Leon, A. C.; Palaganas, J. O.; Pangilinan, K. D.; Lee, Y. J.; Advincula, R. C., 3D Printing of Photocurable Cellulose Nanocrystal Composite for Fabrication of Complex Architectures via Stereolithography. *Acs Applied Materials & Interfaces* **2017,** *9* (39), 34314-34324.
129. Feng, X. H.; Yang, Z. Z.; Chmely, S.; Wang, Q. W.; Wang, S. Q.; Xie, Y. J., Lignin-coated cellulose nanocrystal filled methacrylate composites prepared via 3D stereolithography printing: Mechanical reinforcement and thermal stabilization. *Carbohydrate Polymers* **2017,** *169*, 272-281.
130. Noorani, S.; Simonsen, J.; Atre, S., Nano-enabled microtechnology: polysulfone nanocomposites incorporating cellulose nanocrystals. *Cellulose* **2007,** *14* (6), 577-584.
131. Mi, H. Y.; Jing, X.; Peng, J.; Salick, M. R.; Peng, X. F.; Turng, L. S., Poly(epsilon-caprolactone) (PCL)/cellulose nano-crystal (CNC) nanocomposites and foams. *Cellulose* **2014,** *21* (4), 2727-2741.
132. Sonseca, A.; Camarero-Espinosa, S.; Peponi, L.; Weder, C.; Foster, E. J.; Kenny, J. M.; Gimenez, E., Mechanical and Shape-Memory Properties of Poly(mannitol sebacate)/Cellulose Nanocrystal Nanocomposites. *J. Polym. Sci. Pol. Chem.* **2014,** *52* (21), 3123-3133.
133. Zarina, S.; Ahmad, I., Biodegradable Composite Films based on kappa-carrageenan Reinforced by Cellulose Nanocrystal from Kenaf Fibers. *Bioresources* **2015,** *10* (1), 256-271.
134. Kargarzadeh, H.; Sheltami, R. M.; Ahmad, I.; Abdullah, I.; Dufresne, A., Cellulose nanocrystal: A promising toughening agent for unsaturated polyester nanocomposite. *Polymer* **2015,** *56*, 346-357.
135. Wu, X. D.; Lu, C. H.; Zhang, X. X.; Zhou, Z. H., Conductive natural rubber/carbon black nanocomposites via cellulose nanowhisker templated assembly: tailored hierarchical structure leading to synergistic property enhancements. *J. Mater. Chem. A* **2015,** *3* (25), 13317-13323.
136. Bagheriasl, D.; Carreau, P. J.; Dubois, C.; Riedl, B., Properties of polypropylene and polypropylene/poly(ethylene-co-vinyl alcohol) blend/CNC nanocomposites. *Composites Science and Technology* **2015,** *117*, 357-363.
137. Iyer, K. A.; Flores, A. M.; Torkelson, J. M., Comparison of polyolefin biocomposites prepared with waste cardboard, microcrystalline cellulose, and cellulose nanocrystals via solid-state shear pulverization. *Polymer* **2015,** *75*, 78-87.
138. Huan, S. Q.; Bai, L.; Liu, G. X.; Cheng, W. L.; Han, G. P., Electrospun nanofibrous composites of polystyrene and cellulose nanocrystals: manufacture and characterization. *Rsc Advances* **2015,** *5* (63), 50756-50766.
139. Gu, M. Y.; Jiang, C. Y.; Liu, D. G.; Prempeh, N.; Smalyukh, II, Cellulose Nanocrystal/Poly(ethylene glycol) Composite as an Iridescent Coating on Polymer

Substrates: Structure-Color and Interface Adhesion. *Acs Applied Materials & Interfaces* **2016,** *8* (47), 32565-32573.
140. Huang, S. W.; Zhou, L.; Li, M. C.; Wu, Q. L.; Kojima, Y.; Zhou, D. G., Preparation and Properties of Electrospun Poly (Vinyl Pyrrolidone)/Cellulose Nanocrystal/Silver Nanoparticle Composite Fibers. *Materials* **2016,** *9* (7), 14.
141. Nagalakshmaiah, M.; El Kissi, N.; Dufresne, A., Ionic Compatibilization of Cellulose Nanocrystals with Quaternary Ammonium Salt and Their Melt Extrusion with Polypropylene. *Acs Applied Materials & Interfaces* **2016,** *8* (13), 8755-8764.
142. Zhang, X. Z.; Ma, P. M.; Zhang, Y., Structure and properties of surface-acetylated cellulose nanocrystal/poly(butylene adipate-co-terephthalate) composites. *Polym. Bull.* **2016,** *73* (7), 2073-2085.